DECIPHERING THE GENETIC EFFECTS AND PROTEOMIC CHANGES UNDERLYING NITROGEN USE EFFICIENCY IN POPCORN PLANTS

TALLES DE OLIVEIRA SANTOS

UNIVERSIDADE ESTADUAL DO NORTE FLUMINENSE
DARCY RIBEIRO – UENF

CAMPOS DOS GOYTACAZES – RJ
JULY – 2023

DECIPHERING THE GENETIC EFFECTS AND PROTEOMIC CHANGES UNDERLYING NITROGEN USE EFFICIENCY IN POPCORN PLANTS

TALLES DE OLIVEIRA SANTOS

"Thesis presented to the Centro de Ciências e Tecnologias Agropecuárias (CCTA) of the Universidade Estadual do Norte Fluminense Darcy Ribeiro as part of the requirements for obtaining the title of Doctor of Science in Genetics and Plant Breeding."

Advisor: Prof. Dr. Antônio Teixeira do Amaral Junior

CAMPOS DOS GOYTACAZES – RJ
JULY – 2023

FICHA CATALOGRÁFICA
UENF - Bibliotecas
Elaborada com os dados fornecidos pelo autor.

S237 Santos, Talles de Oliveira.

Deciphering the genetic effects and proteomic changes underlying nitrogen use efficiency in popcorn plants / Talles de Oliveira Santos. - Campos dos Goytacazes, RJ, 2023.

190 f. : il.
Bibliografia: 67 - 90.

Tese (Doutorado em Genética e Melhoramento de Plantas) - Universidade Estadual do Norte Fluminense Darcy Ribeiro, Centro de Ciências e Tecnologias Agropecuárias, 2023.
Orientador: Antonio Teixeira do Amaral Junior.

1. NUE. 2. Diallel Analysis. 3. Sustainable agriculture. 4. *Zea mays everta*. I. Universidade Estadual do Norte Fluminense Darcy Ribeiro. II. Título.

CDD - 631.5233

DECIPHERING THE GENETIC EFFECTS AND PROTEOMIC CHANGES UNDERLYING NITROGEN USE EFFICIENCY IN POPCORN PLANTS

TALLES DE OLIVEIRA SANTOS

"Thesis presented to the Centro de Ciências e Tecnologias Agropecuárias (CCTA) of the Universidade Estadual do Norte Fluminense Darcy Ribeiro as part of the requirements for obtaining the title of Doctor of Science in Genetics and Plant Breeding."

Approved on July 26th, 2023.

Examining committee:

Prof. Dr. Alexandre Pio Viana (D.Sc. Genetics and Plant Breeding) - UENF

Prof. Dr. Geraldo de Amaral Gravina (D.Sc. Plant Science) - UENF

Prof. Dr. Katarzyna Glowacka (Ph.D. Agricultural Sciences) - University of Nebraska - Lincoln

Prof. Dr. Antônio Teixeira do Amaral Junior (D.Sc. Genetics and Breeding) - UENF (Advisor)

DEDICATION

To my parents Alessandro and Rosinei, to my siblings Arthur, Thalita and Marianna.

I DEDICATE THIS THESIS!

ACKNOWLEDGMENTS

To the Universidade Estadual do Norte Fluminense Darcy Ribeiro and the Graduate Program in Genetics and Plant Breeding for providing me with suitable conditions to complete my Ph.D.

To CAPES, FAPERJ, and CNPq for granting the scholarships that ensured the development of my research.

To my advisor Prof. Dr. Antônio Teixeira do Amaral Júnior, for all the teachings, guidance, and valuable contributions that have shaped my education, as well as for the friendship.

I thank the professors of the Genetics and Plant Breeding Program for the companionship and learning.

To Secretary José Daniel for the support throughout the years.

To the Popcorn Breeding group for the support, especially to Rosimeire Barboza Bispo, a research and travel partner, for being so pleasant during our time together.

To my laboratory colleagues at the University of Nebraska – Lincoln for sharing with me the experiences and teachings that significantly contributed to my Ph.D. Sandwich.

To my friends in Lincoln, Nebraska, especially Denny and Roy, for giving me the opportunity to have them as family.

To my parents, for their incomparable support and understanding during all this time that I have been away, and for being my biggest cheerleaders.

To my partner Paulo, for being the best friend, family, and companion on this journey, always being there for me through the ups and downs, and with whom I hope to share infinite other moments.

To my friends, for being an extension of my home.

To my thesis committee for their valuable contributions to this work: Professor Alexandre Pio Viana, Professor Gravina, Professor Kasia Glowacka, for their contributions to the improvement of this work and the knowledge gained throughout my Ph.D. program.

This study was financed in part by the Coordenação de Aperfeiçoamento de Pessoal de Nível Superior - Brasil (CAPES) – Finance Code 001.

SUMMARY

ABSTRACT

SANTOS, Talles de Oliveira; D.Sc.; Universidade Estadual do Norte Fluminense Darcy Ribeiro. July, 2023. Deciphering the genetic effects and proteomic changes underlying nitrogen use efficiency in popcorn plants. Advisor: Antônio Teixeira do Amaral Júnior. Advising Committee: Alexandre Pio Viana and Gonçalo Apolinario de Souza Filho.

Nitrogen (N) is essential for sustaining life on Earth and plays a vital role in plant growth and agricultural production. The excessive use of N fertilizers not only harms the economy but also the environment. In the context of the environmental impacts caused by agriculture, global maize improvement programs aim to develop cultivars with high N-use efficiency (NUE) to reduce the use of N fertilizers, which is the most viable strategy from a sustainable perspective. N is highly mobile in plants, therefore NUE is related to several morphophysiological, and molecular mechanisms and despite being well explored in plants, the genetic effects and molecular mechanisms underlying NUE in popcorn plants still represent a gap in knowledge. In this sense, the objective of this study is to investigate the genetic effects controlling growth and physiological traits in four popcorn lines (P2 and P7 being N-efficient and N-responsive; L75 and L80 being N-inefficient and non-responsive to N) and their 12 hybrids combinations under two contrasting nitrogen conditions: high N (100% – 224.09 mg NO_3^- L^{-1}) and low N (10% – 22.41 mg NO_3^- L^{-1}), in a greenhouse experiment. Additionally, the study aims to investigate the proteomic profile involved in the molecular responses underlying NUE in two NUE-contrasting popcorn lines (P2 and L80). The first chapter consisted of estimating the genetic effects involved

in controlling morphoagronomic, physiological, and NUE-associated traits in four popcorn lines and 12 diallel maize-popping hybrids subjected to contrasting N conditions. By using diallel analysis proposed by Griffing (1956), the additive, non-additive genetic effects, and reciprocal genetic effects controlling these traits were estimated. In both N conditions, the non-additive genetic effects were more pronounced, indicating that exploiting heterosis is the most viable strategy for the development of cultivars with enhanced NUE. The second chapter aimed to evaluate the impact of nitrogen deficiency on the growth and physiological traits in two NUE-contrasting popcorn inbred lines, P2 and L80, under low and high N conditions, as described on the first chapter. Subsequently, the study aimed to investigate the proteomic profile involved in the molecular responses underlying NUE. Despite the limiting N supply significantly affected the growth and development of the lines, as well as physiological traits (such as photochemical and non-photochemical quenching and quantum yield of photosystem II), the N-efficient P2 line exhibited higher averages under both N conditions. A comparative proteomic analysis of leaves detected a total of 215 differentially accumulated proteins (DAPs) in the low/high N comparison for P2, and 168 DAPs in the low/high N comparison for L80. Among the identified DAPs, the N-efficient line showed 18 unique DAPs – five for high N and three for low N – while the N-inefficient line presented 12 unique DAPs, with five under high N and seven under low N. The pathways involved in oxidative stress response, energy metabolism (such as carbon fixation and carbohydrate metabolism), and photosynthesis represented the main differences between P2 and L80. The results shed light on the proteomic changes underlying NUE in popcorn and provide new insights for popcorn improvement programs in the face of negative effects caused by climate change, contributing to the development of a sustainable agriculture model.

Key words: NUE, Diallel Analysis, Sustainable agriculture, *Zea mays everta*.

RESUMO

SANTOS, Talles de Oliveira; D.Sc.; Universidade Estadual do Norte Fluminense Darcy Ribeiro. Julho, 2023. Deciphering the genetic effects and proteomic changes underlying nitrogen use efficiency in popcorn plants. Orientador: Antônio Teixeira do Amaral Junior. Conselheiros: Alexandre Pio Viana e Gonçalo Apolinario de Souza Filho.

O nitrogênio (N) é essencial para sustentar a vida na Terra e desempenha um papel vital no crescimento das plantas e na produção agrícola. O uso excessivo de fertilizantes nitrogenados não apenas prejudica a economia, mas também o meio ambiente. No contexto dos impactos ambientais causados pela agricultura, os programas globais de melhoramento de milho visam desenvolver cultivares com alta eficiência no uso de nitrogênio (NUE) para reduzir o uso de fertilizantes nitrogenados, o que é a estratégia mais viável do ponto de vista sustentável. O nitrogênio é altamente móvel nas plantas, portanto, a NUE está relacionada a vários mecanismos morfofisiológicos e moleculares, e apesar de ter sido bem explorada em nas plantas, os efeitos genéticos e os mecanismos moleculares subjacentes à NUE em plantas de milho-pipoca ainda representam uma lacuna no conhecimento. Nesse sentido, o objetivo deste estudo é investigar os efeitos genéticos que controlam o crescimento e características fisiológicos em quatro linhagens de pipoca (P2 e P7 com eficiência no uso de N e responsivas ao N; L75 e L80 com ineficiência no uso de N e não responsivas ao N) e suas 12 combinações híbridas, sob duas condições contrastantes de nitrogênio: alto N (100% - 224,09 mg NO_3^- L^{-1}) e baixo N (10% - 22,41 mg NO_3^- L^{-1}), em um experimento em casa de vegetação. Além disso, o estudo visa investigar o perfil proteômico envolvido nas respostas

moleculares subjacentes à NUE em duas linhagens de milho-pipoca contrastantes para NUE (P2 e L80). O primeiro capítulo consistiu em estimar os efeitos genéticos envolvidos no controle de características morfofisiológicas e associadas à NUE em quatro linhagens de pipoca e 12 híbridos dialélicos de milho-pipoca submetidos a condições contrastantes de N. Por meio da análise dialélica proposta por Griffing (1956), foram estimados os efeitos genéticos aditivos, efeitos genéticos não-aditivos e efeitos genéticos recíprocos que controlam essas características. Em ambas as condições de N, os efeitos genéticos não-aditivos foram mais pronunciados, indicando que explorar a heterose é a estratégia mais viável para o desenvolvimento de cultivares com maior eficiência de NUE. O segundo capítulo teve como objetivo avaliar o impacto da deficiência de nitrogênio no crescimento e nos traços fisiológicos em duas linhagens de pipoca com características contrastantes de NUE, P2 e L80, sob baixo e alto N, conforme descrito no primeiro capítulo. Posteriormente, o estudo buscou investigar o perfil proteômico envolvido nas respostas moleculares subjacentes à NUE. Apesar de o suprimento limitado de N afetar significativamente o crescimento e desenvolvimento das linhagens, bem como as características fisiológicas (como *quenching* fotoquímico e não fotoquímico e rendimento quântico do fotossistema II), a linhagem P2, eficiente no uso de N, apresentou médias mais altas em ambas as condições de N. Uma análise proteômica comparativa das folhas detectou um total de 215 proteínas acumuladas diferencialmente (DAPs) na comparação de baixo/alto N para P2 e 168 DAPs na comparação de baixo/alto N para L80. Entre as DAPs identificadas, a linhagem eficiente no uso de N apresentou 18 DAPs exclusivas – cinco para alto N e três para baixo N – enquanto a linhagem ineficiente no uso de N apresentou 12 DAPs exclusivas, sendo cinco para alto N e sete para baixo N. As vias envolvidas na resposta ao estresse oxidativo, no metabolismo energético (como fixação de carbono e metabolismo de carboidratos) e na fotossíntese representaram as principais diferenças entre P2 e L80. Os resultados lançam luz sobre as mudanças proteômicas subjacentes à NUE em milho-pipoca e fornecem novas perspectivas para programas de melhoramento de pipoca diante dos efeitos negativos causados pelas mudanças climáticas, contribuindo para o desenvolvimento de um modelo agrícola sustentável.

Palavras-chave: NUE, Análise dialélica, Agricultura sustentável, *Zea mays everta*.

1. INTRODUCTION

With the growing demand for increased food production and the demand for more economically sustainable agriculture, there is a pressing need to use efficient genotypes in the use of nitrogen (N) in crop fields (Zhang et al., 2015). From the economic point of view, only 33% of the N applied to the soil is used by wheat, rice, and maize plants (Almeida et al., 2018a), resulting in a significant increase in expenditure (Tilman et al., 2001; Mascia et al., 2019). The excessive use of nitrogen fertilizers causes not only economic damage, but also environmental, with soil acidification and water and air pollution (Wang et al., 2019; Khan et al., 2020b; Ren et al., 2021). Damage caused by excessive N use in Europe has been estimated at between US$91 and US$466 billion annually. The annual cost of nitrogen fertilizer could be reduced by about $2.3 billion if nitrogen uptake efficiency was improved by only 1% (Andrews e Lea, 2013).

Worldwide, maize (*Zea mays* L.) alone consumes almost a fifth of the nitrogen produced in the world. According to the United States Department of Agriculture (USDA, 2021), in 2020, corn production in the United States (US), China and Brazil – the three largest grain producers in the world, respectively – corresponded to 64.63% of global production. And, according to data from the Assessment of Fertilizer Use by Crop at the Global Level (Heffer et al., 2017), of all the N used in agriculture (102.50 million metric tonnes - Mt), the three countries consumed about 39.8% in the cultivation of wheat, rice, soybean, and corn. In terms of N consumption in agriculture, China ranks first, consuming about 24.5% of global N, followed by the United States, with a consumption of 11.5%, and Brazil with a consumption of 3.8%. In China, the highest consumption of N occurs in corn

cultivation, with 4.65 Mt of N applied in crop fields, followed by rice (3.90 Mt), wheat (3.40 Mt) and soybean (201 thousand metric tonnes). In the United States, corn also accounts for the highest consumption of N in agriculture, with a use of approximately 5.58 Mt, followed by wheat (1.56 Mt), rice (201 Mt), and soybean (178 thousand metric tonnes). In Brazil, similarly, the highest consumption of N in agriculture occurs in corn (1.06 Mt), followed by soybean (266 thousand metric tons), rice (182 thousand metric tons) and wheat (179 thousand metric tonnes).

Since 1960, the global application of nitrogen fertilizers has increased by 9 times and, in the next forty years, it is expected that there will be an increase of 40 to 60% (Sheoran et al., 2021). Therefore, reducing the consumption of nitrogen fertilizers and the environmental impacts resulting from them, through the cultivation of more efficient N-use genotypes (NUE) is an effective strategy to make agriculture more sustainable from an economic and environmental point of view (Han et al., 2016; Pampana e Mariotti, 2021). Nitrogen use efficiency is a complex characteristic consisting of two main components: N uptake efficiency (NUpE) and N utilization efficiency (NUtE), which involve biochemistry, phenology, root architecture and responses to the environment (Hawkesford, 2017; Hawkesford and Griffiths, 2019; Congreves et al., 2021).

Although nitrogen use efficiency has been extensively studied in maize, little is known about the genetic effects controlling morphological, physiological and root traits on popcorn subjected to nitrogen starvation. In addition, the molecular mechanisms underlying the plant response to this stress still represents a knowledge gap (Quan et al., 2019). Such information is important not only for improving plant yields under insufficient nitrogen supply, but also for the development of potential molecular tools for the selection of genotypes with enhanced NUE.

Given the complexity of the processes involved in NUE and the diversity of metabolic pathways involved, it is necessary to fill the gap in knowledge regarding the genetic effects controlling morphological and physiological traits and molecular mechanisms underlying the NUE response of maize under low N supply. In this sense, it was deemed necessary to the development of this thesis, which was divided into two chapters. CHAPTER 1 consists of studying the genetic control of morphophysiological and NUE-related traits in four inbred lines and 12 diallel popcorn hybrids. CHAPTER 2 describes the physiological and proteomic changes caused by nitrogen deprivation in two contrasting popcorn inbred lines.

.

2. OBJECTIVES

2.1 General objective

To analyze the genetic effects that control morphological, physiological and root traits through a diallel crossing of four popcorn inbred lines and to analyze the effect of heterosis on their respective hybrids. From the selection of two NUE-contrasting inbred lines, the objective is to analyze the differential accumulation of proteins on the leaves to identify the molecular mechanisms underlying the NUE response.

2.3 Specific objectives

1) To study the morphological, physiological and root architecture responses of popcorn lines and hybrids under different N availability;
2) To estimate the control parameters of morphological, physiological and root architecture characteristics in contrasting environments of N availability;
3) To evaluate the expression of heterosis for traits related to growth, development and plant physiology in addition to NUE-related traits in popcorn hybrids;
4) To analyze the metabolic pattern involved in the mechanism of nitrogen use and efficiency through comparative proteomics of two NUE-contrasting inbred lines.

3. CHAPTERS

3.1 EXPLORING THE POTENTIAL OF HETEROSIS TO IMPROVE NITROGEN USE EFFICIENCY IN POPCORN PLANTS

3.1.1 INTRODUCTION

In recent decades, world corn production has grown exponentially, and about 50% of this growth can be attributed to plant breeding and 50% to management practices, including nitrogen fertilization (Li et al., 2022). Regarding plant breeding, the exploitation of the heterosis effect has played a vital role in the extraordinary increase in corn yield around the world, especially in the United States of America, where grain yield has increased by 120% since the advent of the first hybrid, in 1930 (Duvick, 2015), being today the largest producer of the grain. According to FAO (FAO, 2020), Brazil is the third largest corn producer in the world and, in 2019, became the largest exporter. In the 2019/2020 harvest, Brazilian production was around 103 million tons, of which approximately 23 million tons were exported (Kist et al., 2021).

In the last 20 years, despite the Brazilian corn yield has grown about 120%, this value remains low (5.72 t ha^{-1}) compared to the United States of America (11.07 t ha^{-1}) and Argentina (8.36 t ha^{-1}), countries where corn is grown in temperate and/or

subtropical conditions and with a large amount of N application. In Brazil, even corn is grown in temperate and/or tropical conditions, about 75% of production comes from regions with a tropical climate, where the grain yield potential of cultivated areas is significantly reduced due to the occurrence of abiotic stresses (Fahad et al., 2017; Yadav et al., 2020; Santos et al., 2021b). Among the abiotic stresses, the low availability of nitrogen in the soil (Anas et al., 2020; Zuffo et al., 2021) is one of the main factors contributing to the grain yield reduction of several crops, including popcorn (*Zea mays* var. *everta*).

As an essential component of critical macromolecules, nitrogen is vital for plants (Quan et al., 2019), and in corn, it is an essential nutrient. N represents up to 5% of total dry matter (Mascia et al., 2019) and is a constituent of leaf pigments, such as chlorophyll, amino acids, nucleic acids, proteins, and plant hormones (Gan et al., 2016; Taiz and Zeiger, 2016). The low availability of nitrogen in the soil directly impacts corn yield, with adverse effects on the weight and length of ears (Abubakar et al., 2019), 100-grain weight, prolificacy (D'andrea et al., 2022; Ludemann et al., 2022), as well as plant height (Hammad et al., 2022). These compromises in the agronomic components of production result from the effects of N limitation on photosynthetic capacity (Wu et al., 2019). This is because N supply has an important impact on carbon assimilation, considering that in a scenario of abiotic stresses, such N deprivation, as first response plants tend to promote the stomata closure, inhibiting the assimilation of CO_2.

Given its great importance in several physiological processes, nitrogen is the nutrient required in greater quantity to produce corn and is considered the second limiting factor for the increase in crop yield (Zuffo et al., 2021). However, despite the high demand for N in corn production, only half of the applied N is used (Jiang et al., 2018). The remaining N is responsible for increasingly severe environmental pollution (Li et al., 2017). Therefore, given the scenario of increased adverse effects on agricultural sustainability, there is a need to develop a more sustainable agriculture model with genotypes efficient in the use of nitrogen (Hammad et al., 2022) since the excessive use of this nutrient causes damage not only to the economy but also to the environment. It must be considered that by 2050, agriculture will need to feed a growing world population, reaching the 10 billion mark (Springmann et al., 2018).

For the popcorn plants, which is highly appreciated in Brazil – and which moved around US$10 billion worldwide in 2020 (Serna-Saldivar, 2022) – there are still few studies aimed at obtaining efficient genotypes in the use of N (NUE), as well as the exploration of heterosis for the release of more efficient hybrids in the use of the nutrient. This is because NUE is a complex trait controlled by several genes and highly influences the environment (Getahun et al., 2022). Therefore, understanding complex traits such as NUE requires a better understanding of the morphophysiological mechanisms underlying its expression, which is an arduous task from the point of view of plant breeding, mainly because it has already been reported that the components of NUE (N uptake efficiency – NUpE, and N utilization efficiency – NUtE) are inherited independently (Torres et al., 2018).

Aiming to understand the mechanism of genetic control of NUE in popcorn, Santos et al. (2017) evaluated the efficiency of nitrogen use in lines evaluated in two environments under adequate and infra-optimal conditions of nutrient availability in the soil. Subsequently, Santos et al. (2019) evaluated the genetic effects involved in nitrogen use efficiency through the characterization of ten lines and 90 popcorn hybrids obtained in a complete diallel scheme for the two variables of interest for the crop – grain yield (GY) and popping expansion (PE). The authors' conclusion is that both additive and non-additive effects contribute to the expression of NUE, along with the influence of the female parent, which is evident from the reciprocal effect's significance. More recently, to understand the physiological mechanisms and proteomic profile of popcorn genotypes grown under different N availability conditions, Khan et al. (2020b) and Khan et al. (2022) evaluated two contrasting lines for NUE together with their hybrid. According to the authors, the interaction between proteins related to the synthesis of L-ascorbate peroxidase and ferredoxin-nitrite reductase showed great importance in the expression of NUE for the species *Zea mays everta*.

However, studies on the morpho-physiological mechanisms associated with heterosis still represent a knowledge gap. Having access to additional knowledge about the genetic regulation of traits related to NUE expression, such as photosynthetic mechanisms, leaf pigments, and photochemical efficiency, would significantly assist in guiding breeding programs. This information would facilitate the reliable selection of parents and the production of superior hybrids, thereby playing a crucial role in the advancement of breeding programs. In this sense, evaluating lines and their hybrid combinations can provide relevant information for the popcorn breeding program (Lima et al., 2019). Through these targeted crosses, estimates of general and specific combining abilities are obtained, which are

associated with the additive and non-additive genetic effects involved in the control of traits (Cruz et al., 2014; Hallauer et al., 2010). In addition, through complete diallel, information can be obtained about reciprocal effects, which may be associated with the expression of extrachromosomal genes (Santos et al., 2019).

Although previous studies have shown that much of the nitrogen supply destined for the grain in maize is absorbed in the reproductive growth stage (Gallais et al., 2007; Ning et al., 2017), the various negative effects of climate changes that intensified abiotic stresses caused a disruption in N assimilation and remobilization patterns (De Oliveira Silva et al., 2017). In this sense, the assimilation of N in the vegetative stage is crucial to compensate for a possible deprivation of N in the grain-filling stage, mainly because between 45 and 65% of the N destined for the grains is provided by N remobilization with the advance of leaf senescence. Therefore, considering a scenario of water scarcity – common in countries with tropical and subtropical climates such as Brazil – genotypes that are more efficient in the use of N may present lower losses in productivity caused by N deprivation. In this perspective, Nasielski et al. (2019) showed that a luxury N accumulation in the pre-anthesis period may be beneficial for plants since it is able to mitigate low N stress and act as an N reserve that buffers grain yield and maintains plant function.

Therefore, given the above, it was considered suitable to develop this study in which the goal is to evaluate the differences in growth, efficiencies of use, uptake, and utilization of nitrogen and the impacts of N starvation in the traits associated with photosynthetic efficiency. In addition, under contrasting conditions of nitrogen availability in the soil, the study aimed to understand the mechanisms involved in the expression of heterosis in popcorn genotypes and the genetic control of these traits under different N availability in plants in the vegetative stage.

3.1.2 LITERATURE REVIEW

3.1.2.1 General aspects of popcorn

Popcorn belongs to the Poaceae family (Goodman and Smith, 1987), Panicoide subfamily, Maydeae tribe, *Zea* genus, *Zea mays* var. *everta* species (Sturtev) L.H. Bailey (Galinat, 1979; Paterniani and Campos, 2005). Popcorn has smaller grains, higher prolificacy, smaller size, thinner and more fragile stalks, fewer

leaves, and higher susceptibility to diseases compared to common corn. The main difference between the two types of corn lies in the popcorn's ability to expand its grains (Larish and Brewbaker, 1999). This process, called popping, is described as an explosion caused by the expansion when the grains are subjected to temperatures above 180 ºC, which leads to the loss of moisture contained in the starch granules and the destruction of the entire cellular structure of the endosperm (Weatherwax, 1922).

Regarding the shape, size, and color of the grain, there is great variability within the species. The types that are most accepted by the consumer market are round grains, pearl type, with orange endosperm (Ziegler and Ashman, 1994). As for its commercialization, popcorn can be classified as extra American popcorn, special American popcorn, extra yellow popcorn, and special yellow popcorn (Zinsly and Machado, 1987).

Although popcorn is exclusively intended for human consumption, it is considered a highly profitable crop and has gained great popular acceptance. For these reasons, there has been an increased interest in grain production in various regions, positioning Brazil as the second-largest popcorn producer in the world. In the agricultural year of 2018, the state of Mato Grosso alone produced 268,402 thousand tons of popcorn (Kist, 2019).

In Brazil, commercial cultivation of popcorn was limited during the 1990s, requiring a large quantity of importation, mainly from the United States, the largest producer of the crop (Galvão et al., 2000). However, many changes have been occurring in the market, and according to Rangel et al. (2008), with the widespread use of Brazilian and American hybrids, grain imports have significantly reduced. In addition to this, the release of the hybrids IAC-112 in 1988 and IAC-125 in 2006 by the Agronomic Institute of Campinas had an immediate effect on the popcorn grain market in Brazil (Scapim et al., 2006). However, even with the increase in the number of available cultivars in Brazil, the commercially available planting area is insufficient to meet the national demand (Vittorazi et al., 2013; Kist, 2019).

There are 166 registered popcorn cultivars in the National Cultivar Registry of the Ministry of Agriculture, Livestock, and Supply (MAPA), with 22 of them developed by the Darcy Ribeiro State University of Northern Rio de Janeiro (UENF) (Brasil, 2023). Among the registered cultivars, only three have indications for tolerance to environments with low nitrogen availability.

3.1.2.2 The physiological and morphological shoot responses of maize under low nitrogen conditions

As an essential component of key macromolecules, nitrogen is of great importance to plants (Quan et al., 2019) and, in maize, it is an extremely important nutrient. N represents up to 5% of the total dry matter (Mascia et al., 2019), and is a constituent of leaf pigments, such as chlorophyll, amino acids, nucleic acids, proteins, and plant hormones (Gan et al., 2016; Taiz and Zeiger, 2016) and plays an important role in photosynthesis. The nitrogen used in all photosynthetic apparatus can be divided into two categories: i) N associated with enzymes related to CO_2 assimilation; and ii) N present in thylakoids and associated with photochemical efficiency.

Regarding the association with enzymes, N is present in the structure of ribulose-1,5-bisphosphate carboxylase (Rubisco), phosphoenolpyruvate carboxylase (PEPC) and pyruvate orthophosphate dikinase (PPDK), which are directly involved in carbon reduction reactions, and are the most abundant enzymes in the assimilation of CO_2 (Mu and Chen, 2021).

Regarding the N associated with thylakoids, the nutrient can be distributed between two types of proteins, which are related to bioenergetics - including Cyt b6f and CF1/CF0, involved in electron transport and phosphorylation (Buchert et a 2022; Urban et al., 2021) – and those involved in the photosystem I (PSI) and photosystem II (PSII) [light-harvesting complex II (LHCII) and I (LHCI)] (Li et al., 2021). In plants with C4 metabolism about 45% of nitrogen is allocated to soluble proteins (20% of which is Rubisco) and 28% to thylakoids. Of this total present in thylakoids, about 75% of N is associated with light-harvesting proteins and the remainder is allocated to bioenergetics (Mu and Chen, 2021).

Therefore, the reduced supply of nitrogen negatively affects many aspects of plant growth and development in diverse morphophysiological stages (Figure 1), such as germination, seedling emergence, tillering, flowering, pollination and ultimately in yield and grain quality (Thi Nong et al., 2020; Liu et al., 2021; Sanagi et al., 2021; Santos et al., 2019). The impact of low N stress depends upon the magnitude and duration of exposure, on the genotype response, soil moisture and status and other environmental aspects. In maize, these negative effects impact plant growth and development in many aspects (Hammad et al., 2022). At early seedling stage it causes poor seedling establishment. At the beginning of the

vegetative development, it affects root and shoot growth, impacting on the acquisition of mineral and water supply, resulting in reduction of leaf area. The prolonged exposure causes reduction in photosynthesis, which directly affects the grain yield by reducing the weight and length of ears (Abubakar et al., 2019), the weight of the grains, the prolificity (D'andrea et al., 2022; Ludemann et al., 2022).

However, plants have numerous morphophysiological mechanisms to respond to the different stresses to which they are subjected, that were obtained through natural or artificial selection (Liu and Qin, 2021), and grant them tolerance to unfavorable environments, as is the case of low nutritional availability. In terms of low nitrogen availability, as a positive response, corn – which is a C_4 plant – can increase the amount of CO_2 available to Rubisco, investing much less N for the synthesis of this protein, which makes the crop more efficient at assimilating carbon per unit of N when compared to rice, for example, a C_3 plant (Makino et al., 1997). In addition, the low amount of Rubisco in corn allows for greater investment in thylakoid components (Mu et al., 2016a), allowing the crop to perform well in scenarios where N demand is not met. Another important mechanism of low N tolerance is the reduction in the relative content of chlorophyll in leaves for the protection of the photosynthetic apparatus, which, according to Khamis et al. (Khamis et al., 1990) and Lu et al. (Lu et al., 2001), means an important strategy for the protection of PSII, since the reduction in the content of this pigment reduces the amount of excitation energy in the system that, in a stressful scenario, could generate oxidative damage due to the presence of reactive oxygen species (ROS) – resulting in low values of stay-green.

Regarding the stay-green, the damage caused by ROS in the plant cells directly affects this trait – which was the most important phenotype for breeding selection, particularly for maize – resulting in early leaf senescence (Fu et al., 2020). Stay-green is a term used to describe genotypes with a delay in leaf senescence when compared other genotypes. Stay-green has a strong correlation with productivity because higher values for this trait translates into greater photosynthetic activity after the flowering period and, therefore, greater production of photoassimilates, positively impacting productivity (Lee and Tollenaar, 2007).

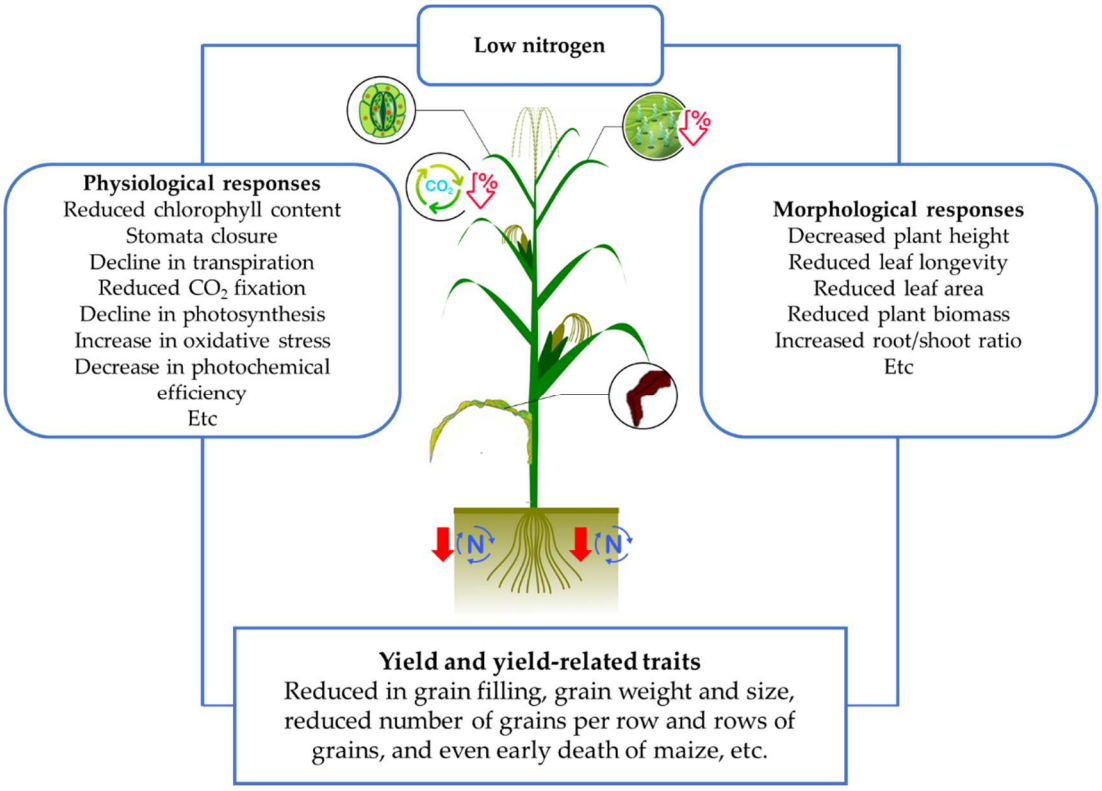

Figure 1. Schematic diagram showing impacts of plants to low nitrogen stress.

In a scenario of adequate N supply, plants use different mechanisms to distribute N among the various metabolic processes in which the nutrient is involved. Among these processes, the remobilization and recycling of N stands out, which, during the reproductive growth, supplies 35 to 55% of the N destined to grains (Hirel et al., 2007; Chen et al., 2014). However, in an infra-optimal condition of N supply, this mechanism is disrupted and the N that should be destined to filling the grain will increasingly depend on remobilized N, since the availability of soil N to be absorbed is low. Therefore, yield is reduced to the extent that, at the expense of N remobilization from leaves – as a component of photosynthetic pigments, nucleic acids, etc. – several cell functions are affected, causing damage to the leaves, through reductions in chlorophyll content, Fv/Fm, and photosynthesis activity (measured as CO_2 interchange) (Mu et al., 2018) and to the roots – which has reduced its supply of photoassimilates. All these effects ultimately significantly affect productivity. Therefore, more N-use efficient genotypes with higher values of stay-green have been the focus of improvement programs for the low N condition, since these plants have, as one of the tolerance mechanisms, a more effective absorption

of N in an environment of limiting N, reducing the need to activate remobilization mechanisms that would damage photosynthetic processes (Nasielski et al., 2019).

Another existing hypothesis about the tolerance mechanisms of maize plants under low N conditions – proposed by Plénet and Lemaire (1999) and by Ciampitti and Vyn (2012) – is that some genotypes would be able to accumulate luxury N, that is, N which is absorbed during vegetative growth and is stored into storage pools, instead of being used in the increment of biomass. According to the authors, this luxury N would then be used later in a scenario of nutritional deprivation during grain filling, a critical phase for the occurrence of stress in corn. Although later studies have found a strong association between high levels of productivity and the accumulation of luxury N, the mechanisms underlying this response of luxury N uptake and better shoot longevity have remained unstudied. In order to clarify this response, subsequent studies with ^{15}N isotope tracking sought to quantify the response of maize to the stress of low N availability during grain filling.

Paponov and Engels (2005), De Oliveira Silva et al. (2017) and, more recently Nasielski et al. (2019), in greenhouse and field experiments showed that during post-silking N stress, maize metabolism adapts to ensure that the necessary N is allocated to the grain at the expense of the N accumulated during the vegetative stage. Therefore, more efficient genotypes with a positive tolerance response to low amounts of N in the soil are more effective in accumulating luxury N in the vegetative stages. In view of the urgent issues related to climate change and the environmental damage caused by agriculture, breeding programs aimed at selecting superior materials for this condition can be highly successful when aimed at evaluating materials that are more efficient for these conditions, so that to reduce the consumption of N.

3.1.2.3 The root adaptation of maize under low N conditions

Roots play a crucial role from the initial development of seedlings to harvest, whether under stress conditions or optimal growth conditions, in addition, root plasticity plays a vital role in the adaptation of plants to stressful environments, whether in the acquisition or transport of nutrients (Gao et al., 2015). For this, root systems have developed anatomical and physiological strategies to exploit resources in complex environments (Lynch, 2015; Schneider et al., 2021). Corn has

an embryonic root system – which includes the primary root/radicle and seminal roots – and a post-embryonic one, which comprises shoot-borne roots, including crown roots (formed below ground) and brace roots (formed at aboveground nodes) (Hochholdinger et al., 2004). Primary, seminal, crown and brace roots are also called axial roots, while roots arising from axial roots are called lateral roots (LRs) (Figure 2).

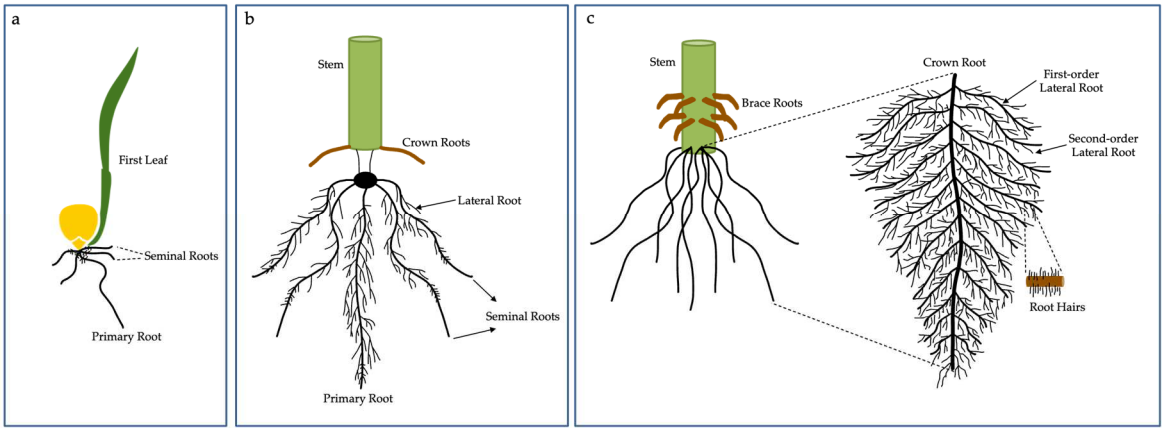

Figure 2. Maize embryonic (a), early post-embryonic (b) and adult post-embryonic (c) root systems are represented. (a) The primary root and seminal roots initiate from the embryo. (b) Lateral roots initiate from primary root and seminal root, while crown roots initiate from the stem. (c) The root system of adult maize is comprised of numerous crown roots and their lateral roots, which goes through several branching orders. The different root organs are terminated by root hairs. The scheme also demonstrates structural brace roots that start above-ground.

Some corn root system responses have been documented. Lynch et al. (Lynch, 2013) proposed a root ideotype called “steep, cheap and deep” to optimize water and N capture in maize. This ideotype consists of a set of architectural, anatomical, and physiological attributes that promote a quick exploration of more distant soil profiles and better acquisition of nitrate – the predominant form of N acquired by plants, highly mobile and soluble. In this more efficient root phenotype proposed by Lynch et al. (2013), regarding architectural attributes, more accentuated angles (in relation to the ground) of root growth favor the exploration of more distant profiles in the soil and, therefore, better acquisition of nitrogen – which, due to its greater mobility when compared to other nutrients, tends to be concentrated on deeper soil layers.

Therefore, a bigger depth of the root system, that is, a smaller root angle, has a direct effect on the accumulation of plant biomass. Another feature associated with the root architecture proposed by Lynch (2013) is the presence de few nodal roots and sparser LR branching which contributes to the reduction of competition between root axes for resources such as carbohydrates (since a greater number of ramifications would require redistribution of carbohydrate between these structures – which represents greater energy expenditure) and available nitrate. This root phenotype has been corroborated by other studies, such as the one developed by Wang et al. (2005) who sought to evaluate the influence of nitrate supply availability on root morphology and N uptake efficiency in five corn lines.

According to the authors, under N deficient situation, a larger root system with a great root length allowed the plants to explore the deep strata of soil, contributed to the efficient N accumulation. Trachsel et al. (2013), evaluating 108 inbred lines of maize in grown in high and low nitrogen under field conditions in the USA and South Africa found that the angles of crown roots were significantly associated with rooting depth – calculated as the depth containing 95% of the root mass, which means that the biggest portion of the crown roots were in the deep soil strata, contributing to a better N acquisition. The study confirms that more accentuated root angles allowed more adapted genotypes, under conditions of N limitation, to potentially explore soil volumes like those genotypes under optimal conditions of N availability, thus avoiding the reduction in grain yield.

Given the large number of characteristics and root phenotypes that affect the search for water and mineral resources in the soil, and the diversity of genetic and molecular mechanisms, it is quite unlikely that genotypes with maximum productive capacity will be reached in breeding programs based on up only on components such as productivity and other secondary characteristics. Despite being rare, breeding programs that employ these characteristics in the search for more adapted root phenotypes are successful (Burridge et al., 2019; Santos et al., 2021).

3.1.2.4 Maize improvement for low N conditions

The development of genotypes tolerant to low N conditions along with the adoption of improved agronomic practices – as reduction of nitrogen fertilizers applied in crop fields – are required to sustain corn productivity under the negative effects of climate changes.

The development of superior varieties for N use is the most viable and efficient strategy to mitigate the negative effects of climate change – which increasingly requires the development of a sustainable agricultural model. Therefore, one of the initial steps in breeding for N-use efficiency involves testing candidate environments and genotypes, then selecting superior varieties. The selection process can be effective for traits that are highly heritable and positively correlated with high productivity under conditions of N limitation (Bänziger et al., 1997; Bänziger and Lafitte, 1997). However, for the most part, the traits that contribute to grain yield and productivity are of a polygenic nature and have relatively low heritability, making direct selection difficult (Caixeta et al., 2015; Ertiro et al., 2020b). In these cases, the use of secondary traits with positive correlation with productivity can serve to assess gains in the selection process. As we mentioned in Topic 2.2, different are the responses of plants under infra-optimal conditions of N availability and, given the advances achieved in plant phenotyping in recent years, evaluating a greater number of secondary characteristics has been less challenging.

Therefore, several breeding programs have sought to evaluate secondary characters that are shown to be associated with higher productivity in maize under low N conditions (Ertiro et al., 2020a), such as photosynthetic rate, relative content of pigments (such as chlorophyll, flavonoids, and anthocyanins), chlorophyll fluorescence, stay-green duration and other traits associated with plant growth. Regarding foliar pigments, several studies with abiotic stresses have pointed to the effectiveness and speed of the evaluation of these parameters), which can be carried out with the aid of portable meters that use non-destructive methods for evaluation (Leite et al., 2021; Santos et al., 2021). Portable chlorophyll meters have been applied in the diagnosis of N status in maize and the significant relationship between chlorophyll meter readings and N status as well as productivity of maize plants has been well documented (Blackmer and Schepers, 1994; Rashid et al., 2005; Scharf et al., 2006; Hawkins et al., 2007; Zhang et al., 2008; Yang et al., 2012). Parameters associated with leaf gas exchange and chlorophyll fluorescence have also proven to be powerful tools to monitor the photochemical efficiency of leaves because they are reliable, non-destructive and can be obtained in vivo to assess important physiological phenomena that have a high correlation with maize productivity under optimal conditions and deprivation of N in the soil, according to

results demonstrated in some studies (Jin et al., 2015; Khamis et al., 1990; Zhang et al., 2021).

Once the stages of selection of superior genotypes for limiting N conditions have been advanced, defining the strategy that will guide the breeding program is crucial for obtaining adapted varieties. In this sense, studies aimed at understanding the genetic control of target traits (and correlated with productivity, as we discussed) are important to understand how to increase the frequency of favorable alleles associated with these traits, as well as assist in the selection of the best genotypes parental. In this sense, several key traits have been studied to understand genetic control, tolerance and nitrogen use efficiency in maize (Table 1), to guide crop improvement programs regarding the most appropriate improvement methods for gains in productivity (Santos et al., 2022).

Table 1. Genetic parameters for NUE-associated traits in maize under limiting nitrogen conditions.

Species	Traits	Type of Inheritance	Population	Number of Environments	Method	Authors
Zea mays everta	Grain yield and two NUE indices (Harmonic Mean of the Relative Performance and Agronomic Efficiency under Low Nitrogen Availability)	Additive and non-additive effects	90 temperate/tropical hybrids	2 environments and 2 N conditions	Classical (SCA and GCA)	Santos et al. (2019)
	Daily growth, shoot, root and total dry weight, root shoot ratio, NUpE, NUtE and NtrE efficiencies, lateral and axial root length, root surface area and root volume	Non-additive effects	2 F_1 hybrids, F_2 and backcross	1 environment and 2 N conditions	Generation Mean Analysis	Almeida et al. (2018a)
Z. mays	Grain yield, anthesis date and silking interval, plant height, ear height and position, ears per plant and senescence	Polygenic	411 testcrosses tropical hybrids	9 high N and 13 low N sites	Genomics (GWAS and GP)	Ertiro et al. (2020a)
	Grain yield, harvest index, nitrogen harvest index, grain protein concentration, NUE, NUpE, NUtE and genetic utilization	Polygenic	89 ex-PVP germplasm and 2 public lines (B73 and Mo17)	11 environments from (location - year, 2011 to 2016)	Classical (GCA, SCA) and genomics (GP)	Mastrodomenico et al. (2019)
	Grain yield and yield related traits (ear length, ear diameter, cob diameter, and grain size)	Non-additive effects	55 tropical hybrids	2 environments and 2 N conditions	Classical (SCA and GCA)	Guedes et al. (2014)
	Shoot dry weight, lateral and axial root length, NUE and its components (NUpE and NUtE)	Additive effects	41 hybrids	1 environment and 2 N conditions	Classical (SCA and GCA)	DoVale et al. (2012)
	Grain yield	Non-additive effects	105 tropical/ subtropical hybrids	Two trials under high and low N conditions each	Classical (SCA and GCA)	Makumbi et al. (2011)
	Grain yield, NUE and its components (NUpE and NUtE)	Additive and non-additive effects	28 hybrids	1 environment and 2 N conditions	Classical (SCA and GCA)	Souza et al. (2008)
	Partial factor productivity, agronomic nitrogen use efficiency, grain nutrient utilization efficiency and protein content	Additive and non-additive effects	15 hybrids	2 N conditions and 2 years	Classical (SCA and GCA)	Riache et al. (RIACHE et al., 2022)

SCA: Specific combining ability; GCA: General combining ability; GP: Genomic prediction; PVP: Plant variety protection.

Studies conducted in recent years on common corn and popcorn (*Zea mays everta*), using classical and molecular genetic approaches, have shown that the inheritance of traits linked to tolerance to low N and efficiency in the use of nitrogen can be additive or non-additive – linked to dominance and/or epistasis effects. Through classical approaches, such as diallel analysis or generation mean analysis, authors show that grain yield and yield-related traits – such as length and diameter of the ear, number of grains per row, number of rows of grain and one hundred grains weight, protein content, etc. – are controlled mostly by non-additive effects, either under optimal or nitrogen-limiting conditions (Almeida et al., 2018a; Dovale et al., 2012; Guedes et al., 2014; Makumbi et al., 2011; Riache et al., 2022; Santos et al., 2019; Souza et al., 2008).

In a recent study, for example, Amegbor et al. (2022) valuated 100 corn hybrids under optimum and limiting nitrogen conditions and, through combinatorial analysis, obtained estimates of the general (GCA) and specific (SCA) combining abilities for traits associated with phenology (days for male and female flowering and interval between flowering) and plant architecture as well as productivity and secondary characters. According to the authors, GCA e SCA varied for grain yield demonstrating the importance of additive and non-additive genetic effects for the hybrids evaluated under contrasting N conditions. Even though significant variations were detected for GCA and SCA, GCA which is the additive gene action component mainly controlled the heritage of grain yield under both conditions (Amegbor et al., 2022).

In terms of efficiency indices in the use of nitrogen and its secondary components – NUpE and NUtE – DoVale et al. (2012) and Mastrodomenico et al. (2019) report a greater contribution of additive effects on these characteristics with the others reporting a greater contribution of additive non-additive effects in common corn (Riache et al., 2022; Souza et al., 2008) and in popcorn (Almeida et al., 2018c; Santos et al., 2019), for example. In a work developed by Souza et al. (2008), thirty-one corn genotypes (28 crosses between commercial hybrids and three controls) were evaluated in soils with high and low N application rates. The authors found that in corn grown in soil with high N content, the GCA and SCA were significant for grain yield, NUE and NUpE. In corn from soils with low N content, only GCA, in NUpE, was significant. As for NUte, GCA and SCA were not significant in any of the environments. Thus, the authors concluded that for the conditions

studied, the additive and non-additive genetic effects are responsible for the genetic control of NUE and grain yield in maize cultivated in soils with high availability of N. Riache et al. (2021), evaluating diallel hybrids of Alegrian varieties of corn under two contrasting N conditions – optimal and infraoptimal – proposed that for the evaluated characteristics (plant height, interval between flowering, productivity, etc.) the best method to assess significant gains would be by exploring the interpopulation recurrent selection method (or reciprocal recurrent selection), since additive and non-additive effects contributed to the expression of genotypic variation in the studied material.

For popcorn, a crop of significant commercial importance (Santos et al., 2021b), although studies aimed at elucidating the inheritance and genetic control of important traits are less expressive (Dofing et al., 1991; Silva et al., 2010; Schwantes et al., 2018; Coan et al., 2019; Gerhardt et al., 2019; Lima et al., 2019; Peterlini et al., 2020; Santos et al., 2022), especially when it comes to abiotic stresses – as it is the case of low N availability. In this perspective, Santos et al. (2019) evaluating 90 hybrids from a complete diallel, under contrasting N availability conditions, for two indices of N use efficiency, grain yield and popping expansion, concluded that both additive and non-additive gene effects were important for selection for NUE. Moreover, the authors also concluded that there was allelic complementarity between the lines and a reciprocal effect for NUE, indicating the importance of the choice of the parents used as male or female. Considering the mentioned studies, the exploitation of heterosis is still the most viable alternative from an economic and sustainable point of view to obtain more tolerant and efficient genotypes in the use of N and, consequently, more productive.

However, not departing from the quantitative nature of the inheritance of essential traits related to low N tolerance, such as those mentioned above, genomic prediction (GP) has been applied to explore the additive effects to improve the response of maize to environments with low N availability (Table 1). Ertiro et al. (2020a), using GP to explore these effects on traits such as grain yield, flowering, plant height, ear height and number of ears per plant, found prediction accuracies ranging between 0.24 and 0.67.

3.1.3 MATERIAL AND METHODS

3.1.3.1 Plant material and growth conditions

Four popcorn lines (S_7) – P2 (derived from the compound CMS-42, adapted to temperate/tropical climates), P7 (derived from the hybrid IAC112, adapted to temperate/tropical climates), L75 and L80 (derived from the open pollination variety Viçosa, adapted to temperate/tropical climates) – and the hybrids, including reciprocal combinations, were evaluated under contrasting conditions of N availability. The lines were selected based on previous studies under contrasting N conditions in the soil and classified as efficient (P2 and P7) and inefficient (L75 and L80) in nitrogen use (Santos et al., 2017, 2019). Following the order of female and male parents, the hybrids P2×P7, P2×L75, P2×L80, P7×P2, P7×L75, P7×L80, L75×P2, L75×P7, L75×L80, L80×P2, L80×P7, and L80×L75 were used.

The experiment took place in a protected cultivation environment within a greenhouse at the Experimental Support Unit of the Universidade Estadual do Norte Fluminense Darcy Ribeiro (21º9′S; 41°10′W, 14 m altitude) from March 10 to April 20, 2021. A lysimetric system, following the description by Elazab et al. (2016), was utilized for the experiment. The system consisted of polyvinyl chloride (PVC) tubes with a diameter of 15 cm and a length of 150 cm, which were cut in half lengthwise. The two halves of the tubes were securely fixed together with adhesive tape. The lower parts of the tubes were sealed with pots of the same diameter, enabling proper drainage. The tubes, known as lysimeters, were filled with sand that had been washed using deionized water. Before commencing the experiment, samples of the substrate were collected and subjected to chemical analysis to evaluate the nutrient availability. The results of the chemical analysis can be found in Supplementary Table 1.

The experiment was arranged in complete randomized blocks, under two nitrogen availability conditions, with three replications per genotype for each nutrient availability in a factorial arrangement. Three seeds per lysimeter were sown, and after thinning (10 days after germination), only one plant per tube was maintained for each genotype (one plant per biological replicate). The spacing between plants was 25 cm and between rows was 1 m (40,000 plants ha^{-1}). The temperature, humidity, and photosynthetically active radiation data followed the seasonal pattern

and were obtained using the WatchDog 2000 Series Experimental Station (Spectrum Technologies Inc., Aurora, IL, USA) (Figure 3).

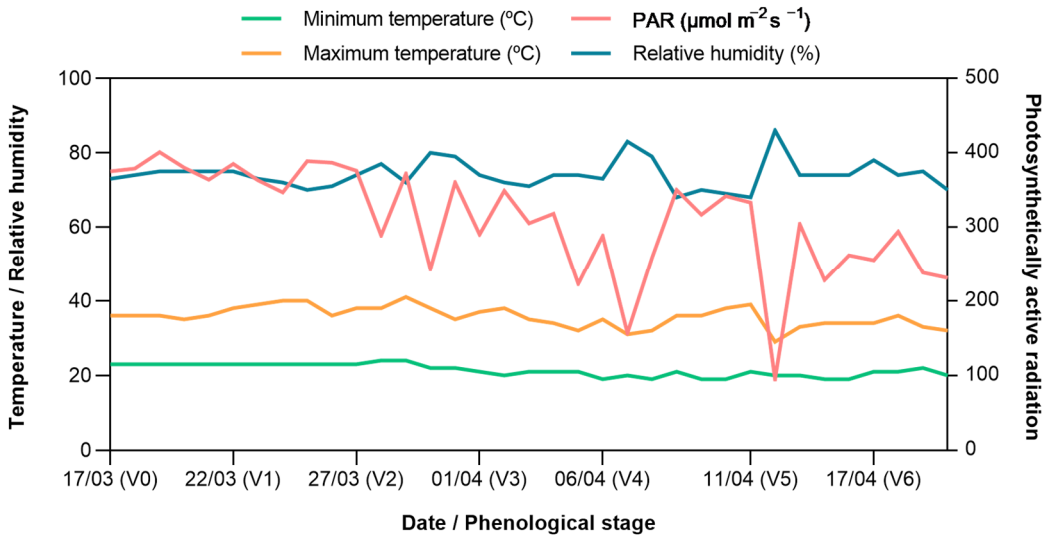

Figure 3 - Means of minimum and maximum temperatures (°C), relative humidity (RH, %), and photosynthetically active radiation (PAR, µmol m^{-2} s^{-1}) along the dates and phenological stages (V) of popcorn plant growth under two N availability conditions (March to April 2021).

The two nitrogen (N) availability conditions were based on 100% N (control condition, 224.09 mg L^{-1}) and 10% N (treatment, 22.41 mg L^{-1}), as established by Khan et al. (2020b), as being the ideal contrasting N levels to better discriminate popcorn genotypes for NUE and other morphophysiological traits. The solutions used were based on the modified Hoagland and Arnon (1950). The plants were irrigated daily with deionized water, and nutrients were supplied from the V2 stage (two fully expanded leaves), applying 200 mL of the nutrient solution with a pH between 5.5 and 5.8. Two contrasting dosages of N were used: 100% N requirement and 10% N requirement (22.41 mg L^{-1}) (90% reduction in soil N availability).

3.1.3.2 Leaf pigments

The measurements of chlorophyll, flavonoids, anthocyanins, and nitrogen balance index were conducted on the middle third of the sixth fully expanded leaf

(V6) one day prior to the conclusion of the experiment, which was 30 days after sowing. A portable meter called Dualex® (manufactured by FORCE-A, Orsay, France) was used for these measurements. The analysis was performed at the specific location on the leaf where chlorophyll fluorescence emission and gas exchange were evaluated.

3.1.3.3 Chlorophyll fluorescence measurements

Chlorophyll fluorescence was evaluated one day before the end of the experiment (V6 stage), in the middle third of the last fully expanded leaf of each plant from 9:00 to 11:00 h, using the Pocket PEA fluorimeter (Hansatech, King's Lynn, UK). The leaf was adapted in the dark for 20 minutes before using the leaf clip. Then, the leaf samples were exposed to a saturating light pulse (3,500 µmol m^{-2} s^{-1}) to evaluate the maximum quantum efficiency of PSII (Fv/Fm).

3.1.3.4 Measurements of leaf gas exchange

Gas exchange [net photosynthetic rate (A), stomatal conductance (gs), and transpiration rate (E)] were evaluated one day before the end of the experiment, in the middle third of the sixth fully expanded leaf of each plant (V6), between 09:00 and 11:00 h, and an infrared gas analyzer, model LI-6400 (LI-COR, Lincoln, NE, USA), equipped with a 6 cm2 leaf chamber and external light source (6400–40 LCF, LI-COR). During the evaluations, the PPFD was set at 1500 µmol m^{-2} s^{-1}, the CO_2 concentration was 400 µmol mol^{-1}, the relative humidity was between 55% and 60%, and the temperature was situated at 25 °C.

3.1.3.5 Morphological traits

At the end of the experiment, the plant height (cm) was measured with a ruler from the tube surface to the last developed leaf (visible ligule). The stem diameter, quantified in mm, was measured at the height of the middle third of the plants. The leaf area (cm^2) was obtained through the product between the width (cm) and length of the leaf (cm) with a tape measure. Then, the leaves were separated from the stems and placed in paper bags for drying in a circulation oven at 65 ˚C for 72 h to

determine the dry matter of the leaf (LDM – g) and stem (SDM – g) on a scale of precision. The shoot dry matter (STDM – g) was obtained by adding the LDM and SDM.

3.1.3.6 Root system analysis

At the end of the experiment, the tubes were opened to separate the substrate from the roots. Then, the samples were gently shaken and washed with running water, using a screen to remove the soil. Root samples were washed with deionized water, lightly dried with paper towels, and placed in a paper envelope. Then they were taken to drying in an oven at 65 °C for 72 h to determine the dry matter (RDM – g) on a precision balance.

3.1.3.7 Concentration of N

The N analysis was determined using the Kjeldahl (1990) method, obtaining the N content in the leaves (CNF: MSF × N content in the leaf – mg), in the stem (CNC: MSC × N in the stem – mg), in the shoot (CNPA: MSPA × N content in the shoot – mg), in the root (CNR: MSR × N content in the root – mg), and in the plant (CNP: sum of CNPA and CNR – mg).

3.1.3.8 Efficiency in the use of nitrogen and components

With the information on N application in the soil and the dry matter produced, the N use efficiency (NUE: MSPA/total applied N), the N uptake efficiency with the root N content (NUpE_cR: CNP/N total applied), the N uptake efficiency without the root N content (NUpE_sR: MSPA/total applied N), the N utilization efficiency with the root N content (NUtE_cR: MSPA/N content in the plant), the N utilization efficiency without the content of N of the root (NUtE_sR: MSPA/N content in the shoot), and the N translocation efficiency (NTrE: N content in the shoot/N content in the plant).

3.1.3.9 Root system analysis

For each trait, heterosis (H) was calculated by the difference between the average value obtained by the hybrid (F1) about the average values obtained by its parents (MP), in absolute and percentage values, respectively, according to the expressions: $\mathrm{MP} = \frac{\mathrm{P1+P2}}{2}$ and $\mathrm{H} = \left(\frac{\mathrm{F1-MP}}{\mathrm{MP}}\right) \times 100$; where P1 and P2 refer to the averages of the parents and F1 refers to the average performance of the hybrid (Hallauer et al., 2010).

3.1.3.10 Statistical analysis

For each trait studied, an individual analysis of variance was performed for each nitrogen availability condition according to the following statistical model: $Y_{ij} = \mu + G_i + B_j + \varepsilon_{ij,}$ on what Y_{ij} is the observed value of the i-th genotype in the j-th block, μ is the general constant, G_i is the effect attributed to the i-th genotype, B_j is the effect of block j, and ε_{ij} is the experimental error associated with the observation Y_{ij}.

Subsequently, a joint analysis of variance was performed based on the following statistical model: $Y_{ijk} = \mu + B_k + G_i + A_j + GA_{ij} + \varepsilon_{ijk}$, on what Y_{ijk} is the observation of the i-th genotype in the j-th availability of N in the k-th block, μ is the general constant, G_i is the fixed effect of the i-th genotype, B_k is the random effect of the k-th block, A_j is the fixed effect of the j-th condition of N, GA_{ij} is the fixed effect of the interaction between the i-th genotype with the j-th condition of N, and ε_{ijk} is the average experimental random error associated with the observation Y_{ijk} with NID (0, σ^2). The differences between lines and hybrids were partitioned for each trait, considered as contrast I (C1 – differences between lines), contrast 2 (C2 – differences between lines and hybrids) and contrast 3 (C3 – differences between hybrids). Statistical analyzes were performed using SAS 9.4 software (SAS Institute Inc., Cary, NC, USA).

The combinatorial abilities were analyzed by the method I of diallel analysis proposed by Griffing (1956), in which the parents, the hybrids, and the reciprocals are evaluated, considering the effect of the fixed genotypes. The effects of the genotypes for the general combining ability (GCA) and the specific combining ability (SCA) were obtained considering the following model: $Y_{ij} = \mu + g_i + g_j + s_{ij} + r_{ij}\ \varepsilon_{ij}$, on what Y_{ij} is the average value of the hybrid combination (i ≠ j) or the parent

(i = j), μ is the overall average, g_i, g_j are the effects of the general combining ability of the i-th or j-th parent (i, j = 1, 2, 3, and 4), s_{ij} is the effect of the specific combining ability for crosses between parents of order i and j, r_{ij} is the reciprocal effect that quantifies the differences resulting from parent i or j when used as a male or female parent in the cross *ij*, and ε_{ij} is the average experimental error associated with the observation of order *ij*.

The quadratic components that express the genetic variability associated with GCA (ϕ_g), SCA (ϕ_s), and reciprocal effects (ϕ_{rc}) were estimated by: $\phi g = \frac{QMG-QMR}{2p}$, $\phi s = QMS - QMR$, and $\phi rc = \frac{QMRC-QMR}{2}$, where QMG is the mean square of the general combining ability, QMS is the mean square of the specific combining ability, QMRC is the mean square of the reciprocal effect, QMR is the mean square of the residual, and *p* is the number of parents. To test the importance (R^2) of the Sources of Variation genotypes (G), N condition (N) and G by N interaction (G × N) for each trait we estimated the ratio between sum of square (SQ) of a given trait and its total SQ (SQT). Therefore, we obtained the following parameters: R^2G (proportional contribution of G) R^2N (proportional contribution of N) and $R^2_{G\times N}$ (proportional contribution of G × N).

The effects of the quadratic components were expressed as percentages concerning the sum of the total effects. Statistical-genetic analyzes were performed using the Genes software (Cruz, 2013). Finally, the PCA was performed on RStudio (R Core Team, 2023) using the packages FactoMineR (Lê et al., 2008).

3.1.4 RESULTS

3.1.4.1 Traits of plant architecture and nitrogen use efficiency

Plant architecture traits, nitrogen content, and N use efficiency differed statistically between lines and hybrids, except stem diameter and root N content in the high N condition. The Principal Component Analysis (PCA) showed that PC1 and PC2 accounted with more than 89% of the variance observed on the inbred lines in both N conditions (Supplementary Table 2). It can be observed that the NUE

related traits had the highest contributions for the two first PC's in both N conditions (Supplementary Figure 1). For all growth traits, soil N deficit affected all evaluated traits, with significant interactions between genotypes and environments (G × N) being found (Table 1). Out of the 18 evaluated traits, the major contribution to the significant differences was given by the source of variation N (14 traits) (Supplementary Table 3).

Plant height, stem diameter, and leaf area were reduced by 8.6%, 33.4%, and 25.9%, respectively, by the reduction in soil N application. Regarding the dry matter, reductions of 60.0% and 53.6% were observed for the dry matter traits of the leaf and stem, respectively, and the reductions were 57.5% and 32.5% for the dry matter of the shoot and root, respectively (Table 2).

Table 2. Summary of joint and individual ANOVA, means and standard deviations of morpho-physiological traits, nitrogen (N) content, and N use efficiency of lines and diallel hybrids of popcorn cultivated under contrasting conditions of N availability.

Trait	Joint Analysis			High N condition						Low N condition					
	G	N	G × N	Lines	C1	Hybrids	C2	C3	H%	Lines	C1	Hybrids	C2	C3	H%
PH	**	**	**	28.28 ± 3.30	**	31.48 ± 4.60	**	**	14.5	24.80 ± 3.01	**	29.09 ± 4.62	**	**	18.8
SD	**	**	**	10.42 ± 1.57	**	10.52 ± 1.64	ns	**	6.9	6.42 ± 1.06	**	7.17 ± 0.91	**	**	12.5
LA	**	**	**	233.37 ± 22.23	**	226.62 ± 49.22	**	**	-2.2	160.29 ± 21.92	**	172.02 ± 25.03	**	**	1.2
LDM	**	**	**	4.27 ± 1.00	**	3.77 ± 1.23	**	**	-8.9	1.47 ± 0.53	**	1.57 ± 0.53	**	**	13.2
SDM	**	**	**	2.55 ± 0.57	**	2.49 ± 1.07	**	**	-0.9	0.96 ± 0.34	**	1.21 ± 0.44	**	**	39.2
STDM	**	**	**	6.82 ± 1.57	**	6.29± 2.21	**	**	-5.2	2.43 ± 0.85	**	2.78 ± 0.92	**	**	23.2
RDM	**	**	**	1.03 ± 0.42	**	1.06 ± 0.35	**	**	23.7	0.54 ± 0.05	**	0.77 ± 0.25	**	**	49.4
LNC	**	**	**	25.55 ± 1.39	**	28.51 ± 3.86	**	**	17.1	17.23 ± 3.72	**	18.15 ± 2.64	**	**	1.1
SNC	**	**	**	22.75 ± 1.51	**	24.62 ± 5.03	**	**	15.0	14.90 ± 1.62	**	13.19 ± 1.42	**	**	-11.3
RNC	**	**	**	13.23 ± 0.26	ns	12.41 ± 2.45	**	**	-1.4	10.26 ± 0.68	**	8.99 ± 0.90	**	**	-18.1
STNC	**	**	**	48.30 ± 2.30	**	53.13 ± 8.55	**	**	16.1	32.13 ± 2.42	**	31.34 ± 3.40	**	**	-6.7
PNC	**	**	**	61.53 ± 2.39	**	65.54 ± 10.79	**	**	12.3	42.39 ± 2.05	**	40.33 ± 4.01	**	**	-9.6
NUE	**	**	**	124.15 ± 28.51	**	114.50 ± 40.27	**	**	14.0	448.45 ± 156.98	**	514.19 ± 169.78	**	**	23.2
NUpE_cR	**	**	**	1.12 ± 0.04	**	1.19 ± 0.20	**	**	12.3	7.84 ± 0.38	**	7.45 ± 0.74	**	**	-9.6
NUpE_sR	**	**	**	0.88 ± 0.04	**	0.97 ± 0.16	**	**	16.1	5.94 ± 0.45	**	5.79 ± 0.63	**	**	-6.7
NUtE_cR	**	**	**	142.41 ± 37.59	**	118.71 ± 41.83	**	**	1.1	75.52 ±26.39	**	89.74 ± 33.16	**	**	33.4
NUtE_sR	**	**	**	111.53 ± 28.56	**	96.43 ± 34.13	**	**	4.6	57.28 ± 20.20	**	69.59 ± 25.48	**	**	36.3
NTrE	**	**	**	0.78 ± 0.01	**	0.81 ± 0.01	**	**	3.4	0.76 ± 0.02	**	0.78 ± 0.02	**	**	3.1

PH – plant height (cm); SD – stem diameter (mm); LA – leaf area (cm^2); LDM – leaf dry matter (g); SDM – stem dry matter (g); STDM – shoot dry matter (g); RDM – root dry matter (g); LNC – leaf N content (mg of N kg^{-1}); SNC – stem N content (mg of N kg^{-1}); RNC – root N content (mg of N kg^{-1}); STNC – shoot N content (mg of N kg^{-1}); PNC – plant N content (mg of N kg^{-1}); (NUE – N use efficiency; NUpE_cR – N uptake efficiency with root N content; NUpE_sR – N uptake efficiency without root N content; NUtE_cR – N utilization efficiency with the content of N in the root; NUtE_sR – N utilization efficiency without the content of N in the root; NTrE – N translocation efficiency. The values in the Lines and Hybrids columns represent the means ± standard deviations of the respective 4 and 12 evaluated genotypes. C1 – statistical differences between strains; C2 – statistical differences between lines and hybrids according to the partition of the effects of lines and hybrids; and C3 – statistical differences between the hybrids; H% – relative heterosis. Joint ANOVA: genotype (G), nitrogen availability condition (N), and genotype × N availability condition (G × N). Significance levels: * $p \leq 0.05$; ** $p \leq 0.01$; and ns = not significant.

N deprivation had the biggest impact on the popcorn lines for plant height, stem diameter, and leaf area, which showed reductions of 12.3%, 38.4%, and 31.3%, respectively. In contrast, these reductions were 7.6%, 31.9%, and 24.5% for the hybrids, respectively. The same can be observed for the dry matter of leaf, stem, shoot, and root, which in the lines were reduced in the order of 65.6%, 62.4%, 64.4%, and 47.6%, while in the hybrids, the reductions were 58.6%, 51.4%, 55.8%, and 27.2%, respectively.

In this sense, the means of these traits (plant height, stem diameter, leaf area, dry matter of leaf, stem, shoot, and root) were higher in the hybrids, except for stem diameter at high N, whose contrast between lines and hybrids (C2) was not significant. The heterosis estimates for these traits were more marked in the limiting N condition. Thus, plant height, stem diameter, leaf area, and stem dry matter under N deficit presented estimates of 18.8%, 12.5%, 1.2%, 13.2%, and 39.2%, respectively. The shoot and dry root matter showed 23.2% and 49.4%, respectively (Table 2).

Regarding the N content in the plant, the joint analysis revealed a significant effect of the limitation of this nutrient in the genotypes studied, which caused decreases of 35.5%, 44.0%, 26.1%, 39.4%, and 36.8% in the N content in the leaf (LNC), stem (SNC), roots (RNC), shoot (STNC), and plant (PNC), respectively. Interestingly, for all these traits, the percentage decreases caused by the reduction of N in the soil were higher in the hybrids than in the lines. In the lines, the adverse effects of N reduction caused a decrease of 32.6%, 34.5%, 22.5%, 33.5%, and 31.1%, respectively, in LNC, SNC, RNC, STNC, and PNC. In the hybrids, the reductions in these traits were in the order of 36.3%, 46.4%, 27.6%, 41.0%, and 38.5%. Except for RNC, the nutrient reduction resulted in higher heterosis estimates in the high nitrogen supply environment for all traits, namely: 17.1% (LNC), 15.0% (SNC), 16.1% (STNC), and 12.3% (PNC) (Table 2).

Regarding the estimates of N use efficiency, the interaction of genotypes with the environment was also significant (Table 1). However, the reduction in the N applied to the soil caused an increase in NUE, in the nitrogen uptake efficiency of the root with the N content (NUpE_cR), and the nitrogen uptake efficiency without the N content (NUpE_sR). For these three traits, the increases caused in the means of lines and hybrids were 431.2%, 641.3%, and 614.9%, respectively. Considering that there was a significant difference ($p \leq 0.01$) for contrast 2 – lines and hybrids –

(Table 2), the increase in these traits was more pronounced in the hybrids only for NUE (449.1% compared to 361.2% increase in lines). Furthermore, for NUpE_cR and NUpE_sR, the most significant increases occurred in the lines, in the order of 699.2% and 675.2%, compared to 624.5% and 598.7%, respectively, in the hybrids.

Conversely, for the nitrogen utilization efficiency with N content in the root (NUtE_cR), as well as for the nitrogen utilization efficiency without N content in the root (NUtE_sR) and the nitrogen translocation efficiency (NTrE), reductions were observed caused by the reduced availability of the nutrient in the soil. For NUtE_cR and NUtE_sR, the reductions were more accentuated than those observed in NTrE (4.2%), with magnitudes of 29.8% and 32.7%, respectively, in the mean of the lines and hybrids. It was detected a significant difference ($p \leq 0.01$) between the lines and hybrids (C2). It appears that the reduction in these traits was more accentuated in the lines so that NUtE_cR and NUtE_sR were reduced by 47.0% and 48.7%, respectively, while in the hybrids this reduction was 24.4% and 27.8%, respectively. NTrE was much less affected in the lines and the hybrids, with respective values of 3.5% and 4.3%, but with a greater reduction in the hybrids (Table 2).

Given the differences observed between the performance of lines and hybrids for NUE in the N deficit conditions, the heterosis estimate was 23.2%, while in high N, the value was 14.0%. As for NUpE_cR and NUpE_sR, in low N, considering the inferior performance of the hybrids compared to the lines, the heterosis estimates were -9.6% and -6.7%, respectively – while in high N, the values were 12.3% and 16.1%, respectively –, which reflects, in this case, the superior performance of the hybrids for these traits in this condition.

For NUtE_cR, NUtE_sR, and NTrE, the heterosis estimates were more modest, with the limiting soil N supply environment being responsible for the highest estimates, in percentages of 33.4%, 36.3%, and 3.1%, respectively. These values were 1.1%, 4.6%, and 3.4% in the high N environment.

For the two N supply conditions, the importance (expressed in %) of the quadratic components pertaining to the general combining ability (ϕ_g), specific combining abilities (ϕ_s), and the reciprocal effects (ϕ_{rc}) of the traits associated with plant architecture, the status of N in the plant, and the efficiencies in the use, uptake, and utilization of N. It was observed that the general (related to ϕ_g) and specific combining ability (related to ϕ_s) differed in the two N supply conditions for all traits (Supplementary Table 4).

Although the mean squares related to the quadratic components ϕ_g were significant at high N, the essential components to explain the observed genetic variability for growth traits, N status, and nutrient use efficiency were those related to the specific combining ability (ϕ_s) and reciprocal effects (ϕ_{rc}). Therefore, for the traits PH, LDM, SDM, STDM, RDM, NUE, NUtE_cR, NUtE_sR, and NTrE, the prevalence of non-additive genetic effects is evident. In the case of the LA, the components ϕ_s and ϕ_{rc} had values very close to the relative contribution, with estimates of 49.01% and 49.02%, for ϕ_s and ϕ_{rc}, respectively. These reciprocal effects were more important for SD, LNC, SNC, RNC, STNC, PNC, NUpE_cR, and NUpE_sR (Figure 4, Supplementary Table 4).

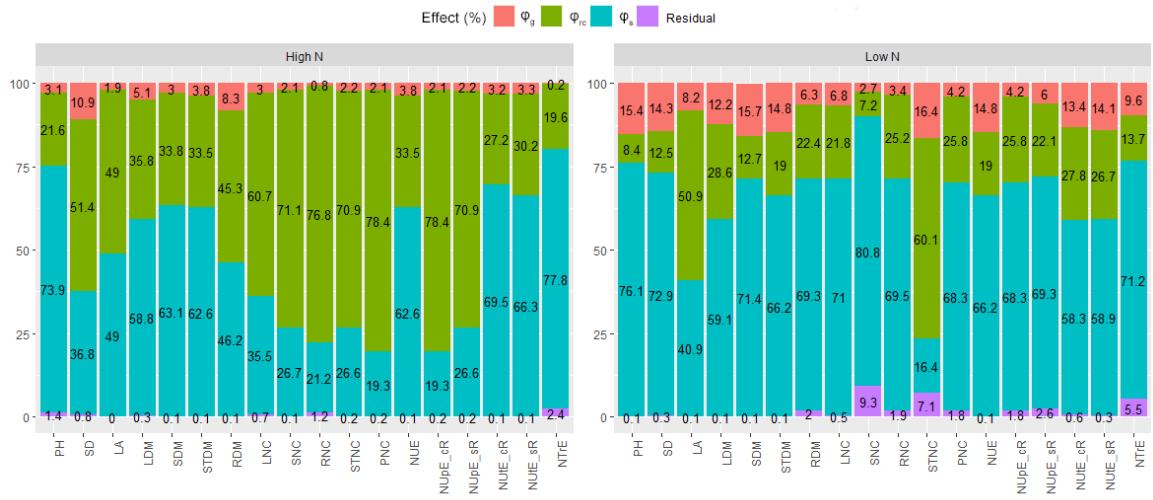

Figure 4. Importance in % of quadratic components related to general (ϕg) and specific (ϕs) combining abilities and reciprocal effects (ϕrc) for plant architecture traits (PH – plant height; SD – stem diameter; LA – leaf area; LDM – leaf dry matter; SDM – stem dry matter; STDM – shoot dry matter; RDM – root dry matter; LNC – leaf N content; SNC – stem N content; RNC – root N content; STNC – shoot N content; PNC – plant N content; NUE – nitrogen use efficiency with (cR) and without (sR) root N content; NUpE – nitrogen uptake efficiency with (cR) and without (sR) root N content; NUtE – nitrogen utilization efficiency with (cR) and without (sR) root N content; and NUtrE – nitrogen translocation efficiency.

In soil N limiting condition, for most traits, there was a predominance of the contribution of the quadratic component associated with non-additive effects (ϕ_s) in the expression of genetic variability (Figure 4, Supplementary Table 4). In this sense, it can be observed that for 16 of the 18 traits related to growth, N status in the plant and nutrient use efficiency - PH, SD, LDM, SDM, STDM, RDM, LNC, SNC,

PNC, NUE, NUPE_cR, NUpE_sR, NUtE_cR, NUtE_sR, NTrE – the quadratic component ϕ_s presented greater contributions. For LA and STNC, it is possible to observe a greater contribution of the quadratic component associated with the reciprocal effect (ϕ_{rc}). It is important to highlight that for the two N availability in the soil, the residual effects were not very expressive and, therefore, of minor importance for the observed results, guaranteeing an unequivocal interpretation of the observed effects (Figure 4, Supplementary Table 4).

3.1.4.2 Gas exchange, photochemical efficiency of chlorophyll and leaf pigments measurements

The joint ANOVA revealed a significant effect of nitrogen limitation on the genotypes – means of lines and hybrids –, with a decrease in the net CO_2 assimilation rate (A) of 28.4%, in addition to reductions in stomatal conductance (g_s) of 36.1%, in the intercellular concentration of CO_2 (Ci), and in the ratio between the intercellular and external concentration of CO_2 (Ci/Ca) of 12.8% and 12.5%, respectively, as well as the transpiration rate (E), of 18.7% (Table 2). In terms of the contribution to significative differences observed, for the gas exchange and related traits and chlorophyll fluorescence, the effect of genotype and N condition were equally relevant, being the G × N interaction, on the other hand, relevant just for one trait (Supplementary Table 2).

In addition to the effects between the genotypes, it can be noticed that the lines presented smaller percentage reductions concerning the hybrids and that there was an increase, even if not very expressive – of magnitude 0.3% - for the transpiration rate. In this sense, for the lines, the reductions caused in A, gs, Ci, and in the Ci/Ca ratio were 19.0%, 15.1%, 6.0%, and 0.6%, respectively. For the hybrids, the reductions for the same traits were 31.4% (A), 41.5% (gs), 14.9% (Ci), and 14.0% (Ci/Ca). However, for the maximum photochemical efficiency of photosystem II (F_v/F_m), with the imposition of stress, there was an increase of 5.7% in the average of the lines and hybrids; however, this increase was mainly due to the increase of 7.9 % in the average of the hybrids, while in the lines there was a negative impact of 0.6% (Table 3).

In the two conditions of N availability in the soil and considering that there is a significant difference ($p \leq 0.01$) for the contrast between lines and hybrids for A, *gs*, E, Ci/Ca, the heterosis estimates in the high nitrogen condition environment were higher for A, *gs*, E, and Ci/Ca, with estimates of 17.5%, 33.9%, 28.4%, and 21.9%, respectively. For F_v/F_m, under the condition of high N in the soil, there was

a significant difference between lines and hybrids, which resulted in a reduced heterosis value (-1.1%). For traits A, g_s, E, Ci/Ca, and F_v/F_m, in N limiting condition, heterosis estimates were 1.0% (A), -4.3% (*gs*), -9.7% (E), 20.3% (Ci/Ca), and 10.1% (F_v/F_m). For Ci, a higher estimate for heterosis was obtained in the low N condition, of 3.5%, while in the high N condition, the estimate was 2.6% (Table 3).

About leaf pigments, except for the relative content of anthocyanin (Anth) in high N, a significant difference was found between the genotypes studied, in addition to a significant interaction between genotype and N condition (G × N), and N being the source of variation the one the most influenced the significant differences observed. In this sense, it can be observed that nitrogen limitation had an impact on the relative content of chlorophyll (Chl), flavonoids (Flav), and the nitrogen balance index (NBI, Chl/Flav ratio). In the relative content of chlorophyll, under N-limited conditions, there was a reduction of 24.1%. In comparison, it caused an increase of 9.5% and 37.1% in the relative contents of the accessory pigments, anthocyanins, and flavonoids, respectively. Regarding the nitrogen balance index, there was a reduction of 31.1% based on the average performance of the lines and hybrids (Table 3).

Considering the significant difference between lines and hybrids, it is noteworthy that the reductions observed in the relative chlorophyll content and nitrogen balance index were more prominent in the hybrids. Specifically, the decrease in relative chlorophyll content caused by soil nitrogen limitation was 25.6% in hybrids, while the reduction in the nitrogen balance index was 33.4%. In contrast, the reductions in these traits for the lines were 18.8% (chlorophyll) and 23.6% (nitrogen balance index). On the other hand, the hybrids exhibited more substantial increases in accessory pigments. The estimated percentage increase was 10.6% for the relative content of flavonoids and 44.0% for the relative content of anthocyanins (Table 3).

In heterosis estimates, nitrogen limitation resulted in more expressive values. At low N, the values for Chl, Flav, and NBI were -10.5%, 10.2%, and -18.4%, respectively. Therefore, no significant difference was observed in contrast between lines and hybrids in this condition. In high nitrogen conditions, a significant difference ($p \leq 0.01$) was observed between lines and hybrids only for anthocyanin content, whose heterosis estimate was -2.7% (Table 3).

Table 3. Summary of joint and individual ANOVA, means, and standard deviations of physiological traits associated with measurements of gas exchange, photochemical efficiency of chlorophyll, and leaf pigments of lines and diallel hybrids of popcorn cultivated under contrasting conditions of N availability.

Trait	Joint Analysis			High N condition						Low N condition					
	G	N	G × N	Lines	C1	Hybrids	C2	C3	H%	Lines	C1	Hybrids	C2	C3	H%
A	**	**	**	23.65 ± 4.34	**	26.15 ± 3.55	**	**	17.5	19.16 ± 3.54	**	17.95 ± 2.88	**	**	-1.4
gs	**	**	**	0.18 ± 0.05	**	0.23 ± 0.05	**	**	33.9	0.16 ± 0.01	**	0.13 ± 0.04	**	**	-4.3
Ci	**	**	**	150.43 ± 22.90	**	158.20 ± 17.77	**	**	2.6	141.46 ± 15.64	**	134.68 ± 24.05	**	**	3.5
E	**	**	**	2.10 ± 0.39	**	2.52 ± 0.56	**	**	28.4	2.11 ± 0.18	**	1.91 ± 0.47	**	**	-9.7
Ci/Ca	**	**	**	0.36 ± 0.09	**	0.43 ± 0.05	**	**	21.9	0.34 ± 0.10	**	0.37 ± 0.09	**	**	20.3
F_v/F_m	**	**	**	0.78 ± 0.01	**	0.79 ± 0.08	ns	**	1.1	0.79 ± 0.02	*	0.85 ± 0.15	**	**	10.1
Chl	**	**	**	30.65 ± 1.84	**	30.06 ± 4.54	ns	**	2.6	24.90 ± 2.47	*	22.37 ± 2.28	**	**	-10.5
Flav	**	**	**	0.70 ± 0.07	ns	0.71 ± 0.13	ns	**	9.9	0.74 ± 0.07	**	0.78 ± 0.08	**	**	10.2
Anth	ns	**	ns	0.17 ± 0.01	**	0.16 ± 0.02	**	**	-2.7	0.21 ±0.01	*	0.23 ± 0.17	ns	ns	26.5
NBI	**	**	**	44.50 ± 5.68	*	43.07 ± 6.94	ns	**	-4.1	33.99 ±3.55	**	28.67 ± 3.00	**	**	-18.4

A – net CO2 assimilation rate; gs – stomatal conductance; Ci – intercellular concentration of CO_2; E – transpiration rate; Ci/Ca – ratio between the intercellular and external concentration of CO2; F_v/F_m – photochemical efficiency of photosystem II; Chl – relative chlorophyll content; Flav – relative content of flavonoids; Anth – relative anthocyanin content; NBI – nitrogen balance index. The values in the Lines and Hybrids columns represent the means ± standard deviations of the respective 4 and 12 evaluated genotypes. C1 – statistical differences between lines; C2 – statistical differences between lines and hybrids according to the partition of the effects of lines and hybrids; and C3 – statistical differences between the hybrids; H% – relative heterosis. Joint ANOVA: genotype (G), nitrogen availability condition (N), and genotype × N availability condition (G × N). Significance levels: * $p \leq 0.05$; ** $p \leq 0.01$; and ns = not significant.

Despite the significance observed in the mean squares of general combining ability, specific combining ability, and reciprocal effects for gas exchange measures, photochemical efficiency of chlorophyll, and leaf pigments in both nitrogen supply conditions, the ϕs component associated with non-additive genetic effects was predominant (Figure 5, Supplementary Table 4). Notably, a substantial contribution of residual effect was observed for the relative content of anthocyanin in low N conditions, indicating great environmental influence. Consequently, negative estimates for the quadratic components ϕ_g and ϕ_s were obtained. In this context, these negative values are interpreted as estimates with a true magnitude equal to zero. Therefore, the quadratic component was not considered further, as it accounted for 0% of the variation and did not explain the genetic variability of the trait.

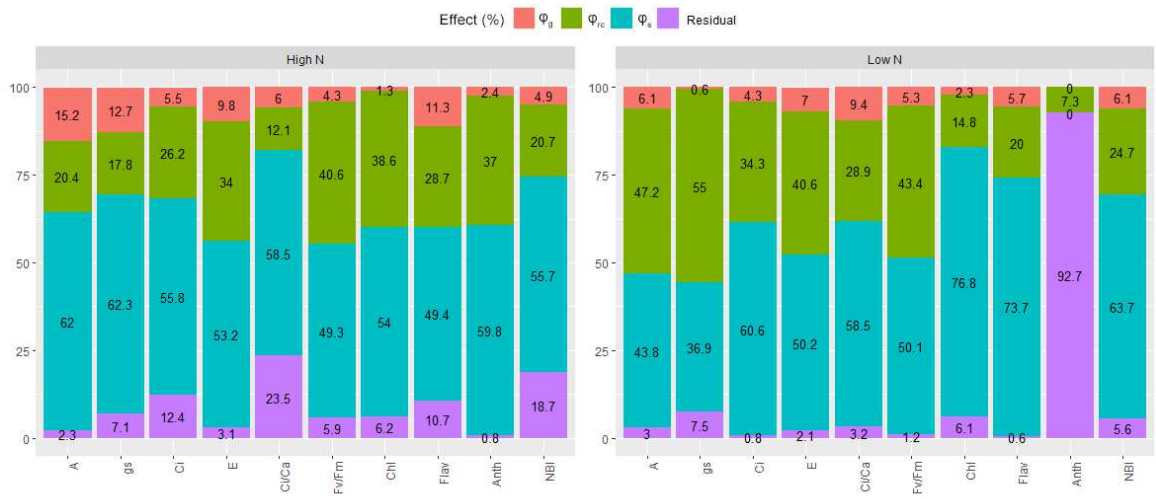

Figure 5 - Importance (expressed in %) of the quadratic components related to general (ϕ_g) and specific combining abilities (ϕ_s) and of reciprocal effects (ϕ_{rc}) for traits related to photosynthesis, leaf pigments and photochemical efficiency of chlorophyll (A – net CO_2 assimilation rate; gs – stomatal conductance; Ci – intercellular concentration of CO_2; E – transpiration rate; Ci/Ca – ratio between the intercellular and external concentration of CO_2; Fv/Fm – maximum quantum efficiency of photosystem II; Chl – relative chlorophyll content; Flav – relative content of flavonoids; Anth – relative content of anthocyanins; and NBI - nitrogen balance index).

3.1.5 DISCUSSION

3.1.5.1 The effect of nitrogen deprivation on photosynthesis, maximum efficiency of PSII, leaf pigments, and its impact on the growth of popcorn genotypes

Nitrogen plays a vital role in plants (Wu et al., 2019) and, in leaves, nitrogen forms include soluble components such as nitrate, amino acids, and proteins, as well as insoluble constituents in cell walls and membranes, among other structures (Bhadmus et al., 2022). The nitrogen utilized by the photosynthetic apparatus can be categorized into two main types: i) nitrogen associated with enzymes involved in CO_2 assimilation, and ii) nitrogen present in thylakoids and associated with photochemical efficiency (Khan et al., 2020a). In terms of the nitrogen's association with enzymes, it is found in the structure of key enzymes such as ribulose-1,5-bisphosphate carboxylase (Rubisco), phosphoenolpyruvate carboxylase (PEPC), and pyruvate orthophosphate dikinase (PPDK). These enzymes play a direct role in the reduction reactions of carbon and are the most abundant enzymes involved in the assimilation of CO_2 (Mu and Chen, 2021).

In relation to nitrogen associated with thylakoids, this nutrient can be divided between two types of proteins. The first type includes proteins involved in bioenergetics, such as Cyt b6f and CF1/CF0, which play roles in electron transport and phosphorylation (Urban et al., 2021; Buchert et al., 2022) The second type of proteins is associated with the light-harvesting complexes II (LHCII) and I (LHCI) (Li et al., 2021).

In plants with C4 metabolisms, like popcorn, approximately 45% of the nitrogen is allocated to soluble proteins, with 20% of this portion being attributed to Rubisco. Another 28% of nitrogen is allocated to thylakoids. Within the thylakoids, approximately 75% of the nitrogen is associated with light-harvesting proteins, while the remaining portion is dedicated to bioenergetics (Mu and Chen, 2021). Consequently, a low supply of nitrogen has a negative impact on the photosynthetic process, ultimately affecting plant development.

Based on the results of the present work, during vegetative growth, N limitation in popcorn plants caused significant reductions in plant height, stem diameter, and leaf area (Table 2). These reductions may be mainly associated with

the decrease observed in traits related to photosynthesis, such as net photosynthetic rate (A), stomatal conductance (gs), intercellular CO_2 concentration (Ci), transpiration (E), and the ratio between the and external concentration of CO_2 (Ci/Ca), which were reduced by the magnitudes of 28.4%, 36.1%, 12.8%, 18.7%, and 12.5%, respectively (Table 3).

The reduction in the traits associated with photosynthesis caused by the N limitation in the soil was more expressive in the hybrids than in the lines. However, the hybrids presented higher values for plant height, stem diameter, and, mainly, leaf area in this N limitation condition (Table 2). The larger leaf area is essential to increase the photosynthetically active radiation (PAR) interception area and, therefore, to increase CO_2 assimilation – under the condition of adequate stomatal conductance values – and transpiration in the plant (Mu and Chen, 2021). Although under soil N limiting conditions, the hybrids reduced the estimates of A, gs, E, and chlorophyll contents by -1.4, -4.3, -9.7, and -10.5%, respectively, these decreases were not enough to cause reductions in the growth variables (Table 3). On the contrary, in the N-limiting condition, the hybrids increased the estimates related to the growth traits (Table 2). In this way, the hybrids produced a greater amount of plant dry matter with a smaller amount of assimilated CO_2 (lines ≅ 7.9 g of shoot dry matter per µmol of CO_2 assimilated; hybrids ≅ 9 g of shoot dry matter per μmol^{-1} CO_2 assimilated), if we could consider a hypothetic scenario where the responses found on the V6 leaf could be extrapolated to the photosynthesis of the whole plant.

In the condition of reduced CO_2 assimilation, the excitation energy surplus due to the decrease in ATP and NADPH consumption promotes an increase in the susceptibility of PSII to the action of photons on this photosystem (photoinhibition) (Ramalho et al., 1997; Grassi et al., 2001; Lu et al., 2001) and PSII damage can compromise the biomass production of plants. However, this did not happen with the hybrids since, in the condition of N limitation in the soil, the F_v/F_m ratio values expressed an increase of 10% concerning the lines. This tolerance of the hybrids may be associated with the reduction in the concentration of chlorophylls in the leaves. The reduction in the relative chlorophyll content in the hybrids was higher than in the lines, with an estimate of 25.6%, when compared to the value of 18.8% in the lines. According to Khamis et al. (1990) and Lu et al. (2001), reducing the relative chlorophyll content may be a strategy to protect the PSII function since it

can avoid the excessive production of excitation energy, which could cause damage to the PSII.

The F_v/F_m ratio, which makes it possible to verify whether there was damage to the photosynthetic apparatus, is a variable that represents the maximum photochemical efficiency of PSII in a condition in which all reaction centers are open and receive a pulse of light saturating. Under stress conditions, such as the reduction of N availability in the plant, there may be a decline in the values of this trait, which indicates possible damage to the photochemical machinery (Lin et al., 2022; Mattila et al., 2022). Therefore, genotypes that present tolerance mechanisms to protect the PSII may show insignificant reductions or even higher values for this measure, even in stressful situations (White et al., 2011; Ramanna et al., 2014; Farooq et al., 2022). As observed in the hybrids under N-limited conditions, it can be suggested that the regulatory mechanisms associated with the reduction in the total chlorophyll content favored the elevation of the F_v/F_m ratio in the hybrids. Based on the results, it can be inferred that the hybrids were more efficient in the assimilation of CO_2 per unit of chlorophyll molecules (Table 3) than the lines, which reflected in the greater capacity to allocate the photoassimilates produced in the production of matter drought, generating positive impacts on the total dry matter of the plant (Table 2).

Among the genotypes evaluated, the hybrids showed essential increases in the relative content of flavonoids (Flav), which are phenolic compounds associated with the adaptive responses of plants to various abiotic stresses, such as drought (Li et al., 2021), the reduced availability of nutrients in the soil, and the excess of solar radiation (Agati et al., 2013; Nascimento and Tattini, 2022). These compounds act mainly as accessory pigments of chlorophyll molecules, protecting against reactive oxygen species (ROS), which can have high rates in plants under suboptimal N conditions. ROS can degrade plant cells through the oxidation of membranes (Chen et al., 2019) and the degradation of molecules, such as DNA (Tripathi et al., 2020). The production of these ROS is mainly associated with the reduction of stomatal conductance, which is regulated by the action of ABA through stress signaling from the roots (Kumari et al., 2022). Therefore, in the hybrids, when compared to the lines, the notable increase in secondary metabolites such as flavonoids (Flav) and anthocyanins (Anth) could potentially provide an adaptive

advantage over the parent plants. This increase in secondary metabolites might have contributed to an improved physiological and agronomic performance.

3.1.5.2 The mechanisms underlying the efficient use of N in popcorn genotypes

Efficiency in the use of N and associated components (efficiency in uptake and utilization) was proposed by Moll et al. (1982). These authors defined that N use efficiency (NUE) as the ratio between the grain weight and the available N in the soil or the product of the N uptake efficiency (NUpE: the ratio between the total N in the plant and the available N in the soil) and the N utilization efficiency (NUtE: the ratio between the weight of grains and the total N in the plant). Subsequently, Good et al. (2004) proposed that NUE is the ratio between dry shoot matter and applied N. NUpE is the ratio between the N content in the plant and the amount of N applied to the rhizosphere, and NUtE is the ratio between the shoot dry matter and the N content in the plant. However, when assessing the efficiency in the uptake and utilization of N, it remains uncertain whether the N content of roots should be included since some authors only use the N content in the shoot (Rodrigues et al., 2017; Menz et al., 2018) and others consider the N content of the plant, including the N content of the roots (Moll et al., 1982; Mundim et al., 2014; Almeida et al., 2018b; Khan et al., 2020b).

Given the significant differences between the genotypes for NUE and the components associated with this variable (with and without the assessment of N content in the root), under high and low N conditions, it can be noted that when considering the N content in the roots, it is possible to obtain more reliable estimates of N uptake and utilization since up to the V6 stage, the N content in the root has a crucial role for the growth of the plants.

Regarding the effect of N reduction, a significant increase in NUE was observed in popcorn genotypes under N-limiting conditions. This increase can also be observed for NUpE_cR and NUpE_sR. For NUtE_cR, NUtE_sR, and NTrE, reductions were observed when the soil had limited nitrogen. In this condition, corn shows an increase in N use efficiency (NUE), either through increased uptake (NUpE) or N utilization (NUtE) (Hirel et al., 2007; Mu et al., 2016). As N is quite mobile and found in deeper soil profiles (Weitzman et al., 2022), the increase in nitrogen uptake may be associated with an increase in area and a deepening of the root system (Lynch, 2013). NUtE can be defined as the amount of dry matter

produced per unit of N in the plant; the increase in the value of this variable is an indicator of how efficiently the plant can use the available N in the photosynthetic machinery (Hammad et al., 2022).

With the N limitation in the soil, the lines had more significant reductions in NUE, while the hybrids stood out with higher values for this trait. However, in this study, the most important mechanism to increase the NUE of the hybrids was the use and transport of the nutrient since the hybrids presented more expressive values compared to the lines. This becomes clear when the N contents in different plant tissues are compared in the limiting N condition. In this condition, the hybrids presented higher N content in the leaves, while the lines concentrated most N in the stem and root (Table 2). Therefore, even with a higher net photosynthetic rate and higher relative chlorophyll content, the lines were not efficient in using N to increase their leaf area and dry matter; however, they were more efficient in the acquisition of the nutrient, considering that in the condition limiting the values for N content in the plant and NUpE were higher in the lines.

3.5.1.3 What is the best strategy for conducting popcorn breeding to increase the nitrogen use efficiency?

In general, the N limitation in the soil caused greater discrimination between the genotypes studied and resulted in higher heterosis estimates in this environment. This is associated with the fact that in this condition, the genotypes have greater differentiation for the traits studied, which is already reported by other studies with common corn (Worku et al., 2007; Granato et al., 2016) and popcorn (Khan et al., 2020b). Therefore, the selection of genotypes in this condition may be more effective in obtaining a high genetic variance. Furthermore, based on the estimates of the mean squares and the quadratic components associated with the general and specific abilities of combination and the reciprocal effect, it was evidenced that there is no difference between the environments regarding the quadratic component that most contributed to the genetic variance of the studied traits. The genetic mode of action is the same for both conditions – high and low N, which may allow the use of the same breeding strategies in both conditions.

For the traits associated with growth – plant height, dry matter of leaf, stem, shoot, and root - in the two N conditions, the contribution of the quadratic component associated with non-additive genetic effects (ϕ_S) predominated. This fact indicates that the exploitation of heterosis is recommended to achieve genetic gains (Hallauer et al., 2010; Cruz et al., 2014). Although ϕ_S was essential for most traits, some

showed a greater predominance of the quadratic component associated with reciprocal effects, as is the case of stem diameter in high N and leaf area in both N conditions. In addition, the genetic effects associated with the reciprocal effect prevailed for the N contents in the leaf, stem, root, shoot, and mining plant. The same could not be observed in low N conditions, prevailing for these traits – except N content in the shoots – the genetic effects associated with ϕ_s. However, even with the predominance of genetic effects associated with ϕs, the other components also showed significance, indicating that there is, even to a lesser degree, the influence of additive genetic effects (ϕ_g) and the female parent (ϕ_{rc}). This fact indicates that, based on the selection of genotypes for NUE, the female parent should be the one with the best values for the evaluated trait. This can be explained by the fact that the mechanisms underlying better performance for NUE, such as the photosynthetic response and the content of leaf pigments, are determined by the female parent through chloroplasts located in the cytoplasm of the female gamete (Wang et al., 2019).

For the variables evaluated for the general and specific combining ability, as well as for the reciprocal effect on the two levels of N used, the significance of the interactions allows us to confirm that the alleles that control the expression of traits under low nutrient supply are partially different from those that control the same traits under optimal nutrient supply (Santos et al., 2019). This implies that the performance of genotypes under low N conditions availability involves genes expressed under optimal N availability and that other genes are expressed or silenced (Liu et al., 2012).

3.1.6 CONCLUSION

In popcorn, in the vegetative stage, the effects of heterosis related to plant biomass resulted in higher production of shoot dry matter. Regarding the parents, the better performance of the hybrids was even more evident in conditions of low N availability in the soil, in which it is established that the adaptation of *Zea mays everta* to environments with N deficiency requires the exploitation of hybrid vigor.

In the hybrids, under limiting conditions of N in the soil, contrary to what was expected, there was a greater reduction in leaf gas exchange, which was not

enough to reduce the growth of these genotypes, guaranteeing higher estimates for NUE, promoted by better use of nitrogen available.

It is suggested that under limiting N condition, the adaptive mechanisms developed by the hybrids were the reduction of the total chlorophyll content and the increase in the levels of accessory pigments – anthocyanins and flavonoids – which could improve the protection of the photosynthetic apparatus and higher maximum photochemical efficiency of the PSII.

Future perspectives based on the results found point in two directions: i) conducting comparative proteomics and mRNA-sequencing studies to comprehend the molecular mechanisms underlying the NUE response in the most contrasting inbred lines; and ii) examining the evaluated genotypes (lines and hybrids) under field conditions throughout the crop development cycle to gain insights into the impacts of N starvation on traits such as grain yield and popping expansion.

3.2 PROTEOMIC CHANGES IN BIOENERGETIC METABOLISM AND ANTIOXIDANT SYSTEM ENHANCE NITROGEN USE EFFICIENCY IN POPCORN LINES UNDER NITROGEN STARVATION

3.2.1 INTRODUCTION

Given the global population is projected to reach 10 billion inhabitants by 2050, the development of a sustainable agricultural model is of a paramount importance (Long et al., 2015). Considering that nitrogen (N) is one of the minerals required in larger quantities in agriculture and directly impacts the yield of several crops, such as maize, there is an urgent need to act through innovative plant breeding strategies to develop cultivars that require reduced application of nitrogen fertilizers.

Since 1960, global application of nitrogen fertilizers has increased approximately ten-fold (from 11 million tons in 1961 to 113 millon tons in 2020) (FAO, 2023), and it is expected to increase by 40 to 60% in the next 40 years. Maize cultivation consumes about 20% of all N produced in the world, and according to data from the Assessment of Fertilizer Use by Crop at the Global Level (Heffer et al., 2017), the United States, China, and Brazil – the three largest producers of maize – accounted for approximately 39.8% of worldwide nitrogen consumption (globally 102.5 metric tons), with maize cultivation being nitrogen consumer.

Despite nitrogen being essential for plant growth and development, and its application as a fertilizer leading to a significant increase in global food production

since 1990 (Mu & Chen, 2021), its excessive use can cause several environmental impacts such as global warming, and air and water pollution (Li et al., 2018b). Furthermore, it is estimated that between 50 and 70% of the nitrogen utilized in agriculture is used by plants, with the remaining being lost, most commonly as ammonia or nitrous oxide through leaching, soil denitrification, surface runoff, and volatilization (Raun e Johnson, 1999; Khan et al., 2022).

In this regard, the development of crops with enhanced nitrogen use efficiency (NUE) is one of the most economically and environmentally viable initiatives to meet global food demand and contribute to the development of a sustainable agricultural model. However, improving NUE remains a complex task. While NUE has been extensively studied in maize, little is known about the underlying molecular mechanisms of plant responses under nitrogen deprivation conditions. This information is crucial not only for improving plant yields under conditions of inadequate nitrogen supply but also for the development of potential molecular tools for selecting nitrogen-efficient genotypes.

NUE is a complex trait that consists of two main components: N-uptake efficiency (NUpE) and N-utilization efficiency (NUtE), which both involve several biological processes. To elucidate these mechanisms in corn, previous studies have used proteomic approaches to understand the efficient response of genotypes under limited N conditions (Liao et al., 2012; Prinsi & Espen, 2018; Wei et al., 2015). However, there is currently a scarcity of research focused on unraveling the molecular mechanisms involved in the expression of an efficient response to low N in popcorn – a highly valued crop that was responsible for circulating US$10 billion worldwide in 2020 (Serna-Saldivar, 2022) – under N deprivation conditions. For our knowledge, only one study, conducted by Khan et al. (2022), has aimed to elucidate the proteomic profiles exhibited by contrasting popcorn lines under different N availability conditions. Furthermore, the physiological and molecular mechanisms associated with NUE in popcorn still lack comprehensive studies.

With this context, the development of the study herein was deemed necessary, where we evaluated plant growth, physiological traits, and proteomic profiles of leaves from two contrasting NUE lines cultivated under high and low N conditions. Our main objective was to study the physiological mechanisms and identify key proteins that contribute to the expression of N use efficiency in popcorn. These results provide new insight into the mechanisms involved in NUE and can be

harnessed to develop novel breeding strategies aimed at developing popcorn cultivars with enhanced NUE, ultimately promoting sustainable agriculture, reducing adverse environmental impacts, and support to the growing global demand for food.

3.2.2 LITERATURE REVIEW

3.2.2.1 The molecular mechanisms involved in nitrogen-use efficiency in maize

Below we highlight other important mechanisms for the tolerance response and efficiency of plants in using available nitrogen in environments with nutrient limitation – such as those related to the acquisition, transport and remobilization of N.

Nitrogen is a nutrient that has great mobility in plants, so its metabolism involves several processes, including absorption, reduction, assimilation, translocation and remobilization. The genetic differences between nitrogen uptake or productivity per unit of nitrogen applied to the soil have been studied for several grasses, especially those of commercial importance, such as wheat, rice, oats and, mainly, maize. The latter, in general, is one of the most produced cereals worldwide and one that most requires nitrogen fertilizers to increase productivity (Bi et al., 2014). However, little is known about the regulation of nitrate assimilation at the molecular and genetic levels in this crop (Cao et al., 2017). In this perspective, each process involved in the use of nitrogen has been widely explored, in order to elucidate the routes by which efficient plants in the use of N can avoid the effects of the lack of this nutrient in the soil. Below, each of these steps involved in the use of nitrogen is highlighted, including the molecular mechanisms described in the literature and how they influence plants in the efficient use of N.

Nitrogen uptake and transport

Nitrogen is a limiting macronutrient for plant growth and development (Kang and Turano, 2003; Raddatz et al., 2020). Soil nitrogen availability is normally low

and can be influenced by factors such as precipitation, temperature, pH and soil type. The form of nitrogen preferred by plants is intrinsically related to their adaptation and soil conditions (Zuluaga and Sonnante, 2019). Plants can use both nitrate (NO_3^-) and ammonium (NH_4^+) as sources of N (Andrews & Lea, 2013; Simons et al., 2014; Plett et al., 2018). NO_3^- is the main and most readily available source of nitrogen for most higher plants (Engineer and Kranz, 2007; Ma et al., 2020), however, NO_3^- concentrations in soils can be very varied, depending on environmental variations and, therefore, plants have developed several specific adaptations for the uptake of available NO_3^- (Vidal et al., 2013; Zuluaga and Sonnante, 2019).

Nitrate is actively transported into cells, mainly by the NO_3^- transcarriers of the *NRT* family, which depend on the energy supply and electrochemical gradient and are divided into two systems existing in the cell membranes of the roots (Fan et al., 2017; Vidal et al., 2013; Wang et al., 2020; Yang et al., 2019). One of them is the high affinity transport system (HATS), which is activated when there is a high concentration of nitrate available to the plant. The other, the low affinity transport system (LATS), is activated under conditions of low nitrate concentration (Fan et al., 2017; Zuluaga and Sonnante, 2019; Dechorgnat et al., 2019; Raddatz et al., 2020).

NRT transporters belong to three main families: the first, NRT1 – or NPF – contains many genes, which can be divided into 8 to 10 subfamilies in Arabidopsis, which are predominantly low-affinity transporters (Fan et al., 2017; Ohkubo et al., 2021; Raddatz et al., 2020; Wang et al., 2020). The other families – *NRT2/NRT3* (*NAR2*) – play an important role in the high-affinity transport of NO_3^- (Zuluaga & Sonnante, 2019; Wang et al., 2020). As in Arabidopsis, *NRTs* have been identified in rice, sorghum and maize and show differences in gene numbers and family structure. Studies show that in the corn genome there are four copies of genes of the *ZmNRT2* family, namely: *ZmNRT2.1*, *ZmNRT2.2*, *ZmNRT2.3* and *ZmNRT2.5*, of which only two were studied: *ZmNRT2.1* and *ZmNRT2.2*, that have about 98% homology in their amino acid sequence (Dechorgnat et al., 2019). Both are inducible to NO_3^- in seedling roots, having been found transcripts of the former in the region of the root cortex while, for the latter, in the cortex, stele and lateral primordia of the roots (Trevisan et al., 2008).

For the NRT3 family, two copies of the NRT3.1 gene were described in the maize genome*: ZmNRT3.1A* and *ZmNRT3.1B*, both never characterized in maize,

but which are strong candidates in the NO_3^- transport complex (Goel et al., 2018; Sinha et al., 2018; Zuluaga & Sonnante, 2019) More recently, Wang et al. (Wang et al., 2022), after analyzing the proteome of two contrasting hybrids for NUE, verified the function of the *ZmTGA* gene and the study found that the gene has an important role in maintaining the tolerance of plants in low conditions. N, giving greater length and area of the root system, greater shoot/root ratio, in addition to lower leaf senescence compared when comparing the mutant with the wild type. *TGA* transcription factors are a very important group of the bZIP (basic leucine zipper) family (Jakoby et al., 2002) and can bind to the -1 (as-1) activation sequence with TGACG as the core and activate or inhibit the translation of downstream target genes, having, therefore, an important role in the defense and response of plants to various biotic and abiotic stresses, such as low nitrogen availability. Furthermore, studies show that plants with overexpression of the *TGA1* or *TGA4* genes show a significant increase in the nitrate transporter genes *NRT2.1* and *NRT2.2* (Alvarez et al., 2014; Zhong et al., 2015), whose functions we discussed earlier.

Ammonium is also a direct source of nitrogen taken up by plant roots, but, in general, the ammonium content in unfertilized soils is up to 1,000 times lower than that of nitrate. (Marschner, 2012). However, efficient ammonium uptake is critical for optimal plant growth and development, as it confers several beneficial effects, such as root density and corn seedling length (Taylor & Bloom, 1998; Bloom et al., 2002) or enhanced H+ proton extrusion, which subsequently acidifies the rhizosphere and leads to increased bioavailability of poorly soluble nutrients such as P or Fe (Gu et al., 2013). Therefore, this NH_4^- absorption process is expected to be highly regulated under adverse conditions of N availability in the soil.

Whenever the ammonium concentration in the soil solution is low, the contribution of high-affinity transport systems (HATSs) becomes more relevant to the overall ammonium uptake by roots (Gu et al., 2013). In general, high-affinity ammonium transport is mediated by AMT1-type ammonium transporters: *ZmAMT1*; *1a* and *ZmAMT1*;*3*, which belong to the ammonium/methylammonium permease/rhesus transporters (AMT/MEP/Rh) (Gu et al., 2013; Zhao et al., 2018).

The two *ZmAMT*s confer high-affinity ammonium transport activities and are localized in the plasma membrane of maize root epidermal cells. Furthermore, their gene expressions are induced by ammonium, and one study revealed high correlations with high-affinity ammonium and increased root influx rates (Gu et al., 2013). Although *ZmAMT1*; *1a* e *ZmAMT1*; *3* are likely to be the main components for ammonium uptake in the root, not much is known about their physiological contribution to N uptake and use efficiency (Zhao et al., 2018).

Nitrogen reduction and assimilation

Once incorporated, nitrate is reduced to nitrite in plant cells in a reaction that takes place in the cytosol and is catalyzed by a nitrate reductase (NR) (Wang et al., 2018; Meyer and Stitt, 2001). The nitrite is then translocated to plastids and chloroplasts, where it is reduced to ammonium by the enzyme nitrite reductase (NiR). Nitrate-derived ammonium, or that produced by photorespiration or amino acid recycling, is more assimilated in plastids by the GS/GOGAT cycle (Masclaux-Daubresse et al., 2010; Asibi et al., 2019).

Ammonium is attached to glutamate to form glutamine by glutamine synthase (GS; family of *Gln* genes), of which there is a plastid isoform (GS2) and a cytosolic isoform (GS1). In maize, a single gene encodes GS2 (*Gln2*), while at least 5 genes encode GS1 (*Gln1-1* to *Gln1-5*), which are differentially expressed during development (Sakakibara et al., 1992; Martin et al., 2006; Liseron-Monfils et al., 2013; Vidal et al., 2013).

Glutamate can serve as an amino acid donor to other amino acids and nitrogen-requiring compounds, or act as an amine acceptor in the GS-GOGAT cycle to regenerate glutamine. Plants have two types of GOGAT enzymes – NADH-GOGAT and Fd-GOGAT – which use NADH and ferredoxin as electron donors, respectively (Suzuki and Knaff, 2005). Different parallels of GOGAT show constitutive or tissue-specific activity in plants, including maize (Sakakibara et al., 1992). Ferridoxine-GOGAT is localized in leaf chloroplasts, while NADH-GOGAT is expressed in non-photosynthetic tissues, including root plastids (Masclaux-Daubresse et al., 2010). After nitrogen assimilation, glutamine, glutamate, and other amino acids, including asparagine and aspartate, are transported by vascular tissues to growing organs (Masclaux-Daubresse et al., 2010). Nitrate and ammonium can also be stored in vacuoles before or after long-distance transport.

Nitrogen translocation and remobilization

During senescence, leaf proteins and photosynthetic proteins are extensively degraded, becoming a huge source of nitrogen, which plants can exploit to supplement the nutrition of growing organs (Masclaux-Daubresse et al., 2010).

During the grain filling period, the absorption and assimilation of nitrogen are often insufficient for the high demand required at this stage, making re-mobilization in the different organs of the plant necessary to direct nitrogen to the seeds (Asibi et al., 2019). The contribution of this process to supplying N in cereals such as rice,

wheat and corn varies according to the cultivar, at rates of 50 to 90% (Masclaux-Daubresse et al., 2010). N remobilization also depends on the environment and is favored under conditions of nitrate limitation (Lemaitre et al., 2008).

In this sense, glutamine (Gln) is the main amino acid translocated in cereals as a source of N. Therefore, in senescence, glutamine concentrations increase in the phloem sap, being remobilized to the reproductive organs. In this process, GS and GOGAT enzymes are important for the remobilization and reuse of N in senescent and developing organs, respectively (Tabuchi et al., 2007; Wang et al., 2020). Some studies have shown that GS1-1 is responsible for this process and that NADH-GOGAT1 plays a key role in the reuse of Gln transported in the developing organs of rice (Uauy et al., 2006; Tabuchi et al., 2007). In maize, wheat, and barley, grain N content is correlated with senescence of flag leaves and appears to play a significant role in N availability for grain filling (Martin et al., 2006; Uauy et al., 2006; Zuluaga & Sonnante, 2019).

3.2.3 MATERIAL AND METHODS

3.2.3.1 Plant material

Two popcorn S_7 inbred lines contrasting for NUE, P2 e L80, developed by the Popcorn Breeding Program of Universidade Estadual do Norte Fluminense Darcy Ribeiro (UENF, Campos dos Goytacazes, RJ, Brazil), were used in this work. These inbred lines were developed after seven cycles of self-pollination and belong to the Germplasm Bank of UENF. P2 is classified as early, temperate/tropical and was derived from Composto CMS-42 (open pollinated variety, OPV), while L80 is classified as late, temperate/tropical and derived from the OPV Viçosa: UFV. Subsequently, these lines were evaluated for NUE by Santos et al. (2017) and (Santos et al., 2019) under field conditions and, later, by Santos et al. (2023) under controlled conditions with contrasting N availability conditions (100% of the N required by corn and 10% of the N needed, *i.e.*, 224.09 mg NO_3^- L^{-1} and 22.41 mg NO_3^- L^{-1}). Based on these previous works, the line P2 was selected as N-efficient and N-responsive and the line L80 classified as N-inefficient and non-responsive to N.

3.2.3.2 Growing conditions and experimental design

The experiment was carried out in the greenhouse (40% of light interception) at UENF from April 29th to June 17th, 2022 (49 days, 21° 9′ 23″ S; 41° 10′ 40″ W; altitude: 14 m; temperature: 25–38 °C; relative air humidity: 70–76%). The nutritive solution for the N source was prepared according to Hoagland and Arnon (1950), with modifications. Two contrasting N doses were used: N100% (224.09 mg NO_3^- L^{-1}) and N10% (22.41 mg NO_3^- L^{-1}), as described in previous work (Khan et al., 2020b, 2022; Santos et al., 2023).

Seeds were grown in plastic pots (35 L) containing sand washed with deionized water. The plants were irrigated daily with deionized water, and nutrients were provided at the V2 stage (7 days after sowing) every day. A randomized complete block design was used with two factorial treatment arrangements (2 genotypes × 2 N levels) with seven blocks, one pot per plot and one plant per pot. Seven blocks were used to evaluate morphological and physiological traits. Out of seven, three blocks were used to obtain the leaf samples to proteomics analysis – each of them considered one biological replicate.

3.2.3.3 Evaluated traits

Plant growth and development

At six fully developed leaves stage (V6) plants were evaluated regarding plant height (PH – cm), leaf area (LA – cm^2, as described by Guimarães et al., 2002), stem diameter (SD – mm), shoot dry weight (SDW – g), root dry weight (RDW – g) and relative water content (RWC – %). To obtain RWC, five discs were collected from the sixth fully developed leaf, weighted to obtain the fresh disc weight (FDW – g) and then soaked in distilled water in 4 ºC for 24h to obtain the turgid disc weight (TDW – g). Finally, the discs were dried at 65 ºC for 72h in an oven to assess the disc dry weight (DDW – g). The RWC was obtained as follows: $\mathrm{RWC} = (\mathrm{FDW} - \mathrm{DDW}/\mathrm{TDW} - \mathrm{DDW}) \times 100.$

Physiological traits

The measurements of total chlorophyll, flavonoids and anthocyanins indexes were evaluated on the middle of the sixth fully expanded leaf (V6) one day prior to

the end of the experiment (30 days after sowing). A portable leaf pigments meter Dualex® (FORCE-A, Orsay, France) was used to measure the indexes.

To obtain the chlorophyll fluorescence parameters, one leaf disk (10 cm^2) was collected from each plant in the middle of V6 leaf. Each leaf was previously adapted in the dark for 30 minutes, to ensure the complete oxidation of the photosystem II (PSII) reaction centers. The discs were placed inside a chlorophyll fluorescence imaging system (CFIS) model FluorCam 800MF (Photon System Instruments, Drásov, Czech Republic) previously configured with the protocol "Light Curve 2", which relates the photochemical efficiency in response to photosynthetic photon flux densities (PFFD) incident on the leaf (Serôdio et al., 2007). Then, fluorescence levels F_o and F_m were determined. Samples were then exposed to 6 increasing irradiance levels, from 145 to 1057 µmol m^{-2} s^{-1}.

This protocol allows obtaining curves of rapid response to light, from a few adjustments to the proper fluorescence measurement procedure. Thus, the measurement flash was defined, which is used to determine the minimum fluorescence (F_0) of the dark-adapted leaf disc, without it inducing the photochemical reaction. The saturation flash (4,000 µmol m^{-2} s^{-1}) was defined, which pulse intensity is related to the ability to completely reduce all open PSII reaction centers, enabling the determination of maximum fluorescence (F_m) leaf discs adapted to dark and light (F_m'). After measuring the variables related to dark adaptation (F_0 and F_m), increasing amounts of actinic radiation (interspersed by measurement flashes and saturation flashes) were applied to determine the basic variables (F_0', F_m', $F_{t'}$ and F_q). Based on the dark and light adaptation variables, for each actinic light intensity, the other variables related to fluorescence emission were determined: effective quantum yield of PSII (ϕPSII), photochemical quenching (qP) and non-photochemical quenching (NPQ), according to the equations 1, 2 and 3, respectively.

$$\phi\mathrm{PSII} = (F_m - F_t') / F_m' \quad \text{Eqn. 1}$$

$$\mathrm{qP} = (F_m' - F_s) / F_m' \quad \text{Eqn. 2}$$

$$\mathrm{NPQ} = (F_m - F_m') / F_m' \quad \text{Eqn. 3}$$

To assess the photosynthetic O_2 evolution (potential photosynthesis, A_{pot} – µmol O_2 m^{-2} s^{-1}), a leaf disc (10 cm^2) was used for each replicate (n = 3). Each disc was placed inside a Clark type oxygen electrode (LD2/2; Hansatech, Pentney, King's Lynn, UK), under CO_2 saturation conditions (1%, supplied by 500 µL 1M $NaHCO_3$), constant temperature (35 ºC) and variation in PPFD supplied by a

Bjorkman type lamp (Han- satech) and filters coupled to a light source (Rodrigues et al., 2018). The A_{pot} was determined under 10 decreasing PPFDs: 1720, 1400, 1010, 749, 458, 233, 179, 139, 96 and 0 µmol m^{-2} s^{-1}. Each point in the O_2 light curve was obtained after a 3 min exposure to the respective PPFD, totaling 30 min for each leaf disc. To obtain the parameters associated to A_{pot} kinetics such as A_{max} (maximum value of O_2 release during the light response curve) and K_A (light intensity in which A_{pot} reaches 63.2% of the maximum values) the hyperbola equation was fitted on Prism GraphPad. Goodness of the fit (R^2) was used to define the discrepancy between measured values and the values expected under the hyperbola equation fits.

3.2.3.4 Leaf proteomics

Protein extraction

Total protein extraction was performed according to Damerval et al. (1986), with modifications. The leaf from each treatment was sampled at V6 stage. Samples (300 mg of fresh material each, three biological replicates per treatment) were first macerated to a fine powder with liquid nitrogen, resuspended in 1 mL of extraction buffer containing 10% (w/v) trichloroacetic acid (TCA; Sigma-Aldrich, St. Louis, MO, USA) in acetone (Merck, Darmstadt, Germany) with 20 mM dithiothreitol (DTT; GE Healthcare, Piscataway, NJ, USA), vortexed for 5 min at 4 °C, kept at -20 °C for 1 h, and then centrifuged at 16,000g for 30 min at 4 °C. The resulting pellets were washed three times with cold acetone containing 20 mM DTT and subsequently air dried. The pellets were resuspended in buffer containing 7 M urea (GE Healthcare), 2 M thiourea (GE Healthcare), 1% DTT, 1 mM phenylmethylsulfonide (PMSF; Sigma-Aldrich), and 2% Triton X-100 (Sigma-Aldrich), vortexed for 30 min, and then centrifuged at 16,000g for 20 min at 4 °C. The supernatants were collected, and the protein concentrations were determined using a 2D-Quant Kit (Cytiva, Marlborough, MA, USA).

Protein digestion

The proteins samples were precipitated using a methanol/chloroform extraction method to remove any interfering compounds from the samples (Nanjo et al., 2012). The samples were then resuspended in a solution consisting of 7 M urea and 2 M thiourea after which tryptic protein digestion (1:100 enzyme: protein,

V5111, Promega, Madison, WI, USA) was performed using Microcon-30 kDa filter units (Merck Millipore, Burlington, MA, USA) with the filter-aided sample preparation (FASP) methodology (Reis et al., 2021). The resulting peptides were quantified with the A205nm protein and peptide method using a NanoDrop 2000c spectrophotometer (Thermo Fisher Scientific, Waltham, MA, USA).

Mass spectrometry and data analysis

The samples were then injected into a nanoAcquity ultra-pure liquid chromatography (UPLC) mass spectrometer connected to a Q-TOF SYNAPT G2-Si instrument (Waters, Manchester, UK). The runs consisted of three biological replicates of 1 µg of peptide samples. The spectra processing and database search were performed using the ProteinLynx Global SERVER (PLGS) software v.3.02 (Waters) and the *Zea mays* protein databank (ID: UP000007305) available on UniProtKB (www.uniprot.org). The label-free quantification analyses were performed using ISOQuant software v.1.7 (Distler et al., 2014). To ensure the quality of the results after data processing, only proteins present in the three runs were accepted for differential abundance analysis.

Proteins were deemed up-accumulated if the log2 value of the foldchange (FC) was > 0.60 and down-accumulated if the log2value of the FC was < 0.60, according to Student's t test (two-tailed, P < 0.05). The functional enrichment analysis was performed using PlantRegMap (Tian et al., 2019; http://plantregmap.gao-lab.org) and KOBAS (Bu et al., 2021; http://kobas.cbi.pku.edu.cn).

3.*2*.3.5 Statistical analysis

For all the morphological and physiological data, at least three biological replicates were accessed. We used Prism GraphPad (https://www.graphpad.com) and RStudio (R Core Team, 2023) to perform statistical analysis and to create the graphs. In all cases, the error bars show SEM, and the letters indicate significant differences (Tukey test, $P < 0.05$).

3.2.4 RESULTS

3.2.4.1 Plant growth, development and physiological responses

The NUE-contrasting inbred lines presented clear phenotypic differences on high and low N conditions (Figure 6).

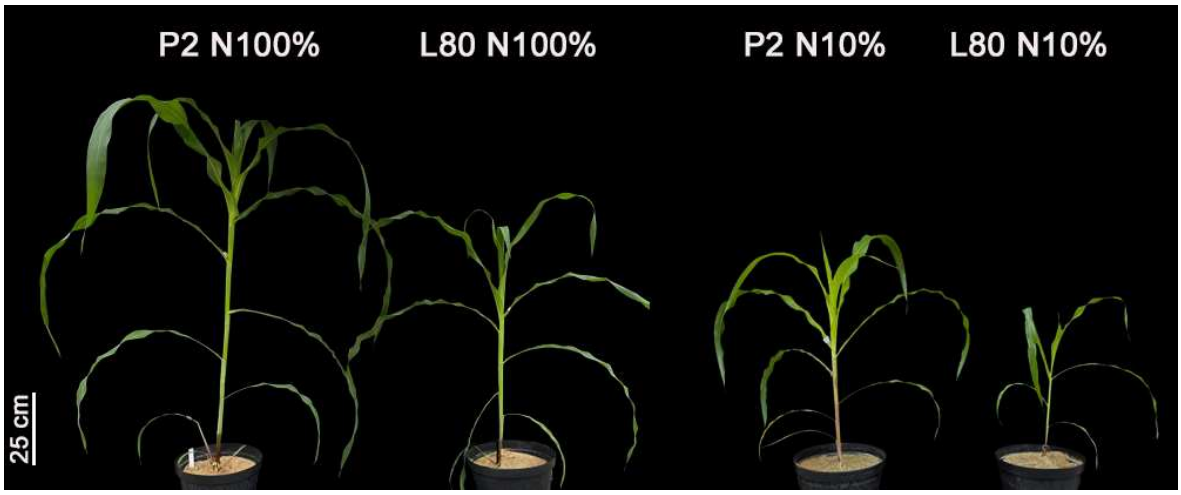

Figure 6. Phenotype of two NUE-contrasting inbred lines (P2: N-efficient; L80: N-inefficient) under high (100% of required N) and low (10% of required N) N conditions.

N limitation in the soil caused significant differences ($P < 0.001$) in the NUE-contrasting inbred lines for growth and development evaluated traits, except for relative water content and root dry weight, the latter tending to decrease when in N-limiting condition (Figure 7).

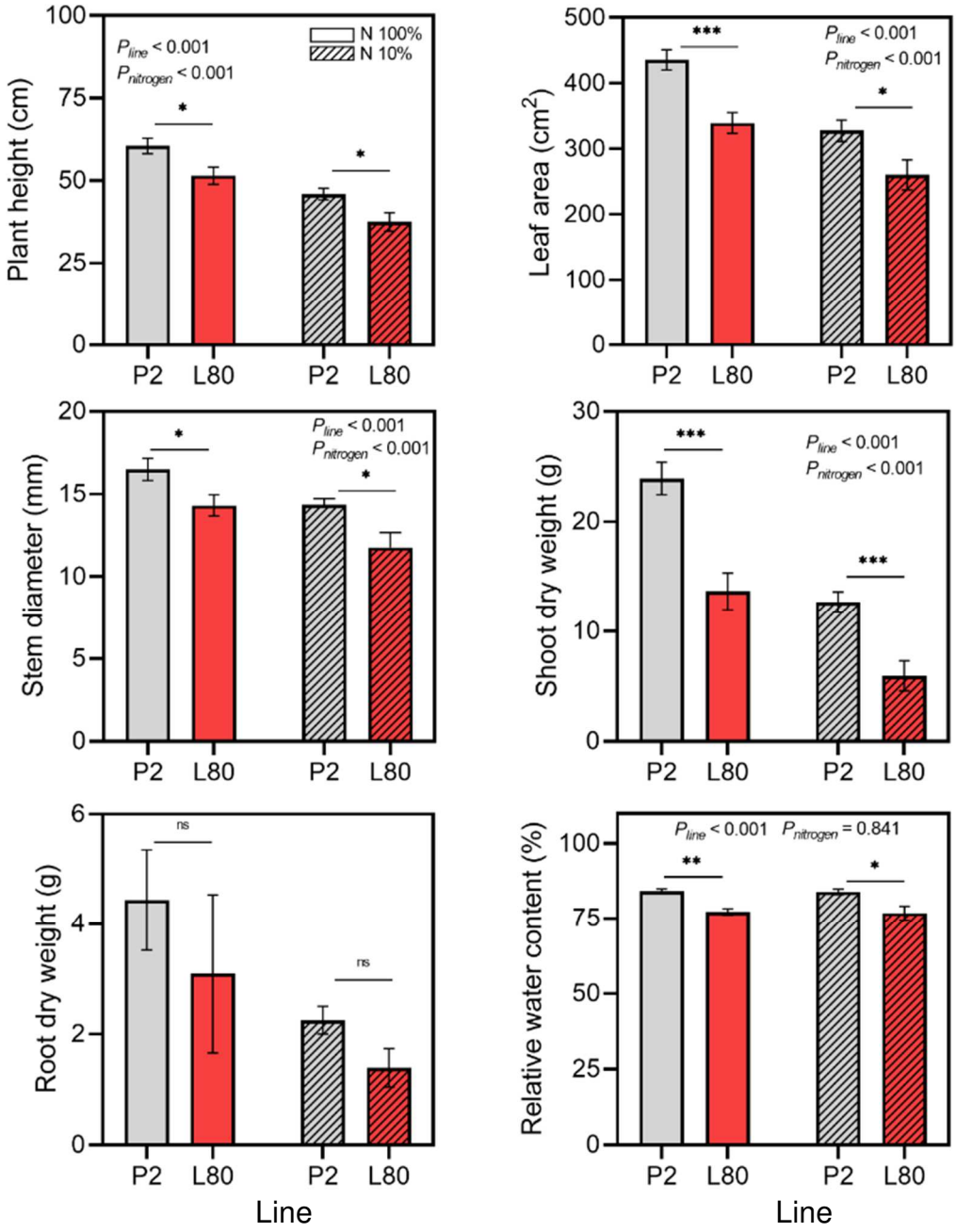

Figure 7 - Growth-related traits measured in popcorn plants grown under high (100% N) and low (10%) nitrogen conditions. Error bars indicate standard error of the mean (n = 7 biological replicates, except for root dry weight and relative water content which n = 3 biological replicates). *, **, *** indicate P-values < 0.05, <0.01 and < 0.001, respectively (Student's t-test).

The N-efficient inbred line P2 showed higher means for all traits in both N conditions compared to the N-inefficient inbred line L80. The reductions caused on P2 due to low N supply in plant height, leaf area, stem diameter and shoot dry matter were 24.2, 24.8, 13.0 and 47.3%, respectively. For L80, losses were more

pronounced for all traits (except for leaf area), in the order of 27.2, 23.4, 56.0 and 17.7%, respectively (Figure 7).

Regarding the O_2 evolution rate (A_{pot}, Figure 8), on the high N condition, both inbred lines showed a similar behavior, mainly at low (below 233 µmol m^{-2} s^{-1}) and saturating (above 1200 µmol m^{-2} s^{-1}) light conditions. According to the hyperbola fitting of A_{pot}, under high N P2 presented 30% less A_{max} than L80 ($P < 0.01$) but with a faster response to light, once it reached 63.2% of the maximum value of the curve (K_A) at 727 PPFD, whereas L80 reached K_A same response at 1360 PPFD (Figure 8a).

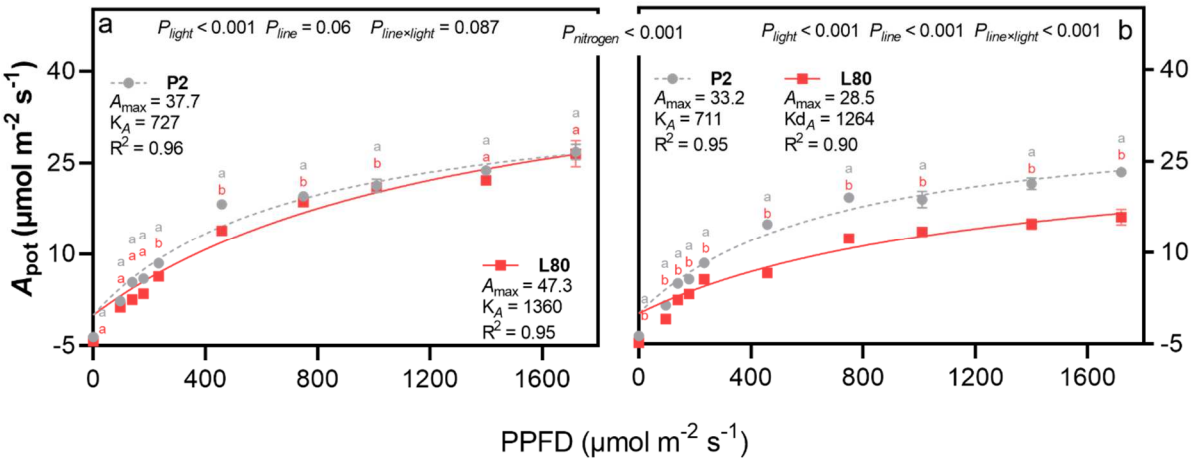

Figure 8 - Light-response curves for net O_2 evolution (µmol m^{-2} s^{-1}) estimated at 35 ºC and ≅ 1% [CO_2], using 10 decreasing photosynthetic photons flux density (PPFD) levels in popcorn plants grown under high (100% N – a) and low (10% N – b) nitrogen conditions. Error bars indicate standard error of the mean (n= 3 biological replicates). Letters above each light point indicate the difference between means by Tukey test (P < 0.05).

However, under low N condition, P2 and L80 showed significant differences ($P < 0.001$) for all points on the light response curve, and even more pronounced under light saturation conditions. This becomes more evident from the light point where the light intensity was higher than the average supply during the growing conditions of the inbred lines (≈ 600 µmol m^{-2} s^{-1}). The N-efficient inbred line P2 showed A_{max} 14.2% higher than the N-inefficient inbred line L80 in addition to a more efficient response to light supply (Figure 8b). The N condition caused significant reductions in the rate of O_2 evolution ($P < 0.001$) in both lines, however this decrease

was more pronounced in L80, with an average reduction of 39.8% in A_{pot} compared to an average reduction of 29.8% in P2.

The limited N supply markedly reduced the chlorophyll content in both lines (Figure 9). Compared with the condition of adequate N supply, the reduction in chlorophyll content under low N was 46.9% for P2 and 33.6% for L80 (Figure 9a). The flavonol content, however, was positively impacted by the stress condition, with increases of 28.6% on P2 and 27.7% on L80 (Figure 4b). The same was observed in the anthocyanin content, with increases of 46.5 and 25% in P2 and L80, respectively (Figure 4c).

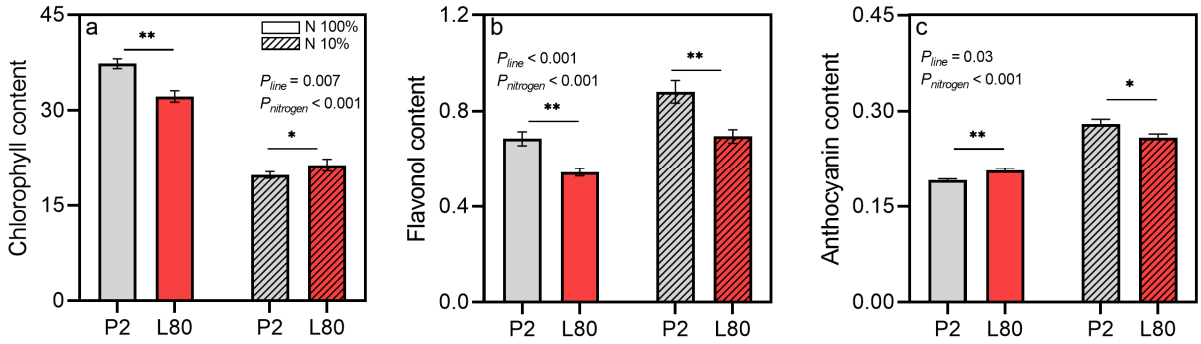

Figure 9 - Leaf pigments measured in popcorn plants grown under high (100% N) and low (10%) nitrogen conditions. Error bars indicate standard error of the mean (n= 7 biological replicates and 5 technical replicates). * and ** indicate P-values < 0.05 and <0.01, respectively (Tukey test).

Regarding chlorophyll fluorescence-related traits, under both nitrogen conditions, the lines showed significant differences in effective quantum yield of photosystem II (ϕPSII), photochemical quenching (qP), and non-photochemical quenching (NPQ). The N-efficient line P2 showed higher values for all three traits under both conditions (P < 0.001, Figure 10). Nitrogen deprivation impacted the performance of all lines for ϕPSII, qP, and NPQ (P < 0.001), with NPQ being the most impacted trait. NPQ increased in both nitrogen-deprived lines, but the largest increase was observed in the N-efficient line P2, with significantly higher averages after 300 PPFD (Figure 10f). Although significant differences between lines were observed for some points on the light response curve for ϕPSII and qP (Figure 10a-d), the difference between P2 and L80 for these variables was not as noticeable as for NPQ.

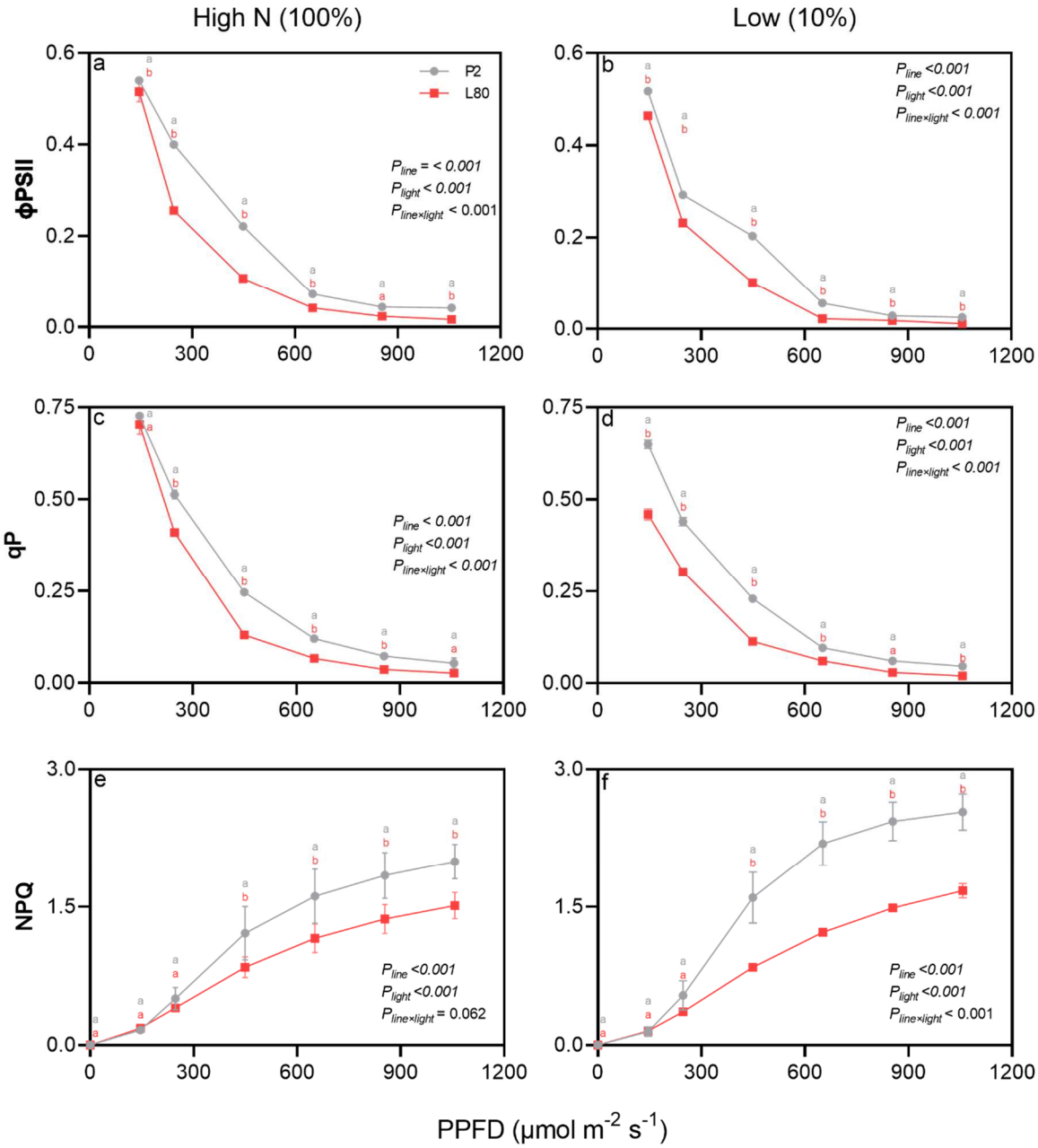

Figure 10 - Light-response curves of effective quantum yield of PSII (ϕPSII – a, b), photochemical quenching (qP – c, d) and non-photochemical quenching (NPQ – e, f) measured in popcorn plants grown under high (100%) and low (10%) nitrogen conditions. Error bars indicate standard error of the mean (n= 3 biological replicates). Letters above each light point indicate the difference between means by Tukey Test (p<0.05).

3.2.4.2 Leaf proteomics

We identified a total of 1276 proteins in maize leaves under high and low N levels (Supplementary Table 5). Among them, 215 different accumulated proteins (DAPs) were observed in P2 inbred line e 168 DAPs were observed in L80 inbred line,

both considering the contrast between low N level and high N level (N10/N100) (Figure 11a, Supplementary Table 5). In P2, 78 DAPs were up-regulated and 119 were down-accumulated, while in L80, 36 DAPs were up-accumulated and 120 were down-accumulated. In P2 inbred line we observed 13 unique proteins in high N level and 5 unique proteins in low N level, while in L80 only 5 and 7 unique proteins were identified in high and low N levels, respectively. In both comparisons we identified 79 shared DAPs between inbred lines (Figure 11b, Supplementary Table 5).

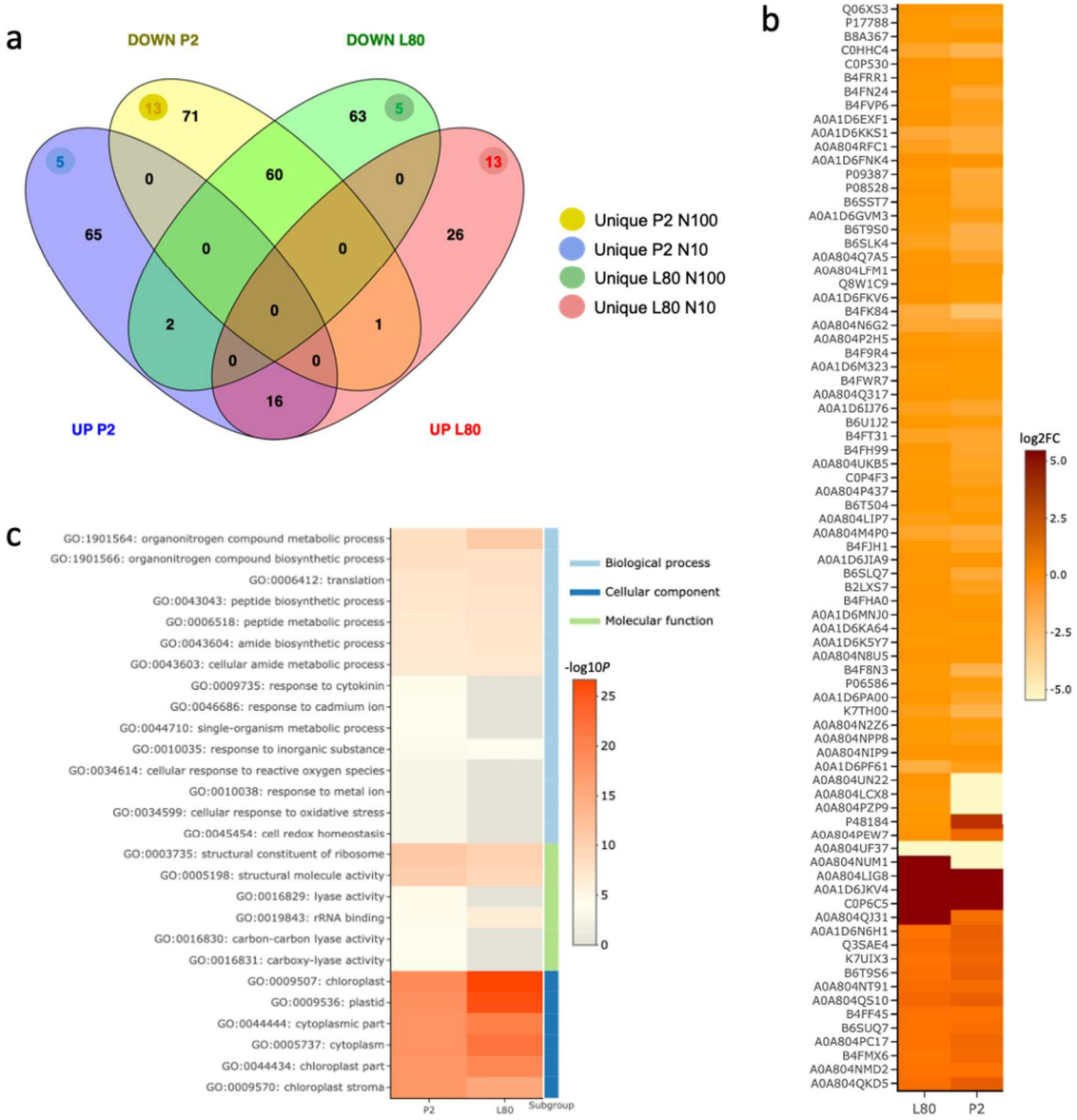

Figure 11 - Leaf proteomic analysis of two popcorn inbred lines grown under contrasting conditions of N in soil (N 100% and N10%). **a** Venn diagram shows the overlap of differentially accumulated proteins. **b** Heatmap of 79 co-regulated proteins between P2 (N-efficient line) and L80 (N-inefficient inbred line). **c** GO enrichment of top 26 GO terms of DAPs using PlantRegMap database with *Zea mays* genome as reference.

The Gene Ontology (GO) enrichment analysis categorized the DAPs into three categories. The most significant terms (P <0.05) were the functional groups o*rganonitrogen compound metabolic process* (GO: 1901564) and *organonitrogen compound biosynthetic process* (GO: 1901566), shared by both lines, *structural constituent of ribosome* (GO : 0003735) and s*tructural molecule activity* (GO: 0005198) in the N-efficient line P2 and *chloroplast* (GO: 0009507), *plastid* (GO: 0009536) in the N-inefficient line L80 (Figure 11c).

We performed the Kyoto Encyclopedia of Genes and Genomes (KEGG) analysis to investigate the biological functions of DAPs. P2 and L80 sequences were mapped in several pathways. A total of 103 sequences were mapped on the P2 line while 118 sequences mapped on L80 (P < 0.05). The most enriched pathway was *metabolic pathways*, followed by *ribosome* and b*iosynthesis of secondary metabolites* (Figure 12).

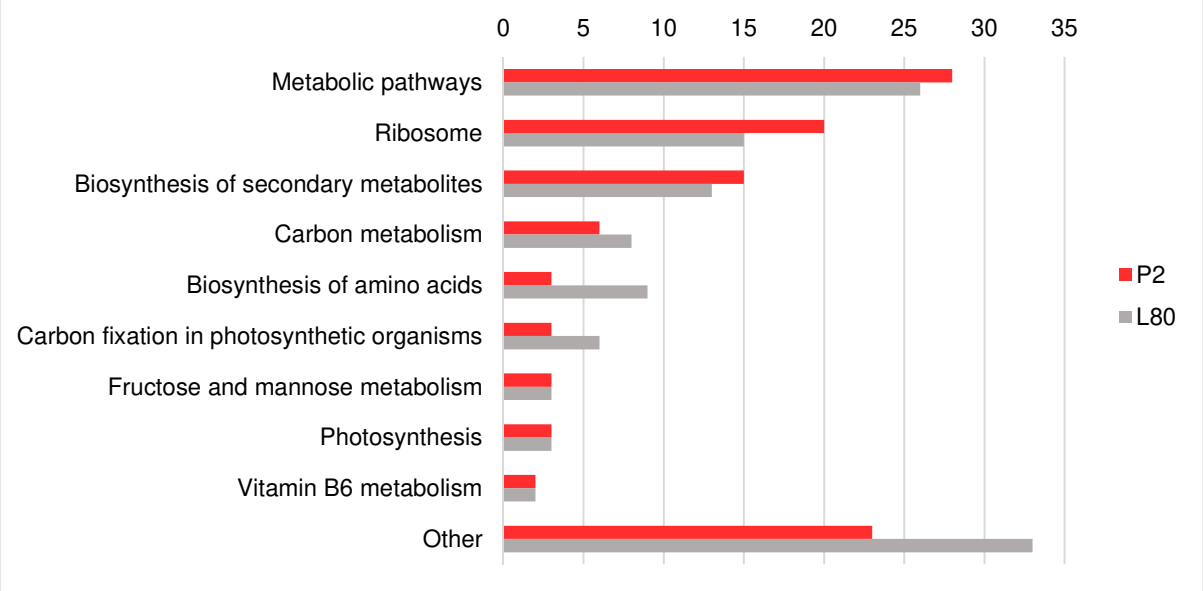

Figure 12 - KEGG pathway analysis of DAPs in P2 and L80 inbred lines under contrasting conditions of N in soil (*x* axis represents the number of proteins involved in each KEGG pathway represented by *y* axis).

3.2.5 DISCUSSION

3.2.5.1 The effects of N starvation on plant growth, development, and physiological traits

Plant growth and development, as well as the regulation of various physiological mechanisms, directly depend on an adequate supply of nutrients. In this sense, N plays a fundamental role in plants, being an essential component of important macromolecules. In maize, N is one of the most used essential nutrients, and represents up to 5% of the total dry weight of the plant (Hawkesford et al., 2012; Mascia et al., 2019). In addition, N is involved in several essential plant functions, including the formation of leaf pigments, synthesis of amino acids, nucleic acids, proteins, and plant hormones.

Our results show that the 90% reduction of nitrogen supply significantly affected the growth of NUE-contrasting inbred lines. This effect was more pronounced in the N-inefficient inbred line L80 for some traits such as plant height, stem diameter, and shoot dry matter (Figure 6). These reductions are likely due to the reduced CO_2 assimilation rate and shoot dry mass, already reported in previous studies for cotton (Zhu et al., 2022), rice (Zhong et al., 2019; Tantray et al., 2020), maize (Wu et al., 2019) and popcorn (Santos et al., 2017; Khan et al., 2020b, 2022; 2019; Santos et al., 2023).

Nitrogen also plays a vital role in photosynthesis. In C_4 plants, about 45% of available N is allocated to soluble proteins (20% of which is ribulose-1,5-bisphosphate carboxylase – Rubisco) and 25% to thylakoids. Out of the total N allocated to thylakoids, about 75% is associated with proteins from light-harvesting complexes and the remainder allocated to bioenergetics (Mu and Chen, 2021). Thus, N limitation can drastically affect the photosynthetic and bioenergetic processes of plants. To assess these effects on NUE-contrasting inbred lines in this study, we used parameters related to chlorophyll fluorescence that have been used in several studies to understand the physiological mechanisms impacted by N limitation.

In this sense, the light response curve of chlorophyll fluorescence is a fast and sensitive method to detect the impacts of abiotic stresses (such as low N

availability) on the photosynthetic processes of plants under different conditions of light availability. The ϕPSII measures the efficiency of PSII photochemistry and represents the proportion of light that, after being absorbed by PSII-associated chlorophyll, will be used in photochemistry. The qP gives an indication of the proportion of PSII reaction centers that are open and ready to function dissipating the light energy absorbed as electron transport (Maxwell and Johnson, 2000). Alternatively, NPQ refers to the photoprotective dissipation mechanism that dissipates excess absorbed light energy in the form of heat, preventing damage to the photosynthetic apparatus (Maxwell and Johnson, 2000). Thus, based on the content of leaf pigments and on the light response curves of chlorophyll fluorescence parameters and photosynthetic O_2 evolution rate, our hypothesis is that the two lines showed different mechanisms to deal with the low N supply.

Under low N, the N-inefficient inbred line L80 had higher chlorophyll and anthocyanin content than the N-efficient inbred line P2 (and less reduction between the two conditions) while the N-efficient line showed higher values for flavonoid content (Figure 9). Anthocyanins and flavonoids are plant pigments that belong to the phenylpropanoid subclass of secondary metabolites and act as non-enzymatic antioxidants protecting plants against the reactive oxygen species (ROS), playing an important role in photoprotection (Hughes et al., 2014; Zhang et al., 2022). In this case, each line used different accessory pigments to mitigate photoinhibition damage. Additionally, in terms of photoprotection, P2 showed higher values of NPQ under low N condition (Figure 10f).

However, these physiological adaptations showed in two inbred lines did not translate into higher ϕPSII, once P2 and L80 both showed a significant reduction for this trait, with a negligible difference in saturating light condition (starting from 600 PPFDs). However, P2 showed significantly higher A_{pot} values. Thus, our hypothesis is that this difference in the performance of the two lines and the superiority of P2 in N-limiting conditions might not directly be associated with light harvesting process, but potentially in the amount and/or regeneration of Rubisco, which could lead to a decrease in photosynthetic activity, as previously described in a study conducted by Tazoe et al., (2006) in *Amaranthus cruentus*, a C_4 plant. In that study, it was observed that the N content in soluble proteins such as Rubisco was reduced by 24% due to N deprivation.

Subsequently, Mu et al. (2016) revealed that, compared to the control treatment (HN – 180 kg N ha^{-1}), N deprivation (0 kg N ha^{-1}) reduced the percentage of N allocated to Rubisco by 24% in maize plants, as well as other light harvesting proteins. On the other hand, there was a 65% increase in the N content allocated to bioenergetics. Therefore, based on previous studies, it can be inferred that C_4 plants tend to invest more N in bioenergetics to support electron transport, in addition to preferably reducing the content of Rubisco, in response to N deprivation. However, in the present study, this could not be verified. Future work will help us understand whether the difference in the photosynthetic efficiency of the two lines is associated with the synthesis or regeneration of this enzyme.

3.2.5.2 Regulation of proteins associated with photosynthesis in conditions of N deprivation

Abiotic stresses significantly affect the productivity of important crops such as popcorn. As one of the first responses of plants to these stresses, stomatal closure occurs, reducing the availability of CO_2 for Rubisco and triggering the generation of ROS (Bai et al., 2023). At a molecular level, these stresses cause a reduction in the activity of photosystem II (PSII) or I (PSI), generating a deficit in the electron transport chain, and consequently, damage by photoinhibition (Ozaki et al., 2022).

In this work, a PSII D2 protein (PsbD – P48184) was up-accumulated in P2 and down-accumulated in L80, while PSI reaction center subunit IV A (PsaE – B6TH55) and Rieske domain-containing protein (PetC – A0A804LDL1) were up-accumulated in P2 and unchanged in L80 (Supplementary Table 5). Among the intrinsic proteins of PSII, PsbD is required for phototropic growth and oxygen evolution, and the lack of this protein can cause severe damage to the functions of PSII.

PsaE and PetC are both involved on the electron tranport chain and are determinants of the rate of electron transport on PSII and PSI. PsaE is involved in electron transfer in PSI, which occurs through its association with ferredoxin (Fd) and previous studies (Varotto et al., 2000; Ihnatowicz et al., 2007) showed that *psae* mutants had significant reductions in electron flow, growth rate and a reduction of up to 50% in the total chlorophyll content. PetC is a component of cytochrome b_6f

complex wich is involved in both linear and cyclic electron transport, and it is considered a limiting step in the photosynthetic electron transport chain (Ermakova et al., 2019) and its overexpression resulted in substancial impact on quantum yield of PSI and PSII, biomass and seed yield on *A. thaliana* (Simkin et al., 2017). Therefore, our results suggest that the increase in the expression of PsbD, PsaE ans PetC likely contributed to an improvement in N utilization and resulted in significantly higher values of photossynthetic O_2 evolution rate in the N-efficient inbred line (Figure 8).

The L80 showed down-accumulation of oxygen-evolving enhancer protein 3 (OOE3 – B4FT19) and plastocyanin (PC – B6SSB9) (Supplementary Table 5). OEE proteins consist of three subunits that are bounded to PSII on the luminal side of the thylakoid membrane and are crucial members of the oxygen-evolving complex (OEC), which is involved in the photo-oxidation of water during the light reactions of photosynthesis and providing protons to PSI (Thornton et al., 2004; Chen et al., 2022). This protein complex is sensitive to abiotic stresses, and alteration in its regulation have been reported in plants under abiotic stresses such as drought (Lu and Zhang, 1999; Hajheidari et al., 2005; Li et al., 2018a; Zadražnik et al., 2019) and salinity (Murota et al., 1994; Sugihara et al., 2000). PC, in turn, shuttles electrons from PSII to PSI, binding to cytocrom f and PSI (CASPY et al., 2021).

Thus, the downregulation of OOE3 and PC in the L80 inbred line may have contributed to the reduction in electron flow in the electron transport chain, which could have led to less pronounced values of A_{pot} in L80 (Figure 8b), impacting its growth and development.

3.2.5.3 N affects the pathways of energy generation and secondary metabolites production

We identified proteins related to energy generation and involved in carbon fixation in both lines. Phosphoenolpyruvate carboxykinase (PEPCK – C0P3W9) was up-accumulated in P2 and unchanged in L80 whereas phosphoenolpyruvate carboxylase (PEPC – K7VCJ9) was down-accumulated in L80 and unchanged in P2 (Supplementary Table 5).

PEPC catalyzes the conversion of CO_2 and phosphoenolpyruvate (PEP) to oxaloacetate (OAA), which is then converted into malate or aspartate and

transported to bundle sheath cells in C_4 plants where CO_2 is released for the Calvin cycle (Carmo-Silva et al., 2008; Torresi et al., 2023). PEPCK is found in the cytosol and mitochondria of plant cells and catalyzes the conversion of OOA to PEP, which is then used in the process of gluconeogenesis to produce glucose (Behera et al., 2023). This conversion is critical for plants when they are experiencing conditions of reduced CO_2 fixation caused by abiotic stresses. Under these conditions, PEPCK helps the plant to conserve energy by using alternative carbon sources allowing them to maintain their metabolic processes even when photosynthesis is limited (Carmo-Silva et al., 2008; Walker et al., 2021).

Glycine cleavage system P (GCS-P – K7TIN2) was up accumulated in P2 line while presented unchanged accumulation in L80 (Supplementary Table 5). The GCS-P is a component of the glycine cleavage system (GCS), a metabolic pathway that is responsible for the breakdown of glycine into serine and one-carbon units during photorespiration. Studies have shown that overexpression of GCS system proteins led to substantial increments in photosynthesis and growth of plants such as *A. thaliana* (Kebeish et al., 2007; Maier et al., 2012) and tobacco (López-Calcagno et al., 2019).

Together, these results suggest that N deficiency regulated the up accumulation of PEPCK and GCS-P in the P2 inbred line and the down accumulation of PEPC in L80, which may have substantially contributed to the difference in energy balance between the two inbred lines, highlighting that P2 is more efficient in regulating key enzymes for alternative carbon metabolism pathways to compensate for the energy deficit. Our findings are consistent with Khan et al. (2022), suggesting that in popcorn, N may regulate enzymes involved in the glycolysis pathway to overcome energy shortage.

3.2.5.4 Antioxidant system to reduce the effects of ROS due to N deprivation

The stress caused by N deprivation increases the amount of excitation energy resulting on damage to the photosynthetic apparatus caused by ROS (Zhang et al., 2012). To deal with these imbalances, plants use a series of enzymes and antioxidant molecules to scavenge ROS and other free radicals. Generally, ROS-scavenging systems in plants are comprised of non-enzymatic and/or enzymatic antioxidants (Soares et al., 2019; Machado et al., 2023).

Ascorbate peroxidase (APX) is a central enzyme for ROS scavenging in plants and can be induced under several biotic and abiotic stresses (Kuo et al. 2020). APX, which is the first step of the ascorbate-glutathione cycle, uses ascorbate as its specific electron donor to reduce H_2O_2 to water (Xiao et al., 2021). The regeneration of the ascorbate involved in this cycle is performed by monodehydroascorbate reductase (MDAR) (Leterrier et al., 2005). In P2, both proteins were up-accumulated on the ascorbate metabolism (peroxidase – K7V8K5; and MDAR – C0P4M0) (Supplementary Table 5).

Cytochrome P450 (CYP 450), RAB-related protein (RAB7 – A0A804QRT8), malic enzyme (ME – A0A804PAE3), aspartate aminotransferase (AST – A0A804ND31) and phytoene dehydrogenase (A0A804LEU1) were up-accumulated on P2 inbred line (Supplementary Table 5). CYP 450 and phytoene dehydrogenase are essential enzymes involved in the ROS-scavenging system. CYP 450 play significant role in various biosynthetic reactions during abiotic stresses (Pandian et al., 2020) and contribute also to the production of carotenoids and flavonoids, which serve as defense mechanisms against ROS (Xu et al., 2015). In popcorn and maize, they have been linked to tolerance to several abiotic stresses such as heavy metal (Pinto et al., 2021), drought stress (Li and Wei, 2020), salinity (Zörb et al., 2005) but their specific role in low N stress is not yet well understood. Phytoene dehydrogenase acts on the production of carotenoids catalyzing the first step in the carotenoid biosynthesis pathway, which is the conversion of colorless phytoene to colored phytofluene (Welsch et al., 2008).

The proteins of the RAB family (GTPases) are involved in the vesicle trafficking system and recent studies have shown that the overexpression of *Rab7* gene have enhanced tolerance to several abiotic stresses on *A. thaliana* (Mazel et al., 2004), tobacco (Agarwal et al., 2008), *Prosopis juliflora* (George and Parida, 2011) and rice (Tripathy et al., 2017). More recently, El-Esawi and Alayafi (2019) demonstrated that the overexpression of *Rab7* in rice promotes drought and heat tolerance by modulating different antioxidants. ME is also described as an important ROS-scavenging protein acting not only balancing the malic acid concentration in cells, but reducing oxidative damage caused by ROS and enhancing plants' abiotic stress tolerance (Zhou et al., 2011). The mechanism by which AST, up accumulated in the inbred line P2, may reduce ROS levels in plant is not yet fully understood. Indirectly, this enzyme acts through the transamination of glutamate with the final

process resulting in the formation of aspartate (Asp). Asp can then be used for several metabolic processes and be converted again to glutamate, a precursor or glutathione (Han et al., 2021) – a powerful ROS-scavenging metabolite (Dorion et al., 2021).

Our hypothesis is that the low N supply triggered the activation of mechanisms that positively regulate both enzymatic and non-enzymatic antioxidants. This is supported by the observed increase in accessory pigments in P2 (Figure 9) and the enhanced accumulation of key ROS-scavenging enzymes. These mechanisms likely played a role in minimizing ROS-induced damage. Consequently, these findings may explain the higher A_{pot} rates observed in P2, which, despite being subjected to N limitation, experienced less reductions and maintained higher values compared to the N-inefficient line L80.

3.2.6 CONCLUSION

In conclusion, both physiological and proteomic analyses contribute to the understanding of the physiological and molecular mechanisms underlying the efficient response of contrasting popcorn genotypes to nitrogen use efficiency (NUE). The increased regulation of proteins involved in plant photochemistry and bioenergetic metabolism in the efficient inbred line plays a crucial role in maintaining photosynthesis and utilizing an alternative pathway to manage the energy imbalance resulting from nitrogen deprivation. Additionally, the abundance of proteins associated with the enzymatic antioxidant system and the increase in accessory pigments constituting the non-enzymatic antioxidant system contribute significantly to a more efficient utilization of nitrogen in the efficient lineage.

Our results provide valuable insights into the adaptive responses of popcorn plants to limited nitrogen availability. Ultimately, this knowledge can be utilized to develop novel breeding strategies aimed at producing popcorn cultivars with enhanced NUE, ultimately promoting sustainable agriculture, reducing environmental impacts, and meeting the growing global demand for food.

REFERENCES

Abubakar, A. W. et al. (2019) Physiological Evaluations of Maize Hybrids under Low Nitrogen. *Advances in Agriculture*, v. 2019, p. 1–6.

Agati, G. et al. (2013) Functional roles of flavonoids in photoprotection: New evidence, lessons from the past. *Plant Physiology and Biochemistry*, v. 72, p. 35–45.

Almeida, V. C. et al. (2018a) Generation mean analysis for nitrogen and phosphorus uptake, utilization, and translocation indexes at vegetative stage in tropical popcorn. *Euphytica*, v. 214, n. 7, p. 103.

Almeida, V. C. et al. (2018b) Genetic diversity and path analysis for nitrogen use efficiency of tropical popcorn (*Zea mays* ssp. *everta*) inbred lines in adult stage. *Plant Breeding*, v. 137, n. 6, p. 839–847.

Alvarez, J. M. et al. (2014) Systems approach identifies TGA1 and TGA4 transcription factors as important regulatory components of the nitrate response of *Arabidopsis thaliana* roots. *The Plant Journal*, v. 80, n. 1, p. 1–13.

Amegbor, I. K. et al. (2022) Genetic analysis and yield assessment of maize hybrids under low and optimal nitrogen environments. *Heliyon*, v. 8, n. 3, p. e09052.

Anas, M. et al. (2020) Fate of nitrogen in agriculture and environment: agronomic, eco-physiological and molecular approaches to improve nitrogen use efficiency. *Biological Research*, v. 53, n. 1, p. 47.

Andrews, M.; Lea, P. J. (2013) Our nitrogen ‘footprint’: the need for increased crop nitrogen use efficiency. *Annals of Applied Biology*, v. 163, n. 2, p. 165–169.

Asibi, A. E.; Chai, Q.; A. Coulter, J. (2019) Mechanisms of Nitrogen Use in Maize. *Agronomy,* v. 9, n. 12, p. 775.

Association Of Official Analytical Chemists - AOAC. *Official methods of analysis*. 15. ed. Arlington: [s.n.].

Bai, Q. et al. (2023) The C 2 H 2 -type zinc finger transcription factor OSIC1 positively regulates stomatal closure under osmotic stress in poplar. *Plant Biotechnology Journal*, v. 21, n. 5, p. 943–960.

Bänziger, M.; Betrán, F. J.; Lafitte, H. R. (1997) Efficiency of High-Nitrogen Selection Environments for Improving Maize for Low-Nitrogen Target Environments. *Crop Science*, v. 37, n. 4, p. 1103–1109.

Bänziger, M.; Lafitte, H. R. (1997) Efficiency of Secondary Traits for Improving Maize for Low-Nitrogen Target Environments. **Crop Science**, v. 37, n. 4, p. 1110–1117.

Behera, D. et al. (2023) Overexpression of Setaria italica phosphoenolpyruvate carboxylase gene in rice positively impacts photosynthesis and agronomic traits. *Plant Physiology and Biochemistry*, v. 194, p. 169–181.

Bhadmus, O. A. et al. (2022) Genome-Wide Association Analysis Reveals Genetic Architecture and Candidate Genes Associated with Grain Yield and Other Traits under Low Soil Nitrogen in Early-Maturing White Quality Protein Maize Inbred Lines. *Genes*, v. 13, n. 5, p. 826.

Bi, Y.-M. et al. (2014) High throughput RNA sequencing of a hybrid maize and its parents shows different mechanisms responsive to nitrogen limitation. *BMC Genomics*, v. 15, n. 1, p. 77.

Blackmer, T. M.; Schepers, J. S. (1994) Techniques for monitoring crop nitrogen status in corn. *Communications in Soil Science and Plant Analysis*, v. 25, n. 9–10, p. 1791–1800.

Bloom, A. J. et al. (2002) Root Development and Absorption of Ammonium and Nitrate from the Rhizosphere. *Journal of Plant Growth Regulation*, v. 21, n. 4, p. 416–431.

Brasil (2023) *Ministério da Agricultura, Pecuária e Abastecimento. Registro Nacional de Cultivares* <https://sistemas.agricultura.gov.br/snpc/cultivarweb/cultivares_registradas.php> Accessed in 11 oct. 2023.

Bu, D. et al. (2021) KOBAS-i: intelligent prioritization and exploratory visualization of biological functions for gene enrichment analysis. *Nucleic Acids Research*, v. 49, n. W1, p. W317–W325.

Buchert, F.; Scholz, M.; Hippler, M. (2022) Electron transfer via cytochrome *b* 6 *f* complex displays sensitivity to antimycin A upon STT7 kinase activation. *Biochemical Journal*, v. 479, n. 1, p. 111–127.

Burridge, J. D. et al. (2019) A case study on the efficacy of root phenotypic selection for edaphic stress tolerance in low-input agriculture: Common bean breeding in Mozambique. *Field Crops Research*, v. 244, p. 107612.

Caixeta, D. S. et al. (2015) Early indirect selection for nitrogen use efficiency in maize. *REVISTA CIÊNCIA AGRONÔMICA*, v. 46, n. 2.

Cao, H. et al. (2017) Overexpression of the Maize ZmNLP6 and ZmNLP8 Can Complement the Arabidopsis Nitrate Regulatory Mutant nlp7 by Restoring Nitrate Signaling and Assimilation. *Frontiers in Plant Science*, v. 8.

Carmo-Silva, A. E. et al. (2008) The activities of PEP carboxylase and the C4 acid decarboxylases are little changed by drought stress in three C4 grasses of different subtypes*. Photosynthesis Research*, v. 97, n. 3, p. 223–233.

Caspy, I. et al. (2021) Structure of plant photosystem I-plastocyanin complex reveals strong hydrophobic interactions*. Biochemical Journal*, v. 478, n. 12, p. 2371–2384.

Chen, S. et al. (2019) NtMYB4 and NtCHS1 Are Critical Factors in the Regulation of Flavonoid Biosynthesis and Are Involved in Salinity Responsiveness. *Frontiers in Plant Science*, v. 10.

Chen, Y. et al. (2014) Characterization of the plant traits contributed to high grain yield and high grain nitrogen concentration in maize. *Field Crops Research*, v. 159, p. 1–9.

Chen, Y. et al. (2022) Mimicking the Oxygen-Evolving Center in Photosynthesis. *Frontiers in Plant Science*, v. 13.

Ciampitti, I. A.; Vyn, T. J. (2012) Physiological perspectives of changes over time in maize yield dependency on nitrogen uptake and associated nitrogen efficiencies: A review. *Field Crops Research*, v. 133, p. 48–67.

Coan, M. M. D. et al. (2019)Inheritance Study for Popping Expansion in Popcorn vs. Flint Corn Genotypes. *Agronomy Journal*, v. 111, n. 5, p. 2174–2183.

Congreves, K. A. et al. (2021) Nitrogen Use Efficiency Definitions of Today and Tomorrow. *Frontiers in Plant Science*, v. 12.

Cruz, C. D. (2013) GENES - a software package for analysis in experimental statistics and quantitative genetics. *Acta Scientiarum. Agronomy*, v. 35, n. 3.

Cruz, C. D.; Carneiro, P. C. S.; Ragazzi, A. J. (2014) *Modelos Biométricos Aplicados ao Melhoramento Genético*. 1. ed. Viçosa-MG: Editora UFV, 2014. v. 2

Damerval, C. et al. (1986) Technical improvements in two-dimensional electrophoresis increase the level of genetic variation detected in wheat-seedling proteins. *Electrophoresis*, v. 7, n. 1, p. 52–54.

D'andrea, K. E.; Parco, M.; Maddonni, G. Á. (2022) Maize prolificacy under contrasting plant densities and N supplies: II. Growth per plant, biomass partitioning to apical and sub-apical ears during the critical period and kernel setting*. Field Crops Research*, v. 284, p. 108557.

De Oliveira Silva, A. et al. (2017) Applicability of a "Multi-Stage Pulse Labeling" 15N Approach to Phenotype N Dynamics in Maize Plant Components during the Growing Season. *Frontiers in Plant Science*, v. 8.

Dechorgnat, J. et al. (2019) Tissue and nitrogen-linked expression profiles of ammonium and nitrate transporters in maize. *BMC Plant Biology*, v. 19, n. 1, p. 206.

Distler, U. et al. (2014) Drift time-specific collision energies enable deep-coverage data-independent acquisition proteomics. *Nature Methods*, v. 11, n. 2, p. 167–170.

Dofing, S. M.; D'croz-Mason, N.; Thomas-Compton, M. A. (1991) Inheritance of Expansion Volume and Yield in Two Popcorn × Dent Corn Crosses. *Crop Science*, v. 31, n. 3, p. 715–718.

Dorion, S.; Ouellet, J. C.; Rivoal, J. (2021) Glutathione Metabolism in Plants under Stress: Beyond Reactive Oxygen Species Detoxification. *Metabolites*, v. 11, n. 9, p. 641.

Dovale, J. C. et al. (2012) Efeitos gênicos de caracteres associados à eficiência no uso de nitrogênio em milho. *Pesquisa Agropecuária Brasileira*, v. 47, n. 3, p. 385–392.

Duvick, D. N. (1996) Heterosis: Feeding People and Protecting Natural Resources. In: Coors, J. G.; Pandey, S. (eds.) *Genetics and Exploitation of Heterosis in Crops.* American Society of Agronomy, p. 19–29.

Elazab, A.; Serret, M. D.; Araus, J. L. (2016) Interactive effect of water and nitrogen regimes on plant growth, root traits and water status of old and modern durum wheat genotypes. *Planta*, v. 244, n. 1, p. 125–144.

El-Esawi, M.; Alayafi, A. (2019) Overexpression of Rice Rab7 Gene Improves Drought and Heat Tolerance and Increases Grain Yield in Rice (*Oryza sativa* L.). *Genes*, v. 10, n. 1, p. 56.

Engineer, C. B.; Kranz, R. G. (2007) Reciprocal Leaf and Root Expression of *AtAmt1.1* and Root Architectural Changes in Response to Nitrogen Starvation. *Plant Physiology*, v. 143, n. 1, p. 236–250.

Ermakova, M. et al. (2019) Overexpression of the Rieske FeS protein of the Cytochrome b6f complex increases C4 photosynthesis in Setaria viridis. *Communications Biology*, v. 2, n. 1, p. 314.

Ertiro, B. T. et al. (2020a) Genetic Dissection of Nitrogen Use Efficiency in Tropical Maize Through Genome-Wide Association and Genomic Prediction. *Frontiers in Plant Science*, v. 11.

Ertiro, B. T. et al. (2020b) Efficiency of indirect selection for grain yield in maize (Zea mays L.) under low nitrogen conditions through secondary traits under low nitrogen and grain yield under optimum conditions. *Euphytica*, v. 216, n. 8, p. 134.

Fahad, S. et al. (2017) Crop Production under Drought and Heat Stress: Plant Responses and Management Options. *Frontiers in Plant Science*, v. 8.

Fan, X. et al.(2017) Plant nitrate transporters: from gene function to application. *Journal of Experimental Botany*, v. 68, n. 10, p. 2463–2475.

FAO (2022) *Food and Agricultural Organization of the United Nations*. Disponível em: <http://www.fao.org/faostat/en/#data/QC>. Accessed in 18 jun. 2022.

FAO (2023) *FAOSTAT - Fertilizers by Nutrient*. Disponível em: <https://www.fao.org/faostat/en/#data/RFN>. Accessed in 19 jun. 2023.

Farooq, W. et al. (2022) Monitoring lipids profile, CO_2 fixation, and water recyclability for the economic viability of microalgae Chlorella vulgaris cultivation at different initial nitrogen. *Journal of Biotechnology*, v. 345, p. 30–39.

Fu, W. et al. (2020) Grain Yields and Nitrogen Use Efficiencies in Different Types of Stay-Green Maize in Response to Nitrogen Fertilizer. **Plants**, v. 9, n. 4, p. 474.

Galinat, W. C. (1979) *Maize: Ciba-Geigy Agrochemicals Technical Monograph.* Basel, Switzerland: Ciba-Geigy, 1979.

Gallais, A. et al. (2007) Estimating the Proportion of Nitrogen Remobilization and of Postsilking Nitrogen Uptake Allocated to Maize Kernels by Nitrogen-15 Labeling. *Crop Science*, v. 47, n. 2, p. 685–691.

Galvão, J. C. C.; Sawazaki, E.; Miranda, G. V. (2000) Comportamento de híbridos de milho pipoca em Coimbra, Minas Gerais. **Ceres**, v. 47, n. 270, p. 201–218.

Gan, H. et al. (2016) Phosphorus and nitrogen physiology of two contrasting poplar genotypes when exposed to phosphorus and/or nitrogen starvation. *Tree Physiology*, v. 36, n. 1, p. 22–38.

Gao, K. et al. (2015) A comprehensive analysis of root morphological changes and nitrogen allocation in maize in response to low nitrogen stress. *Plant, Cell & Environment*, v. 38, n. 4, p. 740–750.

George, S.; Parida, A. (2011) Over-expression of a Rab family GTPase from phreatophyte Prosopis juliflora confers tolerance to salt stress on transgenic tobacco. *Molecular Biology Reports*, v. 38, n. 3, p. 1669–1674.

Getahun, B. B. et al. (2022) Genotype-by-Environment Interaction for Quantitative Trait Loci Affecting Nitrogen Use Efficiency and Associated Traits in Potato. *Potato Research*, v. 65, n. 4, p. 777–807.

Goel, P. et al. (2018) Transcriptome and Co-Expression Network Analyses Identify Key Genes Regulating Nitrogen Use Efficiency in Brassica juncea L. *Scientific Reports*, v. 8, n. 1, p. 7451.

Good, A. G.; Shrawat, A. K.; Muench, D. G. (2004) Can less yield more? Is reducing nutrient input into the environment compatible with maintaining crop production? *Trends in Plant Science*, v. 9, n. 12, p. 597–605.

Goodman, M. M.; Smith, J. S. C. (1987) Botânica. In: Paterniani, E.; Viegas, G. P. (Eds.). *Melhoramento e produção de milho*. Campinas: Fundação Cargill, p. 41–78.

Granato, I. S. C. et al. (2016) Effects of using phenotypic means and genotypic values in GGE biplot analyses on genotype by environment studies on tropical maize (Zea mays). *Genetics and Molecular Research*, v. 15, n. 4.

Grassi, G.; Colom, M. R.; Minotta, G. (2001) Effects of nutrient supply on photosynthetic acclimation and photoinhibition of one-year-old foliage of *Picea abies*. *Physiologia Plantarum*, v. 111, n. 2, p. 245–254.

Gu, R. et al. (2013) Characterization of AMT-Mediated High-Affinity Ammonium Uptake in Roots of Maize (Zea mays L.). *Plant and Cell Physiology*, v. 54, n. 9, p. 1515–1524.

Guedes, F. L. et al. (2013) Inheritance of Nitrogen Use Efficiency in Inbred Progenies of Tropical Maize Based on Multivariate Diallel Analysis. *The Scientific World Journal*, v. 2014, p. 1–7.

Guimarães, D. P.; Sans, L. M. A.; Moraes, A. V. C. (2002) Estimativa da Área Foliar de Cultivares de Milho. *Proceedings of the XXIV Congresso Nacional de Milho e Sorgo*, Minas Gerais: ABMS.

Hajheidari, M. et al. (2005) Proteome analysis of sugar beet leaves under drought stress. *PROTEOMICS*, v. 5, n. 4, p. 950–960.

Hallauer, A. R.; Carena, M. J.; Miranda Filho, J. B. (2010) *Quantitative genetics in maize breeding*. 1. ed. Berlin: Verlag.

Hammad, H. M. et al. (2022) Evaluating the Impact of Nitrogen Application on Growth and Productivity of Maize Under Control Conditions. *Frontiers in Plant Science*, v. 13.

Han, M. et al. (2016) Identification of Nitrogen Use Efficiency Genes in Barley: Searching for QTLs Controlling Complex Physiological Traits. *Frontiers in Plant Science*, v. 7.

Han, M. et al. (2021) l-Aspartate: An Essential Metabolite for Plant Growth and Stress Acclimation. *Molecules*, v. 26, n. 7, p. 1887.

Hawkesford, M. et al. (2012) Functions of Macronutrients. In: Marschner, P. (Ed.) *Marschner's Mineral Nutrition of Higher Plants*. Amsterdam, Holand: Elsevier, p. 135–189.

Hawkesford, M. J. (2017) Genetic variation in traits for nitrogen use efficiency in wheat. *Journal of Experimental Botany*, v. 68, n. 10, p. 2627–2632.

Hawkesford, M. J.; Griffiths, S. (2019) Exploiting genetic variation in nitrogen use efficiency for cereal crop improvement. *Current Opinion in Plant Biology*, v. 49, p. 35–42.

Hawkins, J. A. et al. (2007) Using Relative Chlorophyll Meter Values to Determine Nitrogen Application Rates for Corn. *Agronomy Journal*, v. 99, n. 4, p. 1034–1040.

Heffer, P.; Gruère, A.; Roberts, T. *Assessment of Fertilizer Use by Crop at the Global Level*. Paris, France: International Fertilizer Industry Association (IFA), p. 1– 9.

Hirel, B. et al. (2007) The challenge of improving nitrogen use efficiency in crop plants: towards a more central role for genetic variability and quantitative genetics within integrated approaches. *Journal of Experimental Botany*, v. 58, n. 9, p. 2369–2387.

Hoagland, D. R.; Arnon, D. I. (1959) The water-culture method for growing plants without soil. *California Agricultural Experiment Station*, v. 347, n. 2.

Hochholdinger, F. et al. (2004) Genetic Dissection of Root Formation in Maize (Zea mays) Reveals Root-type Specific Developmental Programmes. *Annals of Botany*, v. 93, n. 4, p. 359–368.

Hughes, N. M. et al. (2014) Photosynthetic costs and benefits of abaxial versus adaxial anthocyanins in Colocasia esculenta 'Mojito'. *Planta*, v. 240, n. 5, p. 971–981.

Ihnatowicz, A.; Pesaresi, P.; Leister, D. (2007) The E subunit of photosystem I is not essential for linear electron flow and photoautotrophic growth in Arabidopsis thaliana. *Planta*, v. 226, n. 4, p. 889–895.

Jakoby, M. et al. (2002) bZIP transcription factors in Arabidopsis. *Trends in Plant Science*, v. 7, n. 3, p. 106–111.

Jiang, L. et al. (2018) Analysis of Gene Regulatory Networks of Maize in Response to Nitrogen. *Genes*, v. 9, n. 3, p. 151.

Jin, X. et al. (2015) Effects of nitrogen stress on the photosynthetic CO2 assimilation, chlorophyll fluorescence and sugar-nitrogen ratio in corn. *Scientific Reports*, v. 5, n. 1, p. 9311.

Kang, J.; Turano, F. J. (2003) The putative glutamate receptor 1.1 (AtGLR1.1) functions as a regulator of carbon and nitrogen metabolism in *Arabidopsis thaliana*. *Proceedings of the National Academy of Sciences*, v. 100, n. 11, p. 6872–6877.

Kebeish, R. et al. (2007) Chloroplastic photorespiratory bypass increases photosynthesis and biomass production in Arabidopsis thaliana. *Nature Biotechnology*, v. 25, n. 5, p. 593–599.

Khamis, S. et al. (1990) Adaptation of the Photosynthetic Apparatus in Maize Leaves as a Result of Nitrogen Limitation. **Plant Physiology**, v. 94, n. 3, p. 1436–1443.

Khan, A. et al. (2020a) Validation of an Enzyme-Driven Model Explaining Photosynthetic Rate Responses to Limited Nitrogen in Crop Plants. *Frontiers in Plant Science*, v. 11.

Khan, S. et al. (2020b) Limited Nitrogen and Plant Growth Stages Discriminate Well Nitrogen Use, Uptake and Utilization Efficiency in Popcorn. **Plants**, v. 9, n. 7, p. 893.

Khan, S. et al. (2022) Revealing the differential protein profiles behind the nitrogen use efficiency in popcorn (*Zea mays* var. *everta*). *Scientific Reports*, v. 12, n. 1, p. 1521.

Kist, B. B.; Carvalho, C.; Beling, R. R. (2021) *Anuário Brasileiro do Milho 2021*. Santa Cruz do Sul: Gazeta.

Kumari, A. et al. (2021) ROS Regulation Mechanism for Mitigation of Abiotic Stress in Plants. In: Ahmad, R (Ed.) *Reactive Oxygen Species*. London, UK: IntechOpen.

Kuo, E. Y.; Cai, M.-S.; Lee, T.-M. (2020) Ascorbate peroxidase 4 plays a role in the tolerance of Chlamydomonas reinhardtii to photo-oxidative stress. *Scientific Reports*, v. 10, n. 1, p. 13287.

Larish, L. B.; Brewbaker, J. L. (1999) Diallel analyses of temperate and tropical popcorn. *Maydica*, v. 44, p. 279–284.

Lê, S.; Josse, J.; Husson, F. (2008) FactoMineR: An *R* Package for Multivariate Analysis. *Journal of Statistical Software*, v. 25, n. 1.

Lee, E. A.; Tollenaar, M. (2007) Physiological Basis of Successful Breeding Strategies for Maize Grain Yield. *Crop Science*, v. 47, p. S-202-S-215.

Leite, J. T. et al. (2021) Water Use Efficiency in Popcorn (Zea mays L. var. everta): Which Physiological Traits Would Be Useful for Breeding? *Pl***ants**, v. 10, n. 7, p. 1450.

Lemaitre, T. et al. (2008) Enzymatic and Metabolic Diagnostic of Nitrogen Deficiency in Arabidopsis thaliana Wassileskija Accession. *Plant and Cell Physiology*, v. 49, n. 7, p. 1056–1065.

Leterrier, M. et al. (2005) Peroxisomal Monodehydroascorbate Reductase. Genomic Clone Characterization and Functional Analysis under Environmental Stress Conditions. *Plant Physiology*, v. 138, n. 4, p. 2111–2123.

Li, B. et al. (2021) Flavonoids improve drought tolerance of maize seedlings by regulating the homeostasis of reactive oxygen species. *Plant and Soil*, v. 461, n. 1–2, p. 389–405.

Li, C. et al. (2018a) Comparative proteomic analysis of key proteins during abscisic acid-hydrogen peroxide-induced adventitious rooting in cucumber (*Cucumis sativus* L.) under drought stress. *Journal of Plant Physiology*, v. 229, p. 185–194.

Li, L.; Zhang, L.; Liu, J. (2021) Proteomic analysis of hydrogen production in Chlorella pyrenoidosa under nitrogen deprivation. *Algal Research*, v. 53, p. 102143.

Li, R. et al. (2022) Heterosis for Nitrogen Use Efficiency of Maize Hybrids Enhanced over Decades in China. *Agriculture*, v. 12, n. 6, p. 764.

Li, W. et al. (2017) Transcriptome and metabolite analysis identifies nitrogen utilization genes in tea plant (Camellia sinensis). *Scientific Reports*, v. 7, n. 1, p. 1693.

Li, W. et al. (2018b) Comprehensive environmental impacts of fertilizer application vary among different crops: Implications for the adjustment of agricultural structure aimed to reduce fertilizer use. *Agricultural Water Management*, v. 210, p. 1–10.

Li, Y.; Wei, K. (2020) Comparative functional genomics analysis of cytochrome P450 gene superfamily in wheat and maize. *BMC Plant Biology*, v. 20, n. 1, p. 93.

Liao, C. et al. (2012) Proteomic Analysis Revealed Nitrogen-mediated Metabolic, Developmental, and Hormonal Regulation of Maize (Zea mays L.) Ear Growth. *Journal of Experimental Botany*, v. 63, n. 14, p. 5275–5288.

Lima, V. J. De et al. (2019) Combined Dominance and Additive Gene Effects in Trait Inheritance of Drought-Stressed and Full Irrigated Popcorn. *Agronomy*, v. 9, n. 12, p. 782.

Lin, S.-Y.; Chen, P.-A.; Zhuang, B.-W. (2022) The Stomatal Conductance and Fv/Fm as the Indicators of Stress Tolerance of Avocado Seedlings under Short-Term Waterlogging. *Agronomy*, v. 12, n. 5, p. 1084.

Liseron-Monfils, C. et al. (2013) Nitrogen transporter and assimilation genes exhibit developmental stage-selective expression in maize (*Zea mays* L.) associated with distinct *cis* -acting promoter motifs. *Plant Signaling & Behavior*, v. 8, n. 10, p. e26056.

Liu, H.; Able, A. J.; Able, J. A. (2021) Nitrogen Starvation-Responsive MicroRNAs Are Affected by Transgenerational Stress in Durum Wheat Seedlings. *Plants*, v. 10, n. 5, p. 826.

Liu, R. et al. (2012) Mining of Candidate Maize Genes for Nitrogen Use Efficiency by Integrating Gene Expression and QTL Data. *Plant Molecular Biology Reporter*, v. 30, n. 2, p. 297–308.

Liu, S.; Qin, F. (2021) Genetic dissection of maize drought tolerance for trait improvement. *Molecular Breeding*, v. 41, n. 2, p. 8.

Long, S. P.; Marshall-Colon, A.; Zhu, X.-G. (2015) Meeting the Global Food Demand of the Future by Engineering Crop Photosynthesis and Yield Potential. *Cell*, v. 161, n. 1, p. 56–66.

López-Calcagno, P. E. et al. (2019) Overexpressing the H-protein of the glycine cleavage system increases biomass yield in glasshouse and field-grown transgenic tobacco plants. *Plant Biotechnology Journal*, v. 17, n. 1, p. 141–151.

Lu, C. et al. (2001) Modification of photosystem II photochemistry in nitrogen deficient maize and wheat plants. *Journal of Plant Physiology*, v. 158, n. 11, p. 1423–1430.

Lu, C.; Zhang, J. (1999) Effects of water stress on photosystem II photochemistry and its thermostability in wheat plants. *Journal of Experimental Botany*, v. 50, n. 336, p. 1199–1206.

Ludemann, C. I. et al. (2022) Estimating maize harvest index and nitrogen concentrations in grain and residue using globally available data. *Field Crops Research*, v. 284, p. 108578.

Lynch, J. P. (2013) Steep, cheap and deep: an ideotype to optimize water and N acquisition by maize root systems. *Annals of Botany*, v. 112, n. 2, p. 347–357.

Lynch, J. P. (2015) Root phenes that reduce the metabolic costs of soil exploration: opportunities for 21st century agriculture. *Plant, Cell & Environment*, v. 38, n. 9, p. 1775–1784.

Ma, N. et al. (2020) Transcriptome analysis of maize seedling roots in response to nitrogen-, phosphorus-, and potassium deficiency. *Plant and Soil*, v. 447, n. 1–2, p. 637–658.

Machado, J. et al. (2023) Enzymatic and Non-Enzymatic Antioxidant Responses of Young Tomato Plants (cv. Micro-Tom) to Single and Combined Mild Nitrogen and Water Deficit: Not the Sum of the Parts. *Antioxidants*, v. 12, n. 2, p. 375.

Maier, A. et al. (2012) Transgenic Introduction of a Glycolate Oxidative Cycle into A. thaliana Chloroplasts Leads to Growth Improvement. *Frontiers in Plant Science*, v. 3.

Makino, A. et al. (1997) Does Decrease in Ribulose-1,5-Bisphosphate Carboxylase by Antisense RbcS Lead to a Higher N-Use Efficiency of Photosynthesis under Conditions of Saturating CO2 and Light in Rice Plants? *Plant Physiology*, v. 114, n. 2, p. 483–491.

Makumbi, D. et al. (2011) Combining ability, heterosis and genetic diversity in tropical maize (Zea mays L.) under stress and non-stress conditions. *Euphytica*, v. 180, n. 2, p. 143–162.

Marschner, H. (2012) *Marschner's Mineral Nutrition of Higher Plants*. Amsterdam, Holand: Elsevier.

Martin, A. et al. (2006) Two Cytosolic Glutamine Synthetase Isoforms of Maize Are Specifically Involved in the Control of Grain Production. *The Plant Cell,* v. 18, n. 11, p. 3252–3274.

Mascia, M. et al. (2019) Nitrogen Starvation Differentially Influences Transcriptional and Uptake Rate Profiles in Roots of Two Maize Inbred Lines with Different NUE*. International Journal of Molecular Sciences*, v. 20, n. 19, p. 4856.

Masclaux-Daubresse, C. et al. (2010) Nitrogen uptake, assimilation and remobilization in plants: challenges for sustainable and productive agriculture. *Annals of Botany*, v. 105, n. 7, p. 1141–1157.

Mastrodomenico, A. T. et al. (2019) Genomic Selection Using Maize Ex-Plant Variety Protection Germplasm for the Prediction of Nitrogen-Use Traits. *Crop Science*, v. 59, n. 1, p. 212–220.

Mattila, H. et al. (2022) Differences in susceptibility to photoinhibition do not determinegrowth rate under moderate light in batch or turbidostat - a studywith five green algae. *Photosynthetica*, v. 60, n. SPECIAL ISSUE 2022, p. 10–20.

Maxwell, K.; Johnson, G. N. (2000) Chlorophyll fluorescence—a practical guide. *Journal of Experimental Botany*, v. 51, n. 345, p. 659–668.

Menz, J. et al. (2018) Molecular basis of differential nitrogen use efficiencies and nitrogen source preferences in contrasting Arabidopsis accessions. *Scientific Reports*, v. 8, n. 1, p. 3373.

Meyer, C.; Stitt, M. (2001) Nitrate Reduction and signalling. Em: *Plant Nitrogen*. Berlin, Heidelberg: Springer Berlin Heidelberg, 2001. p. 37–59.

Moll, R. H.; Kamprath, E. J.; Jackson, W. A. (1982) Analysis and Interpretation of Factors Which Contribute to Efficiency of Nitrogen Utilization [1]. *Agronomy Journal*, v. 74, n. 3, p. 562–564.

Mu, X. et al. (2016) Within-Leaf Nitrogen Allocation in Adaptation to Low Nitrogen Supply in Maize during Grain-Filling Stage. *Frontiers in Plant Science*, v. 7.

Mu, X. et al. (2018) Dynamic remobilization of leaf nitrogen components in relation to photosynthetic rate during grain filling in maize. *Plant Physiology and Biochemistry*, v. 129, p. 27–34.

Mu, X.; Chen, Y. (2021) The physiological response of photosynthesis to nitrogen deficiency. *Plant Physiology and Biochemistry*, v. 158, p. 76–82.

Mundim, G. et al. (2014) Early evaluation of popcorn hybrids for vegetative use efficiencyof nitrogen and phosphorus and secondary traits. *Maydica,* v. 59, p. 331–328.

Murota, K. et al. (1994) Changes Related to Salt Tolerance in Thylakoid Membranes of Photoautotrophically Cultured Green Tobacco Cells. *Plant and Cell Physiology*.

Nanjo, Y. et al. (2012) Mass spectrometry-based analysis of proteomic changes in the root tips of flooded soybean seedlings. *Journal of Proteome Research*, v. 11, n. 1, p. 372–385.

Nascimento, L. B. Dos S.; Tattini, M. (2022) Beyond Photoprotection: The Multifarious Roles of Flavonoids in Plant Terrestrialization. *International Journal of Molecular Sciences*, v. 23, n. 9, p. 5284.

Nasielski, J.; Earl, H.; Deen, B. (2019a) Luxury Vegetative Nitrogen Uptake in Maize Buffers Grain Yield Under Post-silking Water and Nitrogen Stress: A Mechanistic Understanding. *Frontiers in Plant Science*, v. 10.

Ning, P.; Fritschi, F. B.; Li, C. (2017) Temporal dynamics of post-silking nitrogen fluxes and their effects on grain yield in maize under low to high nitrogen inputs. *Field Crops Research*, v. 204, p. 249–259.

Ohkubo, Y.; Kuwata, K.; Matsubayashi, Y. (2021) A type 2C protein phosphatase activates high-affinity nitrate uptake by dephosphorylating NRT2.1. *Nature Plants*, v. 7, n. 3, p. 310–316.

Ozaki, H. et al. (2022) Low N level increases the susceptibility of PSI to photoinhibition induced by short repetitive flashes in leaves of different rice varieties. *Physiologia Plantarum*, v. 174, n. 2.

Pampana, S.; Mariotti, M. (2021) Durum Wheat Yield and N Uptake as Affected by N Source, Timing, and Rate in Two Mediterranean Environments. *Agronomy*, v. 11, n. 7, p. 1299.

Pandian, B. A. et al. (2020) Role of Cytochrome P450 Enzymes in Plant Stress Response. *Antioxidants*, v. 9, n. 5, p. 454.

Paponov, I. A.; Engels, C. (2005) Effect of nitrogen supply on carbon and nitrogen partitioning after flowering in maize. *Journal of Plant Nutrition and Soil Science*, v. 168, n. 4, p. 447–453.

Paterniani, E.; Campos, M. S. (2005) Melhoramento de milho. In: Borém, A. (Ed.). *Melhoramento de espécies cultivadas*. 2. ed. Viçosa, MG: Editora UFV, p. 491–552.

Peterlini, E. et al. Diallel analysis of popcorn populations for yield, popping expansion and resistance to fall armyworm. *Revista Ceres*, v. 67, n. 4, p. 288–295.

Pinto, V. B. et al. (2021) Uncovering the transcriptional response of popcorn (Zea mays L. var. everta) under long-term aluminum toxicity. *Scientific Report***s**, v. 11, n. 1, p. 19644.

Plénet, D.; Lemaire, G. (1999) Relationships between dynamics of nitrogen uptake and dry matter accumulation in maize crops. Determination of critical N concentration. *Plant and Soil*, v. 216, n. 1/2, p. 65–82.

Plett, D. C. et al. (2018) Nitrate uptake and its regulation in relation to improving nitrogen use efficiency in cereals. *Seminars in Cell & Developmental Biology*, v. 74, p. 97–104.

Prinsi, B.; Espen, L. (2018) Time-Course of Metabolic and Proteomic Responses to Different Nitrate/Ammonium Availabilities in Roots and Leaves of Maize. *International Journal of Molecular Sciences*, v. 19, n. 8, p. 2202.

Quan, X. et al. (2019) Transcriptomic analysis reveals adaptive strategies to chronic low nitrogen in Tibetan wild barley. *BMC Plant Biology*, v. 19, n. 1, p. 68.

R Core Team (2023) *R: A Language and ENVIRONMENT for statistical Computing*. Vienna, AustriaR Foundation for Statistical Computing. Available in: <http://www.r-project.org/>

Raddatz, N. et al. (2020) Coordinated Transport of Nitrate, Potassium, and Sodium. *Frontiers in Plant Science*, v. 11.

Ramalho, J. C. et al. (1997) Photosynthetic responses of Coffea arabica leaves to a short-term high light exposure in relation to N availability. *Physiologia Plantarum*, v. 101, n. 1, p. 229–239.

Ramanna, L. et al. (2014) The optimization of biomass and lipid yields of Chlorella sorokiniana when using wastewater supplemented with different nitrogen sources. *Bioresource Technology*, v. 168, p. 127–135.

Rangel, R. M. et al. (2008) Genetic parameters in parents and hybrids of circulant diallel in popcorn. *Genetics and Molecular Research*, v. 7, n. 4, p. 1020–1030.

Rashid, M. T.; Voroney, P.; Parkin, G. (2005) Predicting nitrogen fertilizer requirements for corn by chlorophyll meter under different N availability conditions. *Canadian Journal of Soil Science*, v. 85, n. 1, p. 149–159.

Raun, W. R.; Johnson, G. V. (1999) Improving Nitrogen Use Efficiency for Cereal Production. *Agronomy Journal*, v. 91, n. 3, p. 357–363.

Reis, R. S. et al. (2021) Pretreatment free of 2,4-dichlorophenoxyacetic acid improves the differentiation of sugarcane somatic embryos by affecting the hormonal balance and the accumulation of reserves. *Plant Cell, Tissue and Organ Culture (PCTOC)*, v. 145, n. 1, p. 101–115.

Ren, B. et al. (2021) Effects of Urea-Ammonium Nitrate Solution on Yield, N2O Emission, and Nitrogen Efficiency of Summer Maize Under Integration of Water and Fertilizer. *Frontiers in Plant Science*, v. 12.

Riache, M. et al. (2021) Combining Ability and Heterosis of Algerian Saharan Maize Populations (Zea mays L.) for Tolerance to No-Nitrogen Fertilization and Drought. *Agronomy*, v. 11, n. 3, p. 492..

Riache, M. et al. (2022) Assessment of Nitrogen Use Efficiency in Algerian Saharan Maize Populations for Tolerance under Drought and No-Nitrogen Stresses. *Agronomy*, v. 12, n. 5, p. 1123.

Rodrigues, M. C. et al. (2017) Genotypic variation and relationships among nitrogen-use efficiency and agronomic traits in tropical maize inbred lines. *Genetics and Molecular Research*, v. 16, n. 3.

Rodrigues, W. P. et al. (2018) Stomatal and photochemical limitations of photosynthesis in coffee (Coffea spp.) plants subjected to elevated temperatures. *Crop and Pasture Science*, v. 69, n. 3, p. 317.

Sakakibara H et al. (1992) Differential Effects of Nitrate and Light on the Expression of Glutamine Synthetases and Ferredoxin-Dependent Glutamate Synthase in Maize. *Plant and Cell Physiology*.

Sanagi, M. et al. (2021) Low nitrogen conditions accelerate flowering by modulating the phosphorylation state of FLOWERING BHLH 4 in *Arabidopsis*. *Proceedings of the National Academy of Sciences*, v. 118, n. 19.

Santos, D. L. et al. (2021a) Partial root-zone drying in field-grown papaya: Gas exchange, yield, and water use efficiency. *Agricultural Water Management*, v. 243, p. 106421.

Santos, A. (2017) Dos et al. GGE Biplot projection in discriminating the efficiency of popcorn lines to use nitrogen. *Ciência e Agrotecnologia*, v. 41, n. 1, p. 22–31.

Santos, A. (2019) Dos et al. Relative importance of gene effects for nitrogen-use efficiency in popcorn. *PLOS ONE*, v. 14, n. 9, p. e0222726.

Santos, T. De O. (2021b) et al. Phenotyping Latin American Open-Pollinated Varieties of Popcorn for Environments with Low Water Availability. *Plants*, v. 10, n. 6, p. 1211.

Santos, T. De O. et al. (2022b) Additive and Non-Additive Effects on the Control of Key Agronomic Traits in Popcorn Lines under Contrasting Phosphorus Conditions. *Plants*, v. 11, n. 17, p. 2216.

Santos, T. De O. et al. (2023) Exploring the Potential of Heterosis to Improve Nitrogen Use Efficiency in Popcorn Plants. *Plants*, v. 12, n. 11, p. 2135.

Scapim, C. A. et al. (2006) Componentes genéticos de médias e depressão por endogamia em populações de milho-pipoca. *Ciência Rural*, v. 36, n. 1, p. 36–41.

Scharf, P. C.; Brouder, S. M.; Hoeft, R. G. (2006) Chlorophyll Meter Readings Can Predict Nitrogen Need and Yield Response of Corn in the North-Central USA. *Agronomy Journal*, v. 98, n. 3, p. 655–665.

Gerhardt, I. F. S. et al. (2019) Genetic effects on the efficiency and responsiveness to phosphorus use in popcorn as estimated by diallel analysis. *PLOS ONE*, v. 14, n. 5, p. e0216980.

Schneider, H. M. et al. (2021) Nodal root diameter and node number in maize (*Zea mays* L.) interact to influence plant growth under nitrogen stress. *Plant Direct*, v. 5, n. 3.

Schwantes, I. A. et al. (2018) Inheritance of resistance to Fusarium ear rot in popcorn. *Crop Breeding and Applied Biotechnology*, v. 18, n. 1, p. 81–88.

Serna-Saldivar, S. O. (2022) Popcorn and Other Puffed Grains. In: *Snack Foods: Processing, Innovation, and Nutritional Aspects*. 1. ed. Boca Raton: CRC Press.

Serôdio, J. et al. (2007) Rapid light-response curves of chlorophyll fluorescence in microalgae: relationship to steady-state light curves and non-photochemical quenching in benthic diatom-dominated assemblages. *Photosynthesis Research*, v. 90, n. 1, p. 29–43.

Sheoran, S. et al. (2021) Nitrogen fixation in maize: breeding opportunities. *Theoretical and Applied Genetics*, v. 134, n. 5, p. 1263–1280.

Silva, V. et al. (2010) Inheritance for economically important traits in popcorn from distinct heterotic groups by Hayman's diallel. *Cereal Research Communications*, v. 38, n. 2, p. 272–284.

SimkIN, A. J. et al. (2017) Overexpression of the RieskeFeS Protein Increases Electron Transport Rates and Biomass Yield. *Plant Physiology*, v. 175, n. 1, p. 134–145.

Simons, M. et al. (2014) Nitrogen-use efficiency in maize (Zea mays L.): from "omics" studies to metabolic modelling. *Journal of Experimental Botany*, v. 65, n. 19, p. 5657–5671.

Sinha, S. et al. (2018) ranscriptome Analysis of Two Rice Varieties Contrasting for Nitrogen Use Efficiency under Chronic N Starvation Reveals Differences in Chloroplast and Starch Metabolism-Related Genes. *Genes,* v. 9, n. 4, p. 206.

Soares, C. et al. (2019) Plants facing oxidative challenges—A little help from the antioxidant networks. *Environmental and Experimental Botany*, v. 161, p. 4–25, maio 2019.

Souza, L. V. De et al. (2008) Genetic control of grain yield and nitrogen use efficiency in tropical maize. *Pesquisa Agropecuária Brasileira*, v. 43, n. 11, p. 1517–1523.

Springmann, M. et al. (2018) Options for keeping the food system within environmental limits. *Nature*, v. 562, n. 7728, p. 519–525.

Sugihara, K. et al. (2000) Molecular Characterization of cDNA Encoding Oxygen Evolving Enhancer Protein 1 Increased by Salt Treatment in the Mangrove Bruguiera gymnorrhiza. *Plant and Cell Physiology*, v. 41, n. 11, p. 1279–1285.

Suzuki, A.; Knaff, D. B. (2005) Glutamate synthase: structural, mechanistic and regulatory properties, and role in the amino acid metabolism. *Photosynthesis Research*, v. 83, n. 2, p. 191–217.

Tabuchi, M.; Abiko, T.; Yamaya, T. (2007) Assimilation of ammonium ions and reutilization of nitrogen in rice (Oryza sativa L.). *Journal of Experimental Botany*, v. 58, n. 9, p. 2319–2327.

Taiz, L.; Zeiger, E. (2016*) Plant Physiology*. 6. ed. [s.l.] Sinauer Associates, 2016.

Tantray, A. Y.; Bashir, S. S.; Ahmad, A. (2020) Low nitrogen stress regulates chlorophyll fluorescence in coordination with photosynthesis and Rubisco efficiency of rice. *Physiology and Molecular Biology of Plants*, v. 26, n. 1, p. 83–94.

Taylor, A. R.; Bloom, A. J. (1998) Ammonium, nitrate, and proton fluxes along the maize root. *Plant, Cell and Environment*, v. 21, n. 12, p. 1255–1263.

Thi Nong, H. et al. (2020) Effect of Seedling Nitrogen Condition on Subsequent Vegetative Growth Stages and Its Relationship to the Expression of Nitrogen Transporter Genes in Rice. *Plants*, v. 9, n. 7, p. 861.

Thornton, L. E. et al. (2004) Homologs of Plant PsbP and PsbQ Proteins Are Necessary for Regulation of Photosystem II Activity in the *Cyanobacterium synechocystis* 6803[W]. *The Plant Cell*, v. 16, n. 8, p. 2164–2175.

TIAN, F. et al. (2019) PlantRegMap: charting functional regulatory maps in plants. *Nucleic Acids Research*.

Tilman, D. et al. (2001) Diversity and Productivity in a Long-Term Grassland Experiment. *Science*, v. 294, n. 5543, p. 843–845.

Torres, L. G. et al. (2018) Multi-trait multi-environment Bayesian model reveals G x E interaction for nitrogen use efficiency components in tropical maize. *PLOS ONE*, v. 13, n. 6, p. e0199492.

Torresi, F. et al. (2023) Two phosphoenolpyruvate carboxykinases with differing biochemical properties in *Chlamydomonas reinhardtii*. *FEBS Letters*, v. 597, n. 4, p. 585–597.

Trachsel, S. et al. (2013) Maize root growth angles become steeper under low N conditions. *Field Crops Research*, v. 140, p. 18–31.

Trevisan, S. et al. (2008) Expression of two maize putative nitrate transporters in response to nitrate and sugar availability. *Plant Biology*, v. 10, n. 4, p. 462–475.

Tripathi, D. et al. (2020) Reactive Oxygen Species, Antioxidant Agents, and DNA Damage in Developing Maize Mitochondria and Plastids. *Frontiers in Plant Science*, v. 11.

Tripathy, M. K. et al. (2017) Ectopic expression of PgRab7 in rice plants (Oryza sativa L.) results in differential tolerance at the vegetative and seed setting stage during salinity and drought stress. *Protoplasma*, v. 254, n. 1, p. 109–124.

Uauy, C. et al. (2006) A NAC Gene Regulating Senescence Improves Grain Protein, Zinc, and Iron Content in Wheat. *Science*, v. 314, n. 5803, p. 1298–1301.

Urban, A. et al. (2021) Understanding Maize Response to Nitrogen Limitation in Different Light Conditions for the Improvement of Photosynthesis. *Plants*, v. 10, n. 9, p. 1932.

USDA. **International Baseline Data**.

Vidal, E. A. et al. (2013) Integrated RNA-seq and sRNA-seq analysis identifies novel nitrate-responsive genes in Arabidopsis thaliana roots. *BMC Genomics*, v. 14, n. 1, p. 701.

Vittorazi, C. et al. (2013) Seleção de pré-cultivares de milho-pipoca baseado em índices não paramétricos. *Revista Ciência Agronômica*, v. 44, n. 2, p. 356–362.

Walker, R. P.; Chen, Z.-H.; Famiani, F. (2021) Gluconeogenesis in Plants: A Key Interface between Organic Acid/Amino Acid/Lipid and Sugar Metabolism. *Molecules*, v. 26, n. 17, p. 5129.

Wang, Y. et al. (2005) Response of Root Morphology to Nitrate Supply and its Contribution to Nitrogen Accumulation in Maize. *Journal of Plant Nutrition*, v. 27, n. 12, p. 2189–2202.

Wang, Y. et al. (2020) The Role of Gibberellins in Regulation of Nitrogen Uptake and Physiological Traits in Maize Responding to Nitrogen Availability. *International Journal of Molecular Sciences*, v. 21, n. 5, p. 1824.

Wang, Y. et al. (2022) Comparative Proteomic Analysis of Two Contrasting Maize Hybrids' Responses to Low Nitrogen Stress at the Twelve Leaf Stage and Function Verification of ZmTGA Gene. *Genes*, v. 13, n. 4, p. 670.

Wang, Y.-Y. et al. (2018) Nitrate Transport, Signaling, and Use Efficiency. *Annual Review of Plant Biology*, v. 69, n. 1, p. 85–122.

Wang, Z. et al. (2019) Physiological Basis of Heterosis for Nitrogen Use Efficiency of Maize. *Scientific Reports*, v. 9, n. 1, p. 18708.

Weatherwax, P. (1922) The popping of corn. *Proceedings of the Indiana Academy Science*, v. 31, p. 149–153.

Wei, S. et al. (2015) The role of nitrogen in leaf senescence of summer maize and analysis of underlying mechanisms using comparative proteomics. *Plant Science*, v. 233, p. 72–81.

Weitzman, J. N. et al. (2022) Deep soil nitrogen storage slows nitrate leaching through the vadose zone. *Agriculture, Ecosystems & Environment*, v. 332, p. 107949.

Welsch, R. et al. (2008) A Third Phytoene Synthase Is Devoted to Abiotic Stress-Induced Abscisic Acid Formation in Rice and Defines Functional Diversification of Phytoene Synthase Genes . *Plant Physiology*, v. 147, n. 1, p. 367–380.

White, S.; Anandraj, A.; Bux, F. (2011) PAM fluorometry as a tool to assess microalgal nutrient stress and monitor cellular neutral lipids. *Bioresource Technology*, v. 102, n. 2, p. 1675–1682.

Worku, M. et al. (2007) Nitrogen Uptake and Utilization in Contrasting Nitrogen Efficient Tropical Maize Hybrids. *Crop Science*, v. 47, n. 2, p. 519–528.

Wu, Y. et al. (2019) Effect of low-nitrogen stress on photosynthesis and chlorophyll fluorescence characteristics of maize cultivars with different low-nitrogen tolerances. *Journal of Integrative Agriculture*, v. 18, n. 6, p. 1246–1256.

Xiao, M. et al. (2021) The Multiple Roles of Ascorbate in the Abiotic Stress Response of Plants: Antioxidant, Cofactor, and Regulator. *Frontiers in Plant Science*, v. 12.

Xu, J.; Wang, X.; Guo, W. (2015) The cytochrome P450 superfamily: Key players in plant development and defense. *Journal of Integrative Agriculture*, v. 14, n. 9, p. 1673–1686.

Yadav, S. et al. (2020) Effect of Abiotic Stress on Crops. Em: *Sustainable Crop Production*. [s.l.] IntechOpen, 2020.

Yang, Y. et al. (2012) Nitrogen Concentration and Dry-Matter Accumulation in Maize Crop: Assessing Maize Nitrogen Status with an Allometric Function and a Chlorophyll Meter. *Communications in Soil Science and Plant Analysis*, v. 43, n. 11, p. 1563–1575.

Yang, Z. et al. (2019) Physiological responses and small RNAs changes in maize under nitrogen deficiency and resupply. *Genes & Genomics*, v. 41, n. 10, p. 1183–1194, 16 out. 2019.

Zadražnik, T.; Moen, A.; Šuštar-Vozlič, J. (2019) Chloroplast proteins involved in drought stress response in selected cultivars of common bean (Phaseolus vulgaris L.). *3 Biotech*, v. 9, n. 9, p. 331.

Zhang, H. et al. (2021) Effects of Nitrogen Fertilizer on Photosynthetic Characteristics, Biomass, and Yield of Wheat under Different Shading Conditions. *Agronomy*, v. 11, n. 10, p. 1989.

Zhang, J. et al. (2008) Sensitivity of Chlorophyll Meters for Diagnosing Nitrogen Deficiencies of Corn in Production Agriculture. *Agronomy Journal*, v. 100, n. 3, p. 543–550.

Zhang, Q. et al. (2022) Dynamic Changes in the Antioxidative Defense System in the Tea Plant Reveal the Photoprotection-Mediated Temporal Accumulation of Flavonoids under Full Sunlight Exposure. *Plant and Cell Physiology*, v. 63, n. 11, p. 1695–1708..

Zhang, Q.-Y. et al. (20129 Constitutive accumulation of zeaxanthin in tomato alleviates salt stress-induced photoinhibition and photooxidation. *Physiologia Plantarum*, v. 146, n. 3, p. 363–373..

Zhang, X. et al. (2015) Managing nitrogen for sustainable development. *Nature*, v. 528, n. 7580, p. 51–59.

Zhao, S. et al. (2018) RnaSeqSampleSize: real data based sample size estimation for RNA sequencing. *BMC Bioinformatics*, v. 19, n. 1, p. 191.

Zhong, C. et al. (2019) Nitrogen-mediated alleviation of photosynthetic inhibition under moderate water deficit stress in rice (Oryza sativa L.). *Environmental and Experimental Botany*, v. 157, p. 269–282.

Zhong, L. et al. (2015) AtTGA4, a bZIP transcription factor, confers drought resistance by enhancing nitrate transport and assimilation in Arabidopsis thaliana. *Biochemical and Biophysical Research Communications*, v. 457, n. 3, p. 433–439.

Zhou, H.; Liu, S. K.; Yang, C. P. (2011) Over-Expression of a NAD-Malic Enzyme Gene from Rice in *Arabidopsis thaliana* Confers Tolerances to Several Abiotic Stresses. *Advanced Materials Research*, v. 393–395, p. 863–866.

Zhu, L. et al. (2022) Low nitrogen supply inhibits root growth but prolongs lateral root lifespan in cotton*. Industrial Crops and Products*, v. 189, p. 115733.

Zinsly, J. R.; Machado, J. A. (1987) Milho-pipoca. In: Paterniani, E.; Viegas, G. P. (Eds.). *Melhoramento e produção do milho*. Campinas, SP: Fundação Cargill, 1987. p. 413–421.

Zörb, C. et al. (2005) Does H^+ pumping by plasmalemma ATPase limit leaf growth of maize (*Zea mays*) during the first phase of salt stress? *Journal of Plant Nutrition and Soil Science*, v. 168, n. 4, p. 550–557.

Zuffo, L. T. et al. (2021) Assessing genotypic variation for nitrogen use efficiency and associated traits in Brazilian maize hybrids grown under low and high nitrogen inputs. *Euphytica,* v. 217, n. 4, p. 71.

Zuluaga, D. L.; Sonnante, G. (2019) The Use of Nitrogen and Its Regulation in Cereals: Structural Genes, Transcription Factors, and the Role of miRNAs. *Plants*, v. 8, n. 8, p. 294.

APPENDIX

Supplementary Table 1 Chemical and particle-size analysis of the substrate used to evaluate four lines and 12 diallel popcorn hybrids under contrasting nitrogen conditions

Sample	pH	S-SO_4	P	K	Ca	Mg	Al	Na	H+Al	C	OM	CEC	SB	BS	m	NaSI	Fe	Cu	Zn	Mn	B	N
	H_2O	mg/dm^3							mmol$_c$/dm^3										mg/dm^3							%
1	6.7	2	8	0.6	7.9	1.9	0	0.4	3.3	1.3	2.24	14.1	10.8	77	0	3	217.2	0.12	2.3	33.6	0.33	0.18
2	6.7	2	8	0.5	7.3	1.9	0	0.7	4.1	1.3	2.24	15.5	10.4	74	0	5	245.0	0.04	2.6	34.0	0.37	0.17
3	6.7	2	8	0.6	7.6	1.9	0	0.5	4	1.3	2.24	15	10.6	75	0	5	230.0	0.10	2.5	33.0	0.38	0.17

Extractors: P, Na, K, Fe, Zn, Mn, Cu – Mehlich-1 Extractor; Ca, Mg, Al – KCl Extractor (1 mol/L); H + Al – Calcium Acetate Extractor (0.5 mol/L and pH 7.0); B – Hot water extractor; S – Monocalcium Phosphate Extractor. **Abbreviations:** SB – Sum of Exchangeable Bases; CEC – Cation Exchange Capacity at pH 7.0; BS – Base Saturation Index; m – Aluminum saturation index; NaSI – Sodium saturation index; and OM – Organic matter (C Org × 1,724, Walkley-Black

Supplementary Table 2 Principal component analysis (PCA) for 28 morpho-agronomic and physiological traits evaluated in popcorn genotypes under contrasting nitrogen (N) availability

Principal component	Eigenvalue	Variance (%)	Cumulative variance (%)
High N			
1	14.78	52.80	52.80
2	9.04	32.30	85.10
3	4.17	14.90	100.00
Low N			
1	12.50	44.64	44.64
2	10.10	36.06	80.70
3	5.40	19.30	100.00

Supplementary Table 3 R2 statistics to test the proportional contribution of each source of variation in 28 morpho-agronomic and physiological traits evaluated in popcorn genotypes under contrasting nitrogen (N) availability

Trait	Sum of Squares				R^2 statistics		
	G	N	G × N	Total	R^2_G	R^2_N	$R^2_{G\times N}$
PH	1351.56	166.35	610.74	2128.64	**0.635**	0.078	0.287
SD	112.27	294.39	54.76	461.41	0.243	**0.638**	0.119
LA	46743.95	83920.25	28458.37	159122.57	0.294	**0.527**	0.179
LDM	51.28	131.37	27.61	210.26	0.244	**0.625**	0.131
SDM	33.27	42.75	19.42	95.44	0.349	**0.448**	0.203
STDM	158.28	324.06	81.33	563.67	0.281	**0.575**	0.144
RDM	5.51	2.84	3.46	11.82	**0.467**	0.241	0.293
LNC	582.17	2322.93	432.16	3337.27	0.174	**0.696**	0.129
SNC	585.31	2722.78	471.36	3779.45	0.155	**0.720**	0.125
RNC	126.22	258.19	136.31	520.72	0.242	**0.496**	0.262
STNC	1776.81	10075.55	1512.41	13364.76	0.133	**0.754**	0.113
PNC	2530.05	13559.60	2383.28	18472.93	0.137	**0.734**	0.129
NUE	825099.01	3563988.70	565939.84	4955027.55	0.167	**0.719**	0.114
NUpE_cR	11.84	972.43	11.34	995.61	0.012	**0.977**	0.011
NUpE_sR	8.82	570.26	7.92	587.00	0.015	**0.971**	0.014
NUtE_cR	91009.80	32707.18	39096.94	162813.93	**0.559**	0.201	0.240
NUtE_sR	57696.23	25439.84	22885.31	106021.37	**0.544**	0.240	0.216
NTrE	0.018	0.028	0.015	0.060	0.301	**0.458**	0.241
A	646.64	1250.61	466.58	2363.83	0.274	**0.529**	0.197
gs	0.087	0.149	0.078	0.314	0.277	**0.474**	0.249
Ci	21125.85	9564.15	16386.92	47076.93	**0.449**	0.203	0.348
E	8.79	4.91	13.31	27.02	0.326	0.182	**0.493**
Ci/Ca	0.281	0.065	0.233	0.579	**0.485**	0.112	0.403
Fv/Fm	0.784	0.048	0.294	1.126	**0.696**	0.043	0.261
Chl	628.85	1273.00	364.44	2266.29	0.277	**0.562**	0.161
Flav	0.489	0.107	0.364	0.961	**0.509**	0.111	0.379
Anth	0.172	0.091	0.148	0.411	0.418	0.221	0.361
NBI	1118.23	4388.86	1208.65	6715.75	0.167	**0.654**	0.180

Values in bold represents the ones with biggest contribution to their respective Sum of Square. R^2_G – Genotypic contribution to the observed variation in genotypes; R^2_N – Nitrogen condition contribution to the observed variation in genotypes; $R^2_{G\times N}$ – Genotype by N interaction contribution to the observed variation in genotypes; PH – plant height (cm); SD – stem diameter (mm); LA – leaf area (cm^2); LDM – leaf dry matter (g); SDM – stem dry matter (g); STDM – shoot dry matter (g); RDM – root dry matter (g); LNC – leaf N content (mg of N kg^{-1}); SNC – stem N content (mg of N kg^{-1}); RNC – root N content (mg of N kg^{-1}); STNC – shoot N content (mg of N kg^{-1}); PNC – plant N content (mg of N kg^{-1}); (NUE – N use efficiency; NUpE_cR – N uptake efficiency with root N content; NUpE_sR – N uptake efficiency without root N content; NUtE_cR – N utilization efficiency with the content of N in the root; NUtE_sR – N utilization efficiency without the content of N in the root; NTrE – N translocation efficiency; A – net CO2 assimilation rate; gs – stomatal conductance; Ci – intercellular concentration of CO_2; E – transpiration rate; Ci/Ca – ratio between the intercellular and external concentration of CO2; F_v/F_m – photochemical efficiency of photosystem II; Chl – relative chlorophyll content; Flav – relative content of flavonoids; Anth – relative anthocyanin content; NBI – nitrogen balance index

Supplementary Table 4 Analysis of variance and quadratic components for 28 characters evaluated in 16 popcorn genotypes under contrasting nitrogen conditions, according to the model proposed by Griffing (1956) for a diallel involving four lines, their F1s, and reciprocal hybrids.

Trait	High N condition											Low N condition									
	General combining ability			Specific combining ability			Reciprocal effect			Residual Effect		General combining ability			Specific combining ability			Reciprocal effect			Residual Effect	
	MS	φg	%	MS	φs	%	MS	φrc	%	Value	%	MS	φg	%	MS	φs	%	MS	φrc	%	Value	%
PH	**	1.2	3.1	**	29.57	74	**	8.655	22	0.571	1.4	**	5.65	15.39	**	27.96	76	**	3.077	8.4	0.04	0.1
SD	**	0.4	11	**	1.34	37	**	1.871	51	0.029	0.8	**	0.24	14.31	**	1.21	73	**	0.208	13	0.005	0.3
LA	**	62	1.9	**	1594	49	**	1594	49	1.521	0.1	**	73.67	8.17	**	368	41	**	458.8	51	0.505	0.1
LDM	**	0.1	5.1	**	1.428	59	**	0.868	36	0.008	0.3	**	0.05	12.19	**	0.26	59	**	0.124	29	0.001	0.1
SDM	**	0.1	3	**	1.08	63	**	0.578	34	0.002	0.1	**	0.05	15.74	**	0.22	71	**	0.039	13	4E-04	0.1
STDM	**	0.3	3.9	**	4.813	63	**	2.578	34	0.006	0.1	**	0.20	14.82	**	0.87	66	**	0.25	19	0.001	0.1
RDM	**	0	8.3	**	0.095	46	**	0.093	45	0	0.1	**	0.01	6.25	**	0.07	69	**	0.024	22	0.002	2
LNC	**	0.6	3	**	7.141	36	**	12.2	61	0.15	0.8	**	1.06	6.79	**	11.12	71	**	3.409	22	0.076	0.5
SNC	**	0.6	2.1	**	7.92	27	**	21.05	71	0.041	0.1	**	0.15	2.72	**	4.41	81	**	0.391	7.2	0.509	9.3
RNC	**	0.1	0.8	**	1.417	21	**	5.144	77	0.081	1.2	**	0.07	3.43	**	1.34	70	**	0.484	25	0.037	1.9
STNC	**	2	2.2	**	23.53	27	**	62.72	71	0.213	0.2	**	1.11	16.42	**	1.11	16	**	4.057	60	0.479	7.1
PNC	**	2.7	2.1	**	24.83	19	**	100.9	78	0.286	0.2	**	1.07	4.16	**	17.50	68	**	6.618	26	0.454	1.8
NUE	**	98	3.9	**	1597	63	**	854.9	34	1.857	0.1	**	6671.84	14.82	**	29796	66	**	8535	19	30.08	0.1
NUPE_cR	**	0	2.1	**	0.008	19	**	0.033	78	0	0.2	**	0.04	4.16	**	0.60	68	**	0.226	26	0.016	1.8
NUpE_sR	**	0	2.2	**	0.008	27	**	0.021	71	0	0.2	**	0.04	6.03	**	0.44	69	**	0.139	22	0.016	2.6
NUtE_cR	**	105	3.2	**	2321	70	**	908.2	27	4.047	0.1	**	212.35	13.36	**	926	58	**	441.6	28	9.129	0.6
NUtE_sR	**	68	3.3	**	1365	66	**	622.2	30	2.267	0.1	**	132.65	14.06	**	555	59	**	252.2	27	3.09	0.3
NTrE	**	0	0.2	**	0.001	78	**	0	20	0	2.4	**	0.00	9.56	**	0.00	71	**	0	14	0	5.5

Supplementary Table 4 – Cont.

Trait—	High N condition											Low N condition									
	General combining ability			Specific combining ability			Reciprocal effect			Residual Effect		General combining ability			Specific combining ability			Reciprocal effect			Residual Effect	
	MS	φg	%	MS	φs	%	MS	φrc	%	Value	%	MS	φg	%	MS	φs	%	MS	φrc	%	Value	%
A	**	3.5	15	**	14.25	62	**	4.691	20	0.528	2.3	**	0.88	6.09	**	6.32	44	**	6.799	47	0.426	3
gs	**	0	13	**	0.002	62	**	0.001	18	0	7.1	**	0.00	0.62	**	0.00	37	**	0.001	55	0	7.5
Ci	**	31	5.5	**	317.2	56	**	149	26	70.71	12	**	37.47	4.29	**	530	61	**	299.4	34	7.109	0.8
E	**	0	9.8	**	0.252	53	**	0.161	34	0.015	3.1	**	0.02	7.03	**	0.14	50	**	0.115	41	0.006	2.1
Ci/Ca	**	0	6	**	0.004	58	**	0.001	12	0.002	24	**	0.00	9.4	**	0.01	58	**	0.004	29	4E-04	3.2
Fv/Fm	**	0	4.3	**	0.004	49	**	0.003	41	0	5.9	**	0.00	5.28	**	0.01	50	**	0.013	43	4E-04	1.2
Chl	**	0.4	1.3	**	15.01	54	**	10.73	39	1.716	6.2	**	0.30	2.3	**	10.08	77	**	1.938	15	0.802	6.1
Flav	**	0	11	**	0.01	49	**	0.006	29	0.002	11	**	0.00	5.72	**	0.01	74	**	0.002	20	1E-04	0.6
Anth	**	0	2.4	**	0	60	**	0	37	3E-06	0.8	ns	0.00	0	ns	0.00	0	ns	0.002	7.3	0.02	93
NBI	**	3.4	4.9	**	38.61	56	**	14.39	21	12.99	19	**	1.61	6.1	**	16.80	64	**	6.519	25	1.468	5.6

MS – Mean Square; φg, φs and φrc – quadratic component associated with general and specific combining abilities and reciprocal effects, respectively; PH – plant height (cm); SD – stem diameter (mm); LA – leaf area (cm2); LDM – leaf dry matter (g); SDM – stem dry matter (g); STDM – shoot dry matter (g); RDM – root dry matter (g); LNC – leaf N content (mg of N kg^{-1}); SNC – stem N content (mg of N kg^{-1}); RNC – root N content (mg of N kg^{-1}); STNC – shoot N content (mg of N kg^{-1}); PNC – plant N content (mg of N kg^{-1}); NUE – N use efficiency; NUpE_cR – N uptake efficiency with root N content; NUpE_sR – N uptake efficiency without root N content; NUtE_cR – N utilization efficiency with the N content of the root; NUtE_sR – N utilization efficiency without the N content of the root; NTrE – N translocation efficiency; A – net CO_2 assimilation rate; gs – stomatal conductance; Ci – intercelullar concentration of CO_2; E – transpiration rate; Ci/Ca – ratio between the internal and external concentration of CO2; Fv/Fm – photochemical efficiency of photosystem II; Chl – relative chlorophyll content; Flav – relative flavonoid content; Anth – relative anthocyanin content; NBI – nitrogen balance index. Significance levels: * $p \leq 0.05$; ** $p \leq 0.01$; and ns = not significant.

Supplementary Table 5 Complete list of proteins identified in the leaves of two lines of popcorn lines (Zea mays everta) contrasting for NUE grown under high (HN) and low (LN) N conditions.

Accession	Description	Reported peptides	Average Normalized Ion Count L80 HN	Average Normalized Ion Count L80 LN	Average Normalized Ion Count P2 HN	Average Normalized Ion Count P2 LN	t-test L80 LN/HN	t-test P2 LN/HN	Log_2 FC L80 LN/HN	Log_2 FC P2 LN/HN	Differential Accumulation L80 LN/HN	Differential Accumulation P2 LN/HN
Q06XS3	Lipoxygenase	57	475809	283195	553731	294038	0.00114	0.00301	-0.74858	-0.91318	DOWN	DOWN
P17788	50S ribosomal protein L2, chloroplastic	9	108055	54609	111118	48360	0.00807	0.00587	-0.98454	-1.20020	DOWN	DOWN
B8A367	Cysteine synthase	16	135992	70337	44312	26013	0.00173	0.00248	-0.95115	-0.76848	DOWN	DOWN
C0HHC4	Nucleoside diphosphate kinase	8	101335	35323	98094	21844	0.00292	0.00290	-1.52045	-2.16689	DOWN	DOWN
C0P530	Chaperonin 60 subunit beta 2 chloroplastic	32	163319	104358	129833	68136	0.00125	0.00034	-0.64615	-0.93017	DOWN	DOWN
B4FRR1	Inorganic diphosphatase	15	154301	90899	148622	78890	0.01427	0.02085	-0.76340	-0.91373	DOWN	DOWN
B4FN24	Glutaredoxin-dependent peroxiredoxin	5	79708	45416	174154	56628	0.01188	0.02258	-0.81153	-1.62079	DOWN	DOWN
B4FVP6	Electron carrier/ electron transporter/ iron ion binding protein	4	48131	25229	49951	22852	0.00641	0.04445	-0.93188	-1.12817	DOWN	DOWN
A0A1D6EXF1	PDK regulatory protein1	20	107673	64133	133011	55514	0.00952	0.00199	-0.74751	-1.26062	DOWN	DOWN
A0A1D6KKS1	peptidylprolyl isomerase	8	66821	21595	65741	18429	0.00090	0.03342	-1.62959	-1.83479	DOWN	DOWN
A0A804RFC1	Mg-protoporphyrin IX chelatase	18	81203	33931	42506	12519	0.00162	0.00504	-1.25891	-1.76351	DOWN	DOWN
A0A1D6FNK4	60S ribosomal protein L11-1	3	36789	23431	24669	14862	0.03102	0.04994	-0.65085	-0.73108	DOWN	DOWN
P09387	50S ribosomal protein L23, chloroplastic	3	25836	13195	19808	6077	0.01329	0.00899	-0.96938	-1.70468	DOWN	DOWN
P08528	50S ribosomal protein L16, chloroplastic	2	56356	35119	64701	21289	0.00849	0.00002	-0.68230	-1.60369	DOWN	DOWN
B6SST7	50S ribosomal protein L5, chloroplastic	12	67340	35907	70379	24412	0.01226	0.00938	-0.90719	-1.52757	DOWN	DOWN

Supplementary Table 5 - Cont

Accession	Description	Reported peptides	Average Normalized Ion Count L80 HN	Average Normalized Ion Count L80 LN	Average Normalized Ion Count P2 HN	Average Normalized Ion Count P2 LN	t-test L80 LN/HN	t-test P2 LN/HN	Log_2 FC L80 LN/HN	Log_2 FC P2 LN/HN	Differential Accumulation L80 LN/HN	Differential Accumulation P2 LN/HN
A0A1D6GVM3	Delta-aminolevulinic acid dehydratase	17	105965	49966	42421	19545	0.00018	0.00047	-1.08458	-1.11796	DOWN	DOWN
B6T9S0	Thioredoxin X	6	34206	15833	42463	10878	0.01949	0.04712	-1.11134	-1.96478	DOWN	DOWN
B6SLK4	Elongation factor 1-beta	9	88790	36431	74173	20263	0.00218	0.00323	-1.28525	-1.87205	DOWN	DOWN
A0A804Q7A5	RRM domain-containing protein	10	55605	31760	44928	16901	0.01180	0.04495	-0.80803	-1.41047	DOWN	DOWN
A0A804LFM1	40S ribosomal protein S3a	9	47367	31099	35332	19573	0.02035	0.01734	-0.60701	-0.85209	DOWN	DOWN
Q8W1C9	60S ribosomal protein L33-B	3	34155	20010	26630	13129	0.00658	0.04705	-0.77135	-1.02032	DOWN	DOWN
A0A1D6FKV6	Ketol-acid reductoisomerase	16	97546	58611	75625	36736	0.02457	0.02573	-0.73490	-1.04168	DOWN	DOWN
B4FK84	glutathione transferase	4	34652	10501	40563	6056	0.00671	0.01357	-1.72249	-2.74369	DOWN	DOWN
A0A804N6G2	PsbP domain-containing protein	9	35410	11792	41947	14052	0.00410	0.04330	-1.58639	-1.57781	DOWN	DOWN
A0A804P2H5	50S ribosomal protein L21	4	57555	30077	12680	5939	0.03975	0.00353	-0.93630	-1.09421	DOWN	DOWN
B4F9R4	60S ribosomal protein L2	5	71220	43015	75335	41294	0.00464	0.01516	-0.72744	-0.86736	DOWN	DOWN
A0A1D6M323	Ribosomal protein	7	43049	20756	30566	16234	0.00828	0.00820	-1.05242	-0.91287	DOWN	DOWN
B4FWR7	60S ribosomal protein L13	4	22134	11868	20736	10048	0.04765	0.00449	-0.89920	-1.04527	DOWN	DOWN
A0A804Q317	Isocitrate dehydrogenase [NADP]	9	155518	90070	169908	80473	0.00232	0.04421	-0.78796	-1.07818	DOWN	DOWN
A0A1D6IJ76	Glyceraldehyde-3-phosphate dehydrogenase A	4	38701	16568	42362	15040	0.01435	0.01283	-1.22394	-1.49400	DOWN	DOWN
B6U1J2	50S ribosomal protein L11	2	20043	10505	13886	6518	0.01358	0.01842	-0.93211	-1.09122	DOWN	DOWN

Supplementary Table 5 - Cont

Accession	Description	Reported peptides	Average Normalized Ion Count L80 HN	Average Normalized Ion Count L80 LN	Average Normalized Ion Count P2 HN	Average Normalized Ion Count P2 LN	t-test L80 LN/HN	t-test P2 LN/HN	Log_2 FC L80 LN/HN	Log_2 FC P2 LN/HN	Differential Accumulation L80 LN/HN	Differential Accumulation P2 LN/HN
B4FT31	Dehydroascorbate reductase	5	31665	12324	34548	12354	0.00641	0.04140	-1.36142	-1.48356	DOWN	DOWN
B4FH99	Thylakoid lumenal protein TL20.3 chloroplastic	8	19439	10970	19022	6927	0.01701	0.04900	-0.82540	-1.45740	DOWN	DOWN
A0A804UKB5	ATP-dependent Clp protease proteolytic subunit	3	12959	6189	11942	4699	0.00715	0.01989	-1.06614	-1.34551	DOWN	DOWN
C0P4F3	Multiple organellar RNA editing factor 9 chloroplastic	4	30749	14994	36643	15020	0.00169	0.00686	-1.03611	-1.28665	DOWN	DOWN
A0A804P437	Glyceraldehyde-3-phosphate dehydrogenase	6	7623	4170	8475	4031	0.00032	0.00336	-0.87049	-1.07223	DOWN	DOWN
B6T504	Proteasome subunit alpha type	6	18407	10036	17530	8028	0.01823	0.03311	-0.87497	-1.12677	DOWN	DOWN
A0A804LIP7	40S ribosomal protein S7	3	17851	7796	11990	5860	0.00014	0.03594	-1.19519	-1.03301	DOWN	DOWN
A0A804M4P0	30S ribosomal protein S9, chloroplastic	4	46710	16757	32695	9602	0.00233	0.01575	-1.47898	-1.76770	DOWN	DOWN
B4FJH1	RNA-binding (RRM/RBD/RNP motifs) family protein	2	19000	9723	15587	6080	0.03672	0.02685	-0.96663	-1.35816	DOWN	DOWN
A0A1D6JIA9	K(+) efflux antiporter 2 chloroplastic	6	7792	4657	11340	6952	0.03164	0.01337	-0.74252	-0.70582	DOWN	DOWN
B6SLQ7	60S ribosomal protein L23a	2	24721	13380	40204	12303	0.00733	0.01329	-0.88568	-1.70837	DOWN	DOWN
B2LXS7	Single-stranded DNA-binding protein WHY1, chloroplastic	2	11463	6720	5559	2452	0.02087	0.03003	-0.77042	-1.18067	DOWN	DOWN
B4FHA0	Thylakoid lumenal 17.4 kDa protein chloroplastic	3	26644	15990	27618	14386	0.00772	0.00003	-0.73668	-0.94096	DOWN	DOWN
A0A1D6MNJ0	1-deoxy-D-xylulose-5-phosphate reductoisomerase	4	14875	8480	8161	4955	0.03870	0.01339	-0.81073	-0.71975	DOWN	DOWN
A0A1D6KA64	LrgB-like family protein	2	2907	1598	4777	2374	0.04355	0.00255	-0.86295	-1.00859	DOWN	DOWN
A0A1D6K5Y7	Chaperone protein ClpB3 chloroplastic	5	8568	4544	7107	3814	0.00560	0.03733	-0.91496	-0.89787	DOWN	DOWN

Supplementary Table 5 - Cont

Accession	Description	Reported peptides	Average Normalized Ion Count L80 HN	Average Normalized Ion Count L80 LN	Average Normalized Ion Count P2 HN	Average Normalized Ion Count P2 LN	t-test L80 LN/HN	t-test P2 LN/HN	Log_2 FC L80 LN/HN	Log_2 FC P2 LN/HN	Differential Accumulation L80 LN/HN	Differential Accumulation P2 LN/HN
A0A804N8U5	ABC transporter B family member 26, chloroplastic	4	7711	4809	9342	5354	0.00694	0.02892	-0.68105	-0.80324	DOWN	DOWN
B4F8N3	6-phosphofructo-2-kinase/fructose-26-bisphosphatase	6	13092	6142	19596	4390	0.00004	0.00014	-1.09201	-2.15813	DOWN	DOWN
P06586	30S ribosomal protein S3, chloroplastic	2	20198	10153	17766	8304	0.00062	0.00232	-0.99225	-1.09720	DOWN	DOWN
A0A1D6PA00	50S ribosomal protein L6 chloroplastic	2	17256	10125	12128	4619	0.01329	0.00931	-0.76925	-1.39253	DOWN	DOWN
K7TH00	Polyamine oxidase1	3	8147	3523	14957	3321	0.00189	0.00076	-1.20938	-2.17102	DOWN	DOWN
A0A804N2Z6	Protein translocase subunit SecA	8	18143	9508	20259	9344	0.04620	0.01192	-0.93216	-1.11647	DOWN	DOWN
A0A804NPP8	Nitrate reductase	2	28876	13951	17430	7694	0.00154	0.01390	-1.04950	-1.17975	DOWN	DOWN
A0A804NIP9	Glutaredoxin domain-containing protein	2	10813	6669	11235	7237	0.00799	0.03744	-0.69738	-0.63455	DOWN	DOWN
A0A1D6PF61	Translocase of chloroplast	2	4768	1303	3703	1644	0.01300	0.03378	-1.87108	-1.17166	DOWN	DOWN
P05348	Ribulose bisphosphate carboxylase small subunit, chloroplastic	16	922790	652013	955409	620884	0.00451	0.01209	-0.50110	-0.62180	UNCH.	DOWN
B4FSD8	plastoquinol--plastocyanin reductase	11	232957	168029	271080	141613	0.13845	0.04787	-0.47135	-0.93676	UNCH.	DOWN
Q41864	Thioredoxin M-type, chloroplastic	8	37877	28828	230375	22508	0.00630	0.00398	-0.39386	-3.35546	UNCH.	DOWN
B4FR47	Fructose-bisphosphate aldolase	23	239294	177041	224165	93814	0.00098	0.00149	-0.43470	-1.25668	UNCH.	DOWN
B4FRC8	FAD/NAD(P)-binding oxidoreductase	16	428582	326086	560986	317527	0.03863	0.01120	-0.39432	-0.82109	UNCH.	DOWN
B6UIC1	50S ribosomal protein L12-1	9	181388	128432	207540	83337	0.04169	0.00149	-0.49807	-1.31636	UNCH.	DOWN
A0A804QQG4	Heat shock cognate 70 kDa protein	29	17308	14300	16135	1348	0.25612	0.00000	-0.27541	-3.58179	UNCH.	DOWN

Supplementary Table 5 - Cont

Accession	Description	Reported peptides	Average Normalized Ion Count L80 HN	Average Normalized Ion Count L80 LN	Average Normalized Ion Count P2 HN	Average Normalized Ion Count P2 LN	t-test L80 LN/HN	t-test P2 LN/HN	Log_2 FC L80 LN/HN	Log_2 FC P2 LN/HN	Differential Accumulation L80 LN/HN	Differential Accumulation P2 LN/HN
A0A804NSA7	Glyoxylate/succinic semialdehyde reductase 1	15	314785	254776	334804	199559	0.10286	0.03187	-0.30513	-0.74650	UNCH.	DOWN
B6SRI4	14-3-3-like protein	12	35689	22117	30142	12417	0.24734	0.04644	-0.69034	-1.27947	UNCH.	DOWN
K7TYJ1	Ribonucleoprotein	8	135024	108036	109594	64340	0.15220	0.00949	-0.32170	-0.76839	UNCH.	DOWN
A0A804Q2W1	14_3_3 domain-containing protein	10	71631	22543	61414	31266	0.20883	0.01174	-1.66789	-0.97396	UNCH.	DOWN
A0A804M1R0	5-methyltetrahydropteroyltriglutamate--homocysteine S-methyltransferase	18	8356	7942	6592	2483	0.75699	0.00207	-0.07335	-1.40865	UNCH.	DOWN
Q768R3	Dicarboxylic acid transporter2	5	268588	201315	282285	172262	0.00113	0.00127	-0.41594	-0.71255	UNCH.	DOWN
A0A804PF87	hydroxymethylbilane synthase	11	74510	70114	38264	18364	0.72237	0.04422	-0.08772	-1.05913	UNCH.	DOWN
A0A804LW73	40S ribosomal protein S8	4	10252	11775	14698	7333	0.11260	0.00509	0.19981	-1.00316	UNCH.	DOWN
Q9FQB2	glutathione transferase	8	50110	34721	101518	44326	0.08687	0.04817	-0.52929	-1.19550	UNCH.	DOWN
C0PEC4	30S ribosomal protein S5 chloroplastic	10	132760	89658	103253	62577	0.09790	0.01005	-0.56632	-0.72247	UNCH.	DOWN
B6TN41	4-hydroxy-4-methyl-2-oxoglutarate aldolase	8	97590	68521	94802	39534	0.49253	0.00187	-0.51017	-1.26185	UNCH.	DOWN
B6TGS8	6,7-dimethyl-8-ribityllumazine synthase	5	43032	32976	43264	18663	0.41644	0.00719	-0.38401	-1.21300	UNCH.	DOWN
A0A1D6KL30	Sorbitol dehydrogenase	15	56407	50728	83275	33721	0.31343	0.00137	-0.15309	-1.30423	UNCH.	DOWN
A0A804QZ28	Acetamidase/Formamidase family protein	6	60105	40695	77920	34357	0.48366	0.00763	-0.56263	-1.18141	UNCH.	DOWN
B6SU89	Nascent polypeptide-associated complex alpha subunit-like protein	6	25894	19654	31326	16203	0.27614	0.01307	-0.39774	-0.95104	UNCH.	DOWN
B6SQM0	Major pollen allergen Car b 1 isoforms 1A and 1B	3	27099	19037	31678	12058	0.17045	0.01167	-0.50946	-1.39356	UNCH.	DOWN

Supplementary Table 5 - Cont

Accession	Description	Reported peptides	Average Normalized Ion Count L80 HN	Average Normalized Ion Count L80 LN	Average Normalized Ion Count P2 HN	Average Normalized Ion Count P2 LN	t-test L80 LN/HN	t-test P2 LN/HN	Log_2 FC L80 LN/HN	Log_2 FC P2 LN/HN	Differential Accumulation L80 LN/HN	Differential Accumulation P2 LN/HN
A0A1D6EEW2	Natterin-4	7	40082	8815	24212	3728	0.21242	0.02023	-2.18493	-2.69937	UNCH.	DOWN
B4G1Q5	50S ribosomal protein L10 chloroplastic	4	54105	36144	42372	16858	0.09372	0.03746	-0.58202	-1.32970	UNCH.	DOWN
P31927	Sucrose-phosphate synthase	29	98670	69157	115768	53297	0.00018	0.00188	-0.51273	-1.11910	UNCH.	DOWN
B4FRJ7	Fumarylacetoacetate (FAA) hydrolase family	3	7666	7828	6006	3219	0.89674	0.03669	0.03008	-0.89997	UNCH.	DOWN
A0A096UAZ3	3-isopropylmalate dehydratase small subunit 2	6	30565	32931	32553	10398	0.89838	0.01359	0.10756	-1.64649	UNCH.	DOWN
K7VIA7	Nascent polypeptide-associated complex alpha subunit-like protein	5	39324	35561	35966	23035	0.47994	0.01466	-0.14514	-0.64280	UNCH.	DOWN
B6T8U7	Chaperonin	8	42107	28513	39641	22810	0.01631	0.02013	-0.56241	-0.79734	UNCH.	DOWN
C0PK59	60S ribosomal protein L11	3	20628	15593	17917	7970	0.20296	0.01152	-0.40369	-1.16877	UNCH.	DOWN
A0A804LCL8	PsbP domain-containing protein	5	24513	10882	17268	7335	0.06815	0.01044	-1.17164	-1.23535	UNCH.	DOWN
P25706	NAD(P)H-quinone oxidoreductase subunit 1, chloroplastic	5	140305	109077	176005	113197	0.17790	0.00006	-0.36321	-0.63679	UNCH.	DOWN
B4FQD7	60S ribosomal protein L27a-2	3	32946	23651	31478	17755	0.04378	0.00517	-0.47820	-0.82610	UNCH.	DOWN
A0A1D6G1E0	Putative ubiquitin-conjugating enzyme family	5	35211	22991	30046	18181	0.12416	0.01070	-0.61494	-0.72477	UNCH.	DOWN
C0P7X7	30S ribosomal protein S6 alpha chloroplastic	4	53950	38780	50114	21068	0.00359	0.00983	-0.47632	-1.25016	UNCH.	DOWN
B6SZK3	NAD(P)H-dependent oxidoreductase	11	77049	59529	67435	31291	0.09309	0.00001	-0.37220	-1.10777	UNCH.	DOWN
O24415	60S acidic ribosomal protein P2B	2	21555	11581	24944	9303	0.09015	0.01654	-0.89635	-1.42291	UNCH.	DOWN
B4FBY5	40S ribosomal protein S23	4	20700	15449	22672	12499	0.05332	0.01173	-0.42214	-0.85918	UNCH.	DOWN

Supplementary Table 5 - Cont

Accession	Description	Reported peptides	Average Normalized Ion Count L80 HN	Average Normalized Ion Count L80 LN	Average Normalized Ion Count P2 HN	Average Normalized Ion Count P2 LN	t-test L80 LN/HN	t-test P2 LN/HN	Log_2 FC L80 LN/HN	Log_2 FC P2 LN/HN	Differential Accumulation L80 LN/HN	Differential Accumulation P2 LN/HN
B6SNW4	glutaminase	4	21356	18122	27283	17993	0.36735	0.00724	-0.23694	-0.60051	UNCH.	DOWN
A0A804M812	RCK N-terminal domain-containing protein	14	46423	33936	37894	18741	0.04363	0.00392	-0.45203	-1.01575	UNCH.	DOWN
P11647	NAD(P)H-quinone oxidoreductase chain 4, chloroplastic	4	27694	20561	38469	22441	0.01004	0.01413	-0.42967	-0.77755	UNCH.	DOWN
K7U7K6	Nine-cis-epoxycarotenoid dioxygenase6	12	52879	40466	75202	24792	0.05884	0.02111	-0.38599	-1.60092	UNCH.	DOWN
B4FUS2	40S ribosomal protein S18	3	18952	14976	21788	11189	0.29550	0.01209	-0.33971	-0.96151	UNCH.	DOWN
B4FN43	Haloacid dehalogenase-like hydrolase domain-containing protein Sgpp	4	18033	11578	21297	7209	0.17130	0.00367	-0.63933	-1.56280	UNCH.	DOWN
A0A1D6HG23	TPR_REGION domain-containing protein	3	9331	5508	16308	6243	0.16823	0.01340	-0.76058	-1.38522	UNCH.	DOWN
B6T7B2	30S ribosomal protein S4, chloroplastic	3	27261	20123	24712	14829	0.04379	0.01014	-0.43795	-0.73679	UNCH.	DOWN
A0A804NJ56	Diaminopimelate decarboxylase 2, chloroplastic	6	92165	88809	95006	32615	0.95934	0.00009	-0.05351	-1.54247	UNCH.	DOWN
A0A804UA89	60S ribosomal protein L9	4	32384	21776	22490	13021	0.00219	0.04505	-0.57253	-0.78840	UNCH.	DOWN
B4FRL3	Abhydrolase_3 domain-containing protein	4	15426	14376	19303	10953	0.78470	0.00008	-0.10165	-0.81752	UNCH.	DOWN
B4G0I5	Chlorophyll synthase chloroplastic	2	20780	16411	35341	20891	0.03205	0.03491	-0.34051	-0.75846	UNCH.	DOWN
A0A804QSM4	GTP cyclohydrolase II	5	16497	12934	14361	8770	0.03651	0.01653	-0.35106	-0.71149	UNCH.	DOWN
A0A804PCP6	KOW domain-containing protein	3	208126	210694	205791	11388	0.70927	0.00001	0.01769	-4.17566	UNCH.	DOWN
A0A804RMV0	Protein TIC 40, chloroplastic	6	13814	15532	18461	4412	0.11503	0.00346	0.16911	-2.06513	UNCH.	DOWN
B4FIM3	Uroporphyrinogen decarboxylase	3	23298	14717	12321	5465	0.25265	0.03011	-0.66274	-1.17284	UNCH.	DOWN

Supplementary Table 5 - Cont

Accession	Description	Reported peptides	Average Normalized Ion Count L80 HN	Average Normalized Ion Count L80 LN	Average Normalized Ion Count P2 HN	Average Normalized Ion Count P2 LN	t-test L80 LN/HN	t-test P2 LN/HN	Log_2 FC L80 LN/HN	Log_2 FC P2 LN/HN	Differential Accumulation L80 LN/HN	Differential Accumulation P2 LN/HN
A0A1D6LPF3	40S ribosomal protein S14	3	11184	8084	9798	5826	0.03657	0.01118	-0.46833	-0.74983	UNCH.	DOWN
B4FDG7	RNA-binding (RRM/RBD/RNP motifs) family protein	3	12773	10770	10033	6439	0.21073	0.03342	-0.24617	-0.64001	UNCH.	DOWN
A0A804M7H7	STI1 domain-containing protein	5	22572	13888	23937	7474	0.07492	0.01170	-0.70070	-1.67935	UNCH.	DOWN
B4FYR9	Membrane metalloprotease ARASP chloroplastic	3	7796	5164	10455	6690	0.01528	0.02327	-0.59416	-0.64415	UNCH.	DOWN
A0A804NLI1	6-phosphogluconate dehydrogenase, decarboxylating	3	14830	6664	5516	3329	0.05535	0.03106	-1.15403	-0.72875	UNCH.	DOWN
A0A804QYS3	glycine--tRNA ligase	3	21369	15253	25991	15695	0.04184	0.01254	-0.48645	-0.72768	UNCH.	DOWN
A0A804NYN9	non-reducing end alpha-L-arabinofuranosidase	3	7481	4895	7848	3666	0.24877	0.03309	-0.61177	-1.09812	UNCH.	DOWN
A0A1D6H5B6	50S ribosomal protein L21 chloroplastic	4	0	0	41387	16114	-	0.00509	#DIV/0!	-1.36089	-	DOWN
A0A804UN22	60S ribosomal protein L12	7	14019	9162	7023	0	0.04775	0.00084	-0.61364	-	DOWN	UNIQUE HIGH N
A0A804LCX8	Plasma membrane ATPase	7	3136	1542	1167	0	0.00157	0.00421	-1.02395	-	DOWN	UNIQUE HIGH N
A0A804PZP9	Stem 28 kDa glycoprotein	3	12308	6389	22872	0	0.00765	0.07889	-0.94588	-	DOWN	UNIQUE HIGH N
A0A804UF37	Ribonuclease T(2)	4	26836	0	64996	0	0.00536	0.03631	-	-	UNIQUE HIGH N	UNIQUE HIGH N
A0A804NUM1	Ribulose bisphosphate carboxylase large chain	6	0	94299	18935	0	0.02380	0.00001	-	-	UNIQUE LOW N	UNIQUE HIGH N
A0A804LQR0	Actin	7	2375	1721	1914	0	0.01840	0.00041	-0.46466	-	UNCH.	UNIQUE HIGH N
B4FAV5	Germin-like protein	4	37792	38992	15893	0	0.91531	0.00002	0.04509	-	UNCH.	UNIQUE HIGH N
A0A804LS47	5-methyltetrahydropteroyltriglutamate--homocysteine S-methyltransferase	25	0	0	15437	0	-	0.00014	-	-	-	UNIQUE HIGH N

Supplementary Table 5 - Cont

Accession	Description	Reported peptides	Average Normalized Ion Count L80 HN	Average Normalized Ion Count L80 LN	Average Normalized Ion Count P2 HN	Average Normalized Ion Count P2 LN	t-test L80 LN/HN	t-test P2 LN/HN	Log_2 FC L80 LN/HN	Log_2 FC P2 LN/HN	Differential Accumulation L80 LN/HN	Differential Accumulation P2 LN/HN
Q9ATM8	Aquaporin PIP2-2	3	0	0	2459	0	-	0.00291	-	-	-	UNIQUE HIGH N
A0A804PMF6	Uncharacterized protein	9	0	0	1265	0	-	0.00031	-	-	-	UNIQUE HIGH N
A0A804Q8W4	glutaredoxin-dependent peroxiredoxin	2	0	0	22301	0	-	0.00102	-	-	-	UNIQUE HIGH N
A0A1D6HWJ3	Glucose-1-phosphate adenylyltransferase	4	0	0	3114	0	-	0.00002	-	-	-	UNIQUE HIGH N
A0A804R2I0	Plasma membrane ATPase	6	0	0	2717	0	-	0.03132	-	-	-	UNIQUE HIGH N
P48184	Photosystem II D2 protein	12	222678	124887	19959	218416	0.00010	0.00001	-0.83433	3.45196	DOWN	UP
A0A804PEW7	Eukaryotic initiation factor 4A-11	22	51781	33173	47243	109458	0.00654	0.01335	-0.64242	1.21221	DOWN	UP
A0A1D6N6H1	Actin-7	28	77298	123867	48712	144382	0.00841	0.02005	0.68030	1.56755	UP	UP
Q3SAE4	Glucose-1-phosphate adenylyltransferase	22	28002	55417	26808	75819	0.00045	0.00478	0.98479	1.49988	UP	UP
K7UIX3	Putative plastid-lipid-associated protein 2 chloroplastic	7	24469	41117	18742	46151	0.02720	0.00106	0.74875	1.30012	UP	UP
B6T9S6	Retrotransposon protein SINE subclass	6	19922	35228	10436	29478	0.01031	0.00193	0.82238	1.49801	UP	UP
A0A804NT91	GrpE protein homolog	7	14771	29420	17167	36178	0.03968	0.00900	0.99403	1.07549	UP	UP
A0A804QS10	Subtilisin-like protease SBT1.9	13	15989	37330	21430	62730	0.00389	0.00308	1.22324	1.54954	UP	UP
B4FF45	S-adenosyl-L-methionine-dependent methyltransferase superfamily protein	7	28619	49253	24832	41336	0.02277	0.04326	0.78323	0.73519	UP	UP
B6SUQ7	Violaxanthin de-epoxidase	8	20054	32941	28260	53165	0.00789	0.02274	0.71600	0.91171	UP	UP
A0A804PC17	Saposin B-type domain-containing protein	2	7240	12214	9038	21308	0.00841	0.02170	0.75445	1.23740	UP	UP

Supplementary Table 5 - Cont

Accession	Description	Reported peptides	Average Normalized Ion Count L80 HN	Average Normalized Ion Count L80 LN	Average Normalized Ion Count P2 HN	Average Normalized Ion Count P2 LN	t-test L80 LN/HN	t-test P2 LN/HN	Log_2 FC L80 LN/HN	Log_2 FC P2 LN/HN	Differential Accumulation L80 LN/HN	Differential Accumulation P2 LN/HN
B4FMX6	Thioredoxin reductase	2	14578	22913	8317	18479	0.00256	0.00326	0.65235	1.15182	UP	UP
A0A804NMD2	Gamma aminobutyrate transaminase 3, chloroplastic-like	4	4149	6991	2784	4715	0.00796	0.04200	0.75287	0.76006	UP	UP
A0A804QKD5	Glutathione hydrolase	2	4464	8374	3418	11311	0.02812	0.00591	0.90769	1.72671	UP	UP
A0A804QJ31	Actin-related protein 8	6	0	1711	1775	3606	0.00012	0.01379	-	1.02273	UNIQUE LOW N	UP
C0P3W9	phosphoenolpyruvate carboxykinase (ATP)	42	246271	306147	222328	345333	0.16502	0.01280	0.31398	0.63530	UNCH.	UP
B6TH55	Photosystem I reaction center subunit IV A	8	231391	279280	158324	306719	0.20945	0.02310	0.27138	0.95404	UNCH.	UP
K7UBU0	Glyceraldehyde-3-phosphate dehydrogenase	21	116242	77378	74155	130226	0.06039	0.02269	-0.58714	0.81239	UNCH.	UP
A0A804QN37	ATP synthase subunit beta	20	27946	38609	30996	54775	0.01280	0.00340	0.46630	0.82144	UNCH.	UP
A0A804NGB7	Carbonic anhydrase	10	6040	6563	2520	4048	0.04481	0.01817	0.11985	0.68341	UNCH.	UP
A0A1D6HN61	Leucine aminopeptidase 2 chloroplastic	28	85931	92242	60730	105751	0.40524	0.02228	0.10224	0.80019	UNCH.	UP
B4FRP8	Plastid-lipid-associated protein 2	15	116226	153386	141768	287626	0.11522	0.00033	0.40023	1.02066	UNCH.	UP
A0A1D6HY75	Photosystem I reaction center subunit IV A	6	179827	224869	130629	242818	0.08511	0.00243	0.32247	0.89440	UNCH.	UP
C0P2C3	Glycine-rich protein 2-like	4	91278	97264	44369	79292	0.47935	0.01975	0.09163	0.83763	UNCH.	UP
A0A804UNU3	phosphoglucomutase (alpha-D-glucose-1,6-bisphosphate-dependent)	24	5856	5235	4788	8752	0.20599	0.00034	-0.16192	0.87019	UNCH.	UP
A0A804LIS3	Aminotran_1_2 domain-containing protein	13	2892	2937	1958	5951	0.66458	0.04314	0.02240	1.60390	UNCH.	UP
A0A1D6LJS9	Chaperonin 60 subunit beta 2 chloroplastic	32	62227	65533	31578	53988	0.55607	0.00903	0.07468	0.77369	UNCH.	UP

Supplementary Table 5 - Cont

Accession	Description	Reported peptides	Average Normalized Ion Count L80 HN	Average Normalized Ion Count L80 LN	Average Normalized Ion Count P2 HN	Average Normalized Ion Count P2 LN	t-test L80 LN/HN	t-test P2 LN/HN	Log_2 FC L80 LN/HN	Log_2 FC P2 LN/HN	Differential Accumulation L80 LN/HN	Differential Accumulation P2 LN/HN
C0P429	UTP--glucose-1-phosphate uridylyltransferase	14	25068	25332	19720	38235	0.83804	0.03374	0.01512	0.95529	UNCH.	UP
K7TIN2	Glycine cleavage system P protein	34	166764	200269	120650	229441	0.19910	0.00189	0.26413	0.92730	UNCH.	UP
B6TVL4	Calcium sensing receptor, chloroplastic	18	131396	139557	158528	258006	0.80206	0.02748	0.08693	0.70267	UNCH.	UP
K7V8L3	S-adenosyl-L-methionine-dependent methyltransferase superfamily protein	8	17106	15360	15686	24245	0.64939	0.00405	-0.15536	0.62816	UNCH.	UP
A0A1D6MIP4	1-aminocyclopropane-1-carboxylate oxidase	11	38352	65883	13040	51522	0.12568	0.00257	0.78062	1.98220	UNCH.	UP
A0A096PRE6	Fibrillin1	9	55317	72194	48861	110327	0.16144	0.03244	0.38415	1.17502	UNCH.	UP
A0A804R918	Pept_C1 domain-containing protein	3	43574	48104	16478	51120	0.42481	0.01857	0.14271	1.63334	UNCH.	UP
A0A1D6IKK1	PLASMODESMATA CALLOSE-BINDING PROTEIN 5	4	13974	24241	12672	39068	0.14039	0.01005	0.79471	1.62431	UNCH.	UP
A0A1D6P0E7	Triose phosphate/phosphate translocator TPT chloroplastic	4	97524	124952	53455	116258	0.36894	0.00019	0.35754	1.12093	UNCH.	UP
A0A1D6NUP6	Thiol protease SEN102	11	154512	183332	79868	122114	0.36056	0.00059	0.24673	0.61254	UNCH.	UP
Q9ZQX9	40S ribosomal protein S27	4	32300	41551	12453	31349	0.16273	0.04075	0.36335	1.33199	UNCH.	UP
B4FU15	Extensin-like protein	4	35958	47780	37528	74675	0.45767	0.00453	0.41012	0.99265	UNCH.	UP
A0A1D6PJL0	Aconitate hydratase	34	62337	81273	36193	62063	0.10511	0.00995	0.38269	0.77802	UNCH.	UP
A0A804QPX6	fructose-bisphosphatase	7	3150	4132	4807	11419	0.00151	0.00043	0.39134	1.24816	UNCH.	UP
A0A804LD80	Aconitate hydratase	34	27379	26136	22523	36406	0.55387	0.01840	-0.06704	0.69280	UNCH.	UP
Q41782	Tubulin beta-4 chain	8	4265	6134	2855	5766	0.05276	0.00060	0.52407	1.01413	UNCH.	UP

Supplementary Table 5 - Cont

Accession	Description	Reported peptides	Average Normalized Ion Count L80 HN	Average Normalized Ion Count L80 LN	Average Normalized Ion Count P2 HN	Average Normalized Ion Count P2 LN	t-test L80 LN/HN	t-test P2 LN/HN	Log_2 FC L80 LN/HN	Log_2 FC P2 LN/HN	Differential Accumulation L80 LN/HN	Differential Accumulation P2 LN/HN
A0A804M3X9	Lysosomal beta glucosidase-like	13	63392	64775	35177	54693	0.89612	0.00562	0.03114	0.63672	UNCH.	UP
A0A1D6HW78	ABC2 homolog 13	7	5288	7382	5279	13821	0.20371	0.03519	0.48140	1.38857	UNCH.	UP
A0A804PNY3	Subtilisin-like protease SBT1.7	13	30917	42237	25850	41112	0.07106	0.00061	0.45011	0.66938	UNCH.	UP
A0A804QRT8	Ras-related protein Rab7	7	37706	50997	28822	53697	0.00627	0.00416	0.43562	0.89767	UNCH.	UP
C0PH69	AB hydrolase-1 domain-containing protein	8	31498	45592	41807	68024	0.08143	0.04053	0.53354	0.70232	UNCH.	UP
B4FIV0	Succinate--CoA ligase [ADP-forming] subunit alpha, mitochondrial	8	76479	95181	58806	105561	0.18288	0.01133	0.31562	0.84403	UNCH.	UP
B4FF48	Haloacid dehalogenase-like hydrolase domain-containing protein	6	42883	58083	37677	71486	0.01856	0.04647	0.43773	0.92396	UNCH.	UP
B4FR11	Protein CURVATURE THYLAKOID 1A chloroplastic	2	20396	25539	23015	43053	0.07571	0.00304	0.32443	0.90357	UNCH.	UP
A0A1D6I1V3	phosphoenolpyruvate carboxylase	18	10107	14447	11445	19024	0.03097	0.01746	0.51539	0.73314	UNCH.	UP
C0PGN4	Obg-like ATPase 1	10	19101	20267	17001	28290	0.45768	0.02194	0.08550	0.73470	UNCH.	UP
A0A1D6HFC3	tripeptidyl-peptidase II	25	20764	23215	27334	41731	0.54116	0.01180	0.16097	0.61045	UNCH.	UP
A0A804LEU1	Phytoene dehydrogenase	8	27446	22063	24658	40862	0.29145	0.02007	-0.31497	0.72870	UNCH.	UP
A0A804P187	Aldehyde dehydrogenase	6	23199	31426	19631	43496	0.00104	0.00320	0.43791	1.14775	UNCH.	UP
A0A1D6IBV1	FAD/NAD(P)-binding oxidoreductase family protein	8	9670	13675	14585	29763	0.15474	0.04132	0.49999	1.02902	UNCH.	UP
A0A1D6HQF7	Epimerase family protein SDR39U1 homolog chloroplastic	7	15559	21044	17058	34438	0.01925	0.01925	0.43561	1.01353	UNCH.	UP
B5AK47	Dhurrinase-like B-glucosidase	14	29020	34103	13989	35931	0.26813	0.02441	0.23285	1.36093	UNCH.	UP

Supplementary Table 5 - Cont

Accession	Description	Reported peptides	Average Normalized Ion Count L80 HN	Average Normalized Ion Count L80 LN	Average Normalized Ion Count P2 HN	Average Normalized Ion Count P2 LN	t-test L80 LN/HN	t-test P2 LN/HN	Log_2 FC L80 LN/HN	Log_2 FC P2 LN/HN	Differential Accumulation L80 LN/HN	Differential Accumulation P2 LN/HN
A0A804PAE3	Malic enzyme	3	9140	13705	5417	10558	0.02771	0.02019	0.58439	0.96277	UNCH.	UP
A0A1D6E9W1	12-oxo-phytodienoic acid reductase5	3	17904	18033	14819	29027	0.97553	0.03101	0.01032	0.96995	UNCH.	UP
A0A804Q2F8	assimilatory sulfite reductase (ferredoxin)	5	22911	19781	10356	15866	0.41997	0.00989	-0.21192	0.61551	UNCH.	UP
K7V8K5	Peroxidase	4	8498	8576	8972	19211	0.96871	0.01960	0.01316	1.09843	UNCH.	UP
A0A1D6I540	Eukaryotic initiation factor 4F subunit p150 isoform 1	3	6607	8835	14023	23445	0.23840	0.00704	0.41919	0.74142	UNCH.	UP
B6U6U2	Hexose transporter	6	14386	22923	16041	33074	0.06092	0.00324	0.67209	1.04398	UNCH.	UP
C0P4M0	Monodehydroascorbate reductase 1 peroxisomal	5	7784	10274	3963	9730	0.19570	0.00911	0.40041	1.29600	UNCH.	UP
A0A1D6M0I9	Carboxypeptidase	5	23287	32981	13676	30784	0.25990	0.04888	0.50211	1.17054	UNCH.	UP
A0A804NQX3	Aldedh domain-containing protein	4	5445	4448	4670	10472	0.53207	0.00637	-0.29160	1.16521	UNCH.	UP
A0A804PZZ8	Patellin-3-like	3	10225	13724	6496	13773	0.07215	0.01463	0.42464	1.08425	UNCH.	UP
A0A1D6GQ46	Glycosyltransferase	4	14495	19790	3442	9109	0.00542	0.03448	0.44922	1.40412	UNCH.	UP
A0A804ND31	Aspartate aminotransferase	3	14086	12356	7750	12599	0.31937	0.02643	-0.18906	0.70103	UNCH.	UP
B6SYG2	Carboxypeptidase	2	11270	16145	9888	15548	0.00126	0.01064	0.51857	0.65290	UNCH.	UP
A0A804LDL1	Rieske domain-containing protein	4	10574	10211	7544	12963	0.90284	0.04201	-0.05040	0.78093	UNCH.	UP
A0A096PQR7	Cytochrome P450 CYP74A19	3	4788	6177	8080	14613	0.54278	0.02734	0.36726	0.85494	UNCH.	UP
A0A804RQW4	S-methyl-5-thioribose kinase	2	11650	17553	5779	10678	0.00377	0.00421	0.59135	0.88583	UNCH.	UP

Supplementary Table 5 - Cont

Accession	Description	Reported peptides	Average Normalized Ion Count L80 HN	Average Normalized Ion Count L80 LN	Average Normalized Ion Count P2 HN	Average Normalized Ion Count P2 LN	t-test L80 LN/HN	t-test P2 LN/HN	Log_2 FC L80 LN/HN	Log_2 FC P2 LN/HN	Differential Accumulation L80 LN/HN	Differential Accumulation P2 LN/HN
A0A1D6N309	Dynamin-related protein 3A	3	5995	6949	4054	6512	0.33864	0.03337	0.21308	0.68367	UNCH.	UP
A0A804PHH9	Enoyl-CoA hydratase/3-2-trans-enoyl-CoA isomerase/3-hydroxybutyryl-CoA epimerase	2	2685	2370	2464	3959	0.06011	0.01284	-0.17998	0.68450	UNCH.	UP
C0PFF5	Proteasome subunit beta	7	0	0	6633	15675	-	0.00037	-	1.24074	-	UP
A0A804LIG8	Iso_dh domain-containing protein	2	0	15924	0	18110	0.00061	0.00343	-	-	UNIQUE LOW N	UNIQUE LOW N
A0A1D6JKV4	Actin-related protein 4	3	0	3591	0	3487	0.00002	0.00017	-	-	UNIQUE LOW N	UNIQUE LOW N
C0P6C5	threonine synthase	5	0	9827	0	8020	0.00004	0.00038	-	-	UNIQUE LOW N	UNIQUE LOW N
A0A804MWU3	Aldo_ket_red domain-containing protein	4	0	0	0	1172	-	0.00011	-	-	-	UNIQUE LOW N
B4F8Q2	Heat shock 70 kDa protein, mitochondrial	13	0	0	0	10411	-	0.00001	-	-	-	UNIQUE LOW N
Q7SIC9	Transketolase, chloroplastic	37	500234	292812	177527	180707	0.00081	0.57083	-0.77263	0.02561	DOWN	UNCH.
B6SSB9	Plastocyanin	4	376552	168270	222337	122589	0.04222	0.14560	-1.16207	-0.85892	DOWN	UNCH.
A0A1D6KCZ2	alanine transaminase	30	357961	230961	266686	189633	0.04027	0.03809	-0.63215	-0.49193	DOWN	UNCH.
A0A804LIC6	L-ascorbate peroxidase	10	126798	47854	81815	41682	0.00257	0.07322	-1.40582	-0.97294	DOWN	UNCH.
A0A804QCB0	UTP--glucose-1-phosphate uridylyltransferase	25	135902	86892	121404	99535	0.01337	0.07162	-0.64528	-0.28654	DOWN	UNCH.
P19124	NAD(P)H-quinone oxidoreductase subunit J, chloroplastic	12	150799	86876	142635	75432	0.00549	0.07065	-0.79560	-0.91907	DOWN	UNCH.
B6TSN0	Macrophage migration inhibitory factor	4	144355	85645	168607	83625	0.01115	0.07005	-0.75318	-1.01165	DOWN	UNCH.
A0A804RPL0	Ribulose bisphosphate carboxylase large chain	6	285331	85890	238703	151051	0.00086	0.16153	-1.73207	-0.66018	DOWN	UNCH.

Supplementary Table 5 - Cont

Accession	Description	Reported peptides	Average Normalized Ion Count L80 HN	Average Normalized Ion Count L80 LN	Average Normalized Ion Count P2 HN	Average Normalized Ion Count P2 LN	t-test L80 LN/HN	t-test P2 LN/HN	Log_2 FC L80 LN/HN	Log_2 FC P2 LN/HN	Differential Accumulation L80 LN/HN	Differential Accumulation P2 LN/HN
B4FWJ8	Binding protein homolog2	23	28778	17176	15668	16185	0.00225	0.80483	-0.74459	0.04691	DOWN	UNCH.
K7UKK5	Elongation factor G, chloroplastic	37	40296	24306	26913	20534	0.00395	0.07615	-0.72930	-0.39025	DOWN	UNCH.
B6T927	NAD(P)H-quinone oxidoreductase subunit S chloroplastic	13	148204	97623	174043	107192	0.03131	0.05620	-0.60228	-0.69925	DOWN	UNCH.
B4FT19	Oxygen evolving enhancer protein 3 containing protein	9	68351	31553	76817	24291	0.03319	0.08504	-1.11521	-1.66101	DOWN	UNCH.
B4FU98	Thylakoid lumenal 16.5 kDa protein chloroplastic	6	28279	13336	41744	14709	0.03174	0.11063	-1.08446	-1.50484	DOWN	UNCH.
P08529	50S ribosomal protein L14, chloroplastic	6	116483	57390	70662	32632	0.00786	0.06636	-1.02125	-1.11464	DOWN	UNCH.
A0A804LI62	PsbP domain-containing protein	11	117426	59498	111449	57615	0.00799	0.10994	-0.98085	-0.95186	DOWN	UNCH.
C0P9R5	Outer envelope pore protein 24A chloroplastic	11	53339	33340	47030	40301	0.02205	0.59619	-0.67795	-0.22279	DOWN	UNCH.
A0A1D6MIA3	Phospholipase A1-Igamma1 chloroplastic	20	109345	52392	100780	50534	0.00122	0.27599	-1.06147	-0.99589	DOWN	UNCH.
K7UXK5	Putative alcohol dehydrogenase superfamily protein	10	89950	54480	28233	28132	0.02348	0.98860	-0.72339	-0.00518	DOWN	UNCH.
C0PG07	Dehydroascorbate reductase	11	83678	45111	68441	29628	0.02715	0.16542	-0.89135	-1.20787	DOWN	UNCH.
B4FWP0	Fructose-bisphosphate aldolase	18	54676	33088	21586	24530	0.01951	0.21779	-0.72457	0.18443	DOWN	UNCH.
A0A804MRM8	Oxygen-evolving enhancer protein 3-2, chloroplastic	8	92686	49868	76147	50782	0.02068	0.11691	-0.89424	-0.58447	DOWN	UNCH.
A0A804REQ4	EFP domain-containing protein	8	64340	36022	57995	35771	0.02941	0.31721	-0.83682	-0.69716	DOWN	UNCH.
B4G0R1	Nucleoside diphosphate kinase	5	62441	29543	25034	12014	0.00474	0.12082	-1.07968	-1.05917	DOWN	UNCH.
B4FTF8	glutathione transferase	6	58129	37320	19944	20377	0.01992	0.93971	-0.63932	0.03103	DOWN	UNCH.

Supplementary Table 5 - Cont

Accession	Description	Reported peptides	Average Normalized Ion Count L80 HN	Average Normalized Ion Count L80 LN	Average Normalized Ion Count P2 HN	Average Normalized Ion Count P2 LN	t-test L80 LN/HN	t-test P2 LN/HN	Log_2 FC L80 LN/HN	Log_2 FC P2 LN/HN	Differential Accumulation L80 LN/HN	Differential Accumulation P2 LN/HN
A0A1D6N9E0	PsbP domain-containing protein 6 chloroplastic	5	75215	43850	99430	53014	0.02992	0.10787	-0.77845	-0.90729	DOWN	UNCH.
K7VCJ9	phosphoenolpyruvate carboxylase	13	63920	38134	47891	40066	0.00406	0.06219	-0.74521	-0.25736	DOWN	UNCH.
P18025	Tubulin beta-1 chain	10	9630	4209	2845	3028	0.00583	0.82671	-1.19404	0.08986	DOWN	UNCH.
A0A804NMS4	KH type-2 domain-containing protein	9	41604	25391	23299	19516	0.04613	0.08203	-0.71240	-0.25564	DOWN	UNCH.
A0A804N9W0	NAD(P)H-quinone oxidoreductase subunit N, chloroplastic	9	57063	28287	47651	29822	0.03852	0.31149	-1.01243	-0.67614	DOWN	UNCH.
B6SSG5	Structural molecule	4	19247	6283	30797	9918	0.02214	0.11997	-1.61513	-1.63466	DOWN	UNCH.
B4FQ61	30S ribosomal protein S8, chloroplastic	5	54417	21141	32902	16696	0.00179	0.06521	-1.36402	-0.97867	DOWN	UNCH.
A0A1D6GDM6	DPP6 N-terminal domain-like protein	12	53984	19378	42101	6241	0.02635	0.06049	-1.47810	-2.75393	DOWN	UNCH.
A0A1D6IDV8	Pyruvate phosphate dikinase regulatory protein 2	8	46209	27101	51518	34140	0.00126	0.02698	-0.76982	-0.59362	DOWN	UNCH.
B6SUJ3	Plastid-specific 30S ribosomal protein 2	4	22192	11966	18845	9997	0.04185	0.09073	-0.89113	-0.91455	DOWN	UNCH.
A0A804MIF0	CBS domain-containing protein	6	37503	23678	40157	23768	0.03154	0.07268	-0.66346	-0.75662	DOWN	UNCH.
B4F9G0	60S ribosomal protein L4-1	7	9854	5461	5701	4655	0.04144	0.26509	-0.85168	-0.29256	DOWN	UNCH.
P08530	30S ribosomal protein S8, chloroplastic	3	46207	27518	11006	13353	0.00564	0.07876	-0.74775	0.27878	DOWN	UNCH.
C0PBS1	Lipase-like	7	66650	40585	23060	19126	0.04465	0.52638	-0.71566	-0.26982	DOWN	UNCH.
B6THZ8	threonine synthase	9	34479	21002	26499	11741	0.00040	0.06960	-0.71520	-1.17435	DOWN	UNCH.
A0A804R572	peptidylprolyl isomerase	2	29453	15177	30971	22978	0.01583	0.43004	-0.95647	-0.43067	DOWN	UNCH.

Supplementary Table 5 - Cont

Accession	Description	Reported peptides	Average Normalized Ion Count L80 HN	Average Normalized Ion Count L80 LN	Average Normalized Ion Count P2 HN	Average Normalized Ion Count P2 LN	t-test L80 LN/HN	t-test P2 LN/HN	Log_2 FC L80 LN/HN	Log_2 FC P2 LN/HN	Differential Accumulation L80 LN/HN	Differential Accumulation P2 LN/HN
A0A1D6KKC7	Purple acid phosphatase	7	24625	7458	27837	4211	0.00080	0.09335	-1.72328	-2.72475	DOWN	UNCH.
B4FZN6	40S ribosomal protein S7	3	8739	5556	2591	1601	0.00127	0.18856	-0.65348	-0.69468	DOWN	UNCH.
A0A804P3L6	Citrate synthase	8	23870	12708	8938	8844	0.01868	0.97163	-0.90949	-0.01521	DOWN	UNCH.
B4F938	coproporphyrinogen oxidase	5	53113	32180	23285	16457	0.02182	0.18270	-0.72288	-0.50068	DOWN	UNCH.
B4FTT2	Regulator of chromosome condensation2	6	48414	29800	53036	24601	0.04646	0.08192	-0.70012	-1.10825	DOWN	UNCH.
A0A1D6NNV9	Alpha/beta-Hydrolases superfamily protein	4	26095	14537	16407	7392	0.01463	0.12810	-0.84407	-1.15026	DOWN	UNCH.
P52588	Protein disulfide-isomerase	3	20853	10623	12223	7664	0.03409	0.24544	-0.97308	-0.67343	DOWN	UNCH.
B4FKB3	50S ribosomal protein L31	2	19648	8547	15552	6546	0.04911	0.13036	-1.20092	-1.24848	DOWN	UNCH.
P49727	Cytochrome b-c1 complex subunit Rieske, mitochondrial	4	25827	16714	19379	12028	0.01145	0.10225	-0.62781	-0.68810	DOWN	UNCH.
A0A804PJS0	HMA domain-containing protein	3	23917	8533	27461	15977	0.01075	0.16131	-1.48685	-0.78142	DOWN	UNCH.
A0A804QFQ9	4-alpha-glucanotransferase	7	19560	12824	12967	10899	0.00277	0.24079	-0.60907	-0.25062	DOWN	UNCH.
A0A804Q6H8	S5 DRBM domain-containing protein	2	46968	29065	26269	19510	0.01826	0.16141	-0.69239	-0.42915	DOWN	UNCH.
C0PEH3	ThiC-associated domain-containing protein	5	22770	12207	20400	12789	0.00795	0.05965	-0.89946	-0.67370	DOWN	UNCH.
B4FQ98	NADH dehydrogenase [ubiquinone] flavoprotein 1, mitochondrial	3	12462	7273	6602	6557	0.01595	0.97822	-0.77687	-0.00987	DOWN	UNCH.
A0A804UGG0	Uncharacterized protein	2	9834	5501	7050	3405	0.00646	0.18689	-0.83808	-1.04983	DOWN	UNCH.
B7ZZM8	argininosuccinate synthase	2	32753	20875	20317	14126	0.01556	0.08694	-0.64984	-0.52432	DOWN	UNCH.

Supplementary Table 5 - Cont

Accession	Description	Reported peptides	Average Normalized Ion Count L80 HN	Average Normalized Ion Count L80 LN	Average Normalized Ion Count P2 HN	Average Normalized Ion Count P2 LN	t-test L80 LN/HN	t-test P2 LN/HN	Log_2 FC L80 LN/HN	Log_2 FC P2 LN/HN	Differential Accumulation L80 LN/HN	Differential Accumulation P2 LN/HN
B4FN21	Proteasome subunit beta	2	7675	4711	5279	4821	0.03806	0.65638	-0.70402	-0.13090	DOWN	UNCH.
A0A804MIK3	Cysteine synthase	3	14200	6373	7255	5160	0.00398	0.40112	-1.15583	-0.49138	DOWN	UNCH.
A0A804R1I4	transketolase	36	128593	285566	374079	353671	0.00012	0.45106	1.15102	-0.08094	UP	UNCH.
A0A804RQH4	Phosphoenolpyruvate carboxylase	9	13878	21178	28096	21596	0.00046	0.01666	0.60977	-0.37958	UP	UNCH.
A0A1D6HZE0	Actin-7	11	2462	4443	4068	3044	0.00047	0.14273	0.85176	-0.41805	UP	UNCH.
Q43247	Glyceraldehyde-3-phosphate dehydrogenase 3, cytosolic	18	25003	42277	24392	34766	0.01839	0.11229	0.75777	0.51129	UP	UNCH.
A0A804MWC7	Actin	7	58176	100294	88944	67666	0.03077	0.45313	0.78574	-0.39448	UP	UNCH.
A0A804P2X2	Uncharacterized protein	21	36752	63869	68353	70063	0.00087	0.92563	0.79729	0.03566	UP	UNCH.
A0A804Q7P8	PGR5-like protein 1A, chloroplastic	8	12591	25294	12229	27529	0.01381	0.20415	1.00643	1.17058	UP	UNCH.
B4FK45	Metallo-hydrolase/oxidoreductase superfamily protein	10	54005	83719	36018	49170	0.02247	0.04472	0.63246	0.44905	UP	UNCH.
A0A804P3D7	40S ribosomal protein S8	6	2819	5676	5640	4230	0.00420	0.01791	1.00974	-0.41497	UP	UNCH.
B4F9G8	Pyruvate kinase	21	64384	99736	63407	99468	0.01246	0.05472	0.63142	0.64959	UP	UNCH.
A0A1D6EBV6	Uncharacterized protein	6	10178	19003	21403	37710	0.00055	0.16149	0.90072	0.81712	UP	UNCH.
A0A804MAH5	Gamma-aminobutyrate transaminase POP2, mitochondrial	17	7505	13141	16752	16858	0.00387	0.95564	0.80806	0.00913	UP	UNCH.
A0A1D6F1Q8	alanine transaminase	4	67510	104580	68592	80802	0.00333	0.32817	0.63143	0.23635	UP	UNCH.
C0P6T2	FHA transcription factor	3	21057	33960	37919	53110	0.04640	0.33482	0.68955	0.48606	UP	UNCH.

Supplementary Table 5 - Cont

Accession	Description	Reported peptides	Average Normalized Ion Count L80 HN	Average Normalized Ion Count L80 LN	Average Normalized Ion Count P2 HN	Average Normalized Ion Count P2 LN	t-test L80 LN/HN	t-test P2 LN/HN	Log_2 FC L80 LN/HN	Log_2 FC P2 LN/HN	Differential Accumulation L80 LN/HN	Differential Accumulation P2 LN/HN
C0PDH2	Plasma membrane ATPase	10	4786	22181	18834	19538	0.00388	0.90558	2.21233	0.05290	UP	UNCH.
A0A804PFK1	Proteasome subunit beta	5	32984	59239	52380	80103	0.03878	0.18609	0.84479	0.61282	UP	UNCH.
B4G233	Dirigent protein	3	7195	12469	7104	14196	0.01439	0.07748	0.79333	0.99878	UP	UNCH.
A0A1D6Q3U2	Ypt homolog3	4	9416	16882	13516	10860	0.01355	0.57310	0.84226	-0.31572	UP	UNCH.
A0A804MF56	Protease Do-like 8, chloroplastic	2	25776	39448	13799	18896	0.00451	0.09149	0.61393	0.45350	UP	UNCH.
A0A804PBC5	ACT domain-containing protein ACR	4	47240	75025	57622	78344	0.03655	0.00274	0.66737	0.44320	UP	UNCH.
A0A1D6GM23	Chloroplast post-illumination chlorophyll fluorescence increase protein	4	29260	47638	32230	34298	0.00316	0.54628	0.70319	0.08974	UP	UNCH.
A0A1D6J2J3	Beta-glucosidase 17	6	26895	41032	27758	33212	0.00257	0.00287	0.60941	0.25882	UP	UNCH.
A0A804PYT1	Heat shock 70 kDa protein 14	7	10942	16964	13619	14485	0.00773	0.36114	0.63269	0.08900	UP	UNCH.
A0A804QU81	Myosin motor domain-containing protein	2	65894	103787	88692	82926	0.04232	0.68241	0.65542	-0.09698	UP	UNCH.
B4FZG6	Haloacid dehalogenase-like hydrolase domain-containing protein	5	0	4632	11291	6461	0.00372	0.25334	-	-0.80540	UNIQUE LOW N	UNCH.
P00874	Ribulose bisphosphate carboxylase large chain	42	1855898	1724437	1424036	1606595	0.50041	0.13188	-0.10599	0.17402	UNCH.	UNCH.
P00827	ATP synthase subunit beta, chloroplastic	40	1464184	1720208	1675083	1752548	0.00162	0.11490	0.23249	0.06522	UNCH.	UNCH.
A0A096RZN2	carbonic anhydrase	37	590206	755027	653734	788546	0.00673	0.03033	0.35531	0.27049	UNCH.	UNCH.
Q43267	phosphoenolpyruvate carboxylase	78	1262040	1164578	1219025	1190802	0.02936	0.52866	-0.11595	-0.03379	UNCH.	UNCH.
P46617	Cytochrome f	23	716585	774549	639692	707288	0.44621	0.23141	0.11222	0.14492	UNCH.	UNCH.

Supplementary Table 5 - Cont

Accession	Description	Reported peptides	Average Normalized Ion Count L80 HN	Average Normalized Ion Count L80 LN	Average Normalized Ion Count P2 HN	Average Normalized Ion Count P2 LN	t-test L80 LN/HN	t-test P2 LN/HN	Log_2 FC L80 LN/HN	Log_2 FC P2 LN/HN	Differential Accumulation L80 LN/HN	Differential Accumulation P2 LN/HN
O24574	Ribulose bisphosphate carboxylase small subunit, chloroplastic	16	955562	810815	1051292	736998	0.21472	0.03548	-0.23698	-0.51243	UNCH.	UNCH.
B6T3B2	Oxygen evolving complex 33kDa subunit	20	1126548	1285342	935596	1211598	0.04812	0.05773	0.19024	0.37295	UNCH.	UNCH.
P06671	Chlorophyll a-b binding protein, chloroplastic	10	747073	763720	674570	757450	0.05380	0.14986	0.03180	0.16718	UNCH.	UNCH.
P12329	Chlorophyll a-b binding protein 1, chloroplastic	12	734250	859351	847004	804775	0.04577	0.55927	0.22698	-0.07378	UNCH.	UNCH.
A0A1D6M7C2	Phosphoglycerate kinase	32	802283	879301	849040	869582	0.10246	0.42315	0.13225	0.03449	UNCH.	UNCH.
A0A804PCP1	Oxygen-evolving enhancer protein 1, chloroplastic	19	477892	510057	327616	382568	0.36784	0.25062	0.09397	0.22371	UNCH.	UNCH.
B4F8L7	Glyceraldehyde-3-phosphate dehydrogenase	29	938961	989525	1080843	948609	0.43073	0.40621	0.07567	-0.18827	UNCH.	UNCH.
P11155	Pyruvate, phosphate dikinase 1, chloroplastic	82	936955	936110	1063943	987744	0.99072	0.12387	-0.00130	-0.10721	UNCH.	UNCH.
C0P441	Carbonic anhydrase	19	202734	215598	103527	129577	0.05795	0.04568	0.08875	0.32380	UNCH.	UNCH.
B4FUA1	Chlorophyll a-b binding protein, chloroplastic	13	737032	796065	747704	760867	0.29105	0.90122	0.11116	0.02518	UNCH.	UNCH.
B4FRH8	Actin-7	27	283365	267965	271319	348663	0.65207	0.01690	-0.08062	0.36184	UNCH.	UNCH.
B4G143	Chlorophyll a-b binding protein, chloroplastic	12	691082	663164	677236	540852	0.70024	0.01130	-0.05949	-0.32442	UNCH.	UNCH.
P05022	ATP synthase subunit alpha, chloroplastic	34	1131489	1129754	1061334	1151121	0.97502	0.24547	-0.00221	0.11716	UNCH.	UNCH.
B6U5I1	peptidylprolyl isomerase	24	488537	601142	438985	621251	0.08401	0.00642	0.29924	0.50101	UNCH.	UNCH.
B4FL55	Chlorophyll a-b binding protein, chloroplastic	16	660445	636895	654554	741401	0.57945	0.00852	-0.05238	0.17974	UNCH.	UNCH.
A0A804MUG2	Chlorophyll a-b binding protein, chloroplastic	13	262296	332727	281661	335783	0.01097	0.00253	0.34314	0.25357	UNCH.	UNCH.

Supplementary Table 5 - Cont

Accession	Description	Reported peptides	Average Normalized Ion Count L80 HN	Average Normalized Ion Count L80 LN	Average Normalized Ion Count P2 HN	Average Normalized Ion Count P2 LN	t-test L80 LN/HN	t-test P2 LN/HN	Log_2 FC L80 LN/HN	Log_2 FC P2 LN/HN	Differential Accumulation L80 LN/HN	Differential Accumulation P2 LN/HN
A0A804LCX5	Glyceraldehyde-3-phosphate dehydrogenase	23	43066	47996	53025	45900	0.15520	0.35059	0.15635	-0.20817	UNCH.	UNCH.
A0A1D6M438	pyruvate, phosphate dikinase	64	1049143	993326	1097432	1001534	0.33738	0.37619	-0.07887	-0.13192	UNCH.	UNCH.
A0A096QRW1	Chlorophyll a-b binding protein, chloroplastic	11	595985	616284	550946	605994	0.61274	0.20947	0.04832	0.13739	UNCH.	UNCH.
P48183	Photosystem II protein D1	13	715235	740448	715305	679323	0.34030	0.28510	0.04998	-0.07446	UNCH.	UNCH.
Q9SLP5	Ferredoxin--NADP reductase, chloroplastic	33	507518	484450	551796	490692	0.65778	0.15117	-0.06711	-0.16932	UNCH.	UNCH.
A0A804M304	Actin	24	86007	84121	81839	86839	0.80891	0.37001	-0.03198	0.08556	UNCH.	UNCH.
B4FTJ0	Triosephosphate isomerase	21	593101	629566	640257	711377	0.06677	0.25080	0.08608	0.15196	UNCH.	UNCH.
B4F989	Actin-7	27	303897	298310	228262	276702	0.87967	0.03619	-0.02677	0.27765	UNCH.	UNCH.
Q9ZT00	Ribulose bisphosphate carboxylase/oxygenase activase, chloroplastic	29	807408	609021	678020	522789	0.00541	0.05282	-0.40681	-0.37510	UNCH.	UNCH.
P26301	Enolase 1	29	426184	405111	453360	352506	0.08820	0.02251	-0.07316	-0.36301	UNCH.	UNCH.
K7TXI5	Chlorophyll a-b binding protein, chloroplastic	11	761120	819986	688416	737528	0.01458	0.07091	0.10747	0.09942	UNCH.	UNCH.
P09315	Glyceraldehyde-3-phosphate dehydrogenase A, chloroplastic	23	1126113	1126432	1026512	1140474	0.99465	0.12575	0.00041	0.15188	UNCH.	UNCH.
B4FTI5	Fructose-bisphosphate aldolase	20	994243	854678	973851	830317	0.14356	0.13108	-0.21822	-0.23004	UNCH.	UNCH.
A0A804M0C2	Chlorophyll a-b binding protein, chloroplastic	12	1025688	978602	1067277	1105842	0.70147	0.60938	-0.06780	0.05121	UNCH.	UNCH.
Q6TM44	Germin-like protein	7	1352061	1404895	1437573	1193957	0.67966	0.05842	0.05530	-0.26788	UNCH.	UNCH.
B4F8P6	Malic enzyme	41	782590	790981	792510	860179	0.89710	0.38654	0.01539	0.11821	UNCH.	UNCH.

Supplementary Table 5 - Cont

Accession	Description	Reported peptides	Average Normalized Ion Count L80 HN	Average Normalized Ion Count L80 LN	Average Normalized Ion Count P2 HN	Average Normalized Ion Count P2 LN	t-test L80 LN/HN	t-test P2 LN/HN	Log_2 FC L80 LN/HN	Log_2 FC P2 LN/HN	Differential Accumulation L80 LN/HN	Differential Accumulation P2 LN/HN
A0A804MQ93	Triose-phosphate isomerase	17	132332	108594	97328	93413	0.01428	0.54988	-0.28522	-0.05923	UNCH.	UNCH.
A0A804QTN9	Phosphoglycerate kinase	26	430556	450783	356985	399718	0.40546	0.06028	0.06623	0.16312	UNCH.	UNCH.
C0HIK4	Carbonic anhydrase	15	362042	359685	302289	292672	0.95505	0.72447	-0.00943	-0.04664	UNCH.	UNCH.
B4FV94	Chlorophyll a-b binding protein, chloroplastic	9	237591	207832	220669	237074	0.08375	0.19936	-0.19306	0.10345	UNCH.	UNCH.
P00835	ATP synthase epsilon chain, chloroplastic	6	128249	77098	103684	42003	0.06266	0.14492	-0.73419	-1.30363	UNCH.	UNCH.
A0A804U716	Oxygen-evolving enhancer protein 1, chloroplastic	19	245852	236890	171884	185521	0.74581	0.48406	-0.05357	0.11015	UNCH.	UNCH.
A0A1D6F9C2	Oxygen-evolving enhancer protein 2-1 chloroplastic	16	760899	836237	783679	888040	0.19593	0.05893	0.13621	0.18036	UNCH.	UNCH.
B4FUM2	Ferredoxin--NADP reductase, chloroplastic	30	356871	318993	274789	220028	0.22592	0.34710	-0.16188	-0.32064	UNCH.	UNCH.
A0A804NHQ4	Chlorophyll a-b binding protein, chloroplastic	9	51802	46025	128805	149453	0.19879	0.27591	-0.17057	0.21451	UNCH.	UNCH.
A0A804NR66	Chlorophyll a-b binding protein, chloroplastic	7	274254	315786	302804	245683	0.04511	0.00743	0.20343	-0.30159	UNCH.	UNCH.
B4F9N4	plastoquinol--plastocyanin reductase	13	294936	226112	258984	205538	0.19935	0.36940	-0.38336	-0.33345	UNCH.	UNCH.
Q08062	Malate dehydrogenase, cytoplasmic	17	505737	464831	377204	344574	0.07488	0.11416	-0.12168	-0.13053	UNCH.	UNCH.
P19023	ATP synthase subunit beta, mitochondrial	26	301861	322802	267661	400063	0.08254	0.04012	0.09677	0.57982	UNCH.	UNCH.
P11601	Photosystem I iron-sulfur center	4	372714	271925	254903	342658	0.12362	0.16702	-0.45486	0.42682	UNCH.	UNCH.
A0A804Q515	PsbP domain-containing protein	14	782809	834569	606068	558574	0.63845	0.51441	0.09237	-0.11773	UNCH.	UNCH.
P24993	Photosystem II reaction center protein H	4	520314	492222	376036	463619	0.44922	0.05883	-0.08007	0.30207	UNCH.	UNCH.

Supplementary Table 5 - Cont

Accession	Description	Reported peptides	Average Normalized Ion Count L80 HN	Average Normalized Ion Count L80 LN	Average Normalized Ion Count P2 HN	Average Normalized Ion Count P2 LN	t-test L80 LN/HN	t-test P2 LN/HN	Log_2 FC L80 LN/HN	Log_2 FC P2 LN/HN	Differential Accumulation L80 LN/HN	Differential Accumulation P2 LN/HN
K7TXW7	Thioredoxin M-type, chloroplastic	10	499205	437615	421003	478620	0.07350	0.06259	-0.18997	0.18505	UNCH.	UNCH.
B4FM07	thioredoxin-dependent peroxiredoxin	17	509277	505305	470983	535888	0.77085	0.08629	-0.01130	0.18626	UNCH.	UNCH.
B4FQW6	Glyceraldehyde-3-phosphate dehydrogenase	20	404613	381743	267150	260266	0.12451	0.80120	-0.08394	-0.03766	UNCH.	UNCH.
B6TPG0	Elongation factor Tu	33	496315	422823	391543	435520	0.00205	0.35509	-0.23120	0.15357	UNCH.	UNCH.
P08735	Glyceraldehyde-3-phosphate dehydrogenase 1, cytosolic	23	194787	257951	256524	201197	0.04085	0.11097	0.40520	-0.35048	UNCH.	UNCH.
A0A096RAV0	Photosystem I reaction center subunit III	10	680627	735174	564558	749264	0.31823	0.03203	0.11122	0.40835	UNCH.	UNCH.
B4FCL1	Plastocyanin	5	3637	3810	307278	228873	0.88865	0.32601	0.06696	-0.42500	UNCH.	UNCH.
P48187	Photosystem II CP43 reaction center protein	15	258265	301254	269334	317480	0.09053	0.08171	0.22213	0.23727	UNCH.	UNCH.
B4FZU8	Malate dehydrogenase	14	145442	151967	154605	169085	0.64202	0.58066	0.06332	0.12917	UNCH.	UNCH.
B6T2L2	Sedoheptulose-1,7-bisphosphatase	21	235546	298497	390083	527141	0.01364	0.09974	0.34171	0.43441	UNCH.	UNCH.
A0A804PNJ3	Phosphoribulokinase	19	481019	443284	408923	327444	0.56836	0.28703	-0.11786	-0.32058	UNCH.	UNCH.
P05641	Photosystem II CP47 reaction center protein	21	922581	1070860	1023108	1021564	0.13319	0.97694	0.21502	-0.00218	UNCH.	UNCH.
B7ZZ42	Heat shock 70 kDa protein 3	34	90947	82187	52534	75248	0.06407	0.00419	-0.14611	0.51841	UNCH.	UNCH.
C0P699	Elongation factor Tu	32	247205	201592	176066	211894	0.13593	0.34506	-0.29427	0.26723	UNCH.	UNCH.
A0A1D6KE29	Heat shock protein 70	35	209106	195607	206702	194562	0.28567	0.17252	-0.09627	-0.08733	UNCH.	UNCH.
B4G0K4	Phosphoglycerate kinase	23	348722	325850	261399	251696	0.17969	0.53516	-0.09787	-0.05457	UNCH.	UNCH.

Supplementary Table 5 - Cont

Accession	Description	Reported peptides	Average Normalized Ion Count L80 HN	Average Normalized Ion Count L80 LN	Average Normalized Ion Count P2 HN	Average Normalized Ion Count P2 LN	t-test L80 LN/HN	t-test P2 LN/HN	Log_2 FC L80 LN/HN	Log_2 FC P2 LN/HN	Differential Accumulation L80 LN/HN	Differential Accumulation P2 LN/HN
Q9SLP6	Ferredoxin--NADP reductase, chloroplastic	29	226293	221601	171791	226417	0.75625	0.00606	-0.03023	0.39832	UNCH.	UNCH.
B4FVH1	Malate dehydrogenase	13	84996	71448	82803	92768	0.03310	0.47147	-0.25050	0.16395	UNCH.	UNCH.
B6SKI1	Photosystem I reaction center subunit II, chloroplastic	15	492260	429716	534856	440824	0.20537	0.02920	-0.19604	-0.27895	UNCH.	UNCH.
A0A804LV69	malate dehydrogenase (NADP(+))	25	715198	724173	673279	736458	0.86059	0.06977	0.01799	0.12940	UNCH.	UNCH.
A0A1D6JXJ7	fructose-bisphosphatase	18	568715	462542	451239	411641	0.00160	0.46867	-0.29812	-0.13251	UNCH.	UNCH.
A0A1X7YHF7	Photosystem II D2 protein	15	942825	909746	1083923	881397	0.40040	0.05706	-0.05153	-0.29840	UNCH.	UNCH.
K7VFF7	Glutaredoxin-dependent peroxiredoxin	14	376363	350968	369082	281386	0.58162	0.04811	-0.10078	-0.39139	UNCH.	UNCH.
A0A804PAT4	Malate dehydrogenase	14	5175	4281	203885	191515	0.02253	0.54137	-0.27386	-0.09030	UNCH.	UNCH.
B4FJP7	Photosynthetic NDH subunit of subcomplex B 2 chloroplastic	23	237558	249869	226600	262183	0.22206	0.35154	0.07289	0.21043	UNCH.	UNCH.
A0A804QNL6	Malate dehydrogenase	13	4947	5869	4810	4815	0.03253	0.99302	0.24666	0.00144	UNCH.	UNCH.
A0A804RTY6	FAD dependent oxidoreductase	6	525049	418376	373703	395692	0.00306	0.63293	-0.32765	0.08248	UNCH.	UNCH.
B6SZ69	Heat shock cognate 70 kDa protein 2	36	175058	146823	117521	90441	0.52320	0.23209	-0.25376	-0.37787	UNCH.	UNCH.
Q42368	Pyruvate, phosphate dikinase 2	62	390385	456478	437096	431318	0.33755	0.84987	0.22565	-0.01920	UNCH.	UNCH.
P62787	Histone H4	8	280416	300607	289884	338241	0.41318	0.10014	0.10031	0.22258	UNCH.	UNCH.
P15719	Malate dehydrogenase [NADP], chloroplastic	27	324383	279817	306414	302878	0.03398	0.79621	-0.21321	-0.01674	UNCH.	UNCH.
A0A804RQC9	Glutamine synthetase	18	278354	219989	151548	148197	0.10314	0.88062	-0.33949	-0.03226	UNCH.	UNCH.

Supplementary Table 5 - Cont

Accession	Description	Reported peptides	Average Normalized Ion Count L80 HN	Average Normalized Ion Count L80 LN	Average Normalized Ion Count P2 HN	Average Normalized Ion Count P2 LN	t-test L80 LN/HN	t-test P2 LN/HN	Log_2 FC L80 LN/HN	Log_2 FC P2 LN/HN	Differential Accumulation L80 LN/HN	Differential Accumulation P2 LN/HN
A0A5P8KLV9	Photosystem I P700 chlorophyll a apoprotein A2	15	727293	695734	815732	724180	0.31817	0.15959	-0.06400	-0.17175	UNCH.	UNCH.
B4FRJ1	Malate dehydrogenase	13	16261	16776	15864	23307	0.73769	0.15425	0.04504	0.55499	UNCH.	UNCH.
A0A1D6N672	Photosystem II subunit PsbS1	11	758769	818591	850982	911262	0.02002	0.37992	0.10948	0.09874	UNCH.	UNCH.
P38561	Glutamine synthetase root isozyme 3	17	233523	261624	156072	195223	0.22993	0.31507	0.16393	0.32291	UNCH.	UNCH.
P0C1M0	ATP synthase subunit gamma, chloroplastic	19	431422	461865	360113	388493	0.59880	0.45833	0.09837	0.10944	UNCH.	UNCH.
B6SSU6	fructose-bisphosphate aldolase	22	307406	350801	289657	337123	0.04064	0.05527	0.19051	0.21893	UNCH.	UNCH.
A0A804PPF4	Aminotran_1_2 domain-containing protein	33	644169	567219	630542	575032	0.13746	0.24615	-0.18353	-0.13295	UNCH.	UNCH.
P05642	Cytochrome b6	5	651762	694003	790838	767388	0.53779	0.60945	0.09060	-0.04343	UNCH.	UNCH.
B6T2W9	Thylakoid lumenal 19 kDa protein	14	107088	74149	106514	69817	0.17325	0.22145	-0.53029	-0.60940	UNCH.	UNCH.
P25462	Glutamine synthetase, chloroplastic	18	32132	38742	46862	43857	0.30421	0.37530	0.26985	-0.09559	UNCH.	UNCH.
O24561	Chlorophyll a-b binding protein, chloroplastic	14	726975	815880	628665	732897	0.09550	0.17365	0.16645	0.22132	UNCH.	UNCH.
A0A804NRX6	thioredoxin-dependent peroxiredoxin	16	174816	182907	144628	186210	0.27309	0.02550	0.06528	0.36458	UNCH.	UNCH.
O80429	Ferredoxin-2, chloroplastic	2	9615	6812	10941	8695	0.13845	0.37547	-0.49716	-0.33137	UNCH.	UNCH.
A0A804QDB7	Chlorophyll a-b binding protein, chloroplastic	8	533306	597174	464010	461209	0.10508	0.96508	0.16319	-0.00873	UNCH.	UNCH.
A0A804M6X3	Actin	12	6806	8286	7551	9980	0.00646	0.03330	0.28375	0.40240	UNCH.	UNCH.
Q41834	Nucleic acid-binding protein	14	292055	297327	269279	246825	0.76155	0.38677	0.02581	-0.12561	UNCH.	UNCH.

Supplementary Table 5 - Cont

Accession	Description	Reported peptides	Average Normalized Ion Count L80 HN	Average Normalized Ion Count L80 LN	Average Normalized Ion Count P2 HN	Average Normalized Ion Count P2 LN	t-test L80 LN/HN	t-test P2 LN/HN	Log_2 FC L80 LN/HN	Log_2 FC P2 LN/HN	Differential Accumulation L80 LN/HN	Differential Accumulation P2 LN/HN
A0A1D6IAT0	UTP--glucose-1-phosphate uridylyltransferase	30	196315	186368	183072	153461	0.41983	0.08728	-0.07502	-0.25454	UNCH.	UNCH.
B4FXB0	Chlorophyll a-b binding protein, chloroplastic	13	348485	354518	304701	397151	0.93680	0.05561	0.02476	0.38229	UNCH.	UNCH.
A0A1D6L6A9	Malate dehydrogenase	18	190293	236266	165533	157211	0.01623	0.76326	0.31219	-0.07442	UNCH.	UNCH.
P11143	Heat shock 70 kDa protein	35	55373	74492	76615	65489	0.10778	0.37338	0.42790	-0.22638	UNCH.	UNCH.
K7VN08	ATP synthase B chain	11	269358	259234	244627	229522	0.79660	0.73619	-0.05527	-0.09195	UNCH.	UNCH.
A0A096R6Z8	Heat shock 70 kDa protein 6 chloroplastic	34	197098	180796	204492	223927	0.05821	0.15835	-0.12456	0.13099	UNCH.	UNCH.
A0A804UKE7	L-ascorbate peroxidase	8	86871	60578	85262	67822	0.08610	0.41258	-0.52008	-0.33016	UNCH.	UNCH.
B4FJG1	Chlorophyll a-b binding protein, chloroplastic	14	276058	252546	255601	216997	0.20005	0.12742	-0.12843	-0.23622	UNCH.	UNCH.
A0A804QVR5	Tr-type G domain-containing protein	42	170836	162948	171061	134599	0.60972	0.02408	-0.06820	-0.34585	UNCH.	UNCH.
B6T171	alanine--glyoxylate transaminase	16	280791	180187	412308	356507	0.11911	0.58516	-0.64000	-0.20979	UNCH.	UNCH.
K7UUB7	Elongation factor 1-alpha	22	345672	229513	228330	204807	0.01314	0.17778	-0.59083	-0.15685	UNCH.	UNCH.
Q947B9	Glucose-1-phosphate adenylyltransferase	25	91752	92823	98788	106606	0.77182	0.63662	0.01674	0.10988	UNCH.	UNCH.
P93804	Phosphoglucomutase, cytoplasmic 1	35	163093	129714	147834	121708	0.04087	0.00966	-0.33036	-0.28056	UNCH.	UNCH.
A0A1D6LIK1	Peptidyl-prolyl cis-trans isomerase	14	285882	239895	221590	221212	0.13666	0.99428	-0.25301	-0.00246	UNCH.	UNCH.
A0A3L6E0R4	Glycolate oxidase 1	21	225833	330420	171315	130910	0.01236	0.04146	0.54905	-0.38807	UNCH.	UNCH.
A0A1D6LAW0	Elongation factor 2	44	72064	47666	46449	47103	0.00368	0.90251	-0.59630	0.02014	UNCH.	UNCH.

Supplementary Table 5 - Cont

Accession	Description	Reported peptides	Average Normalized Ion Count L80 HN	Average Normalized Ion Count L80 LN	Average Normalized Ion Count P2 HN	Average Normalized Ion Count P2 LN	t-test L80 LN/HN	t-test P2 LN/HN	Log_2 FC L80 LN/HN	Log_2 FC P2 LN/HN	Differential Accumulation L80 LN/HN	Differential Accumulation P2 LN/HN
P38559	Glutamine synthetase root isozyme 1	13	80474	107155	79475	108871	0.05476	0.02254	0.41310	0.45405	UNCH.	UNCH.
B6T4R3	UTP--glucose-1-phosphate uridylyltransferase	26	17303	12078	11642	13954	0.01257	0.06859	-0.51868	0.26127	UNCH.	UNCH.
K7VJF3	Heat shock 70 kDa protein 5	26	33186	34260	25675	30816	0.46845	0.07492	0.04597	0.26332	UNCH.	UNCH.
O22655	Profilin-4	6	176593	202015	161536	176448	0.51030	0.40295	0.19404	0.12738	UNCH.	UNCH.
A0A1D6LZ57	USP family protein	8	120555	114356	116521	86266	0.70116	0.12422	-0.07616	-0.43372	UNCH.	UNCH.
A0A1D6E4M0	Elongation factor G, chloroplastic	38	121760	102095	106008	83402	0.18965	0.00776	-0.25414	-0.34601	UNCH.	UNCH.
P69388	Cytochrome b559 subunit alpha	3	240096	179139	237162	243351	0.37147	0.93910	-0.42254	0.03716	UNCH.	UNCH.
A0A804PQT3	CYTOSOL_AP domain-containing protein	21	204499	229450	226943	267987	0.02413	0.04950	0.16608	0.23983	UNCH.	UNCH.
A0A1D6GK64	Heat shock 70 kDa protein 6 chloroplastic	32	59660	48479	67925	73967	0.00370	0.09886	-0.29943	0.12293	UNCH.	UNCH.
B4FFK3	ADP-ribosylation factor	11	104559	104155	84150	107143	0.97108	0.09542	-0.00559	0.34851	UNCH.	UNCH.
P93805	Phosphoglucomutase, cytoplasmic 2	33	76740	69070	66314	50744	0.27077	0.00312	-0.15193	-0.38608	UNCH.	UNCH.
B6SSN3	Chlorophyll a-b binding protein, chloroplastic	7	322594	347641	309011	331556	0.17082	0.57293	0.10788	0.10159	UNCH.	UNCH.
A0A804PQ35	Ferredoxin	4	96299	103044	136238	104490	0.70341	0.28883	0.09767	-0.38276	UNCH.	UNCH.
B6U4G5	Beta-propeller domain of methanol dehydrogenase type	8	239232	171581	190711	141047	0.03000	0.08479	-0.47952	-0.43521	UNCH.	UNCH.
B4FUZ3	fructose-bisphosphatase	19	279572	281837	292799	268965	0.88243	0.51953	0.01164	-0.12249	UNCH.	UNCH.
B6TCE9	Peptidyl-prolyl cis-trans isomerase	11	139024	108339	100739	95951	0.06159	0.85014	-0.35978	-0.07024	UNCH.	UNCH.

Supplementary Table 5 - Cont

Accession	Description	Reported peptides	Average Normalized Ion Count L80 HN	Average Normalized Ion Count L80 LN	Average Normalized Ion Count P2 HN	Average Normalized Ion Count P2 LN	t-test L80 LN/HN	t-test P2 LN/HN	Log_2 FC L80 LN/HN	Log_2 FC P2 LN/HN	Differential Accumulation L80 LN/HN	Differential Accumulation P2 LN/HN
A0A804PDW7	Luminal-binding protein 5	23	46356	45525	16436	20605	0.83746	0.16613	-0.02609	0.32615	UNCH.	UNCH.
A0A804UKA2	30S ribosomal protein S1, chloroplastic	17	170283	173186	151585	121854	0.78307	0.11332	0.02438	-0.31498	UNCH.	UNCH.
P12863	Triosephosphate isomerase, cytosolic	13	146227	188890	140799	177387	0.04095	0.06964	0.36934	0.33326	UNCH.	UNCH.
A0A804RH33	Thioredoxin domain-containing protein	7	134343	101534	129976	91081	0.04661	0.03559	-0.40395	-0.51302	UNCH.	UNCH.
A0A804MS63	Chlorophyll a-b binding protein, chloroplastic	8	39199	45894	63538	63509	0.19171	0.99669	0.22748	-0.00066	UNCH.	UNCH.
C0P6Z6	ATP synthase subunit delta chloroplastic	9	189557	254028	178326	203010	0.01251	0.34473	0.42235	0.18703	UNCH.	UNCH.
K7TGE1	Beta-glucosidase2	28	358036	250022	212685	236285	0.01393	0.48931	-0.51805	0.15181	UNCH.	UNCH.
A0A1D6MUE8	Heat shock 70 kDa protein 6 chloroplastic	35	297621	369935	330681	343084	0.20982	0.64828	0.31379	0.05312	UNCH.	UNCH.
K7TWV7	Peptidyl-prolyl cis-trans isomerase	9	166141	115273	110936	91958	0.09905	0.12223	-0.52735	-0.27069	UNCH.	UNCH.
A0A804PCR6	Eukaryotic initiation factor 4A-11	24	141907	146222	135932	107335	0.75210	0.29346	0.04321	-0.34077	UNCH.	UNCH.
A0A804LRW1	SAM_MPBQ_MSBQ_MT domain-containing protein	12	259032	264170	236066	266422	0.80355	0.46844	0.02834	0.17452	UNCH.	UNCH.
A0A1D6IKI2	RNA binding protein 1	6	75697	64924	62148	52265	0.43262	0.20290	-0.22148	-0.24986	UNCH.	UNCH.
A0A804NUX3	Phosphoribulokinase	12	21844	25511	24153	25499	0.25148	0.61025	0.22383	0.07826	UNCH.	UNCH.
B4FAD1	S-adenosylmethionine synthase	14	94881	93151	37967	52930	0.87133	0.05237	-0.02655	0.47935	UNCH.	UNCH.
A0A804Q076	RuBisCO large subunit-binding protein subunit alpha, chloroplastic	29	244124	228578	239670	202799	0.14220	0.19672	-0.09493	-0.24099	UNCH.	UNCH.
O65101	Photosystem I reaction center subunit VI, chloroplastic	3	209792	165880	248668	164441	0.02063	0.12451	-0.33881	-0.59665	UNCH.	UNCH.

Supplementary Table 5 - Cont

Accession	Description	Reported peptides	Average Normalized Ion Count L80 HN	Average Normalized Ion Count L80 LN	Average Normalized Ion Count P2 HN	Average Normalized Ion Count P2 LN	t-test L80 LN/HN	t-test P2 LN/HN	Log_2 FC L80 LN/HN	Log_2 FC P2 LN/HN	Differential Accumulation L80 LN/HN	Differential Accumulation P2 LN/HN
A5GZ73	Glucose-1-phosphate adenylyltransferase	32	101315	101873	139914	154407	0.95277	0.31881	0.00791	0.14220	UNCH.	UNCH.
A0A1D6H2R4	H(+)-exporting diphosphatase	19	313340	314208	246202	178514	0.95936	0.39779	0.00399	-0.46381	UNCH.	UNCH.
A0A804RMT2	Photosystem II CP43 chlorophyll apoprotein	6	336895	352321	323485	312104	0.60304	0.83301	0.06459	-0.05167	UNCH.	UNCH.
A0A804RHB6	S-adenosylmethionine synthase	11	79406	96095	56984	59780	0.12149	0.63350	0.27520	0.06912	UNCH.	UNCH.
A0A804R8A0	AAA domain-containing protein	35	175070	197638	202461	164402	0.10003	0.08625	0.17492	-0.30042	UNCH.	UNCH.
A0A804UAT5	Tr-type G domain-containing protein	21	54267	53953	60577	65937	0.95623	0.46951	-0.00835	0.12231	UNCH.	UNCH.
A0A804P2X3	Uncharacterized protein	26	123262	112575	76441	93462	0.45228	0.06857	-0.13084	0.29004	UNCH.	UNCH.
K7TL05	General regulatory factor2	17	126524	77889	101452	45094	0.24440	0.07143	-0.69991	-1.16978	UNCH.	UNCH.
A0A804RB13	Photosynthetic NDH subunit of subcomplex B 2, chloroplastic	19	179541	160833	206106	164354	0.11116	0.11992	-0.15875	-0.32658	UNCH.	UNCH.
B4FRG1	14-3-3-like protein	15	45414	37791	50503	32967	0.34885	0.12197	-0.26509	-0.61535	UNCH.	UNCH.
A0A804RDP0	Stromal 70 kDa heat shock-related protein, chloroplastic	25	19871	16163	19363	19236	0.02660	0.94833	-0.29796	-0.00943	UNCH.	UNCH.
B1PEY4	Superoxide dismutase [Cu-Zn]	6	188801	155704	96085	60882	0.28882	0.21979	-0.27806	-0.65830	UNCH.	UNCH.
A0A1D6I3L1	Elongation factor 2	14	196675	133829	232574	195221	0.14324	0.17873	-0.55542	-0.25258	UNCH.	UNCH.
B8A306	phosphoglycerate mutase (2,3-diphosphoglycerate-independent)	30	82830	104112	130930	89896	0.03652	0.14208	0.32991	-0.54248	UNCH.	UNCH.
A0A804QZU4	Aldedh domain-containing protein	24	239867	211655	163557	170191	0.25012	0.78844	-0.18052	0.05736	UNCH.	UNCH.
B6TR16	PSI-K	5	722385	595978	777589	711431	0.04273	0.32344	-0.27751	-0.12829	UNCH.	UNCH.

Supplementary Table 5 - Cont

Accession	Description	Reported peptides	Average Normalized Ion Count L80 HN	Average Normalized Ion Count L80 LN	Average Normalized Ion Count P2 HN	Average Normalized Ion Count P2 LN	t-test L80 LN/HN	t-test P2 LN/HN	Log_2 FC L80 LN/HN	Log_2 FC P2 LN/HN	Differential Accumulation L80 LN/HN	Differential Accumulation P2 LN/HN
A0A804UAN9	AAA domain-containing protein	36	236187	211735	264955	292057	0.13156	0.36889	-0.15767	0.14050	UNCH.	UNCH.
A0A804NE51	Malic enzyme	15	431572	388166	361055	361890	0.09155	0.98154	-0.15293	0.00333	UNCH.	UNCH.
A0A804RET3	Photosynthetic NDH subunit of subcomplex B 1, chloroplastic	19	247183	224164	266039	252055	0.10560	0.18062	-0.14102	-0.07790	UNCH.	UNCH.
C0PFV4	Chaperone protein ClpC1 chloroplastic	43	132190	134856	137385	138878	0.78357	0.88197	0.02881	0.01559	UNCH.	UNCH.
B7ZYV4	Arginine decarboxylase	29	102317	101863	222154	167382	0.97080	0.32137	-0.00641	-0.40842	UNCH.	UNCH.
C3UZ63	HSP protein	34	211586	172485	174657	159483	0.06853	0.28256	-0.29477	-0.13112	UNCH.	UNCH.
K7UUB0	Triose phosphate isomerase3	14	65902	86898	62212	90391	0.05145	0.04136	0.39899	0.53898	UNCH.	UNCH.
K7VH58	Peroxidase	19	166508	187673	150977	175764	0.27668	0.47875	0.17263	0.21931	UNCH.	UNCH.
K7UGM3	Catalase	18	426279	356725	353020	315717	0.06179	0.37537	-0.25699	-0.16112	UNCH.	UNCH.
B6TVG1	Malic enzyme	13	13449	22314	9390	11186	0.06160	0.02796	0.73039	0.25261	UNCH.	UNCH.
A0A1D6FQN8	Malic enzyme	12	10730	7953	14007	9605	0.06870	0.05152	-0.43217	-0.54423	UNCH.	UNCH.
A0A804Q265	glutamate-1-semialdehyde 2,1-aminomutase	19	162513	130915	136670	97326	0.11581	0.02679	-0.31193	-0.48980	UNCH.	UNCH.
P43188	Adenylate kinase, chloroplastic	16	230644	172030	172439	112350	0.15987	0.18602	-0.42301	-0.61808	UNCH.	UNCH.
A0A804R153	Malic enzyme	6	66374	82835	121989	114458	0.18401	0.77599	0.31963	-0.09193	UNCH.	UNCH.
P80607	Probable UDP-arabinopyranose mutase 1	19	77907	64067	25326	37384	0.24809	0.41382	-0.28216	0.56182	UNCH.	UNCH.
A0A804PZ34	Tr-type G domain-containing protein	15	84373	85876	62724	45463	0.83457	0.24092	0.02549	-0.46433	UNCH.	UNCH.

Supplementary Table 5 - Cont

Accession	Description	Reported peptides	Average Normalized Ion Count L80 HN	Average Normalized Ion Count L80 LN	Average Normalized Ion Count P2 HN	Average Normalized Ion Count P2 LN	t-test L80 LN/HN	t-test P2 LN/HN	Log_2 FC L80 LN/HN	Log_2 FC P2 LN/HN	Differential Accumulation L80 LN/HN	Differential Accumulation P2 LN/HN
B4G1K9	Photosystem I reaction center subunit V, chloroplastic	4	326970	289079	305809	309827	0.25678	0.91797	-0.17770	0.01883	UNCH.	UNCH.
A0A804R0D4	H(+)-exporting diphosphatase	17	12404	11781	18339	20804	0.36408	0.49592	-0.07445	0.18196	UNCH.	UNCH.
Q5QJA2	Harpin binding protein 1	15	258355	289228	217336	313460	0.29333	0.00838	0.16285	0.52836	UNCH.	UNCH.
A0A1D6N0R5	Protein RETICULATA-RELATED 4 chloroplastic	18	303962	331453	304861	312144	0.20877	0.62076	0.12491	0.03406	UNCH.	UNCH.
A0A096S2Q4	ATP-dependent zinc metalloprotease FTSH 5 chloroplastic	30	217481	198483	239598	220527	0.37852	0.50706	-0.13188	-0.11966	UNCH.	UNCH.
A0A804PFG1	V-type proton ATPase catalytic subunit A	32	138146	133755	154212	138007	0.71536	0.04281	-0.04661	-0.16017	UNCH.	UNCH.
B6SR38	NAD(P)-linked oxidoreductase superfamily protein	3	38243	39480	37312	46713	0.82875	0.28638	0.04591	0.32417	UNCH.	UNCH.
B4FIE9	S-adenosylmethionine synthase	17	54600	55632	23349	32743	0.86607	0.06667	0.02702	0.48780	UNCH.	UNCH.
A0A804NLS4	Adenosylhomocysteinase	15	121769	108140	89437	64117	0.15290	0.13177	-0.17125	-0.48017	UNCH.	UNCH.
Q5IBC6	DANA2	15	91805	79054	82451	93516	0.30420	0.59292	-0.21574	0.18168	UNCH.	UNCH.
A0A1D6GD70	Monothiol glutaredoxin-S14 chloroplastic	4	61591	55885	57020	44757	0.46641	0.07662	-0.14025	-0.34937	UNCH.	UNCH.
A0A804LEC3	ribulose-phosphate 3-epimerase	7	41019	30101	12320	16395	0.01343	0.00182	-0.44646	0.41228	UNCH.	UNCH.
A0A804LEC6	Ribulose-phosphate 3-epimerase	7	305825	282889	302305	264569	0.34532	0.03936	-0.11247	-0.19236	UNCH.	UNCH.
A0A804R4K2	Vacuolar proton pump subunit B	21	145044	166257	152848	182067	0.11417	0.02439	0.19693	0.25237	UNCH.	UNCH.
A0A1D6Q3E2	2-hydroxy-3-oxopropionate reductase	12	6075	7707	6889	9293	0.19599	0.03060	0.34324	0.43177	UNCH.	UNCH.
C0PB44	LL-diaminopimelate aminotransferase chloroplastic	14	46471	42601	44408	45170	0.14190	0.95517	-0.12543	0.02453	UNCH.	UNCH.

Supplementary Table 5 - Cont

Accession	Description	Reported peptides	Average Normalized Ion Count L80 HN	Average Normalized Ion Count L80 LN	Average Normalized Ion Count P2 HN	Average Normalized Ion Count P2 LN	t-test L80 LN/HN	t-test P2 LN/HN	Log_2 FC L80 LN/HN	Log_2 FC P2 LN/HN	Differential Accumulation L80 LN/HN	Differential Accumulation P2 LN/HN
A0A804NBQ9	phosphoglycerate mutase (2,3-diphosphoglycerate-independent)	25	53998	46370	54310	49622	0.06162	0.49448	-0.21973	-0.13022	UNCH.	UNCH.
A0A804PVH3	Vacuolar proton pump subunit B	19	50306	34473	42162	40806	0.00383	0.51521	-0.54524	-0.04716	UNCH.	UNCH.
P42895	Enolase 2	23	224681	266941	257032	256490	0.13469	0.97905	0.24864	-0.00304	UNCH.	UNCH.
B6U534	Photosystem I reaction center subunit V, chloroplastic	5	248087	265255	226779	234299	0.44091	0.61068	0.09654	0.04706	UNCH.	UNCH.
P80608	Cysteine synthase	15	53437	51677	132311	99340	0.75687	0.11413	-0.04831	-0.41349	UNCH.	UNCH.
C0PE12	Protein plastid transcriptionally active 16 chloroplastic	29	140323	99063	94569	72058	0.02842	0.12063	-0.50232	-0.39221	UNCH.	UNCH.
A0A804PTC6	Photosystem II stability/assembly factor	20	169662	182447	166415	178670	0.18913	0.55371	0.10481	0.10252	UNCH.	UNCH.
P49087	V-type proton ATPase catalytic subunit A (Fragment)	32	192590	167865	208393	163238	0.15708	0.00337	-0.19823	-0.35233	UNCH.	UNCH.
A0A804MZV7	Histone H2B	4	124303	114969	155711	108894	0.41834	0.07100	-0.11262	-0.51595	UNCH.	UNCH.
B4FFH8	Adenosine kinase	15	105898	111199	76867	60757	0.69957	0.43821	0.07047	-0.33931	UNCH.	UNCH.
A0A804PS86	Epimerase domain-containing protein	19	147277	126269	89558	126238	0.50079	0.28060	-0.22203	0.49524	UNCH.	UNCH.
Q6R987	ATP synthase subunit alpha	24	183098	210788	159161	217310	0.09735	0.06204	0.20318	0.44927	UNCH.	UNCH.
A0A804QR85	Protein plastid transcriptionally active 16, chloroplastic	28	45232	51386	65764	54696	0.31039	0.25018	0.18405	-0.26585	UNCH.	UNCH.
A0A1D6HT76	Protein containing PDZ domain a K-box domain and a TPR region	18	239472	194834	220290	193741	0.24393	0.23258	-0.29761	-0.18528	UNCH.	UNCH.
B4FWD0	NAD(P)H dehydrogenase (quinone)	6	72319	95676	46709	57467	0.14181	0.13244	0.40378	0.29903	UNCH.	UNCH.
A0A096RYW9	alanine transaminase	17	88321	114682	71354	86877	0.04802	0.28501	0.37682	0.28399	UNCH.	UNCH.

Supplementary Table 5 - Cont

Accession	Description	Reported peptides	Average Normalized Ion Count L80 HN	Average Normalized Ion Count L80 LN	Average Normalized Ion Count P2 HN	Average Normalized Ion Count P2 LN	t-test L80 LN/HN	t-test P2 LN/HN	Log_2 FC L80 LN/HN	Log_2 FC P2 LN/HN	Differential Accumulation L80 LN/HN	Differential Accumulation P2 LN/HN
B4G072	DIMBOA UDP-glucosyltransferase BX9	15	165135	133598	152423	137006	0.14418	0.48681	-0.30575	-0.15385	UNCH.	UNCH.
K7TX67	Plasma membrane ATPase	38	105593	97310	65853	92430	0.37088	0.18546	-0.11785	0.48910	UNCH.	UNCH.
A0A1D6FI91	H(+)-exporting diphosphatase	14	40647	10205	10617	12113	0.30446	0.66098	-1.99393	0.19013	UNCH.	UNCH.
A0A804NPT2	Photosynthetic NDH subunit of subcomplex B 1, chloroplastic	17	83717	100756	89885	112374	0.09199	0.02650	0.26726	0.32216	UNCH.	UNCH.
A0A804MP57	Carboxypeptidase	12	209808	159437	146225	173037	0.20003	0.18921	-0.39608	0.24289	UNCH.	UNCH.
B4FR08	Cysteine synthase	18	68396	57140	83104	84417	0.08082	0.79024	-0.25943	0.02261	UNCH.	UNCH.
A0A804M915	Plasma membrane ATPase	35	73430	74994	55471	58924	0.66293	0.71683	0.03042	0.08713	UNCH.	UNCH.
C0P5X6	Ribulose bisphosphate carboxylase/oxygenase activase, chloroplastic	11	16461	22881	23592	19509	0.00460	0.03872	0.47510	-0.27420	UNCH.	UNCH.
A0A804QPC1	Actin	22	39536	47204	24629	33040	0.26719	0.20242	0.25575	0.42387	UNCH.	UNCH.
B6STG2	PSI subunit V	6	323087	329890	368774	362864	0.84414	0.67456	0.03006	-0.02331	UNCH.	UNCH.
P21569	Peptidyl-prolyl cis-trans isomerase	7	157331	123207	89990	121643	0.16740	0.13031	-0.35272	0.43482	UNCH.	UNCH.
A0A1D6GRB4	alanine transaminase	21	10806	9986	15210	11488	0.43932	0.39367	-0.11383	-0.40497	UNCH.	UNCH.
P02582	Actin-1	21	17457	22291	23574	26315	0.27508	0.69870	0.35269	0.15864	UNCH.	UNCH.
A0A1D6LZ61	H(+)-exporting diphosphatase	9	100288	107924	128349	136823	0.74279	0.81356	0.10587	0.09224	UNCH.	UNCH.
P06670	NAD(P)H-quinone oxidoreductase subunit K, chloroplastic	6	160835	157531	188727	183540	0.78268	0.70783	-0.02995	-0.04021	UNCH.	UNCH.
A0A804Q8Y9	PGR5-like protein 1A, chloroplastic	10	63974	71523	95677	95303	0.51786	0.97552	0.16092	-0.00566	UNCH.	UNCH.

Supplementary Table 5 - Cont

Accession	Description	Reported peptides	Average Normalized Ion Count L80 HN	Average Normalized Ion Count L80 LN	Average Normalized Ion Count P2 HN	Average Normalized Ion Count P2 LN	t-test L80 LN/HN	t-test P2 LN/HN	Log_2 FC L80 LN/HN	Log_2 FC P2 LN/HN	Differential Accumulation L80 LN/HN	Differential Accumulation P2 LN/HN
A1XCI1	Lipoxygenase	25	2160	2906	95401	25913	0.38632	0.11038	0.42817	-1.88035	UNCH.	UNCH.
O49010	Herbicide safener binding protein	10	3905	3724	88895	52157	0.34788	0.31544	-0.06858	-0.76925	UNCH.	UNCH.
C4J4E4	Monodehydroascorbate reductase homolog1	19	152545	145258	155556	143743	0.64682	0.54482	-0.07061	-0.11395	UNCH.	UNCH.
P80639	Eukaryotic translation initiation factor 5A	11	107219	105822	84824	85542	0.88565	0.94206	-0.01892	0.01216	UNCH.	UNCH.
A0A804PH50	Rhodanese domain-containing protein	15	276813	295306	286997	353908	0.30746	0.05857	0.09330	0.30234	UNCH.	UNCH.
A0A804NCD4	NAD(P)H dehydrogenase (quinone)	7	34110	30440	33824	34071	0.52188	0.95022	-0.16421	0.01049	UNCH.	UNCH.
P46722	NAD(P)H-quinone oxidoreductase subunit I, chloroplastic	9	174715	177567	167693	196304	0.83909	0.40766	0.02336	0.22726	UNCH.	UNCH.
A0A804NLS3	Adenosylhomocysteinase	17	9542	8305	8026	7425	0.38784	0.30326	-0.20024	-0.11230	UNCH.	UNCH.
A0A804QXX4	UBC core domain-containing protein	3	40726	26072	18274	23944	0.10077	0.27232	-0.64346	0.38985	UNCH.	UNCH.
A0A804PN54	peptidylprolyl isomerase	8	90427	50588	67316	56807	0.06671	0.50085	-0.83794	-0.24488	UNCH.	UNCH.
A0A804PE80	Glycerate dehydrogenase HPR, peroxisomal	23	98673	105132	86449	71210	0.73244	0.11201	0.09147	-0.27977	UNCH.	UNCH.
K7VNE0	phosphoenolpyruvate carboxykinase (ATP)	25	34528	37599	46547	33591	0.52204	0.08702	0.12293	-0.47062	UNCH.	UNCH.
B6T398	Putative plastid-lipid-associated protein 13 chloroplastic	17	47987	53643	39710	52508	0.41220	0.10627	0.16073	0.40305	UNCH.	UNCH.
B4FU39	Enoyl reductase (ER) domain-containing protein	17	109947	117939	109997	96419	0.31653	0.52228	0.10123	-0.19008	UNCH.	UNCH.
Q06509	Caffeic acid 3-O-methyltransferase	13	89397	118470	12778	19753	0.39284	0.36285	0.40622	0.62843	UNCH.	UNCH.
A0A804NPV4	glucose-1-phosphate adenylyltransferase	14	99546	126471	67815	100664	0.04130	0.15234	0.34537	0.56987	UNCH.	UNCH.

Supplementary Table 5 - Cont

Accession	Description	Reported peptides	Average Normalized Ion Count L80 HN	Average Normalized Ion Count L80 LN	Average Normalized Ion Count P2 HN	Average Normalized Ion Count P2 LN	t-test L80 LN/HN	t-test P2 LN/HN	Log_2 FC L80 LN/HN	Log_2 FC P2 LN/HN	Differential Accumulation L80 LN/HN	Differential Accumulation P2 LN/HN
A0A804N5Z9	Acyl carrier protein	3	61200	29169	48057	37916	0.16784	0.35886	-1.06909	-0.34194	UNCH.	UNCH.
A0A804MHD2	Isocitrate lyase	12	107147	108286	89891	91746	0.82461	0.90263	0.01526	0.02948	UNCH.	UNCH.
B6SZ37	Chlorophyll a-b binding protein, chloroplastic	8	54353	58755	50810	48338	0.49753	0.76800	0.11236	-0.07195	UNCH.	UNCH.
A0A804UGZ9	Usp domain-containing protein	5	16198	14374	21937	8377	0.02519	0.13543	-0.17242	-1.38896	UNCH.	UNCH.
Q9ZQY2	Pyruvate dehydrogenase E1 component subunit beta	11	58317	46006	39406	58180	0.40351	0.04310	-0.34211	0.56210	UNCH.	UNCH.
B4FR80	Post-illumination chlorophyll fluorescence increase	10	128203	108588	95136	99932	0.31790	0.60772	-0.23957	0.07097	UNCH.	UNCH.
A0A1D6EC46	Double Clp-N motif-containing P-loop nucleoside triphosphate hydrolase superfamily protein	38	86799	86499	82592	85331	0.93342	0.77222	-0.00499	0.04707	UNCH.	UNCH.
A0A804UMX9	PAP_fibrillin domain-containing protein	14	28552	25493	19296	23970	0.57287	0.29617	-0.16347	0.31290	UNCH.	UNCH.
A0A804LS44	5-methyltetrahydropteroyltriglutamate--homocysteine S-methyltransferase	27	170327	132228	87461	70488	0.16906	0.15179	-0.36529	-0.31127	UNCH.	UNCH.
A0A1D6ES19	Heat shock protein 90-2	34	45623	56501	38967	38100	0.08380	0.77327	0.30852	-0.03245	UNCH.	UNCH.
A0A804QI52	PLD phosphodiesterase domain-containing protein	2	130963	132448	128767	127978	0.85832	0.97705	0.01627	-0.00886	UNCH.	UNCH.
B4FGC8	40S ribosomal protein S12	3	67411	49108	49431	34957	0.28667	0.23866	-0.45702	-0.49984	UNCH.	UNCH.
A0A804ML65	Cytosol aminopeptidase	9	5230	5029	4942	7695	0.70390	0.05177	-0.05658	0.63891	UNCH.	UNCH.
B6TRZ5	ATP-dependent Clp protease proteolytic subunit	12	130402	91267	130171	99523	0.01302	0.25434	-0.51480	-0.38730	UNCH.	UNCH.
B4G054	Photosynthetic NDH subunit of subcomplex B 5 chloroplastic	6	98203	95556	107332	106834	0.76041	0.95511	-0.03942	-0.00671	UNCH.	UNCH.
C0P439	UDP-arabinopyranose mutase	11	44927	34602	29025	29194	0.04378	0.98140	-0.37676	0.00841	UNCH.	UNCH.

Supplementary Table 5 - Cont

Accession	Description	Reported peptides	Average Normalized Ion Count L80 HN	Average Normalized Ion Count L80 LN	Average Normalized Ion Count P2 HN	Average Normalized Ion Count P2 LN	t-test L80 LN/HN	t-test P2 LN/HN	Log_2 FC L80 LN/HN	Log_2 FC P2 LN/HN	Differential Accumulation L80 LN/HN	Differential Accumulation P2 LN/HN
A0A804NYY2	DUF3700 domain-containing protein	6	70750	89024	50360	56475	0.25766	0.27341	0.33147	0.16533	UNCH.	UNCH.
B6SKA0	glutathione transferase	9	74650	71636	46400	48985	0.76454	0.82537	-0.05945	0.07822	UNCH.	UNCH.
A0A804MHD0	Isocitrate lyase	13	22136	26498	20562	22608	0.06667	0.56885	0.25948	0.13690	UNCH.	UNCH.
A0A1D6KKP0	Putative 14-3-3 protein	13	169823	226875	167902	204062	0.04087	0.11907	0.41787	0.28139	UNCH.	UNCH.
B4G031	L-ascorbate peroxidase	13	72602	49816	33099	26824	0.09257	0.48527	-0.54339	-0.30327	UNCH.	UNCH.
P12653	Glutathione S-transferase 1	9	14677	11754	13658	11852	0.14569	0.55247	-0.32043	-0.20466	UNCH.	UNCH.
B4FS77	Methyltransf_11 domain-containing protein	8	96423	90824	112617	109094	0.77644	0.77311	-0.08631	-0.04585	UNCH.	UNCH.
A0A1D6M250	Malic enzyme	15	17146	24104	19913	27234	0.02295	0.07100	0.49141	0.45173	UNCH.	UNCH.
A0A804RCZ7	Rubredoxin-like domain-containing protein	4	45407	45367	171233	179185	0.99633	0.84166	-0.00128	0.06549	UNCH.	UNCH.
A0A804LU84	Pyruvate dehydrogenase E1 component subunit beta	8	39742	34189	41703	34617	0.10154	0.08530	-0.21712	-0.26867	UNCH.	UNCH.
Q8H6A5	Translationally-controlled tumor protein homolog	12	114733	125155	109021	96523	0.23695	0.28182	0.12543	-0.17566	UNCH.	UNCH.
Q41738	Thiamine thiazole synthase 1, chloroplastic	11	58491	43461	61307	92092	0.14590	0.09468	-0.42851	0.58701	UNCH.	UNCH.
P49133	Triose phosphate/phosphate translocator, chloroplastic	7	350606	300330	438376	306200	0.40912	0.03881	-0.22330	-0.51769	UNCH.	UNCH.
P48186	ATP synthase subunit b, chloroplastic	8	100100	63691	69597	35589	0.08912	0.08237	-0.65229	-0.96758	UNCH.	UNCH.
A0A804QAJ3	HATPase_c domain-containing protein	34	41682	51308	55535	61983	0.09322	0.25880	0.29977	0.15847	UNCH.	UNCH.
B6T3B4	Succinate dehydrogenase10	8	31246	41545	32808	35920	0.13406	0.62817	0.41101	0.13074	UNCH.	UNCH.

Supplementary Table 5 - Cont

Accession	Description	Reported peptides	Average Normalized Ion Count L80 HN	Average Normalized Ion Count L80 LN	Average Normalized Ion Count P2 HN	Average Normalized Ion Count P2 LN	t-test L80 LN/HN	t-test P2 LN/HN	Log_2 FC L80 LN/HN	Log_2 FC P2 LN/HN	Differential Accumulation L80 LN/HN	Differential Accumulation P2 LN/HN
P04966	Photosystem I P700 chlorophyll a apoprotein A1	15	677441	568950	757819	676783	0.18607	0.12674	-0.25179	-0.16316	UNCH.	UNCH.
A0A804PZM5	Heat shock protein family A (Hsp70) member 13	4	2221	3112	3705	3275	0.00633	0.26185	0.48641	-0.17770	UNCH.	UNCH.
A0A1D6JPH3	Glutathione reductase	21	127369	111042	82390	81328	0.23439	0.94746	-0.19791	-0.01873	UNCH.	UNCH.
A0A1D6LSP5	Elongation factor gamma1	14	89973	71426	53889	44780	0.04136	0.08907	-0.33304	-0.26714	UNCH.	UNCH.
B4FY73	Germin-like protein	6	116448	97976	113437	122266	0.53694	0.30465	-0.24918	0.10813	UNCH.	UNCH.
B4FKM1	Guanine nucleotide-binding protein beta subunit-like protein	20	57947	49935	53881	48977	0.10832	0.65182	-0.21466	-0.13767	UNCH.	UNCH.
C0PDS1	Plastidal glycolate/glycerate translocator 1 chloroplastic	8	173691	222957	205710	209041	0.12834	0.80245	0.36024	0.02318	UNCH.	UNCH.
B4F836	Lactoylglutathione lyase	13	104229	86795	74886	60986	0.38546	0.38345	-0.26408	-0.29622	UNCH.	UNCH.
P27923	Ubiquitin-40S ribosomal protein S27a	6	253938	216760	184800	207847	0.06155	0.31190	-0.22838	0.16956	UNCH.	UNCH.
P12857	ADP,ATP carrier protein 2, mitochondrial	15	155281	156483	107504	147312	0.90512	0.04356	0.01113	0.45448	UNCH.	UNCH.
B4FK49	Nucleoside diphosphate kinase 1	7	102786	90810	109986	85756	0.44882	0.02052	-0.17873	-0.35901	UNCH.	UNCH.
B4FAL9	Fructose-bisphosphate aldolase	20	60671	60505	42516	42117	0.98396	0.91993	-0.00395	-0.01361	UNCH.	UNCH.
B6SJ21	Guanine nucleotide-binding protein beta subunit-like protein	19	103028	109839	62127	80904	0.59703	0.07699	0.09235	0.38099	UNCH.	UNCH.
Q41739	Thiamine thiazole synthase 2, chloroplastic	15	106362	76920	160852	92581	0.12794	0.15205	-0.46755	-0.79694	UNCH.	UNCH.
A0A804QCX5	Elongation factor 1-alpha	11	175648	194956	156094	170913	0.06414	0.30745	0.15046	0.13085	UNCH.	UNCH.
B6TI56	ribose-5-phosphate isomerase	9	223937	226590	219512	179672	0.89452	0.24686	0.01700	-0.28893	UNCH.	UNCH.

Supplementary Table 5 - Cont

Accession	Description	Reported peptides	Average Normalized Ion Count L80 HN	Average Normalized Ion Count L80 LN	Average Normalized Ion Count P2 HN	Average Normalized Ion Count P2 LN	t-test L80 LN/HN	t-test P2 LN/HN	Log_2 FC L80 LN/HN	Log_2 FC P2 LN/HN	Differential Accumulation L80 LN/HN	Differential Accumulation P2 LN/HN
B4FZ35	CHL-Zea mays Chloroplastic lipocalin	11	50625	51582	51998	67666	0.92507	0.29395	0.02699	0.37998	UNCH.	UNCH.
A0A804Q738	Rhodanese domain-containing protein	11	77579	86048	65216	91821	0.30365	0.00989	0.14948	0.49360	UNCH.	UNCH.
K7TP58	Cysteine protease 1	10	167096	187696	156663	187409	0.44060	0.13106	0.16772	0.25852	UNCH.	UNCH.
A0A804NG48	GTP-binding nuclear protein	10	93745	83053	68042	65113	0.35949	0.80737	-0.17471	-0.06350	UNCH.	UNCH.
A0A804MZR1	phosphoglycerate mutase (2,3-diphosphoglycerate-independent)	9	16532	15915	16699	12193	0.75398	0.03580	-0.05481	-0.45366	UNCH.	UNCH.
B4FPG9	Phosphoglycolate phosphatase 1A chloroplastic	12	77476	70402	72737	55939	0.31207	0.00418	-0.13815	-0.37883	UNCH.	UNCH.
B4FBC2	GDP-mannose 35-epimerase	14	97323	80196	50325	40798	0.01714	0.07976	-0.27926	-0.30279	UNCH.	UNCH.
P25709	NAD(P)H-quinone oxidoreductase subunit H, chloroplastic	18	153744	141162	177778	149867	0.49562	0.11011	-0.12317	-0.24639	UNCH.	UNCH.
B8A1H0	glucose-6-phosphate 1-epimerase	11	73265	56259	52338	42287	0.23968	0.38856	-0.38105	-0.30767	UNCH.	UNCH.
B6SQV5	Photosystem II 10 kDa polypeptide, chloroplastic	3	338721	346888	354950	289482	0.91429	0.14039	0.03437	-0.29414	UNCH.	UNCH.
B6TQ06	Aminomethyltransferase	19	143204	106473	101693	121600	0.17758	0.35025	-0.42758	0.25792	UNCH.	UNCH.
B8A1R8	5-methyltetrahydropteroyltriglutamate--homocysteine S-methyltransferase	18	38495	44882	40550	49577	0.24628	0.49410	0.22147	0.28997	UNCH.	UNCH.
B4FRM7	60S ribosomal protein L12	9	52455	46071	24475	33982	0.55396	0.17180	-0.18722	0.47346	UNCH.	UNCH.
A0A804NTN9	ATP-dependent Clp protease proteolytic subunit	8	52367	64483	37343	39214	0.09499	0.84583	0.30025	0.07053	UNCH.	UNCH.
A0A1D6EGN6	adenosylhomocysteinase	4	17098	17130	21350	14453	0.98579	0.00829	0.00273	-0.56284	UNCH.	UNCH.
Q43260	Glutamate dehydrogenase	15	158772	202692	156775	226738	0.13933	0.06650	0.35233	0.53233	UNCH.	UNCH.

Supplementary Table 5 - Cont

Accession	Description	Reported peptides	Average Normalized Ion Count L80 HN	Average Normalized Ion Count L80 LN	Average Normalized Ion Count P2 HN	Average Normalized Ion Count P2 LN	t-test L80 LN/HN	t-test P2 LN/HN	Log_2 FC L80 LN/HN	Log_2 FC P2 LN/HN	Differential Accumulation L80 LN/HN	Differential Accumulation P2 LN/HN
A0A1D6FA18	alanine transaminase	19	399207	383375	258230	367747	0.38759	0.33090	-0.05838	0.51006	UNCH.	UNCH.
A0A804LD34	40S ribosomal protein SA	12	96845	101821	81067	76603	0.81240	0.71648	0.07229	-0.08171	UNCH.	UNCH.
K7TFI4	NAD(P)H-quinone oxidoreductase subunit U chloroplastic	11	127525	118781	149790	125592	0.38047	0.31710	-0.10247	-0.25420	UNCH.	UNCH.
A0A804RJL5	Aconitate hydratase	21	29918	26385	20575	24595	0.31029	0.34672	-0.18132	0.25747	UNCH.	UNCH.
A0A804R0N6	Proteasome subunit alpha type	7	28307	33039	43342	57311	0.24892	0.00111	0.22300	0.40303	UNCH.	UNCH.
B4FA32	Peroxidase	11	59717	27200	20573	11003	0.09762	0.45303	-1.13455	-0.90289	UNCH.	UNCH.
Q6XZ78	Fructokinase-2	14	53075	59069	51991	36328	0.10845	0.29099	0.15436	-0.51718	UNCH.	UNCH.
A0A1D6F3N9	Elongation factor Ts, mitochondrial	29	62647	59383	30696	31458	0.63970	0.89357	-0.07719	0.03542	UNCH.	UNCH.
C0PCV2	40S ribosomal protein S8	8	68933	64244	62647	47763	0.51463	0.02381	-0.10163	-0.39135	UNCH.	UNCH.
B4FKM0	NADPH-protochlorophyllide oxidoreductase	16	173274	139390	139286	110483	0.04456	0.02665	-0.31393	-0.33423	UNCH.	UNCH.
B4FNM4	60S acidic ribosomal protein P0	10	113786	121966	89147	102502	0.26858	0.32518	0.10015	0.20140	UNCH.	UNCH.
A0A1D6PUK8	Aconitate hydratase	34	131433	146461	124428	123138	0.17012	0.91385	0.15619	-0.01503	UNCH.	UNCH.
C0P317	Phosphoenolpyruvate/phosphate translocator 1 chloroplastic	5	177395	173171	158994	161005	0.78876	0.90892	-0.03477	0.01813	UNCH.	UNCH.
A0A804Q189	Lactoylglutathione lyase	13	12684	14750	27279	24244	0.23492	0.11690	0.21779	-0.17021	UNCH.	UNCH.
Q941P2	Glucose-1-phosphate adenylyltransferase	10	11831	14490	12691	8416	0.00422	0.00363	0.29242	-0.59252	UNCH.	UNCH.
B4FRJ3	Proteasome subunit beta	11	16935	22080	10875	14107	0.02759	0.04287	0.38271	0.37539	UNCH.	UNCH.

Supplementary Table 5 - Cont

Accession	Description	Reported peptides	Average Normalized Ion Count L80 HN	Average Normalized Ion Count L80 LN	Average Normalized Ion Count P2 HN	Average Normalized Ion Count P2 LN	t-test L80 LN/HN	t-test P2 LN/HN	Log_2 FC L80 LN/HN	Log_2 FC P2 LN/HN	Differential Accumulation L80 LN/HN	Differential Accumulation P2 LN/HN
K7TM64	Pyruvate kinase	21	61432	64208	70510	53859	0.63384	0.03003	0.06375	-0.38863	UNCH.	UNCH.
C4J6E4	Peroxidase 42	5	68237	53546	41015	12262	0.47348	0.18758	-0.34978	-1.74198	UNCH.	UNCH.
B6TTP0	Histone H3	4	140654	109894	157971	153046	0.09997	0.71133	-0.35603	-0.04569	UNCH.	UNCH.
A0A804P454	hydroxymethylbilane synthase	16	45688	32504	52204	40550	0.10060	0.19254	-0.49117	-0.36447	UNCH.	UNCH.
A0A804MAX7	PEROXIDASE_4 domain-containing protein	12	267749	219106	333045	273588	0.34852	0.30045	-0.28926	-0.28371	UNCH.	UNCH.
B6TXY3	Quinone oxidoreductase-like protein	15	93150	76852	83059	76153	0.43324	0.30124	-0.27748	-0.12523	UNCH.	UNCH.
A0A1D6HK97	Photosynthetic NDH subunit of subcomplex B 4 chloroplastic	6	72041	71466	90708	60589	0.91324	0.09873	-0.01156	-0.58219	UNCH.	UNCH.
A0A1D6M2W3	Heavy metal transport/detoxification superfamily protein	6	137413	126295	95921	99206	0.61257	0.87369	-0.12172	0.04859	UNCH.	UNCH.
B4G1J8	50S ribosomal protein L3-1 chloroplastic	8	68754	73370	22405	33521	0.53559	0.48858	0.09376	0.58123	UNCH.	UNCH.
P55240	Glucose-1-phosphate adenylyltransferase small subunit (Fragment)	7	24844	24060	23814	19136	0.76953	0.31992	-0.04626	-0.31548	UNCH.	UNCH.
A0A1D6EEB5	transketolase	9	168240	171854	132362	88949	0.84028	0.00368	0.03066	-0.57345	UNCH.	UNCH.
B4FRZ2	Pyridoxal 5'-phosphate synthase-like subunit PDX1.2	13	124964	133420	99823	95281	0.23715	0.64277	0.09446	-0.06718	UNCH.	UNCH.
A0A804REY1	Beta-glucosidase	13	140689	211726	225024	212098	0.00682	0.45275	0.58969	-0.08535	UNCH.	UNCH.
A0A1D6EGA9	Aconitate hydratase	20	50314	36126	33970	45328	0.03899	0.12417	-0.47794	0.41615	UNCH.	UNCH.
B4FMY6	V-type proton ATPase subunit C	11	49215	42274	44709	48824	0.21531	0.36062	-0.21933	0.12703	UNCH.	UNCH.
A0A1D6QNZ7	DUF3119 family protein	7	50039	67038	62780	99143	0.01923	0.11662	0.42192	0.65920	UNCH.	UNCH.

Supplementary Table 5 - Cont

Accession	Description	Reported peptides	Average Normalized Ion Count L80 HN	Average Normalized Ion Count L80 LN	Average Normalized Ion Count P2 HN	Average Normalized Ion Count P2 LN	t-test L80 LN/HN	t-test P2 LN/HN	Log_2 FC L80 LN/HN	Log_2 FC P2 LN/HN	Differential Accumulation L80 LN/HN	Differential Accumulation P2 LN/HN
C4J4Q0	NTF2 domain-containing protein	6	65048	67863	69034	47389	0.56268	0.07096	0.06112	-0.54277	UNCH.	UNCH.
Q9SAZ6	phosphoenolpyruvate carboxylase	26	42418	41048	46200	46587	0.78865	0.97490	-0.04739	0.01203	UNCH.	UNCH.
A0A804MR04	2Fe-2S ferredoxin-type domain-containing protein	4	4517	3644	3458	2275	0.30713	0.13636	-0.30972	-0.60428	UNCH.	UNCH.
C0P455	60S ribosomal protein L4-1	13	96447	103724	134864	113707	0.48442	0.44135	0.10493	-0.24618	UNCH.	UNCH.
A0A804LJN9	phosphoglycerate mutase (2,3-diphosphoglycerate-independent)	7	7965	10992	9216	8427	0.05661	0.53397	0.46473	-0.12920	UNCH.	UNCH.
A0A804QVR8	Clp R domain-containing protein	6	7360	10878	7247	10293	0.00514	0.07726	0.56357	0.50611	UNCH.	UNCH.
A0A804M6T6	FAA_hydrolase domain-containing protein	4	58239	73662	41433	63640	0.39648	0.30011	0.33893	0.61915	UNCH.	UNCH.
K7UGR2	Putative TCP-1/cpn60 chaperonin family protein isoform 1	16	11981	13008	9338	11255	0.36598	0.22010	0.11866	0.26931	UNCH.	UNCH.
B4G010	Putative inactive linolenate hydroperoxide lyase	20	70480	52221	101450	82815	0.01040	0.29991	-0.43258	-0.29281	UNCH.	UNCH.
A0A3L6EVG8	inorganic diphosphatase	4	5588	3012	3822	2949	0.10231	0.56036	-0.89147	-0.37412	UNCH.	UNCH.
B4FT85	Isochorismate synthase 1	12	98844	95527	83599	103297	0.72556	0.34115	-0.04925	0.30524	UNCH.	UNCH.
B4FMF7	Aldose 1-epimerase	8	40022	25379	17047	12334	0.12598	0.40493	-0.65718	-0.46684	UNCH.	UNCH.
A0A804NQB4	Uncharacterized protein	7	55305	40675	37990	24729	0.14215	0.16715	-0.44327	-0.61940	UNCH.	UNCH.
A0A1D6EJC0	Clathrin heavy chain	41	83279	82724	82906	108207	0.96346	0.12887	-0.00964	0.38425	UNCH.	UNCH.
A0A1D6GEX5	Short chain alcohol dehydrogenase1	11	77458	69809	29428	47092	0.21462	0.06105	-0.15000	0.67830	UNCH.	UNCH.
B4FZL4	Chlorophyll a-b binding protein, chloroplastic	6	139187	140637	176359	126557	0.84816	0.02810	0.01495	-0.47872	UNCH.	UNCH.

Supplementary Table 5 - Cont

Accession	Description	Reported peptides	Average Normalized Ion Count L80 HN	Average Normalized Ion Count L80 LN	Average Normalized Ion Count P2 HN	Average Normalized Ion Count P2 LN	t-test L80 LN/HN	t-test P2 LN/HN	Log_2 FC L80 LN/HN	Log_2 FC P2 LN/HN	Differential Accumulation L80 LN/HN	Differential Accumulation P2 LN/HN
A0A804MWG4	Ribos_L4_asso_C domain-containing protein	14	41808	37807	38582	30884	0.53639	0.02690	-0.14511	-0.32106	UNCH.	UNCH.
Q9FQ11	Sucrose-phosphatase 1	11	44417	44167	53388	48633	0.94282	0.43245	-0.00817	-0.13458	UNCH.	UNCH.
A0A804M720	Mevalonate kinase	6	9596	12837	8317	11329	0.05956	0.00094	0.41993	0.44581	UNCH.	UNCH.
B6SUH9	PsbP domain-containing protein 3 chloroplastic	9	46317	55934	50148	41072	0.21021	0.24325	0.27218	-0.28804	UNCH.	UNCH.
A0A804LI35	Cysteine-rich repeat secretory protein 55	7	49956	35954	17604	19963	0.29118	0.77106	-0.47449	0.18149	UNCH.	UNCH.
A0A804LJR2	ABC transporter domain-containing protein	8	159130	146189	155371	142795	0.13834	0.42089	-0.12237	-0.12178	UNCH.	UNCH.
C0HHH9	Stress-response A/B barrel domain-containing protein UP3	5	75384	94710	46215	58558	0.13866	0.51821	0.32926	0.34150	UNCH.	UNCH.
A0A1D6HIF8	ADP/ATP translocase	6	12252	12436	10716	17838	0.93182	0.11231	0.02142	0.73514	UNCH.	UNCH.
C4J6K9	Guanosine nucleotide diphosphate dissociation inhibitor	14	26336	24209	24989	17710	0.03210	0.07482	-0.12146	-0.49677	UNCH.	UNCH.
A0A804NC60	Phosphoglycerate kinase	10	164705	167008	135276	183248	0.73245	0.02621	0.02003	0.43789	UNCH.	UNCH.
A0A804NJL3	Heat shock protein 70 family	9	18668	19808	35438	51208	0.66016	0.44799	0.08556	0.53106	UNCH.	UNCH.
B4FR32	Glyceraldehyde-3-phosphate deHaseN1	23	69623	78322	81102	75101	0.22817	0.52566	0.16986	-0.11090	UNCH.	UNCH.
P41040	Calmodulin	7	66664	43120	55897	24516	0.09283	0.09599	-0.62854	-1.18904	UNCH.	UNCH.
B4FTR5	NAD(P)-bd_dom domain-containing protein	8	57671	69992	79347	111491	0.25888	0.02001	0.27933	0.49068	UNCH.	UNCH.
A0A804M241	Succinate dehydrogenase assembly factor 4, mitochondrial	3	13994	12142	13853	9649	0.49227	0.28410	-0.20483	-0.52171	UNCH.	UNCH.
A0A317Y708	Chitin elicitor-binding protein	3	39308	30320	22447	15725	0.24071	0.32677	-0.37455	-0.51349	UNCH.	UNCH.

Supplementary Table 5 - Cont

Accession	Description	Reported peptides	Average Normalized Ion Count L80 HN	Average Normalized Ion Count L80 LN	Average Normalized Ion Count P2 HN	Average Normalized Ion Count P2 LN	t-test L80 LN/HN	t-test P2 LN/HN	Log_2 FC L80 LN/HN	Log_2 FC P2 LN/HN	Differential Accumulation L80 LN/HN	Differential Accumulation P2 LN/HN
B6TCN7	Threonine endopeptidase	4	70613	79836	68792	97906	0.13534	0.01810	0.17710	0.50915	UNCH.	UNCH.
Q84RL7	Aquaporin PIP2-1	5	97065	106320	62279	89378	0.56420	0.24372	0.13138	0.52116	UNCH.	UNCH.
A0A1D6L0I4	Adenylosuccinate synthetase, chloroplastic	15	79362	85847	52485	70375	0.65102	0.40864	0.11332	0.42315	UNCH.	UNCH.
A0A804LQP0	Shikimate kinase	7	60095	51217	32538	33336	0.40212	0.89117	-0.23061	0.03493	UNCH.	UNCH.
A0A1D6EZ36	peptidylprolyl isomerase	12	61374	70722	63622	71518	0.01888	0.35410	0.20453	0.16878	UNCH.	UNCH.
A0A096RG04	SOUL heme-binding family protein	8	114839	149423	191427	137353	0.47753	0.00500	0.37979	-0.47890	UNCH.	UNCH.
A0A804LUS4	NAD(P)-bd_dom domain-containing protein	8	4879	5523	33171	54018	0.15538	0.25340	0.17883	0.70351	UNCH.	UNCH.
B4FAD4	Isocitrate dehydrogenase [NAD] catalytic subunit 5 mitochondrial	8	30953	36976	22212	38012	0.18652	0.10134	0.25649	0.77514	UNCH.	UNCH.
P05643	Cytochrome b6-f complex subunit 4	3	227576	231472	270644	222055	0.84037	0.19070	0.02449	-0.28548	UNCH.	UNCH.
A0A804PXM9	Ribosomal_L18e/L15P domain-containing protein	7	185743	186446	185035	175500	0.96093	0.47944	0.00546	-0.07632	UNCH.	UNCH.
A0A1D6H1J8	Glyceraldehyde-3-phosphate dehydrogenase	6	6295	6490	7589	8186	0.70911	0.51168	0.04406	0.10926	UNCH.	UNCH.
A0A1D6IJP9	alanine transaminase	18	49037	50841	34539	37836	0.83633	0.63521	0.05212	0.13153	UNCH.	UNCH.
B4FSZ7	Putative mitochondrial-processing peptidase subunit alpha-2 chloroplastic/mitochondrial	17	45675	44335	51112	66456	0.73280	0.21130	-0.04297	0.37873	UNCH.	UNCH.
A0A804PZZ1	DLH domain-containing protein	6	33704	35027	22592	35465	0.89210	0.16096	0.05554	0.65057	UNCH.	UNCH.
A0A804MNZ3	Glucose-6-phosphate isomerase	15	32097	37216	30954	47032	0.17873	0.17868	0.21349	0.60351	UNCH.	UNCH.
A0A804P3H7	Fumarylacetoacetase	6	23582	22832	48443	27319	0.53034	0.10208	-0.04664	-0.82640	UNCH.	UNCH.

Supplementary Table 5 - Cont

Accession	Description	Reported peptides	Average Normalized Ion Count L80 HN	Average Normalized Ion Count L80 LN	Average Normalized Ion Count P2 HN	Average Normalized Ion Count P2 LN	t-test L80 LN/HN	t-test P2 LN/HN	Log_2 FC L80 LN/HN	Log_2 FC P2 LN/HN	Differential Accumulation L80 LN/HN	Differential Accumulation P2 LN/HN
A0A3L6E7C1	Proteasome subunit beta	9	33503	37185	31699	37460	0.06238	0.05580	0.15043	0.24090	UNCH.	UNCH.
A0A804PG82	lactoylglutathione lyase	14	51395	61523	52560	70396	0.42243	0.36347	0.25949	0.42154	UNCH.	UNCH.
A0A1D6MSE3	Dihydrolipoyl dehydrogenase	21	58062	53466	49541	56344	0.35814	0.19257	-0.11897	0.18564	UNCH.	UNCH.
A0A1D6FI07	Dihydrolipoyl dehydrogenase	19	40049	40729	40905	42955	0.79751	0.58064	0.02430	0.07054	UNCH.	UNCH.
A0A804MNL0	aldehyde dehydrogenase (NAD(+))	15	62367	69881	65927	71001	0.42502	0.38349	0.16412	0.10695	UNCH.	UNCH.
Q43272	NADP-dependent glyceraldehyde-3-phosphate dehydrogenase	22	49085	47465	53278	63810	0.77611	0.40739	-0.04841	0.26024	UNCH.	UNCH.
A0A804QU08	Uncharacterized protein	2	29835	13695	52107	20580	0.13231	0.09758	-1.12339	-1.34026	UNCH.	UNCH.
A0A1D6JS28	Outer mitochondrial membrane protein porin	11	68620	70174	64398	112814	0.77303	0.13470	0.03232	0.80885	UNCH.	UNCH.
A0A804Q3T0	PDZ domain-containing protein	10	34345	39960	70733	87498	0.18077	0.16262	0.21846	0.30686	UNCH.	UNCH.
A0A804M0B1	Ribosomal_L16 domain-containing protein	5	46027	32969	40526	29397	0.06405	0.12479	-0.48136	-0.46321	UNCH.	UNCH.
A0A1D6I644	Glucose-6-phosphate isomerase	15	17531	25805	22686	20390	0.01162	0.65034	0.55774	-0.15395	UNCH.	UNCH.
A0A1D6I2X6	Voltage-dependent anion channel protein1b	7	51270	46915	31474	43307	0.42066	0.10025	-0.12809	0.46047	UNCH.	UNCH.
C0PA91	Iso_dh domain-containing protein	9	40076	42516	43145	49985	0.53146	0.04161	0.08527	0.21228	UNCH.	UNCH.
C0PC61	transaldolase	12	52933	50371	37846	48550	0.60563	0.16212	-0.07157	0.35933	UNCH.	UNCH.
C4JBJ3	Calmodulin-7	2	41048	24134	36149	26556	0.09144	0.64209	-0.76625	-0.44490	UNCH.	UNCH.
A0A804QY51	transaldolase	14	27620	31992	19595	23518	0.24141	0.13416	0.21196	0.26327	UNCH.	UNCH.

Supplementary Table 5 - Cont

Accession	Description	Reported peptides	Average Normalized Ion Count L80 HN	Average Normalized Ion Count L80 LN	Average Normalized Ion Count P2 HN	Average Normalized Ion Count P2 LN	t-test L80 LN/HN	t-test P2 LN/HN	Log_2 FC L80 LN/HN	Log_2 FC P2 LN/HN	Differential Accumulation L80 LN/HN	Differential Accumulation P2 LN/HN
A0A804LV96	30S ribosomal protein S4, chloroplastic	8	39557	28884	39031	29785	0.01849	0.15602	-0.45365	-0.39005	UNCH.	UNCH.
A5H454	Peroxidase 66	3	39980	31939	30912	23120	0.36113	0.21792	-0.32397	-0.41905	UNCH.	UNCH.
P49105	Glucose-6-phosphate isomerase, cytosolic	22	158781	143316	204300	171578	0.08335	0.29397	-0.14784	-0.25183	UNCH.	UNCH.
A0A3L6E5Y7	Plasma membrane ATPase	20	37183	42455	41019	55494	0.49733	0.14464	0.19131	0.43604	UNCH.	UNCH.
B4FLJ3	Isocitrate dehydrogenase [NADP]	13	23455	21275	23458	19741	0.65037	0.63282	-0.14074	-0.24886	UNCH.	UNCH.
A0A1D6MV33	Plasma membrane ATPase	20	32938	32625	30913	36199	0.92715	0.14459	-0.01375	0.22770	UNCH.	UNCH.
A0A804MFU1	Protein TIC 40 chloroplastic	14	53790	49020	48604	45344	0.42439	0.67427	-0.13394	-0.10015	UNCH.	UNCH.
B6SXW8	RuBisCO large subunit-binding protein subunit alpha	21	73119	67714	59059	76085	0.65160	0.21257	-0.11079	0.36546	UNCH.	UNCH.
A0A804NIZ3	V-type proton ATPase subunit C	9	60531	76720	65535	67267	0.23698	0.85809	0.34194	0.03765	UNCH.	UNCH.
A0A1D6HAE3	L-ascorbate peroxidase	15	160931	142901	129380	179298	0.68319	0.35179	-0.17142	0.47074	UNCH.	UNCH.
A0A804MAH4	Myosin-11-like	61	80624	88639	87657	81373	0.21155	0.55536	0.13674	-0.10733	UNCH.	UNCH.
B4F9V1	Ferredoxin	2	13651	8717	3823	5439	0.17401	0.38160	-0.64722	0.50867	UNCH.	UNCH.
K7TK74	Putative alcohol dehydrogenase superfamily protein	13	26317	33312	47635	50484	0.04383	0.59065	0.34004	0.08380	UNCH.	UNCH.
C0PK05	Lactoylglutathione lyase	9	84238	82977	59381	59305	0.92673	0.99584	-0.02176	-0.00185	UNCH.	UNCH.
A0A1D6GQ42	Cell division cycle protein 48	29	43913	47982	33337	42572	0.13204	0.04485	0.12786	0.35278	UNCH.	UNCH.
A0A1D6N1Z8	6-phosphogluconate dehydrogenase, decarboxylating	16	46081	39712	32809	34874	0.28413	0.69786	-0.21461	0.08804	UNCH.	UNCH.

Supplementary Table 5 - Cont

Accession	Description	Reported peptides	Average Normalized Ion Count L80 HN	Average Normalized Ion Count L80 LN	Average Normalized Ion Count P2 HN	Average Normalized Ion Count P2 LN	t-test L80 LN/HN	t-test P2 LN/HN	Log_2 FC L80 LN/HN	Log_2 FC P2 LN/HN	Differential Accumulation L80 LN/HN	Differential Accumulation P2 LN/HN
B4FZ14	Protein CHLORORESPIRATORY REDUCTION 6 chloroplastic	5	31415	31644	24079	19332	0.95719	0.12107	0.01045	-0.31680	UNCH.	UNCH.
A0A804MLU6	Aldo_ket_red domain-containing protein	10	47927	43229	43968	49545	0.17882	0.56000	-0.14882	0.17228	UNCH.	UNCH.
C0HHM6	Thioredoxin family protein	4	40065	37329	24983	16101	0.61129	0.26934	-0.10203	-0.63378	UNCH.	UNCH.
K7U9F9	GDP-mannose 3,5-epimerase 2 isoform 1	8	22170	19642	18847	23112	0.37698	0.18667	-0.17466	0.29430	UNCH.	UNCH.
A0A804LVL8	NmrA domain-containing protein	10	49283	56463	68761	54945	0.38539	0.09773	0.19622	-0.32360	UNCH.	UNCH.
O22453	40S ribosomal protein S4	10	66407	49811	62234	49174	0.03999	0.20091	-0.41488	-0.33980	UNCH.	UNCH.
B4FBF6	Mitochondrial dicarboxylate/tricarboxylate transporter DTC	13	75853	94499	57320	79800	0.23037	0.12878	0.31710	0.47733	UNCH.	UNCH.
A0A1D6KZT2	Plasma membrane ATPase	16	69765	57056	64352	64759	0.13261	0.98071	-0.29014	0.00910	UNCH.	UNCH.
B6SRJ5	sulfate adenylyltransferase	16	50026	44891	33653	21177	0.14657	0.09386	-0.15626	-0.66824	UNCH.	UNCH.
A0A1D6I845	Proteasome subunit beta	8	27335	26319	24799	24697	0.79462	0.98437	-0.05463	-0.00594	UNCH.	UNCH.
A0A804PNL1	M16C_associated domain-containing protein	49	76517	85018	74133	75690	0.13643	0.90219	0.15199	0.02998	UNCH.	UNCH.
Q41785	Tubulin beta-8 chain	11	21301	26081	37857	32773	0.11251	0.56532	0.29207	-0.20806	UNCH.	UNCH.
C0PGG5	Pyruvate kinase	15	58027	58351	63772	59395	0.93838	0.21365	0.00803	-0.10258	UNCH.	UNCH.
B6TGL3	Proteasome subunit beta	10	219714	262229	232307	276331	0.00237	0.05604	0.25520	0.25036	UNCH.	UNCH.
B4F891	Tyrosine aminotransferase	16	54863	40208	28020	32342	0.01977	0.60561	-0.44837	0.20694	UNCH.	UNCH.
B4FTE0	Protein TIC 21, chloroplastic	4	56705	53449	72474	68550	0.49045	0.61067	-0.08532	-0.08031	UNCH.	UNCH.

Supplementary Table 5 - Cont

Accession	Description	Reported peptides	Average Normalized Ion Count L80 HN	Average Normalized Ion Count L80 LN	Average Normalized Ion Count P2 HN	Average Normalized Ion Count P2 LN	t-test L80 LN/HN	t-test P2 LN/HN	Log_2 FC L80 LN/HN	Log_2 FC P2 LN/HN	Differential Accumulation L80 LN/HN	Differential Accumulation P2 LN/HN
A0A804QBE8	CAAD domain-containing protein	2	77109	102508	69034	64540	0.05926	0.71296	0.41078	-0.09711	UNCH.	UNCH.
A0A804R6C0	Complex1_30kDa domain-containing protein	4	16239	10052	9894	7458	0.12381	0.29543	-0.69192	-0.40768	UNCH.	UNCH.
A0A804QKB5	Pentapeptide repeat-containing protein	6	15353	10199	31803	17934	0.01278	0.06199	-0.59009	-0.82641	UNCH.	UNCH.
K7URV3	Inositol-1-monophosphatase	7	53752	64714	85620	86698	0.52562	0.95993	0.26776	0.01805	UNCH.	UNCH.
Q41784	Tubulin beta-7 chain	11	19018	15434	11936	16024	0.27977	0.17987	-0.30122	0.42490	UNCH.	UNCH.
A0A804P8Y0	Proteasome subunit beta	8	38041	44003	33569	23744	0.16092	0.02177	0.21004	-0.49955	UNCH.	UNCH.
B6UB52	Cysteine synthase	7	25955	26930	21167	24939	0.54271	0.31833	0.05324	0.23660	UNCH.	UNCH.
C4IYM7	Mitochondrial outer membrane protein porin 2	10	22679	24846	18549	28358	0.44655	0.15204	0.13164	0.61245	UNCH.	UNCH.
C0PBY7	Nucleoside diphosphate kinase	6	45161	34429	33971	23072	0.08179	0.13048	-0.39146	-0.55816	UNCH.	UNCH.
B4FSV6	6-phosphogluconate dehydrogenase, decarboxylating	15	35984	33764	33979	38864	0.48528	0.35515	-0.09189	0.19377	UNCH.	UNCH.
A0A804P3H8	Fumarylacetoacetase	9	10110	10670	15177	8643	0.57734	0.07797	0.07774	-0.81221	UNCH.	UNCH.
A0A804NQ82	adenylate kinase	20	64391	49379	45375	53816	0.06662	0.30739	-0.38297	0.24615	UNCH.	UNCH.
A0A804M7N9	PGR5-like protein 1A, chloroplastic	9	35888	31278	54462	42196	0.20863	0.14222	-0.19833	-0.36814	UNCH.	UNCH.
B6SS42	Reticulon-like protein	6	50401	45743	48221	39056	0.10958	0.17828	-0.13989	-0.30413	UNCH.	UNCH.
B6T207	Cytochrome P450 71A26	6	4949	5491	6382	9260	0.23625	0.05135	0.15008	0.53699	UNCH.	UNCH.
B6TDR5	geranylgeranyl diphosphate reductase	11	40607	31192	36307	29526	0.09531	0.25869	-0.38056	-0.29829	UNCH.	UNCH.

Supplementary Table 5 - Cont

Accession	Description	Reported peptides	Average Normalized Ion Count L80 HN	Average Normalized Ion Count L80 LN	Average Normalized Ion Count P2 HN	Average Normalized Ion Count P2 LN	t-test L80 LN/HN	t-test P2 LN/HN	Log_2 FC L80 LN/HN	Log_2 FC P2 LN/HN	Differential Accumulation L80 LN/HN	Differential Accumulation P2 LN/HN
B4G1T3	chitinase	2	112956	82557	67576	42134	0.31072	0.32274	-0.45229	-0.68152	UNCH.	UNCH.
A0A1D6N2M7	Rieske domain containing protein	5	24644	31044	66788	84678	0.28406	0.13254	0.33307	0.34239	UNCH.	UNCH.
B6TGG7	3-oxoacyl-[acyl-carrier-protein] synthase	14	25835	31693	16125	15970	0.07981	0.97134	0.29484	-0.01392	UNCH.	UNCH.
A0A804R0S3	Starch synthase, chloroplastic/amyloplastic	10	190726	208773	167554	202233	0.04264	0.35814	0.13043	0.27139	UNCH.	UNCH.
A0A804QZ77	3-oxoacyl-[acyl-carrier-protein] synthase	11	43903	46151	20517	21782	0.63784	0.74620	0.07206	0.08636	UNCH.	UNCH.
A0A804Q121	Mitochondrial 2-oxoglutarate/malate carrier protein	11	32047	35121	32111	53070	0.69442	0.13407	0.13218	0.72483	UNCH.	UNCH.
C4J4B7	Rhodanese/Cell cycle control phosphatase superfamily protein	15	44076	53401	69457	81012	0.04430	0.02318	0.27689	0.22202	UNCH.	UNCH.
A0A1D6JX93	Peroxisomal nicotinamide adenine dinucleotide carrier	8	82503	62939	60722	46129	0.07672	0.01397	-0.39049	-0.39653	UNCH.	UNCH.
A0A1D6GYN4	Protein LOW PSII ACCUMULATION 3 chloroplastic	11	19498	16320	30979	29168	0.12920	0.18792	-0.25674	-0.08689	UNCH.	UNCH.
A0A804U9A8	Mitochondrial phosphate carrier protein 3, mitochondrial	14	151523	182697	114223	158846	0.06908	0.01212	0.26992	0.47577	UNCH.	UNCH.
A0A1D6J0S0	Monodehydroascorbate reductase 5 mitochondrial	16	86076	77393	84198	94158	0.53909	0.66336	-0.15340	0.16129	UNCH.	UNCH.
B4FNT1	Elongation factor 1-beta	8	79391	86566	75849	61656	0.37541	0.40370	0.12482	-0.29890	UNCH.	UNCH.
P23225	Ferredoxin-dependent glutamate synthase, chloroplastic	50	103413	80488	88551	70266	0.03755	0.26861	-0.36156	-0.33368	UNCH.	UNCH.
B4FSA7	ADP/ATP translocase	8	35879	31650	35064	31728	0.00309	0.40002	-0.18093	-0.14425	UNCH.	UNCH.
A0A804PIP4	Guanosine nucleotide diphosphate dissociation inhibitor	5	6740	5061	4172	5731	0.02486	0.19861	-0.41339	0.45820	UNCH.	UNCH.
B4FSB0	Guanosine nucleotide diphosphate dissociation inhibitor	7	22802	28808	33733	27246	0.06714	0.20457	0.33731	-0.30811	UNCH.	UNCH.

Supplementary Table 5 - Cont

Accession	Description	Reported peptides	Average Normalized Ion Count L80 HN	Average Normalized Ion Count L80 LN	Average Normalized Ion Count P2 HN	Average Normalized Ion Count P2 LN	t-test L80 LN/HN	t-test P2 LN/HN	Log_2 FC L80 LN/HN	Log_2 FC P2 LN/HN	Differential Accumulation L80 LN/HN	Differential Accumulation P2 LN/HN
K7VKM2	Peptidase beta subunit	17	56570	52362	39860	41618	0.66674	0.77282	-0.11152	0.06227	UNCH.	UNCH.
Q6XZ79	Fructokinase-1	8	23902	23985	16310	20349	0.97482	0.56277	0.00502	0.31918	UNCH.	UNCH.
A0A096RWW7	Chlorophyll a-b binding protein, chloroplastic	5	127769	140916	130084	154812	0.30612	0.42879	0.14129	0.25108	UNCH.	UNCH.
A0A804UDC9	Enoyl-[acyl-carrier-protein] reductase [NADH] chloroplastic	9	46182	51858	44264	45081	0.29899	0.91968	0.16721	0.02639	UNCH.	UNCH.
Q41764	Actin-depolymerizing factor 3	6	20308	21128	23311	16536	0.85552	0.30888	0.05713	-0.49537	UNCH.	UNCH.
C0P7Q1	Iso_dh domain-containing protein	5	14300	20080	15316	18308	0.04295	0.20704	0.48977	0.25745	UNCH.	UNCH.
A0A1D6L3U6	Aluminum induced protein with YGL and LRDR motifs	5	41016	53915	22737	22477	0.00643	0.93502	0.39451	-0.01658	UNCH.	UNCH.
A0A1D6GN34	Putative plastid-lipid-associated protein 10 chloroplastic	5	3051	4405	10018	18527	0.13221	0.06406	0.52980	0.88701	UNCH.	UNCH.
A0A1D6E5Z5	Adenosine kinase	7	3310	3225	2848	3078	0.77803	0.63021	-0.03740	0.11229	UNCH.	UNCH.
A0A1D6L8H4	Rubredoxin-like superfamily protein	4	22803	30566	27938	37919	0.00405	0.36151	0.42270	0.44072	UNCH.	UNCH.
B4FL79	Nascent polypeptide-associated complex subunit alpha-like protein 3	7	10042	11192	7250	11457	0.45966	0.15845	0.15646	0.66013	UNCH.	UNCH.
B4F9Q7	Ascorbate transporter chloroplastic	6	60302	63515	58089	54682	0.63023	0.71663	0.07489	-0.08720	UNCH.	UNCH.
B4FVT1	Peroxidase	11	50908	34372	28089	29033	0.17794	0.89941	-0.56665	0.04767	UNCH.	UNCH.
K7TSD2	Serine hydroxymethyltransferase	10	44051	49770	38708	41797	0.26952	0.56868	0.17610	0.11080	UNCH.	UNCH.
K7UQT7	Putative elongation factor 1-gamma 2	8	25741	19342	26809	26018	0.08016	0.83039	-0.41231	-0.04320	UNCH.	UNCH.
A0A804LX79	Uncharacterized protein	9	64075	74705	84832	74963	0.17336	0.45162	0.22143	-0.17843	UNCH.	UNCH.

Supplementary Table 5 - Cont

Accession	Description	Reported peptides	Average Normalized Ion Count L80 HN	Average Normalized Ion Count L80 LN	Average Normalized Ion Count P2 HN	Average Normalized Ion Count P2 LN	t-test L80 LN/HN	t-test P2 LN/HN	Log_2 FC L80 LN/HN	Log_2 FC P2 LN/HN	Differential Accumulation L80 LN/HN	Differential Accumulation P2 LN/HN
A0A804QTB0	isocitrate dehydrogenase (NADP(+))	10	12456	21377	13311	22850	0.07038	0.12275	0.77925	0.77959	UNCH.	UNCH.
A0A804PCL4	Peroxidase	9	55036	45773	34247	19343	0.26111	0.12264	-0.26587	-0.82416	UNCH.	UNCH.
A0A804LCC3	Dihydrodipicolinate reductase-like protein CRR1, chloroplastic	7	36973	39952	17428	28116	0.77586	0.09807	0.11180	0.68994	UNCH.	UNCH.
A0A1D6IKD2	FAD/NAD(P)-binding oxidoreductase family protein	10	25472	30420	33394	41034	0.14958	0.11067	0.25609	0.29723	UNCH.	UNCH.
A0A1D6EBS5	1,4-alpha-glucan branching enzyme	20	55480	54869	44423	62836	0.90475	0.08916	-0.01598	0.50030	UNCH.	UNCH.
A0A804Q5A4	GTP-binding nuclear protein	5	14598	11506	7447	7547	0.10224	0.93791	-0.34338	0.01926	UNCH.	UNCH.
A0A804QU06	uroporphyrinogen decarboxylase	4	27767	22115	19070	16800	0.44547	0.11839	-0.32836	-0.18281	UNCH.	UNCH.
B4FEA2	Mitochondrial carnitine/acylcarnitine carrier-like protein	11	29191	38700	55419	52069	0.21936	0.70493	0.40679	-0.08994	UNCH.	UNCH.
A0A804NPM9	Uncharacterized protein	6	20510	23712	15542	19954	0.25380	0.02153	0.20928	0.36056	UNCH.	UNCH.
A0A1D6MN18	Fructose-bisphosphate aldolase	4	4448	3166	3964	3612	0.24641	0.52680	-0.49022	-0.13397	UNCH.	UNCH.
C0PF34	Heme-binding-like protein chloroplastic	7	7728	7621	19052	25165	0.93993	0.40978	-0.02003	0.40149	UNCH.	UNCH.
Q08277	Heat shock protein 82	13	108454	99459	114719	89275	0.35563	0.19027	-0.12490	-0.36176	UNCH.	UNCH.
K7UY19	Fructose-bisphosphate aldolase	4	1723	1476	2109	1877	0.46079	0.61333	-0.22328	-0.16818	UNCH.	UNCH.
A0A1D6DW28	UDP-glycosyltransferase 89B1	10	25814	34568	29701	33764	0.11266	0.55967	0.42127	0.18500	UNCH.	UNCH.
A0A1D6E3E9	Prolyl endopeptidase	14	208388	140282	152944	296686	0.36035	0.28163	-0.57094	0.95593	UNCH.	UNCH.
A0A804MR62	ATP-synt_DE_N domain-containing protein	5	47694	47346	44046	43256	0.96802	0.94860	-0.01055	-0.02610	UNCH.	UNCH.

Supplementary Table 5 - Cont

Accession	Description	Reported peptides	Average Normalized Ion Count L80 HN	Average Normalized Ion Count L80 LN	Average Normalized Ion Count P2 HN	Average Normalized Ion Count P2 LN	t-test L80 LN/HN	t-test P2 LN/HN	Log_2 FC L80 LN/HN	Log_2 FC P2 LN/HN	Differential Accumulation L80 LN/HN	Differential Accumulation P2 LN/HN
B4FL64	Ribosomal protein L19	3	54077	40401	50633	38504	0.28754	0.08130	-0.42063	-0.39509	UNCH.	UNCH.
A0A804MAH6	Gamma-aminobutyrate transaminase POP2, mitochondrial	17	61617	74149	57311	73666	0.11587	0.11721	0.26710	0.36220	UNCH.	UNCH.
P17847	Ferredoxin--nitrite reductase, chloroplastic (Fragment)	17	34419	25362	31445	25515	0.00363	0.64454	-0.44053	-0.30149	UNCH.	UNCH.
A0A804PF16	3-isopropylmalate dehydratase	10	65021	75305	51588	41724	0.63029	0.26454	0.21184	-0.30616	UNCH.	UNCH.
B6TIP7	Peptidyl-prolyl cis-trans isomerase	4	30361	28012	14030	32415	0.45624	0.08596	-0.11620	1.20814	UNCH.	UNCH.
A0A1D6H9K5	Mitochondrial import inner membrane translocase subunit Tim17/Tim22/Tim23 family protein	9	17657	21645	16215	22575	0.13319	0.06738	0.29378	0.47740	UNCH.	UNCH.
A0A804M7G3	Elongation factor Tu	12	16600	14166	19118	19790	0.03090	0.71872	-0.22877	0.04983	UNCH.	UNCH.
B4FZB8	Signal recognition particle 54 kDa protein chloroplastic	10	51770	46878	39620	33176	0.54260	0.10040	-0.14322	-0.25611	UNCH.	UNCH.
A0A804UIM1	DUF1995 domain-containing protein	5	28885	39206	23009	31456	0.01468	0.01033	0.44077	0.45114	UNCH.	UNCH.
B6TLW3	Fiber protein Fb19	4	36787	32752	18248	23458	0.74146	0.38975	-0.16763	0.36234	UNCH.	UNCH.
A0A804LY89	TIC110	26	65891	56317	65351	61090	0.13759	0.75330	-0.22651	-0.09729	UNCH.	UNCH.
A0A804N6L9	Alpha-galactosidase	9	41429	35995	40935	29686	0.16583	0.04013	-0.20284	-0.46355	UNCH.	UNCH.
A0A1D6HJS1	Pyruvate dehydrogenase E1 component subunit alpha	11	39385	24905	28277	25258	0.05612	0.58355	-0.66121	-0.16291	UNCH.	UNCH.
Q84TL7	Legumin-like protein	6	25007	19524	10403	11243	0.29051	0.45731	-0.35705	0.11203	UNCH.	UNCH.
Q8W2B7	DIMBOA UDP-glucosyltransferase BX8	10	25586	25722	19731	23629	0.94224	0.30508	0.00769	0.26011	UNCH.	UNCH.
B4FH57	Elongation factor Tu	16	13387	16630	10081	10089	0.08983	0.99577	0.31291	0.00119	UNCH.	UNCH.

Supplementary Table 5 - Cont

Accession	Description	Reported peptides	Average Normalized Ion Count L80 HN	Average Normalized Ion Count L80 LN	Average Normalized Ion Count P2 HN	Average Normalized Ion Count P2 LN	t-test L80 LN/HN	t-test P2 LN/HN	Log_2 FC L80 LN/HN	Log_2 FC P2 LN/HN	Differential Accumulation L80 LN/HN	Differential Accumulation P2 LN/HN
B4FH62	NAD(P)-binding Rossmann-fold superfamily protein	7	53321	35165	32711	27978	0.12999	0.64553	-0.60056	-0.22550	UNCH.	UNCH.
B4FR28	uracil phosphoribosyltransferase	5	44548	57525	52444	71677	0.43633	0.43869	0.36884	0.45073	UNCH.	UNCH.
B4FAE1	Ras-related protein RABD2c	5	48281	48065	34711	48760	0.96006	0.01878	-0.00646	0.49030	UNCH.	UNCH.
B6SGQ2	SAM domain family protein	6	12795	14665	11710	14064	0.28176	0.09605	0.19673	0.26433	UNCH.	UNCH.
A0A1D6JSL7	inositol-3-phosphate synthase	5	8298	12411	5852	12601	0.01057	0.07272	0.58080	1.10655	UNCH.	UNCH.
A0A1D6N4X3	60S ribosomal protein L5-1 homolog a	5	47226	31794	33192	26590	0.01593	0.03837	-0.57082	-0.31994	UNCH.	UNCH.
A0A804PQ98	Ribosome-recycling factor, chloroplastic	4	40631	29590	29858	25279	0.18409	0.62115	-0.45747	-0.24016	UNCH.	UNCH.
A0A804NGW1	phosphoglucomutase (alpha-D-glucose-1,6-bisphosphate-dependent)	19	67360	60923	65687	71816	0.25617	0.51816	-0.14491	0.12870	UNCH.	UNCH.
A0A1D6J5V6	Amidohydro-rel domain-containing protein	7	26109	22701	34764	27456	0.27313	0.28794	-0.20177	-0.34048	UNCH.	UNCH.
B6T7Q7	Serine hydroxymethyltransferase	14	44873	37509	40811	33446	0.33771	0.13699	-0.25863	-0.28711	UNCH.	UNCH.
B4FS55	thioredoxin-dependent peroxiredoxin	5	22432	34751	22260	43107	0.09485	0.23215	0.63152	0.95346	UNCH.	UNCH.
A0A804NMP5	fructose-bisphosphate aldolase	4	8024	7606	7499	8952	0.89124	0.46729	-0.07706	0.25566	UNCH.	UNCH.
C0PHG6	Dicarboxylic acid transporter1	3	84808	71916	99840	102331	0.02128	0.85801	-0.23789	0.03555	UNCH.	UNCH.
B4FRM5	Red chlorophyll catabolite reductase chloroplastic	10	42388	53669	47757	49606	0.17778	0.71100	0.34044	0.05478	UNCH.	UNCH.
B6TAJ3	Proteasome subunit alpha type	9	36109	34128	33545	42519	0.67690	0.02841	-0.08137	0.34201	UNCH.	UNCH.
Q05737	GTP-binding protein YPTM2	4	36345	33272	22881	27902	0.41254	0.12735	-0.12745	0.28625	UNCH.	UNCH.

Supplementary Table 5 - Cont

Accession	Description	Reported peptides	Average Normalized Ion Count L80 HN	Average Normalized Ion Count L80 LN	Average Normalized Ion Count P2 HN	Average Normalized Ion Count P2 LN	t-test L80 LN/HN	t-test P2 LN/HN	Log_2 FC L80 LN/HN	Log_2 FC P2 LN/HN	Differential Accumulation L80 LN/HN	Differential Accumulation P2 LN/HN
C0P618	Phosphoenolpyruvate carboxylase family protein	10	30218	33521	18505	33723	0.69821	0.25389	0.14963	0.86578	UNCH.	UNCH.
P18122	Catalase isozyme 1	4	12253	8444	5382	6334	0.04207	0.56874	-0.53715	0.23482	UNCH.	UNCH.
A0A804LV58	Peptidase_M1 domain-containing protein	22	70570	87981	67491	82398	0.12330	0.05575	0.31813	0.28792	UNCH.	UNCH.
B4F9Z6	Enzyme of the cupin superfamily	4	22764	16535	44258	40654	0.12879	0.74214	-0.46127	-0.12255	UNCH.	UNCH.
B4FKD5	Eukaryotic translation initiation factor 6	2	27602	21062	17712	19396	0.17175	0.60721	-0.39015	0.13101	UNCH.	UNCH.
A0A1R3QF47	Chloroplast stem-loop binding protein of 41 kDa a chloroplastic	14	244307	226076	274457	233356	0.28775	0.04763	-0.11188	-0.23405	UNCH.	UNCH.
P46620	NAD(P)H-quinone oxidoreductase subunit 5, chloroplastic	13	171223	165485	214473	172113	0.78838	0.04974	-0.04918	-0.31744	UNCH.	UNCH.
B4FRJ4	Photosystem II 11 kD protein	2	17100	13391	20003	15101	0.05512	0.07370	-0.35273	-0.40560	UNCH.	UNCH.
C0HFQ0	Thioredoxin superfamily protein	6	20088	20263	29823	35150	0.95699	0.53243	0.01255	0.23713	UNCH.	UNCH.
Q1PBH6	Gamma-tocopherol methyltransferase	3	5709	8058	4858	13793	0.03753	0.07964	0.49733	1.50559	UNCH.	UNCH.
B4FTJ9	PBA1 homolog1	2	86479	87756	40820	43357	0.89161	0.86552	0.02115	0.08697	UNCH.	UNCH.
B4FBM9	60S ribosomal protein L3-1	14	73007	57385	61951	51664	0.22793	0.36122	-0.34735	-0.26199	UNCH.	UNCH.
A0A804Q3T4	Succinate dehydrogenase [ubiquinone] flavoprotein subunit, mitochondrial	12	405656	418509	409497	381293	0.74723	0.27884	0.04500	-0.10296	UNCH.	UNCH.
B6SPL7	Copper chaperone	2	14492	17380	10489	16891	0.18945	0.10694	0.26215	0.68736	UNCH.	UNCH.
C0P6B2	Glyceraldehyde-3-phosphate dehydrogenase-like family protein	11	46723	44678	26300	24988	0.66534	0.89040	-0.06457	-0.07382	UNCH.	UNCH.
A0A804P234	Aminotran_1_2 domain-containing protein	10	227061	210829	273760	257002	0.48830	0.69069	-0.10701	-0.09113	UNCH.	UNCH.

Supplementary Table 5 - Cont

Accession	Description	Reported peptides	Average Normalized Ion Count L80 HN	Average Normalized Ion Count L80 LN	Average Normalized Ion Count P2 HN	Average Normalized Ion Count P2 LN	t-test L80 LN/HN	t-test P2 LN/HN	Log_2 FC L80 LN/HN	Log_2 FC P2 LN/HN	Differential Accumulation L80 LN/HN	Differential Accumulation P2 LN/HN
B4F9K0	Late embryogenesis abundant protein group 2	5	27333	21402	17541	19420	0.16983	0.77062	-0.35293	0.14675	UNCH.	UNCH.
A0A804M5N9	H15 domain-containing protein	2	149991	142996	96168	157660	0.74907	0.05495	-0.06890	0.71318	UNCH.	UNCH.
A0A1D6GMB8	Membrane metalloprotease ARASP chloroplastic	5	9275	11309	11430	11211	0.17231	0.87569	0.28607	-0.02786	UNCH.	UNCH.
A0A1D6QK75	Heat shock protein 90-5 chloroplastic	18	168997	154325	240292	195274	0.12725	0.39557	-0.13103	-0.29929	UNCH.	UNCH.
B4F871	Protein DJ-1 homolog D	10	101125	93429	108355	89300	0.27607	0.12809	-0.11420	-0.27904	UNCH.	UNCH.
K7VKH1	Tubulin alpha chain	10	19360	17857	10767	17309	0.69413	0.15525	-0.11655	0.68486	UNCH.	UNCH.
A0A804PP22	Uncharacterized protein	4	18917	20169	21718	19854	0.54747	0.56623	0.09241	-0.12947	UNCH.	UNCH.
B8A0F3	Hydroxymethylbutenyl diphosphate synthase1	16	285418	320462	343637	303868	0.34032	0.16568	0.16708	-0.17744	UNCH.	UNCH.
B4FH88	methenyltetrahydrofolate cyclohydrolase	8	38439	27778	26736	18064	0.03094	0.11038	-0.46863	-0.56565	UNCH.	UNCH.
A0A804Q433	Mitochondrial-processing peptidase subunit alpha	11	30767	37105	27480	33179	0.14525	0.50093	0.27027	0.27190	UNCH.	UNCH.
A0A1D6HKA8	Arsenical pump-driving ATPase	9	25088	25687	23889	33278	0.71788	0.16158	0.03405	0.47822	UNCH.	UNCH.
A0A1D6LCQ2	SLH domain-containing protein	21	84139	63193	114075	91590	0.12305	0.20748	-0.41302	-0.31673	UNCH.	UNCH.
B4G1P2	NADH dehydrogenase2	2	15713	16734	11316	14414	0.79900	0.46940	0.09082	0.34908	UNCH.	UNCH.
B6SUD1	Alcohol dehydrogenase 2	8	15328	18453	42851	48008	0.14589	0.66907	0.26770	0.16394	UNCH.	UNCH.
A0A1D6GGL9	aspartate-semialdehyde dehydrogenase	11	29792	32882	33876	41082	0.20252	0.31107	0.14237	0.27825	UNCH.	UNCH.
A0A804NG04	Ketol-acid reductoisomerase	7	39440	28968	19260	15875	0.03116	0.30321	-0.44518	-0.27888	UNCH.	UNCH.

Supplementary Table 5 - Cont

Accession	Description	Reported peptides	Average Normalized Ion Count L80 HN	Average Normalized Ion Count L80 LN	Average Normalized Ion Count P2 HN	Average Normalized Ion Count P2 LN	t-test L80 LN/HN	t-test P2 LN/HN	Log_2 FC L80 LN/HN	Log_2 FC P2 LN/HN	Differential Accumulation L80 LN/HN	Differential Accumulation P2 LN/HN
A0A1D6NV83	Proteasome subunit beta	8	24901	30237	19065	26599	0.05935	0.09976	0.28013	0.48044	UNCH.	UNCH.
A0A804PQ06	3-ketoacyl-CoA thiolase 2, peroxisomal	9	35406	55049	39922	53978	0.06350	0.32579	0.63671	0.43517	UNCH.	UNCH.
O04014	40S ribosomal protein S6	5	45018	41143	51361	50999	0.51147	0.97134	-0.12985	-0.01019	UNCH.	UNCH.
A0A804PS72	Cysteine-rich repeat secretory protein 55	5	15806	21756	15560	19153	0.04723	0.37382	0.46088	0.29971	UNCH.	UNCH.
B4FJK0	Histone H2A	2	30632	21200	30219	35649	0.00293	0.24149	-0.53102	0.23839	UNCH.	UNCH.
A0A804QHI6	MPN domain-containing protein	4	20938	18915	11830	12335	0.43940	0.78403	-0.14664	0.06039	UNCH.	UNCH.
A0A804UCH1	Glucose-1-phosphate adenylyltransferase	6	24395	20234	16985	16829	0.00746	0.94845	-0.26983	-0.01328	UNCH.	UNCH.
B6SS34	PsbP domain-containing protein 1 chloroplastic	6	19647	10239	45578	14090	0.07659	0.31595	-0.94021	-1.69365	UNCH.	UNCH.
B4FAL8	Methanethiol oxidase	10	43130	38625	10865	11845	0.32745	0.74138	-0.15915	0.12457	UNCH.	UNCH.
C0PC75	Thioredoxin	2	20005	13710	26598	22592	0.25595	0.67166	-0.54516	-0.23549	UNCH.	UNCH.
B4FTK9	Alpha/beta-Hydrolases superfamily protein	3	9752	7695	3975	5126	0.58111	0.32027	-0.34171	0.36700	UNCH.	UNCH.
B6SRY5	Glycosyltransferase	16	39155	34250	56599	42260	0.31552	0.27837	-0.19308	-0.42149	UNCH.	UNCH.
A0A804QPM5	Alpha/beta-Hydrolases superfamily protein	5	26336	26021	19594	20008	0.87772	0.92961	-0.01735	0.03017	UNCH.	UNCH.
A0A804UCT7	tryptophan synthase	4	12869	8500	11920	10479	0.00485	0.02585	-0.59837	-0.18584	UNCH.	UNCH.
B6U2F2	Protein phosphatase	7	41252	43551	26428	32453	0.86109	0.27352	0.07824	0.29630	UNCH.	UNCH.
B4FNN8	Soluble epoxide hydrolase	4	19016	15268	10363	10482	0.13822	0.96541	-0.31668	0.01643	UNCH.	UNCH.

Supplementary Table 5 - Cont

Accession	Description	Reported peptides	Average Normalized Ion Count L80 HN	Average Normalized Ion Count L80 LN	Average Normalized Ion Count P2 HN	Average Normalized Ion Count P2 LN	t-test L80 LN/HN	t-test P2 LN/HN	Log_2 FC L80 LN/HN	Log_2 FC P2 LN/HN	Differential Accumulation L80 LN/HN	Differential Accumulation P2 LN/HN
C0P9S6	Thioredoxin Y1 chloroplastic	2	14568	11205	13765	6847	0.34094	0.37590	-0.37862	-1.00755	UNCH.	UNCH.
A0A1D6LHK9	Histone H2A	2	30972	30643	33792	35564	0.84657	0.77581	-0.01537	0.07376	UNCH.	UNCH.
A0A804RJT6	Zeaxanthin epoxidase, chloroplastic	8	29110	27177	37030	49884	0.40861	0.00622	-0.09914	0.42988	UNCH.	UNCH.
A0A804MFG4	Zeaxanthin epoxidase, chloroplastic	12	11607	9857	25561	27668	0.10696	0.49957	-0.23585	0.11425	UNCH.	UNCH.
B6SRX9	fructose-bisphosphatase	10	32206	38242	24322	30597	0.04200	0.25931	0.24782	0.33114	UNCH.	UNCH.
A0A804UIB7	Pyr_redox_2 domain-containing protein	7	7701	6372	12924	24820	0.54588	0.13238	-0.27336	0.94142	UNCH.	UNCH.
B4F8B9	S-(hydroxymethyl)glutathione dehydrogenase	9	52776	46092	37825	38642	0.10213	0.88591	-0.19538	0.03083	UNCH.	UNCH.
B4FDT0	40S ribosomal protein S20	2	28238	26858	14302	27540	0.79777	0.10873	-0.07232	0.94535	UNCH.	UNCH.
A0A804PL55	M20_dimer domain-containing protein	13	41838	43017	29133	29853	0.60289	0.88721	0.04008	0.03520	UNCH.	UNCH.
B6TS21	Succinate--CoA ligase [ADP-forming] subunit beta, mitochondrial	11	38795	40377	29515	34692	0.76925	0.37938	0.05765	0.23315	UNCH.	UNCH.
B4FKW0	Thioredoxin superfamily protein	2	29582	34605	27597	35398	0.38549	0.38183	0.22628	0.35918	UNCH.	UNCH.
B4FS03	adenine phosphoribosyltransferase	6	20233	25387	19417	22397	0.02415	0.55599	0.32737	0.20600	UNCH.	UNCH.
B4FPA4	Non-specific lipid transfer protein-like 1	3	17783	12589	12309	21541	0.02977	0.05391	-0.49827	0.80738	UNCH.	UNCH.
B6TAE7	Tropinone reductase	3	11012	10622	14125	14278	0.76911	0.98277	-0.05204	0.01561	UNCH.	UNCH.
A0A804PVR0	HATPase_c domain-containing protein	19	55902	40895	16066	17400	0.09936	0.74643	-0.45097	0.11504	UNCH.	UNCH.
A0A1D6HTL7	Germin-like protein	3	14062	23329	19201	22174	0.06584	0.73088	0.73029	0.20765	UNCH.	UNCH.

Supplementary Table 5 - Cont

Accession	Description	Reported peptides	Average Normalized Ion Count L80 HN	Average Normalized Ion Count L80 LN	Average Normalized Ion Count P2 HN	Average Normalized Ion Count P2 LN	t-test L80 LN/HN	t-test P2 LN/HN	Log_2 FC L80 LN/HN	Log_2 FC P2 LN/HN	Differential Accumulation L80 LN/HN	Differential Accumulation P2 LN/HN
A0A804PIC6	Aspartate aminotransferase	10	28791	21235	24768	16962	0.22684	0.09663	-0.43917	-0.54619	UNCH.	UNCH.
B6U666	Fructokinase-1	6	8455	12414	7068	8832	0.04470	0.28724	0.55413	0.32142	UNCH.	UNCH.
A0A804QJT3	Sodium/calcium exchanger NCL2	6	31959	21964	26773	15786	0.10064	0.21210	-0.54105	-0.76211	UNCH.	UNCH.
B4FA06	L-ascorbate peroxidase	6	22136	20617	33811	28160	0.49450	0.54831	-0.10251	-0.26388	UNCH.	UNCH.
A0A1D6L096	Myelin-associated oligodendrocyte basic protein isoform 1	6	21911	20780	31173	28029	0.40563	0.46313	-0.07644	-0.15336	UNCH.	UNCH.
A0A1D6LKF6	Serine/threonine-protein phosphatase 2A 65 kDa regulatory subunit A beta isoform	13	24712	33022	26917	31537	0.28321	0.14593	0.41818	0.22857	UNCH.	UNCH.
A0A1D6K8P1	peptide-methionine (S)-S-oxide reductase	6	14887	20980	23067	43115	0.13496	0.12259	0.49499	0.90235	UNCH.	UNCH.
B4FUZ2	Dihydrolipoamide acetyltransferase component of pyruvate dehydrogenase complex	4	29463	30397	17208	17506	0.93359	0.97112	0.04501	0.02478	UNCH.	UNCH.
K7UDG5	proline--tRNA ligase	6	9627	7798	8863	6237	0.22550	0.01654	-0.30400	-0.50691	UNCH.	UNCH.
A0A1D6QTB3	methenyltetrahydrofolate cyclohydrolase	7	11866	13355	9624	11758	0.49519	0.62597	0.17054	0.28899	UNCH.	UNCH.
A0A804Q9W9	Starch synthase, chloroplastic/amyloplastic	9	30188	35798	29123	43721	0.74216	0.44320	0.24591	0.58617	UNCH.	UNCH.
B4FIV1	DUF1338 domain-containing protein	2	17555	19480	13778	12010	0.73985	0.74868	0.15012	-0.19816	UNCH.	UNCH.
A0A804QEI0	Usp domain-containing protein	4	31579	25811	22713	23834	0.33391	0.78607	-0.29096	0.06950	UNCH.	UNCH.
A0A1D6JE77	DUF869 domain containing family protein	4	7797	6535	8658	7967	0.54899	0.60270	-0.25482	-0.11989	UNCH.	UNCH.
P52580	Isoflavone reductase homolog IRL	8	110978	125862	140381	123603	0.41211	0.47352	0.18157	-0.18364	UNCH.	UNCH.
A0A804QAX6	Cysteine proteinase 2	2	31096	21302	34901	13487	0.23028	0.11349	-0.54575	-1.37175	UNCH.	UNCH.

Supplementary Table 5 - Cont

Accession	Description	Reported peptides	Average Normalized Ion Count L80 HN	Average Normalized Ion Count L80 LN	Average Normalized Ion Count P2 HN	Average Normalized Ion Count P2 LN	t-test L80 LN/HN	t-test P2 LN/HN	Log_2 FC L80 LN/HN	Log_2 FC P2 LN/HN	Differential Accumulation L80 LN/HN	Differential Accumulation P2 LN/HN
B5AMJ8	Alpha-1,4 glucan phosphorylase	20	27686	31479	37326	40079	0.38483	0.67392	0.18524	0.10267	UNCH.	UNCH.
A0A1D6JJK6	Plasma membrane ATPase	7	650	1125	1713	1610	0.30817	0.88463	0.79065	-0.08932	UNCH.	UNCH.
A0A804UF95	IU_nuc_hydro domain-containing protein	6	22408	24750	18533	20171	0.52715	0.72597	0.14339	0.12220	UNCH.	UNCH.
C0P848	Formate dehydrogenase, mitochondrial	2	5979	4544	4080	2765	0.23681	0.01600	-0.39576	-0.56141	UNCH.	UNCH.
A0A1D6ENR2	Plastid phosphate/phosphoenolpyruvate translocator1	3	333891	305001	380850	328687	0.00235	0.21597	-0.13056	-0.21251	UNCH.	UNCH.
C0PFK3	Proteasome subunit alpha type	5	35212	39963	30040	37537	0.48953	0.23613	0.18260	0.32143	UNCH.	UNCH.
B4F9M9	Isocitrate dehydrogenase [NADP]	9	21022	21807	12327	15448	0.49368	0.31868	0.05289	0.32558	UNCH.	UNCH.
C0P472	Protein TIC 55 chloroplastic	7	30049	28411	21847	34765	0.81343	0.08986	-0.08087	0.67019	UNCH.	UNCH.
A0A1D6H5M1	Chalcone-flavonone isomerase family protein	7	26201	23663	22443	16758	0.66315	0.15187	-0.14697	-0.42139	UNCH.	UNCH.
A0A1D6G9Q0	Proteasome subunit alpha type	6	32647	36123	34204	34042	0.25295	0.98320	0.14596	-0.00683	UNCH.	UNCH.
B6T9P0	UDP-glucose 6-dehydrogenase	12	25954	24411	10136	22787	0.53541	0.21928	-0.08841	1.16874	UNCH.	UNCH.
A0A804LD07	Catalase	11	52677	47606	52259	51886	0.61992	0.97858	-0.14605	-0.01032	UNCH.	UNCH.
A0A1D6E225	proline--tRNA ligase	5	10417	9279	6049	4849	0.22836	0.33591	-0.16678	-0.31896	UNCH.	UNCH.
A0A804LR56	Serine hydroxymethyltransferase	7	23310	19945	14045	8202	0.44800	0.08420	-0.22494	-0.77598	UNCH.	UNCH.
A0A804RAP5	Carotenoid 9,10(9',10')-cleavage dioxygenase 1	10	50489	45229	35422	51292	0.24157	0.24534	-0.15870	0.53408	UNCH.	UNCH.
A0A1D6GWE1	Shepherd-like1	19	20122	15777	13914	14312	0.02283	0.91005	-0.35094	0.04069	UNCH.	UNCH.

Supplementary Table 5 - Cont

Accession	Description	Reported peptides	Average Normalized Ion Count L80 HN	Average Normalized Ion Count L80 LN	Average Normalized Ion Count P2 HN	Average Normalized Ion Count P2 LN	t-test L80 LN/HN	t-test P2 LN/HN	Log_2 FC L80 LN/HN	Log_2 FC P2 LN/HN	Differential Accumulation L80 LN/HN	Differential Accumulation P2 LN/HN
B6U151	Glutamyl-tRNA(Gln) amidotransferase subunit A, chloroplastic/mitochondrial	8	20988	19487	20689	17713	0.64332	0.54867	-0.10706	-0.22410	UNCH.	UNCH.
B4F848	20 kDa chaperonin chloroplastic	4	45248	37439	35425	27404	0.09731	0.27192	-0.27334	-0.37037	UNCH.	UNCH.
B4FG53	Malate dehydrogenase	5	43392	58442	58903	66242	0.01564	0.59982	0.42956	0.16940	UNCH.	UNCH.
B4F9M7	Protein CURVATURE THYLAKOID 1B chloroplastic	3	14320	13658	21557	17096	0.86427	0.47248	-0.06834	-0.33445	UNCH.	UNCH.
A0A804MEH5	peptide-methionine (S)-S-oxide reductase	3	9604	3475	10712	9084	0.08324	0.60425	-1.46669	-0.23769	UNCH.	UNCH.
B4FRI1	Phosphoserine aminotransferase	7	27878	24705	19636	15401	0.47580	0.27503	-0.17433	-0.35055	UNCH.	UNCH.
B6THR9	3-isopropylmalate dehydrogenase	7	18868	16711	11330	12707	0.50218	0.75211	-0.17516	0.16548	UNCH.	UNCH.
B4FWU6	Glutathione reductase	8	27680	27563	23228	26777	0.98163	0.46963	-0.00611	0.20513	UNCH.	UNCH.
C0HEH4	O-methyltransferase family protein	5	37150	40792	29820	30075	0.18209	0.90543	0.13490	0.01228	UNCH.	UNCH.
P46252	60S acidic ribosomal protein P2A	2	14412	13591	8125	11562	0.76765	0.28750	-0.08458	0.50893	UNCH.	UNCH.
B4G066	methylmalonate-semialdehyde dehydrogenase (CoA acylating)	10	30278	29096	18201	15211	0.85260	0.29462	-0.05742	-0.25891	UNCH.	UNCH.
B4FFV3	Malate dehydrogenase	5	1344	1180	2329	1860	0.81523	0.44403	-0.18758	-0.32422	UNCH.	UNCH.
P29185	Chaperonin CPN60-1, mitochondrial	14	62455	72214	54394	78451	0.10788	0.02462	0.20948	0.52833	UNCH.	UNCH.
B7ZWY9	Citrate synthase	10	20247	18309	24679	19878	0.68963	0.26649	-0.14515	-0.31215	UNCH.	UNCH.
B6T969	Proteasome subunit alpha type	4	46777	41092	37358	26647	0.53675	0.13369	-0.18692	-0.48747	UNCH.	UNCH.
A0A804M535	Amino_oxidase domain-containing protein	4	12833	17543	10688	13555	0.15690	0.50121	0.45110	0.34290	UNCH.	UNCH.

Supplementary Table 5 - Cont

Accession	Description	Reported peptides	Average Normalized Ion Count L80 HN	Average Normalized Ion Count L80 LN	Average Normalized Ion Count P2 HN	Average Normalized Ion Count P2 LN	t-test L80 LN/HN	t-test P2 LN/HN	Log_2 FC L80 LN/HN	Log_2 FC P2 LN/HN	Differential Accumulation L80 LN/HN	Differential Accumulation P2 LN/HN
A0A804PPC5	CobW C-terminal domain-containing protein	8	36894	37735	32440	27209	0.88719	0.03907	0.03252	-0.25367	UNCH.	UNCH.
B6TVM7	4-methyl-5-thiazole monophosphate biosynthesis protein	6	31475	27846	17894	27438	0.67244	0.17883	-0.17674	0.61672	UNCH.	UNCH.
Q9SPD7	Outer mitochondrial membrane protein porin	4	30368	37086	21362	30581	0.33832	0.20871	0.28833	0.51755	UNCH.	UNCH.
A0A1D6E501	3-isopropylmalate dehydrogenase	6	9335	6576	7911	6519	0.01745	0.50837	-0.50548	-0.27919	UNCH.	UNCH.
K7V2Z8	carbamoyl-phosphate synthase (glutamine-hydrolyzing)	22	48743	34095	40466	30193	0.09754	0.27004	-0.51563	-0.42253	UNCH.	UNCH.
Q768R5	Oxo-glutarate/malate transporter1	2	214247	204652	235364	210230	0.47116	0.26202	-0.06610	-0.16293	UNCH.	UNCH.
E1AFV5	Beta-1,3-glucanase	4	19783	15115	10006	8843	0.23407	0.54133	-0.38836	-0.17828	UNCH.	UNCH.
B6T2Y5	S-formylglutathione hydrolase	4	20179	17779	13719	11967	0.31176	0.66083	-0.18269	-0.19703	UNCH.	UNCH.
A0A804MIU2	Fe-S cluster assembly factor HCF101, chloroplastic	8	22847	19691	17803	14694	0.23617	0.14809	-0.21442	-0.27691	UNCH.	UNCH.
A0A1D6L554	60S ribosomal protein L13a-1	2	28611	26734	18334	20581	0.58507	0.39320	-0.09792	0.16679	UNCH.	UNCH.
C0P4T5	aspartate--tRNA ligase	9	48337	51846	58515	46715	0.22327	0.20439	0.10110	-0.32492	UNCH.	UNCH.
O63066	Preprotein translocase subunit SECY, chloroplastic	5	26547	20454	19443	12855	0.06287	0.03143	-0.37619	-0.59688	UNCH.	UNCH.
B6TVI5	3-hydroxyisobutyrate dehydrogenase-like 1, mitochondrial	5	22990	20970	20594	16468	0.47833	0.25720	-0.13267	-0.32257	UNCH.	UNCH.
B8A270	Protease Do-like 2 chloroplastic	5	24535	21189	13206	14459	0.33977	0.57237	-0.21152	0.13084	UNCH.	UNCH.
K7VUU0	Protein DJ-1 homolog B	7	27171	21876	14225	20842	0.13770	0.07540	-0.31274	0.55109	UNCH.	UNCH.
A0A317YCE2	Thylakoid soluble phosphoprotein TSP9	3	10233	10981	18752	14129	0.44476	0.05004	0.10180	-0.40839	UNCH.	UNCH.

Supplementary Table 5 - Cont

Accession	Description	Reported peptides	Average Normalized Ion Count L80 HN	Average Normalized Ion Count L80 LN	Average Normalized Ion Count P2 HN	Average Normalized Ion Count P2 LN	t-test L80 LN/HN	t-test P2 LN/HN	Log_2 FC L80 LN/HN	Log_2 FC P2 LN/HN	Differential Accumulation L80 LN/HN	Differential Accumulation P2 LN/HN
B7ZZ56	Glycosyltransferase	7	18377	16091	11529	12491	0.48036	0.65361	-0.19170	0.11570	UNCH.	UNCH.
A0A804Q2I3	Calreticulin	3	23790	19435	15479	11715	0.04740	0.35276	-0.29169	-0.40191	UNCH.	UNCH.
B4FAI1	N-acetyl-gamma-glutamyl-phosphate reductase	6	31445	37421	21245	35238	0.52945	0.05256	0.25102	0.73003	UNCH.	UNCH.
B4FJY5	Proteasome subunit beta	2	26422	23632	20856	24188	0.45536	0.48839	-0.16102	0.21380	UNCH.	UNCH.
A0A804MH53	dihydrolipoyllysine-residue succinyltransferase	7	57411	54469	46990	52249	0.77131	0.58908	-0.07588	0.15307	UNCH.	UNCH.
A0A804R1M2	PALP domain-containing protein	3	4453	4612	4808	3729	0.71106	0.17775	0.05063	-0.36635	UNCH.	UNCH.
K7U4C2	Uncharacterized protein	3	18361	13123	14107	11159	0.11629	0.39454	-0.48457	-0.33819	UNCH.	UNCH.
A0A804Q5M1	RNA-binding protein	3	22171	20433	17241	11780	0.65962	0.06502	-0.11779	-0.54955	UNCH.	UNCH.
A0A804LJ69	Thioredoxin domain-containing protein	10	14646	11757	17949	12812	0.03321	0.00545	-0.31702	-0.48637	UNCH.	UNCH.
Q9M582	Hypersensitive induced reaction3	9	23730	34019	5083	10145	0.15552	0.06511	0.51960	0.99686	UNCH.	UNCH.
A0A1D6KJW6	5'-methylthioadenosine/S-adenosylhomocysteine nucleosidase 2	4	15055	17187	14199	14756	0.08506	0.79056	0.19109	0.05555	UNCH.	UNCH.
A0A1D6ICL3	Adenosine 5'-phosphosulfate reductase	7	28336	33933	21038	24743	0.25833	0.37962	0.26008	0.23403	UNCH.	UNCH.
C4J5P0	Aspartyl protease AED1	4	12504	13571	13206	22219	0.82734	0.09870	0.11815	0.75060	UNCH.	UNCH.
B6TEK2	GroES-like zinc-binding alcohol dehydrogenase family protein	4	14154	15012	13763	18275	0.75934	0.11051	0.08486	0.40909	UNCH.	UNCH.
C0HGN2	NAD(P)-linked oxidoreductase superfamily protein	8	31195	25490	29770	29033	0.30981	0.94663	-0.29139	-0.03617	UNCH.	UNCH.
A0A804LJ17	Peptidase_S9 domain-containing protein	15	32685	29399	30935	28663	0.46971	0.78740	-0.15287	-0.11001	UNCH.	UNCH.

Supplementary Table 5 - Cont

Accession	Description	Reported peptides	Average Normalized Ion Count L80 HN	Average Normalized Ion Count L80 LN	Average Normalized Ion Count P2 HN	Average Normalized Ion Count P2 LN	t-test L80 LN/HN	t-test P2 LN/HN	Log_2 FC L80 LN/HN	Log_2 FC P2 LN/HN	Differential Accumulation L80 LN/HN	Differential Accumulation P2 LN/HN
A0A804NQ44	CBS domain-containing protein CBSX1, chloroplastic	3	95247	115425	102538	140386	0.11749	0.32190	0.27720	0.45324	UNCH.	UNCH.
A0A804Q6Z7	Calreticulin	5	22834	20987	8665	12537	0.57197	0.16717	-0.12170	0.53301	UNCH.	UNCH.
A0A804N4G2	Malate dehydrogenase	9	24175	33082	12160	17265	0.01727	0.30200	0.45251	0.50570	UNCH.	UNCH.
K7WFV1	ATP synthase subunit gamma	7	227968	203555	264226	205735	0.24277	0.00278	-0.16341	-0.36099	UNCH.	UNCH.
A0A1D6MY43	Beta-glucosidase 17	10	18755	15185	16130	21296	0.22471	0.12975	-0.30458	0.40087	UNCH.	UNCH.
B4FLR0	GrpE protein homolog	4	7913	6939	8626	11401	0.50233	0.30052	-0.18957	0.40247	UNCH.	UNCH.
B4G011	D-3-phosphoglycerate dehydrogenase	5	22293	16090	18178	12061	0.00569	0.16780	-0.47043	-0.59180	UNCH.	UNCH.
A0A1D6HP95	Carboxyl-terminal-processing peptidase 2 chloroplastic	8	20483	25517	18595	24528	0.36824	0.08488	0.31701	0.39954	UNCH.	UNCH.
A0A1D6E3W6	Acetylglutamate kinase	4	15088	13641	14358	14629	0.57797	0.94289	-0.14539	0.02698	UNCH.	UNCH.
A0A804MS97	Glycosyltransferase	2	23302	23933	22548	23057	0.85244	0.96633	0.03854	0.03222	UNCH.	UNCH.
A0A804PZW0	Tr-type G domain-containing protein	9	21697	15500	20750	18495	0.01582	0.52011	-0.48518	-0.16599	UNCH.	UNCH.
A0A804UDX0	HATPase_c domain-containing protein	17	23364	18299	16457	17013	0.04269	0.83463	-0.35251	0.04793	UNCH.	UNCH.
A0A804UBX1	Uncharacterized protein	2	16154	11741	13832	6212	0.21306	0.09205	-0.46037	-1.15479	UNCH.	UNCH.
B6U038	thioredoxin-dependent peroxiredoxin	4	21918	17207	17002	13517	0.24530	0.38375	-0.34912	-0.33091	UNCH.	UNCH.
C0HGT2	Alpha/beta-Hydrolases superfamily protein	4	20116	15672	17794	19884	0.03564	0.37561	-0.36011	0.16017	UNCH.	UNCH.
B6T6S5	glucose-6-phosphate 1-epimerase	3	13176	14723	11548	11162	0.45854	0.84936	0.16016	-0.04903	UNCH.	UNCH.

Supplementary Table 5 - Cont

Accession	Description	Reported peptides	Average Normalized Ion Count L80 HN	Average Normalized Ion Count L80 LN	Average Normalized Ion Count P2 HN	Average Normalized Ion Count P2 LN	t-test L80 LN/HN	t-test P2 LN/HN	Log_2 FC L80 LN/HN	Log_2 FC P2 LN/HN	Differential Accumulation L80 LN/HN	Differential Accumulation P2 LN/HN
B4FIE5	Nascent polypeptide-associated complex subunit beta	2	6845	7315	3776	5835	0.62073	0.13570	0.09577	0.62788	UNCH.	UNCH.
A0A804NQN6	PHB domain-containing protein	7	11220	16294	8552	8488	0.16913	0.97046	0.53820	-0.01069	UNCH.	UNCH.
A0A804QNP8	DLH domain-containing protein	4	11026	11528	11414	6880	0.58506	0.25654	0.06422	-0.73028	UNCH.	UNCH.
A0A1D6H703	Aminopeptidase	11	31921	26248	33437	24788	0.11794	0.01374	-0.28228	-0.43178	UNCH.	UNCH.
A0A804MNC3	AB hydrolase-1 domain-containing protein	6	26037	32434	21696	15678	0.31267	0.33371	0.31691	-0.46868	UNCH.	UNCH.
A0A804QHI8	Thioredoxin reductase	6	23106	30001	26206	34068	0.08367	0.34950	0.37677	0.37853	UNCH.	UNCH.
B4FWX5	dihydroxy-acid dehydratase	7	25502	26589	11742	15912	0.76919	0.17832	0.06022	0.43850	UNCH.	UNCH.
A0A1D6K5D2	Nucleoredoxin1	6	7524	7856	13478	15801	0.61052	0.40336	0.06226	0.22939	UNCH.	UNCH.
A0A1D6LKG8	Magnesium protoporphyrin IX methyltransferase chloroplastic	4	20329	19358	13790	11624	0.82399	0.49848	-0.07058	-0.24658	UNCH.	UNCH.
A0A804PIC7	ADP,ATP carrier protein	8	20140	22331	24954	36938	0.41521	0.16679	0.14898	0.56584	UNCH.	UNCH.
K7TMN5	4-coumarate--CoA ligase	9	15730	11206	19030	13191	0.00697	0.10520	-0.48919	-0.52869	UNCH.	UNCH.
Q6R9J5	ATP synthase protein MI25	2	20278	20369	17420	23829	0.92486	0.09951	0.00645	0.45202	UNCH.	UNCH.
B6T671	Uncharacterized protein	3	14120	15895	13727	12732	0.22813	0.52795	0.17079	-0.10860	UNCH.	UNCH.
B4G0V9	Seed gene 3	2	5312	5962	6694	7891	0.46157	0.58433	0.16647	0.23726	UNCH.	UNCH.
K7V9L0	Putative peptidyl-prolyl cis-trans isomerase family protein	5	28898	32060	34033	39593	0.47525	0.51000	0.14978	0.21830	UNCH.	UNCH.
B6UAC7	Cortical cell-delineating protein	3	15637	19908	14986	22672	0.01800	0.02029	0.34842	0.59729	UNCH.	UNCH.

Supplementary Table 5 - Cont

Accession	Description	Reported peptides	Average Normalized Ion Count L80 HN	Average Normalized Ion Count L80 LN	Average Normalized Ion Count P2 HN	Average Normalized Ion Count P2 LN	t-test L80 LN/HN	t-test P2 LN/HN	Log_2 FC L80 LN/HN	Log_2 FC P2 LN/HN	Differential Accumulation L80 LN/HN	Differential Accumulation P2 LN/HN
B6T484	Mitogen-activated protein kinase	3	20310	14835	11096	12636	0.17935	0.61714	-0.45314	0.18761	UNCH.	UNCH.
A0A804UD50	PABS domain-containing protein	4	22094	30407	20727	23610	0.10381	0.06930	0.46077	0.18794	UNCH.	UNCH.
A0A1D6KIN5	PfkB-like carbohydrate kinase family protein	2	11625	12584	8564	15716	0.22699	0.05712	0.11432	0.87588	UNCH.	UNCH.
B6SNA1	Putative thioredoxin superfamily protein	2	10478	7706	13480	10030	0.35694	0.20739	-0.44321	-0.42660	UNCH.	UNCH.
C0P5E7	Leukotriene A-4 hydrolase-like protein	4	8307	11483	9954	9855	0.09716	0.96856	0.46717	-0.01453	UNCH.	UNCH.
A0A804LIH8	Rhodanese domain-containing protein	2	9349	8731	9870	5980	0.81275	0.22855	-0.09864	-0.72280	UNCH.	UNCH.
Q9AQU5	Aquaporin PIP1-3/PIP1-4	3	16430	15443	12718	16727	0.67205	0.20861	-0.08936	0.39533	UNCH.	UNCH.
A0A804NAJ7	chitinase	2	15122	19108	4594	4517	0.16951	0.94522	0.33754	-0.02438	UNCH.	UNCH.
B4FFP2	Glutamate dehydrogenase	5	7028	5736	6072	11037	0.30380	0.29978	-0.29308	0.86207	UNCH.	UNCH.
A0A804PP02	Thioredoxin-disulfide reductase	3	14437	15487	11267	15010	0.62549	0.05816	0.10127	0.41372	UNCH.	UNCH.
A0A804MTM8	Carboxypeptidase	4	19428	12567	5967	10293	0.20872	0.44105	-0.62850	0.78658	UNCH.	UNCH.
C0HEE6	Peroxidase	5	22403	16590	10164	15705	0.50520	0.44038	-0.43332	0.62772	UNCH.	UNCH.
A0A804N7B9	SRP54 domain-containing protein	4	12216	10921	11519	10342	0.27416	0.52275	-0.16168	-0.15544	UNCH.	UNCH.
C0P5U0	Protoporphyrinogen oxidase	8	25964	22711	14826	14355	0.44058	0.86681	-0.19314	-0.04654	UNCH.	UNCH.
A0A1D6M324	Protein RETICULATA-RELATED 4 chloroplastic	5	17566	17217	24386	39444	0.89852	0.14477	-0.02893	0.69372	UNCH.	UNCH.
A0A804NV14	AB hydrolase-1 domain-containing protein	4	11038	11686	5091	5994	0.75616	0.45777	0.08226	0.23552	UNCH.	UNCH.

Supplementary Table 5 - Cont

Accession	Description	Reported peptides	Average Normalized Ion Count L80 HN	Average Normalized Ion Count L80 LN	Average Normalized Ion Count P2 HN	Average Normalized Ion Count P2 LN	t-test L80 LN/HN	t-test P2 LN/HN	Log_2 FC L80 LN/HN	Log_2 FC P2 LN/HN	Differential Accumulation L80 LN/HN	Differential Accumulation P2 LN/HN
O65107	Photosystem I reaction center subunit N, chloroplastic (Fragment)	3	13327	13287	18688	10497	0.99164	0.10314	-0.00430	-0.83221	UNCH.	UNCH.
A0A804QIX8	DHQ_synthase domain-containing protein	6	19295	18324	16861	16204	0.68237	0.68581	-0.07446	-0.05736	UNCH.	UNCH.
A0A1D6I600	Gibberellin receptor GID1L2	4	11767	15320	18701	19679	0.12049	0.79744	0.38065	0.07353	UNCH.	UNCH.
C4J9R0	PLAT domain-containing protein 3	2	11946	16024	17663	25377	0.08670	0.33784	0.42371	0.52278	UNCH.	UNCH.
B6TEP3	Mitochondrial import receptor subunit TOM40	3	10658	12003	10222	13156	0.28076	0.06800	0.17157	0.36403	UNCH.	UNCH.
B6UAK0	Probable 6-phosphogluconolactonase	4	26376	22687	36777	20194	0.43255	0.12337	-0.21735	-0.86486	UNCH.	UNCH.
A0A1D6GMN4	Heat shock 70 kDa protein	14	21257	25706	17391	16690	0.03327	0.66770	0.27422	-0.05941	UNCH.	UNCH.
A0A1D6NAC9	Glycosyl hydrolase family protein	2	3417	5503	7926	5145	0.13877	0.08402	0.68749	-0.62345	UNCH.	UNCH.
A0A1D6HBA0	ATATH13	3	19271	22501	19793	21522	0.05052	0.27398	0.22358	0.12080	UNCH.	UNCH.
A0A804R4D4	homogentisate 1,2-dioxygenase	2	3124	3417	8846	14086	0.84080	0.06085	0.12963	0.67123	UNCH.	UNCH.
A0A804NCX6	Acetamidase/Formamidase family protein	3	39509	30832	27465	14338	0.19691	0.15417	-0.35777	-0.93781	UNCH.	UNCH.
A0A804QHI7	Carboxypeptidase	3	10360	13835	6106	10898	0.16832	0.39876	0.41736	0.83562	UNCH.	UNCH.
A0A1D6MK41	Alba DNA/RNA-binding protein	2	10440	7492	5912	6401	0.03125	0.72639	-0.47872	0.11469	UNCH.	UNCH.
Q84VG9	Lycopene beta cyclase chloroplastic	5	10462	8275	3113	3735	0.08888	0.30747	-0.33830	0.26267	UNCH.	UNCH.
C0PC84	Starch synthase, chloroplastic/amyloplastic	12	17300	20144	14718	16219	0.02814	0.75360	0.21957	0.14014	UNCH.	UNCH.
A0A1D6H558	Chloroplast processing peptidase	3	18276	12938	15994	9050	0.13814	0.07704	-0.49837	-0.82161	UNCH.	UNCH.

Supplementary Table 5 - Cont

Accession	Description	Reported peptides	Average Normalized Ion Count L80 HN	Average Normalized Ion Count L80 LN	Average Normalized Ion Count P2 HN	Average Normalized Ion Count P2 LN	t-test L80 LN/HN	t-test P2 LN/HN	Log_2 FC L80 LN/HN	Log_2 FC P2 LN/HN	Differential Accumulation L80 LN/HN	Differential Accumulation P2 LN/HN
A0A1D6MVN6	Glycosyltransferase	5	18097	17797	16277	15295	0.89809	0.79666	-0.02416	-0.08974	UNCH.	UNCH.
B4FBT1	(+)-neomenthol dehydrogenase	3	17351	15056	16434	12970	0.14357	0.28008	-0.20474	-0.34154	UNCH.	UNCH.
B6TB55	4-(cytidine 5'-diphospho)-2-C-methyl-D-erythritol kinase	6	19133	18217	17677	26431	0.23231	0.24093	-0.07076	0.58036	UNCH.	UNCH.
A0A1D6HSW9	proline--tRNA ligase	4	15732	12195	8523	7698	0.19261	0.67596	-0.36740	-0.14699	UNCH.	UNCH.
A0A1D6DW07	D-3-phosphoglycerate dehydrogenase	8	23062	17957	19808	19418	0.11129	0.93710	-0.36093	-0.02867	UNCH.	UNCH.
A0A1D6F5U0	Alpha-mannosidase	9	44991	36978	28937	24723	0.31105	0.24858	-0.28298	-0.22708	UNCH.	UNCH.
A0A804QD56	formate--tetrahydrofolate ligase	10	38967	38112	38632	39948	0.87671	0.81906	-0.03201	0.04834	UNCH.	UNCH.
A0A804R296	Ras-related protein RABE1c	3	14789	11589	14145	12345	0.04342	0.40005	-0.35177	-0.19632	UNCH.	UNCH.
A0A804M974	6,7-dimethyl-8-ribityllumazine synthase	3	9886	14114	16262	15454	0.18526	0.80754	0.51368	-0.07356	UNCH.	UNCH.
A0A804MLL1	Polyadenylate-binding protein	9	33329	36833	22939	25612	0.61046	0.56595	0.14424	0.15899	UNCH.	UNCH.
B6TKC8	Gibberellin receptor GID1L2	4	13519	14453	11544	12010	0.73002	0.78199	0.09645	0.05711	UNCH.	UNCH.
A0A1D6QNT3	3-hydroxybutyryl-CoA epimerase	8	17431	19969	11736	23215	0.09597	0.07336	0.19609	0.98410	UNCH.	UNCH.
Q6R985	Cytochrome c oxidase subunit 2	2	50385	58724	40402	50126	0.09355	0.33938	0.22096	0.31114	UNCH.	UNCH.
B4FBJ7	26S protease regulatory subunit 6A homolog A	4	20472	18574	16008	19192	0.32861	0.66357	-0.14035	0.26171	UNCH.	UNCH.
A0A804QBD0	PAP_fibrillin domain-containing protein	2	6020	5539	7228	11297	0.67061	0.14492	-0.12023	0.64421	UNCH.	UNCH.
A0A1D6DQH1	Acetyl-coenzyme A synthetase	11	12869	13013	13089	18438	0.89475	0.14083	0.01603	0.49437	UNCH.	UNCH.

Supplementary Table 5 - Cont

Accession	Description	Reported peptides	Average Normalized Ion Count L80 HN	Average Normalized Ion Count L80 LN	Average Normalized Ion Count P2 HN	Average Normalized Ion Count P2 LN	t-test L80 LN/HN	t-test P2 LN/HN	Log_2 FC L80 LN/HN	Log_2 FC P2 LN/HN	Differential Accumulation L80 LN/HN	Differential Accumulation P2 LN/HN
B6U5L3	UDP-glucose 6-dehydrogenase	4	23533	28878	19567	22755	0.01104	0.44643	0.29529	0.21776	UNCH.	UNCH.
A0A804QMD0	AAA domain-containing protein	3	8538	7959	13057	11791	0.69089	0.65974	-0.10132	-0.14704	UNCH.	UNCH.
A0A804PIG9	Citrate synthase	2	6784	8560	10848	14513	0.18153	0.11790	0.33532	0.41997	UNCH.	UNCH.
A0A804P4D4	CCT-eta	5	14700	11056	9415	8720	0.12480	0.69340	-0.41102	-0.11074	UNCH.	UNCH.
A0A804UFI5	Aminotran_1_2 domain-containing protein	5	10940	10606	9186	11298	0.81922	0.18190	-0.04473	0.29851	UNCH.	UNCH.
A0A804LY71	Alpha-galactosidase	4	18623	10872	12032	10274	0.05440	0.53716	-0.77656	-0.22785	UNCH.	UNCH.
B4FFM6	Tropinone reductase-like protein	4	54300	41940	32307	30002	0.14409	0.70910	-0.37262	-0.10677	UNCH.	UNCH.
A0A1D6EU26	3-dehydroquinate synthase chloroplastic	6	7068	6534	3635	4857	0.60331	0.19151	-0.11323	0.41789	UNCH.	UNCH.
K7VQG5	Phospholipase D	9	122871	137909	116455	123606	0.01657	0.45693	0.16657	0.08598	UNCH.	UNCH.
A0A804UBH4	ATP-grasp domain-containing protein	4	16214	18365	14386	15692	0.40050	0.81501	0.17971	0.12542	UNCH.	UNCH.
A0A1D6K836	Branched-chain-amino-acid aminotransferase	4	15054	12142	12434	11802	0.03286	0.43011	-0.31015	-0.07522	UNCH.	UNCH.
B4G1D2	CBS domain protein	2	7899	4563	10419	4343	0.12648	0.14452	-0.79182	-1.26242	UNCH.	UNCH.
K7TJV6	oxoglutarate dehydrogenase (succinyl-transferring)	13	51584	61054	79513	66237	0.01389	0.18676	0.24316	-0.26355	UNCH.	UNCH.
C0HH81	NAD(P)-binding Rossmann-fold superfamily protein	2	14197	14935	11324	10444	0.76991	0.59478	0.07313	-0.11673	UNCH.	UNCH.
A0A804PF81	Clp R domain-containing protein	3	84233	93220	78494	69658	0.05108	0.33679	0.14627	-0.17229	UNCH.	UNCH.
A0A1D6MUR8	Outer envelope pore protein 37 chloroplastic	3	29337	34475	26726	28799	0.04242	0.51548	0.23285	0.10777	UNCH.	UNCH.

Supplementary Table 5 - Cont

Accession	Description	Reported peptides	Average Normalized Ion Count L80 HN	Average Normalized Ion Count L80 LN	Average Normalized Ion Count P2 HN	Average Normalized Ion Count P2 LN	t-test L80 LN/HN	t-test P2 LN/HN	Log_2 FC L80 LN/HN	Log_2 FC P2 LN/HN	Differential Accumulation L80 LN/HN	Differential Accumulation P2 LN/HN
A0A1D6KVM4	Serine/threonine-protein phosphatase	4	13817	17491	10236	13499	0.04344	0.24042	0.34022	0.39924	UNCH.	UNCH.
A0A1D6ND62	phenylalanine--tRNA ligase	6	21436	15648	13304	10591	0.00528	0.38699	-0.45403	-0.32905	UNCH.	UNCH.
A0A804LTH4	L-ascorbate peroxidase	5	10554	12388	17859	22990	0.41462	0.29765	0.23125	0.36438	UNCH.	UNCH.
B6SZW0	Divinyl chlorophyllide a 8-vinyl-reductase, chloroplastic	2	17023	15357	14713	13342	0.61423	0.56750	-0.14860	-0.14112	UNCH.	UNCH.
A0A804LWM9	Aldedh domain-containing protein	5	9389	9573	8106	10118	0.92731	0.24065	0.02791	0.31983	UNCH.	UNCH.
K7U311	Uncharacterized protein	2	15030	21474	23268	30856	0.14214	0.28624	0.51470	0.40721	UNCH.	UNCH.
B4FBF2	Carboxypeptidase	5	30764	22627	21601	25403	0.40193	0.56255	-0.44322	0.23389	UNCH.	UNCH.
B4G1C1	Putative desiccation-related protein LEA14	2	19324	17571	19019	15608	0.65331	0.26504	-0.13721	-0.28517	UNCH.	UNCH.
A0A1D6F1V0	Amidase 1	2	9118	8576	9021	10009	0.50853	0.34562	-0.08830	0.14986	UNCH.	UNCH.
A0A804U9E0	AAA domain-containing protein	4	11534	8884	6966	7461	0.28773	0.69778	-0.37668	0.09901	UNCH.	UNCH.
A0A1D6P7V2	hydroxyisourate hydrolase	2	6856	7103	5952	6116	0.58303	0.89088	0.05116	0.03925	UNCH.	UNCH.
B6SZS2	30S ribosomal protein S4, chloroplastic	3	5787	5350	4867	5110	0.51278	0.59251	-0.11319	0.07046	UNCH.	UNCH.
A0A804U748	NAD(P)-bd_dom domain-containing protein	2	15104	10549	21632	11074	0.04203	0.21077	-0.51780	-0.96595	UNCH.	UNCH.
B4F8Z3	Adenylosuccinate lyase	3	10323	9434	8045	7498	0.25512	0.70286	-0.12997	-0.10156	UNCH.	UNCH.
A0A1D6IKH4	malate dehydrogenase	2	11515	13201	6559	4437	0.20392	0.22810	0.19714	-0.56380	UNCH.	UNCH.
B6TNM0	[acyl-carrier-protein] S-malonyltransferase	4	25453	17122	12402	13414	0.10254	0.83917	-0.57201	0.11314	UNCH.	UNCH.

Supplementary Table 5 - Cont

Accession	Description	Reported peptides	Average Normalized Ion Count L80 HN	Average Normalized Ion Count L80 LN	Average Normalized Ion Count P2 HN	Average Normalized Ion Count P2 LN	t-test L80 LN/HN	t-test P2 LN/HN	Log_2 FC L80 LN/HN	Log_2 FC P2 LN/HN	Differential Accumulation L80 LN/HN	Differential Accumulation P2 LN/HN
C0PB60	Gamma carbonic anhydrase 2 mitochondrial	4	21449	26646	15150	22681	0.25831	0.04035	0.31304	0.58215	UNCH.	UNCH.
B4FAM1	Protein HHL1, chloroplastic	2	17691	16204	15502	11544	0.53123	0.22557	-0.12664	-0.42529	UNCH.	UNCH.
A0A804LEJ9	CN hydrolase domain-containing protein	3	17114	16498	14785	10388	0.78171	0.20142	-0.05293	-0.50919	UNCH.	UNCH.
A0A804LX34	LOV domain-containing protein	6	13980	12106	12289	10199	0.11759	0.21146	-0.20767	-0.26892	UNCH.	UNCH.
B4FRN6	Methionyl-tRNA formyltransferase	2	9340	8372	9426	9933	0.58204	0.60183	-0.15780	0.07558	UNCH.	UNCH.
A0A804QPC7	Importin subunit alpha	4	17276	16731	11527	16532	0.78500	0.25341	-0.04617	0.52022	UNCH.	UNCH.
A0A1D6N4Z9	Membrane-associated protein VIPP1 chloroplastic	2	14841	8108	9784	6940	0.11450	0.32613	-0.87209	-0.49562	UNCH.	UNCH.
A0A1D6HLQ1	Bifunctional D-cysteine desulfhydrase/1-aminocyclopropane-1-carboxylate deaminase mitochondrial	4	17100	17109	28829	28109	0.99669	0.78828	0.00071	-0.03647	UNCH.	UNCH.
C0PM63	DUF1995 domain-containing protein	3	14987	13973	9016	17207	0.61681	0.17849	-0.10109	0.93251	UNCH.	UNCH.
B6SKS5	3-oxoacyl-[acyl-carrier-protein] synthase III chloroplastic	2	6910	9645	6188	8927	0.02050	0.00949	0.48105	0.52874	UNCH.	UNCH.
A0A1D6N084	ABC-type transport system periplasmic component	4	13457	13011	13893	12515	0.72902	0.61724	-0.04867	-0.15078	UNCH.	UNCH.
B6SMC4	Ycf3-interacting protein 1, chloroplastic	2	11593	15858	10970	15711	0.06249	0.04706	0.45197	0.51822	UNCH.	UNCH.
A0A804MZX1	Shikimate O-hydroxycinnamoyltransferase	5	14408	14613	7412	10996	0.93062	0.05560	0.02034	0.56905	UNCH.	UNCH.
A0A804LQM2	diaminopimelate epimerase	5	15862	14693	15970	15000	0.20944	0.60118	-0.11047	-0.09038	UNCH.	UNCH.
B4FWY6	Tyrosine--tRNA ligase	2	7550	10283	6385	7420	0.02974	0.13079	0.44571	0.21691	UNCH.	UNCH.
A0A804LHA1	Beta-galactosidase	5	22291	24056	11318	17957	0.51703	0.32141	0.10992	0.66591	UNCH.	UNCH.

Supplementary Table 5 - Cont

Accession	Description	Reported peptides	Average Normalized Ion Count L80 HN	Average Normalized Ion Count L80 LN	Average Normalized Ion Count P2 HN	Average Normalized Ion Count P2 LN	t-test L80 LN/HN	t-test P2 LN/HN	Log_2 FC L80 LN/HN	Log_2 FC P2 LN/HN	Differential Accumulation L80 LN/HN	Differential Accumulation P2 LN/HN
A0A804QU15	Aldo_ket_red domain-containing protein	2	13662	11617	10356	9789	0.58801	0.87219	-0.23397	-0.08126	UNCH.	UNCH.
A0A1D6EJ39	E1 ubiquitin-activating enzyme	8	32713	30985	28686	27225	0.66365	0.69242	-0.07832	-0.07540	UNCH.	UNCH.
A0A804LBV9	Enoyl reductase (ER) domain-containing protein	2	7351	7498	5768	6731	0.85354	0.14270	0.02863	0.22295	UNCH.	UNCH.
A0A1D6NMW5	protein-serine/threonine phosphatase	4	26788	25733	28192	29812	0.74605	0.69244	-0.05792	0.08060	UNCH.	UNCH.
C0PFI3	Sulfurtransferase	3	8057	9428	4397	4091	0.16535	0.87246	0.22668	-0.10380	UNCH.	UNCH.
A0A1D6JW69	V-type proton ATPase subunit a	8	21124	22250	22418	24394	0.82053	0.52325	0.07492	0.12183	UNCH.	UNCH.
C0PDB6	HXXXD-type acyl-transferase family protein	7	15183	17029	10305	17386	0.14100	0.31369	0.16554	0.75465	UNCH.	UNCH.
A0A804MVE0	CCT-theta	2	15720	18781	17007	13018	0.14889	0.43309	0.25663	-0.38557	UNCH.	UNCH.
A0A804PM63	Plasma membrane intrinsic protein 1	2	29791	36376	18853	26648	0.14778	0.22227	0.28812	0.49926	UNCH.	UNCH.
A0A1D6ICG6	Glycosyltransferase	2	15047	21415	20994	25682	0.14200	0.43157	0.50914	0.29081	UNCH.	UNCH.
A0A1D6L8D1	Pheophorbide a oxygenase	4	8129	9053	9100	6108	0.42985	0.44100	0.15523	-0.57522	UNCH.	UNCH.
B4G1Q6	SERPIN domain-containing protein	5	8959	11508	16139	16830	0.29810	0.87712	0.36136	0.06046	UNCH.	UNCH.
P17344	ATP synthase subunit a, chloroplastic	2	42513	58179	55429	59516	0.35500	0.87363	0.45260	0.10265	UNCH.	UNCH.
A0A804M666	Mitochondrial Rho GTPase	5	15714	15925	11480	15728	0.93492	0.01701	0.01922	0.45420	UNCH.	UNCH.
C4JAI3	Cyclase family protein	2	21875	18333	7891	10176	0.41546	0.37406	-0.25479	0.36688	UNCH.	UNCH.
A0A804PKE2	WPP domain-containing protein	6	25234	27810	24352	27680	0.04151	0.07428	0.14028	0.18480	UNCH.	UNCH.

Supplementary Table 5 - Cont

Accession	Description	Reported peptides	Average Normalized Ion Count L80 HN	Average Normalized Ion Count L80 LN	Average Normalized Ion Count P2 HN	Average Normalized Ion Count P2 LN	t-test L80 LN/HN	t-test P2 LN/HN	Log_2 FC L80 LN/HN	Log_2 FC P2 LN/HN	Differential Accumulation L80 LN/HN	Differential Accumulation P2 LN/HN
A0A804P7H7	ribose-5-phosphate isomerase	2	5810	5390	8289	8486	0.69539	0.95182	-0.10821	0.03392	UNCH.	UNCH.
A0A804M883	Pyruvate kinase	5	25775	28111	19611	27597	0.11665	0.12118	0.12519	0.49285	UNCH.	UNCH.
A0A804ULF4	Obg-like ATPase 1	4	18524	15738	13935	12442	0.17030	0.44519	-0.23520	-0.16350	UNCH.	UNCH.
A0A1D6ENT5	leucine--tRNA ligase	7	17851	17870	16299	17055	0.99418	0.74913	0.00153	0.06539	UNCH.	UNCH.
C0PDA6	fumarate hydratase	5	25242	23467	26814	24749	0.55268	0.71979	-0.10516	-0.11564	UNCH.	UNCH.
A0A1D6ICF2	UDP-glycosyltransferase 71B1	5	16715	13577	5788	8628	0.63458	0.23845	-0.29995	0.57601	UNCH.	UNCH.
A0A804Q2Y4	Nucleosome assembly protein 1	3	21303	23036	17424	17951	0.51377	0.74171	0.11286	0.04293	UNCH.	UNCH.
A0A804LNK8	Haloacid dehalogenase-like hydrolase domain-containing protein Sgpp	2	4874	9189	6243	10376	0.05865	0.28718	0.91485	0.73295	UNCH.	UNCH.
A0A1D6K4Z5	Putative acetyl-CoA acetyltransferase cytosolic 2	2	6886	8500	6365	8223	0.12531	0.11246	0.30367	0.36968	UNCH.	UNCH.
A0A804M793	30S ribosomal protein S1, chloroplastic	4	16946	19482	16252	15856	0.50710	0.74338	0.20118	-0.03555	UNCH.	UNCH.
A0A804U8G0	Photosynthetic NDH subunit of lumenal location 2, chloroplastic	2	10646	9454	9823	6379	0.58723	0.17564	-0.17141	-0.62296	UNCH.	UNCH.
Q9SE94	Methylenetetrahydrofolate reductase (NADH) 1	2	25111	24442	15049	18094	0.81270	0.53726	-0.03897	0.26585	UNCH.	UNCH.
B4G0Y4	Translocase of chloroplast	2	41384	43246	49751	34872	0.71432	0.02833	0.06349	-0.51263	UNCH.	UNCH.
A0A804R2U0	Ubiquitin receptor RAD23	4	9508	7866	6292	5257	0.44657	0.53977	-0.27356	-0.25935	UNCH.	UNCH.
A0A1D6K641	3-oxo-Delta(45)-steroid 5-beta-reductase	4	11981	13093	9296	14536	0.50574	0.05552	0.12800	0.64503	UNCH.	UNCH.
A0A804Q1C9	Pept_C1 domain-containing protein	3	10865	12620	10897	13688	0.19728	0.26523	0.21612	0.32900	UNCH.	UNCH.

Supplementary Table 5 - Cont

Accession	Description	Reported peptides	Average Normalized Ion Count L80 HN	Average Normalized Ion Count L80 LN	Average Normalized Ion Count P2 HN	Average Normalized Ion Count P2 LN	t-test L80 LN/HN	t-test P2 LN/HN	Log_2 FC L80 LN/HN	Log_2 FC P2 LN/HN	Differential Accumulation L80 LN/HN	Differential Accumulation P2 LN/HN
A0A804R1N6	Epimerase domain-containing protein	2	16043	11345	8135	6915	0.00397	0.18546	-0.49983	-0.23428	UNCH.	UNCH.
A0A804PKC2	Succinate--CoA ligase [ADP-forming] subunit beta, mitochondrial	6	5657	6878	4728	5515	0.12121	0.32680	0.28195	0.22208	UNCH.	UNCH.
Q4TZJ2	Pyrroline-5-carboxylate reductase	2	11914	10450	12283	15366	0.75121	0.30326	-0.18911	0.32305	UNCH.	UNCH.
A0A804NKA7	serine--tRNA ligase	2	7734	9684	7364	9589	0.34047	0.17723	0.32442	0.38083	UNCH.	UNCH.
B4FTP2	Thioredoxin-like protein CDSP32 chloroplastic	2	11249	10501	8931	13787	0.51811	0.18965	-0.09938	0.62638	UNCH.	UNCH.
C4IZ62	DEAD-box ATP-dependent RNA helicase 56	5	17520	16146	12189	16650	0.55493	0.11402	-0.11790	0.44992	UNCH.	UNCH.
A0A1D6QLG5	4-coumarate--CoA ligase	2	58244	46716	44139	27621	0.30531	0.13891	-0.31819	-0.67626	UNCH.	UNCH.
A0A096S9C5	Ribonuclease	2	31566	27407	15682	20174	0.14650	0.25156	-0.20381	0.36338	UNCH.	UNCH.
A0A804NLJ5	Probable methylthioribulose-1-phosphate dehydratase	4	14342	11374	9836	9360	0.06826	0.80519	-0.33447	-0.07153	UNCH.	UNCH.
K7V686	Eukaryotic translation initiation factor 3 subunit F	2	11884	13393	9402	12946	0.27338	0.02044	0.17252	0.46153	UNCH.	UNCH.
A0A804PQM0	Enoyl reductase (ER) domain-containing protein	2	11485	11939	9166	11751	0.81689	0.33854	0.05587	0.35840	UNCH.	UNCH.
A0A804QW31	NAD(P)H-quinone oxidoreductase subunit O, chloroplastic	2	27211	25620	29048	22809	0.50640	0.52102	-0.08691	-0.34887	UNCH.	UNCH.
C0P4P5	non-reducing end alpha-L-arabinofuranosidase	10	9933	11619	10158	9310	0.24352	0.67395	0.22613	-0.12569	UNCH.	UNCH.
C4JAX7	UDP-sulfoquinovose synthase chloroplastic	4	11265	8354	13783	7261	0.07638	0.06879	-0.43130	-0.92461	UNCH.	UNCH.
A0A804QM97	asparagine--tRNA ligase	2	22503	25317	21339	19110	0.56287	0.30306	0.16994	-0.15917	UNCH.	UNCH.
A0A1D6N617	Amidophosphoribosyltransferase	2	7391	6656	10250	11454	0.75681	0.26169	-0.15122	0.16020	UNCH.	UNCH.

Supplementary Table 5 - Cont

Accession	Description	Reported peptides	Average Normalized Ion Count L80 HN	Average Normalized Ion Count L80 LN	Average Normalized Ion Count P2 HN	Average Normalized Ion Count P2 LN	t-test L80 LN/HN	t-test P2 LN/HN	Log_2 FC L80 LN/HN	Log_2 FC P2 LN/HN	Differential Accumulation L80 LN/HN	Differential Accumulation P2 LN/HN
K7V1I3	E1 ubiquitin-activating enzyme	11	10587	10387	8418	11338	0.94599	0.09002	-0.02744	0.42962	UNCH.	UNCH.
B6TCZ1	Spermidine synthase 1	3	205192	193486	226986	163094	0.39290	0.03586	-0.08474	-0.47690	UNCH.	UNCH.
C4J473	oligopeptidase A	6	26662	25267	25611	23446	0.67659	0.49558	-0.07752	-0.12739	UNCH.	UNCH.
C0PFA1	Adenylosuccinate synthetase, chloroplastic	2	14082	13752	13253	14001	0.52387	0.67779	-0.03412	0.07922	UNCH.	UNCH.
A0A1D6HT50	polyribonucleotide nucleotidyltransferase	2	32997	26116	32249	20518	0.08308	0.07073	-0.33740	-0.65234	UNCH.	UNCH.
A0A804RE32	Tr-type G domain-containing protein	2	14925	10103	9188	7165	0.00328	0.30679	-0.56293	-0.35878	UNCH.	UNCH.
A0A804UFY0	ATP citrate synthase	6	15017	17189	13006	17391	0.24596	0.37387	0.19491	0.41917	UNCH.	UNCH.
K7TSU4	Beta-D-xylosidase 4	5	21441	22254	16536	17976	0.79132	0.70369	0.05373	0.12045	UNCH.	UNCH.
A0A804N3D8	Protein LOW PSII ACCUMULATION 1, chloroplastic	2	4977	5254	5770	6892	0.62176	0.55887	0.07833	0.25634	UNCH.	UNCH.
C0HJ53	3-hydroxyacyl-[acyl-carrier-protein] dehydratase	2	20266	19668	12223	19196	0.80256	0.11554	-0.04321	0.65117	UNCH.	UNCH.
A0A804P4U4	Aldo_ket_red domain-containing protein	4	32693	26599	14826	11922	0.11569	0.44881	-0.29758	-0.31455	UNCH.	UNCH.
A0A804PGI5	AAA domain-containing protein	2	20760	14849	15472	12087	0.20937	0.09931	-0.48339	-0.35623	UNCH.	UNCH.
B6TFE4	Ribokinase	3	12955	9868	11639	14811	0.33232	0.44576	-0.39263	0.34771	UNCH.	UNCH.
A0A3L6ER98	Epimerase domain-containing protein	2	20262	22535	23307	20230	0.20975	0.61713	0.15336	-0.20428	UNCH.	UNCH.
A0A1D6GDI4	Carotene isomerase3	2	5934	8522	10530	12906	0.17908	0.35146	0.52225	0.29357	UNCH.	UNCH.
B4FE28	E2F transcription factor-like E2FE	2	8280	9076	6187	8658	0.19203	0.34078	0.13249	0.48475	UNCH.	UNCH.

Supplementary Table 5 - Cont

Accession	Description	Reported peptides	Average Normalized Ion Count L80 HN	Average Normalized Ion Count L80 LN	Average Normalized Ion Count P2 HN	Average Normalized Ion Count P2 LN	t-test L80 LN/HN	t-test P2 LN/HN	Log_2 FC L80 LN/HN	Log_2 FC P2 LN/HN	Differential Accumulation L80 LN/HN	Differential Accumulation P2 LN/HN
A0A1D6N8X5	Cytochrome b5 reductase	2	10015	9701	6163	9241	0.73415	0.08722	-0.04598	0.58426	UNCH.	UNCH.
A0A804LE35	Ion channel POLLUX-like 2	7	25012	33931	25379	32603	0.02422	0.09804	0.43996	0.36138	UNCH.	UNCH.
A0A804PRS4	PRK domain-containing protein	3	18677	20751	18644	13887	0.32534	0.33883	0.15191	-0.42491	UNCH.	UNCH.
A0A804UGF5	Heat shock 70 kDa protein 14	6	15510	15487	9641	14308	0.98977	0.02777	-0.00217	0.56960	UNCH.	UNCH.
A0A804Q0C1	arginine--tRNA ligase	2	8820	7091	6407	5830	0.02900	0.36320	-0.31474	-0.13624	UNCH.	UNCH.
A0A804N8M1	AB hydrolase-1 domain-containing protein	2	19191	18623	14169	25593	0.74967	0.12841	-0.04332	0.85302	UNCH.	UNCH.
A0A804QJX5	3-hydroxybutyryl-CoA epimerase	3	35510	24633	24775	23783	0.01019	0.81492	-0.52761	-0.05892	UNCH.	UNCH.
B7ZZM5	Cell wall invertase	2	22009	15118	5796	4782	0.17952	0.50128	-0.54180	-0.27740	UNCH.	UNCH.
A0A804LHB7	imidazole glycerol-phosphate synthase	2	11248	8466	9003	10435	0.19532	0.34583	-0.40987	0.21288	UNCH.	UNCH.
A0A804MJ52	DUF6598 domain-containing protein	2	7323	9104	9334	10411	0.00703	0.57565	0.31407	0.15746	UNCH.	UNCH.
A0A804UH55	UBP1-associated protein 2C	2	11010	14686	9106	13493	0.09382	0.00593	0.41556	0.56729	UNCH.	UNCH.
A0A1D6HV45	Coatomer subunit gamma	4	13064	11569	9395	10851	0.22387	0.41801	-0.17540	0.20784	UNCH.	UNCH.
A0A1D6L245	phosphoribosylformylglycinamidine synthase	6	22957	19144	19215	13701	0.05940	0.04570	-0.26201	-0.48791	UNCH.	UNCH.
A0A804PUY8	AIG1-type G domain-containing protein	4	16505	16688	16030	17549	0.90758	0.45348	0.01598	0.13060	UNCH.	UNCH.
A0A1D6EDQ6	acetyl-CoA carboxylase	6	23716	15275	16072	10885	0.07982	0.07827	-0.63471	-0.56212	UNCH.	UNCH.
A0A1D6L2Q2	Adenylyl cyclase-associated protein	3	18436	22685	22447	19139	0.08633	0.42939	0.29920	-0.23003	UNCH.	UNCH.

Supplementary Table 5 - Cont

Accession	Description	Reported peptides	Average Normalized Ion Count L80 HN	Average Normalized Ion Count L80 LN	Average Normalized Ion Count P2 HN	Average Normalized Ion Count P2 LN	t-test L80 LN/HN	t-test P2 LN/HN	Log_2 FC L80 LN/HN	Log_2 FC P2 LN/HN	Differential Accumulation L80 LN/HN	Differential Accumulation P2 LN/HN
B6ST57	DNA photolyase	4	8471	8501	12500	12515	0.97936	0.99348	0.00521	0.00174	UNCH.	UNCH.
C4J6R6	V-type proton ATPase subunit	2	16502	15577	18127	19114	0.85424	0.71192	-0.08322	0.07644	UNCH.	UNCH.
A0A804R1S6	Kinesin motor domain-containing protein	8	30575	28324	34705	24340	0.22647	0.24922	-0.11032	-0.51185	UNCH.	UNCH.
A0A1D6LWI0	4-coumarate--CoA ligase	2	6597	4953	5406	4869	0.13138	0.63056	-0.41351	-0.15098	UNCH.	UNCH.
A0A804MU73	T-complex protein 1 subunit zeta	2	8245	6970	6217	6213	0.05946	0.99659	-0.24246	-0.00093	UNCH.	UNCH.
A0A096R382	Alpha-1,4 glucan phosphorylase	2	6168	6332	8587	11491	0.89714	0.24168	0.03767	0.42018	UNCH.	UNCH.
Q8S532	Aldehyde dehydrogenase3	2	14518	17357	10268	20785	0.45283	0.45105	0.25769	1.01733	UNCH.	UNCH.
B4F917	WPP domain-containing protein	4	12604	14484	11502	9352	0.21732	0.20491	0.20054	-0.29854	UNCH.	UNCH.
A0A1D6KV33	acylaminoacyl-peptidase	3	14268	14228	9540	12626	0.94743	0.11355	-0.00402	0.40443	UNCH.	UNCH.
A0A804M9M5	Uncharacterized protein	2	8257	7902	8760	10438	0.53479	0.50723	-0.06337	0.25292	UNCH.	UNCH.
B4F8V5	NADH dehydrogenase [ubiquinone] iron-sulfur protein 1 mitochondrial	4	12794	11368	8660	11265	0.56885	0.13461	-0.17057	0.37930	UNCH.	UNCH.
A0A804NVG0	SET domain-containing protein	2	7245	6861	6029	5247	0.71673	0.51453	-0.07857	-0.20064	UNCH.	UNCH.
C4J164	Starch synthase, chloroplastic/amyloplastic	3	26497	35948	25034	28431	0.13096	0.42286	0.44011	0.18357	UNCH.	UNCH.
B4FAT6	Glycosyltransferase	2	14027	13284	5090	4556	0.81369	0.81296	-0.07853	-0.15979	UNCH.	UNCH.
B4FQ24	Cytochrome P450 family 706 subfamily A polypeptide 5	4	14294	11131	20378	16046	0.10248	0.07246	-0.36076	-0.34483	UNCH.	UNCH.
K7TFH9	Prolyl endopeptidase	5	14216	14696	8954	12829	0.61777	0.00494	0.04786	0.51876	UNCH.	UNCH.

Supplementary Table 5 - Cont

Accession	Description	Reported peptides	Average Normalized Ion Count L80 HN	Average Normalized Ion Count L80 LN	Average Normalized Ion Count P2 HN	Average Normalized Ion Count P2 LN	t-test L80 LN/HN	t-test P2 LN/HN	Log_2 FC L80 LN/HN	Log_2 FC P2 LN/HN	Differential Accumulation L80 LN/HN	Differential Accumulation P2 LN/HN
A0A804LRN9	Sulfurtransferase	2	8539	9316	7726	7087	0.58030	0.70294	0.12559	-0.12461	UNCH.	UNCH.
A0A804NZC5	Glutamyl-tRNA(Gln) amidotransferase subunit B, chloroplastic/mitochondrial	3	9971	7565	7733	5544	0.15961	0.09112	-0.39841	-0.48014	UNCH.	UNCH.
A0A1D6PRY2	Protein kinase superfamily protein	4	6665	6663	7567	10730	0.99924	0.06767	-0.00031	0.50394	UNCH.	UNCH.
A0A804QJZ5	Dihydrolipoyl dehydrogenase	2	17118	11571	10027	11415	0.13260	0.47320	-0.56499	0.18708	UNCH.	UNCH.
A0A804ML74	Uncharacterized protein	2	16593	18617	11714	16246	0.18405	0.21543	0.16607	0.47182	UNCH.	UNCH.
Q9SWR9	Acetyltransferase component of pyruvate dehydrogenase complex	3	15090	14042	12585	13200	0.76498	0.72523	-0.10390	0.06889	UNCH.	UNCH.
A0A1D6MID5	glutamine--tRNA ligase	2	13132	12468	7610	10066	0.58736	0.02858	-0.07493	0.40359	UNCH.	UNCH.
A0A804R5C9	Omp85 domain-containing protein	2	12955	17448	12830	14100	0.13077	0.43447	0.42950	0.13623	UNCH.	UNCH.
A0A1D6KE02	Thaumatin-like protein	2	11897	12155	10445	11758	0.85827	0.07159	0.03093	0.17083	UNCH.	UNCH.
K7TLJ6	valine--tRNA ligase	2	13228	10526	10076	9496	0.00838	0.71513	-0.32968	-0.08543	UNCH.	UNCH.
K7TY03	Alanine--tRNA ligase	2	14602	11066	7688	9099	0.14980	0.30632	-0.40003	0.24301	UNCH.	UNCH.
A0A804UC68	Chaperonin Cpn	2	3986	3632	4604	6316	0.61157	0.04936	-0.13422	0.45602	UNCH.	UNCH.
A0A1D6JDW6	26S proteasome non-ATPase regulatory subunit 1 homolog	2	14149	13561	11105	15322	0.77780	0.01182	-0.06117	0.46441	UNCH.	UNCH.
A0A1D6IHP1	ARM repeat superfamily protein	3	8454	8310	7576	8309	0.86558	0.61714	-0.02483	0.13324	UNCH.	UNCH.
A0A804NSQ8	glycerophosphodiester phosphodiesterase	2	10877	12982	7402	10605	0.15000	0.14162	0.25517	0.51869	UNCH.	UNCH.
A0A8X5E9J0	Uncharacterized protein	21	0	0	141252	200797	-	0.00767	-	0.50746	-	UNCH.

Supplementary Table 5 - Cont

Accession	Description	Reported peptides	Average Normalized Ion Count L80 HN	Average Normalized Ion Count L80 LN	Average Normalized Ion Count P2 HN	Average Normalized Ion Count P2 LN	t-test L80 LN/HN	t-test P2 LN/HN	Log_2 FC L80 LN/HN	Log_2 FC P2 LN/HN	Differential Accumulation L80 LN/HN	Differential Accumulation P2 LN/HN
A0A804NB58	Heat shock cognate 70 kDa protein	28	0	0	1971	1350	-	0.11671	-	-0.54608	-	UNCH.
B4FB80	Thioredoxin F2 chloroplastic	8	0	0	46671	24948	-	0.17108	-	-0.90364	-	UNCH.
A0A804RMW6	ATP synthase subunit alpha	24	0	0	2563	3804	-	0.01639	-	0.56946	-	UNCH.
A0A804MWU5	Aldo_ket_red domain-containing protein	4	0	0	19827	37739	-	0.19756	-	0.92861	-	UNCH.
A0A804QY97	Fruit bromelain	7	0	0	99930	93769	-	0.25048	-	-0.09180	-	UNCH.
A0A804MUN7	Subtilisin-like protease SBT3.9	9	0	0	20788	10381	-	0.35841	-	-1.00183	-	UNCH.
A0A1D6I7Z1	Chloroplastic quinone-oxidoreductase	3	0	0	7963	8058	-	0.96161	-	0.01709	-	UNCH.
A0A804M8C9	Haloacid dehalogenase-like hydrolase domain-containing protein	5	13913	4632	0	0	0.00793	-	-1.58676	-	DOWN	-
Q41803	Elongation factor 1-alpha	23	9767	0	0	0	0.00019	-	-	-	UNIQUE HIGH N	-
P08440	Fructose-bisphosphate aldolase, cytoplasmic isozyme	20	3112	0	0	0	0.00030	-	-	-	UNIQUE HIGH N	-
A0A804RIH1	Clp R domain-containing protein	13	1634	0	0	0	0.00001	-	-	-	UNIQUE HIGH N	-
A0A1D6MAI5	Putative mitochondrial-processing peptidase subunit alpha-2 chloroplastic/mitochondrial	10	1745	0	0	0	0.00064	-	-	-	UNIQUE HIGH N	-
A0A804M8Z4	Ribulose bisphosphate carboxylase/oxygenase activase, chloroplastic	3	0	3054	0	0	0.00021	-	-	-	UNIQUE LOW N	-
A0A804PN57	Phosphoribulokinase	16	5335	6812	0	0	0.18272	-	0.35262	-	UNCH.	-
A0A804NPL3	31 kDa ribonucleoprotein, chloroplastic	7	5434	4407	0	0	0.07791	-	-0.30224	-	UNCH.	-
B4FAR8	Proteasome subunit alpha type	6	22908	19535	0	0	0.19043	-	-0.22983	-	UNCH.	-

Supplementary Table 5 - Cont

Accession	Description	Reported peptides	Average Normalized Ion Count L80 HN	Average Normalized Ion Count L80 LN	Average Normalized Ion Count P2 HN	Average Normalized Ion Count P2 LN	t-test L80 LN/HN	t-test P2 LN/HN	Log_2 FC L80 LN/HN	Log_2 FC P2 LN/HN	Differential Accumulation L80 LN/HN	Differential Accumulation P2 LN/HN
B7ZXK9	Thioredoxin family protein	2	11342	8022	0	0	0.07769	-	-0.49966	-	UNCH.	-
A0A804P3S4	Kynurenine formamidase	5	45896	46792	16001	10067	-	-	0.02791	-0.66857	-	-
A0A804MIE1	Agglutinin domain-containing protein	7	55363	7143	26198	8266	-	-	-2.95428	-1.66416	-	-
C0PK04	inorganic diphosphatase	3	24687	13974	24073	8262	-	-	-0.82099	-1.54277	-	-
B4FV96	Uncharacterized protein	4	58514	53503	52788	58966	-	-	-0.12917	0.15966	-	-
A0A1D6F9W9	Putative carboxylesterase 15	6	35309	33673	34119	11325	-	-	-0.06843	-1.59099	-	-
A0A804QG64	Peroxidase	5	4278	10138	7757	19816	-	-	1.24472	1.35313	-	-
B4FWN1	NAD(P)H dehydrogenase (quinone)	4	17086	7529	5105	0	-	-	-1.18216	#NÚM!	-	-
Q84TL6	Legumin-like protein	7	17157	21816	3922	14354	-	-	0.34659	1.87194	-	-
A0A1D6MUQ1	Beta-glucosidase 17	4	2110	2316	986	1415	-	-	0.13447	0.52145	-	-
B4FUN3	GST N-terminal domain-containing protein	2	30892	23634	6496	3125	-	-	-0.38633	-1.05575	-	-
B4FHM1	Cytochrome c1 1 heme protein mitochondrial	2	8353	2965	7736	3654	-	-	-1.49456	-1.08211	-	-
B6T391	Lichenase-2	4	21562	8772	22522	7495	-	-	-1.29746	-1.58733	-	-
B6SVI7	Nascent polypeptide-associated complex subunit beta	2	9406	5432	5089	5925	-	-	-0.79195	0.21966	-	-
A0A804ULR4	Tyrosinase_Cu-bd domain-containing protein	5	2811	1284	11862	10380	-	-	-1.13048	-0.19252	-	-
P49237	Glucan endo-1,3-beta-glucosidase, acidic isoform	3	58472	21488	28707	24336	-	-	-1.44423	-0.23833	-	-

Supplementary Table 5 - Cont

Accession	Description	Reported peptides	Average Normalized Ion Count L80 HN	Average Normalized Ion Count L80 LN	Average Normalized Ion Count P2 HN	Average Normalized Ion Count P2 LN	t-test L80 LN/HN	t-test P2 LN/HN	Log_2 FC L80 LN/HN	Log_2 FC P2 LN/HN	Differential Accumulation L80 LN/HN	Differential Accumulation P2 LN/HN
B4FJV4	Putative carboxylesterase 15	2	22498	20920	9519	11018	-	-	-0.10494	0.21099	-	-
B4FI53	60S ribosomal protein L32	2	39156	7849	34414	34971	-	-	-2.31874	0.02317	-	-
B4FCK8	Protein LOW PSII ACCUMULATION 1 chloroplastic	2	7848	9096	15795	11879	-	-	0.21292	-0.41104	-	-
P27324	Photosystem I assembly protein Ycf3	2	14474	10097	11404	7444	-	-	-0.51953	-0.61542	-	-
B8A187	Putative quinone-oxidoreductase homolog chloroplastic	3	3470	8637	2390	13624	-	-	1.31587	2.51111	-	-
A0A804MDQ3	Aldo_ket_red domain-containing protein	2	2024	2612	20635	16572	-	-	0.36830	-0.31637	-	-
A0A1D6ITY9	5-formyltetrahydrofolate cyclo-ligase1	2	5298	0	9544	5533	-	-	-	-0.78653	-	-
A0A804NP34	Threonylcarbamoyl-AMP synthase	3	6757	6135	6072	5000	-	-	-0.13928	-0.28012	-	-
B4FTK0	Early nodulin-like protein 9	2	15332	11140	6619	17514	-	-	-0.46080	1.40390	-	-
A0A804UNF4	Nudix hydrolase domain-containing protein	2	14106	3280	8593	1364	-	-	-2.10458	-2.65529	-	-
K7VI25	AAA-ATPase ASD mitochondrial	4	31137	19890	5564	6337	-	-	-0.64663	0.18756	-	-
A0A1D6EBE5	NDR1/HIN1-like 1	2	5156	8131	6089	11120	-	-	0.65732	0.86880	-	-
A0A804Q663	FAD-binding PCMH-type domain-containing protein	3	13359	13268	4903	2667	-	-	-0.00985	-0.87845	-	-
B4FQB3	M20_dimer domain-containing protein	2	10436	5374	6993	9845	-	-	-0.95763	0.49358	-	-
A0A804QKF6	phosphoribosylamine--glycine ligase	2	8948	8307	7160	7794	-	-	-0.10723	0.12237	-	-
A0A804RFZ5	Aldo_ket_red domain-containing protein	2	11833	10315	0	4300	-	-	-0.19818	#DIV/0!	-	-

Supplementary Table 5 - Cont

Accession	Description	Reported peptides	Average Normalized Ion Count L80 HN	Average Normalized Ion Count L80 LN	Average Normalized Ion Count P2 HN	Average Normalized Ion Count P2 LN	t-test L80 LN/HN	t-test P2 LN/HN	Log_2 FC L80 LN/HN	Log_2 FC P2 LN/HN	Differential Accumulation L80 LN/HN	Differential Accumulation P2 LN/HN
A0A1D6HSR3	Putative carboxylesterase 15	2	2821	2757	8103	15625	-	-	-0.03311	0.94737	-	-
C0PHF6	AAA-ATPase ASD mitochondrial	2	10365	9975	0	3225	-	-	-0.05545	#DIV/0!	-	-
B4F9X0	Alpha-galactosidase	3	6752	3020	3449	2378	-	-	-1.16070	-0.53662	-	-
A0A804NA49	Patellin-3-like	2	14463	23625	13733	25864	-	-	0.70798	0.91328	-	-
A0A804UF48	Peptidyl-prolyl cis-trans isomerase	2	5538	1557	20985	16441	-	-	-1.83068	-0.35202	-	-
A0A804RGI3	shikimate dehydrogenase (NADP(+))	2	7992	6317	7154	7166	-	-	-0.33939	0.00237	-	-
B4F8K5	NAD(P)-binding Rossmann-fold superfamily protein	2	0	0	35479	0	-	-	-	-	-	-
B6TWA5	Phenolic glucoside malonyltransferase 1	3	5536	6367	1581	3780	-	-	0.20185	1.25759	-	-
C0HF58	Solanesyl-diphosphate synthase 3, chloroplastic	2	12900	11560	10826	13555	-	-	-0.15817	0.32434	-	-
A0A804UD81	ABC transporter B family member 28	2	12656	13136	18067	9915	-	-	0.05374	-0.86565	-	-
A0A1D6K484	Cystathionine gamma-synthase 1 chloroplastic	2	7887	5226	2769	1938	-	-	-0.59388	-0.51504	-	-
A0A1D6FKD0	Putative 3-hydroxyisobutyrate dehydrogenase-like 3 mitochondrial	2	7542	7218	6039	5991	-	-	-0.06331	-0.01157	-	-
K7V8I9	UvrB/uvrC motif-containing protein	2	8033	4825	10257	4982	-	-	-0.73551	-1.04188	-	-

LN/HN: Comparison between proteins accumulated in the condition of low (LN) and high (HN) N; FC: Fold change; UNCh.: Unchanged.

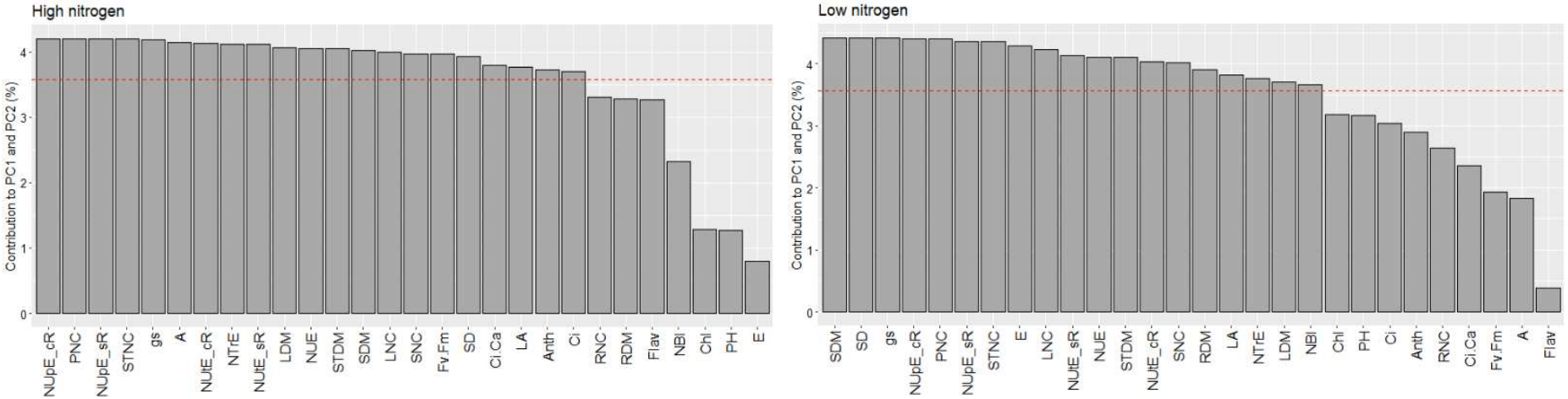

Supplementary Figure 1 – Relative contribution of 28 morpho-agronomic and physiological traits evaluated in popcorn genotypes under contrasting nitrogen (N) availability to the first 2 Principal Components. The red line indicates the average contribution. PH – plant height (cm); SD – stem diameter (mm); LA – leaf area (cm^2); LDM – leaf dry matter (g); SDM – stem dry matter (g); STDM – shoot dry matter (g); RDM – root dry matter (g); LNC – leaf N content (mg of N kg^{-1}); SNC – stem N content (mg of N kg^{-1}); RNC – root N content (mg of N kg^{-1}); STNC – shoot N content (mg of N kg^{-1}); PNC – plant N content (mg of N kg^{-1}); (NUE – N use efficiency; NUpE_cR – N uptake efficiency with root N content; NUpE_sR – N uptake efficiency without root N content; NUtE_cR – N utilization efficiency with the content of N in the root; NUtE_sR – N utilization efficiency without the content of N in the root; NTrE – N translocation efficiency; A – net CO_2 assimilation rate; gs – stomatal conductance; Ci – intercellular concentration of CO_2; E – transpiration rate; Ci/Ca – ratio between the intercellular and external concentration of CO_2; Fv/Fm – photochemical efficiency of photosystem II; Chl – relative chlorophyll content; Flav – relative content of flavonoids; Anth – relative anthocyanin content; NBI – nitrogen balance index.